

1 Global Carbon Budget 2025

2 Pierre Friedlingstein[1,2], Michael O'Sullivan[1], Matthew W. Jones[3], Robbie M. Andrew[4],
3 Dorothee C. E. Bakker[5], Judith Hauck[6,7], Peter Landschützer[8], Corinne Le Quéré[3], Hongmei
4 Li[9,10], Ingrid T. Lujikx[11], Glen P. Peters[4], Wouter Peters[11,12], Julia Pongratz[13,10], Clemens
5 Schwingshackl[13], Stephen Sitch[1], Josep G. Canadell[14], Philippe Ciais[15], Kjetil Aas[4], Simone
6 R. Alin[16], Peter Anthoni[17], Leticia Barbero[18], Nicholas R. Bates[19,20], Nicolas Bellouin[21],
7 Alice Benoit-Cattin[22], Carla F. Berghoff[23], Raffaele Bernardello[24], Laurent Bopp[2], Ida Bagus
8 Mandhara Brasika[1,25], Matthew A. Chamberlain[26], Naveen Chandra[27], Frédéric Chevallier[15],
9 Louise P. Chini[28], Nathan O. Collier[29], Thomas H. Colligan[30], Margot Cronin[31], Laique M.
10 Djeutchouang[32,33,34], Xinyu Dou[35], Matt P. Enright[19,20], Kazutaka Enyo[36], Michael
11 Erb[37,38], Wiley Evans[39], Richard A. Feely[16], Liang Feng[40,41], Daniel J. Ford[1], Adriana
12 Foster[42], Filipa Fransner[43,44], Thomas Gasser[45], Marion Gehlen[15], Thanos Gkritzalis[8],
13 Jefferson Goncalves De Souza[1], Giacomo Grassi[46], Luke Gregor[47,48], Nicolas Gruber[47],
14 Bertrand Guenet[49], Özgür Gürses[6], Kirsty Harrington[50], Ian Harris[51], Jens Heinke[52], George
15 C. Hurtt[28], Yosuke Iida[36], Tatiana Ilyina[53,9,10], Akihiko Ito[54], Andrew R. Jacobson[55,56],
16 Atul K. Jain[57], Tereza Jarníková[3], Annika Jersild[30], Fei Jiang[58], Steve D. Jones[8], Etsushi
17 Kato[59], Ralph F. Keeling[60], Kees Klein Goldewijk[61], Jürgen Knauer[62], Yawen Kong[63,64],
18 Jan Ivar Korsbakken[4], Charles Koven[65], Taro Kunimitsu[4], Xin Lan[55,56], Junjie Liu[66,67],
19 Zhiqiang Liu[68], Zhu Liu[69], Claire Lo Monaco[70], Lei Ma[28], Gregg Marland[37,38], Patrick C.
20 McGuire[71], Galen A. McKinley[72], Joe R. Melton[73], Natalie Monacchi[74], Erwan Monier[75,76],
21 Eric J. Morgan[60], David R. Munro[55,56], Jens D. Müller[77], Shin-Ichiro Nakaoka[78], Lorna R.
22 Nayagam[78], Yosuke Niwa[78], Tobias Nutz[13], Are Olsen[43,44], Abdirahman M. Omar[79,44],
23 Naiqing Pan[80], Sudhanshu Pandey[66], Denis Pierrot[81], Zhangcai Qin[82], Pierre Regnier[83],
24 Gregor Rehder[84], Laure Resplandy[85], Alizée Roobaert[8], Thais M. Rosan[1], Christian
25 Rödenbeck[86], Jörg Schwinger[44,79], Ingunn Skjelvan[79,44], T. Luke Smallman[40,41], Victoria
26 Spada[87], Mohanan G. Sreesh[6], Qing Sun[88], Adrienne J. Sutton[16], Colm Sweeney[56], Didier
27 Swingedouw[89], Roland Séférian[90], Shintaro Takao[78], Hiroaki Tatebe[91,92], Hanqin Tian[80],
28 Xiangjun Tian[93,94], Bronte Tilbrook[26,95], Hiroyuki Tsujino[96], Francesco Tubiello[97], Erik van
29 Ooijen[26], Guido R. van der Werf[11], Sebastiaan J. van de Velde[98,99], Anthony P. Walker[100],
30 Rik Wanninkhof[81], Xiaojuan Yang[100], Wenping Yuan[101], Xu Yue[102], Jiye Zeng[78]

31
32 1: Faculty of Environment, Science and Economy, University of Exeter, Exeter, EX4 4QF, UK

33 2: Laboratoire de Météorologie Dynamique, Institut Pierre-Simon Laplace, CNRS, École Normale
34 Supérieure, Université PSL, Sorbonne Université, École Polytechnique, Paris, France

35 3: Tyndall Centre for Climate Change Research, School of Environmental Sciences, University of East

36 Anglia, Norwich Research Park, Norwich NR4 7TJ, UK

Style Definition: Heading 1

Style Definition: Heading 2

Style Definition: Heading 3

Style Definition: Heading 4

Style Definition: Heading 5

Style Definition: Heading 6

Style Definition: Heading 7: Outline numbered + Level: 7 +
Numbering Style: 1, 2, 3, ... + Start at: 1 + Alignment: Left +
Aligned at: 8.25 cm + Indent at: 8.89 cm

Style Definition: Heading 8: Outline numbered + Level: 8 +
Numbering Style: a, b, c, ... + Start at: 1 + Alignment: Left +
Aligned at: 9.52 cm + Indent at: 10.16 cm

Style Definition: Heading 9: Outline numbered + Level: 9 +
Numbering Style: i, ii, iii, ... + Start at: 1 + Alignment: Right
+ Aligned at: 11.11 cm + Indent at: 11.43 cm

37 4: CICERO Center for International Climate Research, Oslo 0349, Norway
38 5: School of Environmental Sciences, University of East Anglia, Norwich NR4 7TJ, UK
39 6: Alfred-Wegener-Institut, Helmholtz-Zentrum für Polar- und Meeresforschung, Am Handelshafen 12,
40 27570 Bremerhaven
41 7: Universität Bremen, FB02 Biology/Chemistry Bremen, Germany
42 8: Flanders Marine Institute (VLIZ), Jacobsenstraat 1, 8400, Ostend, Belgium
43 9: Helmholtz-Zentrum Hereon, Max-Planck-Straße 1, 21502 Geesthacht, Germany
44 10: Max Planck Institute for Meteorology, Bundesstraße 53, 20146 Hamburg, Germany
45 11: Wageningen University, Environmental Sciences Group, P.O. Box 47, 6700AA, Wageningen, The
46 Netherlands
47 12: University of Groningen, Centre for Isotope Research, Groningen, The Netherlands
48 13: Ludwig-Maximilians-Universität München, Luisenstr. 37, 80333 München, Germany
49 14: CSIRO Oceans and Atmosphere, Canberra, ACT 2101, Australia
50 15: Laboratoire des Sciences du Climat et de l'Environnement, LSCE/IPSL, CEA-CNRS-UVSQ,
51 Université Paris-Saclay, F-91198 Gif-sur-Yvette, France
52 16: National Oceanic and Atmospheric Administration, Pacific Marine Environmental Laboratory
53 (NOAA/PMEL), 7600 Sand Point Way NE, Seattle, WA 98115, USA
54 17: Karlsruhe Institute of Technology, Institute of Meteorology and Climate Research/Atmospheric
55 Environmental Research, 82467 Garmisch-Partenkirchen, Germany
56 18: Rosenstiel School of Marine Atmospheric and Earth Science, Cooperative Institute for Marine and
57 Atmospheric Studies (CIMAS), University of Miami, 4600 Rickenbacker Causeway, Miami, FL, USA
58 19: Arizona State University, Tempe, Arizona, AZ 85287-5502, USA
59 20: Bermuda Institute of Ocean Sciences (BIOS), 17 Biological Lane, St. Georges, GE01, Bermuda
60 21: Department of Meteorology, University of Reading, Reading, RG6 6BB, UK
61 22: Marine and Freshwater Research Institute, Reykjavik, Iceland
62 23: Instituto Nacional de Investigación y Desarrollo Pesquero (INIDEP), Paseo Victoria Ocampo N°1,
63 B7602HSA, Mar del Plata, Argentina
64 24: Barcelona Supercomputing Center, Barcelona, Spain
65 25: Faculty of Marine Science & Fisheries, Udayana University, Denpasar, Bali, 80361, Indonesia
66 26: CSIRO Environment, Castray Esplanade, Hobart, Tasmania 7004, Australia
67 27: Research Institute for Global Change, JAMSTEC, 3173-25 Showa-machi, Kanazawa, Yokohama,
68 236-0001, Japan
69 28: Department of Geographical Sciences, University of Maryland, College Park, MD 20742, USA
70 29: Computer Science and Engineering Division, Oak Ridge National Laboratory, Oak Ridge, TN
71 37831, USA
72 30: Earth System Science Interdisciplinary Center, University of Maryland, College Park, MD 20740,
73 USA

74 31: Marine Institute, Rinville, Oranmore, Co Galway H91 R673, Ireland
75 32: School for Climate Studies, Stellenbosch University, Private Bag X1, Matieland, Stellenbosch,
76 7602, South Africa
77 33: Southern Ocean Carbon – Climate Observatory, CSIR, Rosebank, Cape Town, 7700, South Africa
78 34: Engr. Computer Science, University of California, Davis, CA 95616, USA
79 35: Department of Earth System Science, Stanford University, Stanford, CA 94305, USA
80 36: Japan Meteorological Agency, 3-6-9 Toranomon, Minato City, Tokyo, 105-8431, Japan
81 37: Research Institute for Environment, Energy, and Economics, Appalachian State University, Boone,
82 North Carolina, USA
83 38: Department of Geological and Environmental Sciences, Appalachian State University, Boone,
84 North Carolina, USA
85 39: Hakai Institute, 1713 Hyacinthe Bay Rd, Heriot Bay, BC, V0P 1H0, Canada
86 40: National Centre for Earth Observation, University of Edinburgh, Edinburgh, EH9 3FE, UK
87 41: School of Geosciences, University of Edinburgh, Edinburgh, EH9 3FE, UK
88 42: Climate and Global Dynamics Laboratory, National Center for Atmospheric Research
89 43: Geophysical Institute, University of Bergen, Allégaten 70, 5007 Bergen, Norway
90 44: Bjerknes Centre for Climate Research, Bergen, Norway
91 45: International Institute for Applied Systems Analysis (IIASA), Schlossplatz 1 A-2361 Laxenburg,
92 Austria
93 46: European Commission, Joint Research Centre (JRC), Ispra, Italy
94 47: Environmental Physics Group, Institute of Biogeochemistry and Pollutant Dynamics and Center for
95 Climate Systems Modeling (C2SM), ETH Zürich, Zurich, Switzerland
96 48: Swiss Data Science Center, 8050 Zurich, Switzerland
97 49: Laboratoire de Géologie, Ecole Normale Supérieure, CNRS UMR 8538, Institut Pierre-Simon
98 Laplace, PSL Research University, Paris, France
99 50: Smith School for Enterprise and the Environment, University of Oxford, Oxford, UK
100 51: NCAS-Climate, Climatic Research Unit, School of Environmental Sciences, University of East
101 Anglia, Norwich Research Park, Norwich, NR4 7TJ, UK
102 52: Potsdam Institute for Climate Impact Research (PIK), member of the Leibniz Association, P.O. Box
103 60 12 03, 14412 Potsdam, Germany
104 53: Universität Hamburg, Bundesstraße 55, 20146 Hamburg, Germany
105 54: Graduate School of Agricultural and Life Sciences, University of Tokyo, Tokyo, Japan
106 55: Cooperative Institute for Research in Environmental Sciences (CIRES), University of Colorado
107 Boulder, Boulder, CO 80305, USA
108 56: National Oceanic and Atmospheric Administration Global Monitoring Laboratory (NOAA/GML),
109 325 Broadway R/GML, Boulder, CO 80305, USA

110 57: Department of Climate, Meteorology and Atmospheric Sciences, University of Illinois, Urbana, IL
111 61801, USA
112 58: Jiangsu Provincial Key Laboratory for Advanced Remote Sensing and Geographic Information
113 Technology, International Institute for Earth System Science, Nanjing University, Nanjing, 210023,
114 China.
115 59: Institute of Applied Energy (IAE), Minato-ku, Tokyo 105-0003, Japan
116 60: University of California, San Diego, Scripps Institution of Oceanography, La Jolla, CA 92093-
117 0244, USA
118 61: Utrecht University, Faculty of Geosciences, Department IMEW, Copernicus Institute of Sustainable
119 Development, Heidelberglaan 2, P.O. Box 80115, 3508 TC, Utrecht, the Netherlands
120 62: School of Life Sciences, Faculty of Science, University of Technology Sydney, Ultimo, NSW 2007,
121 Australia
122 63: State Key Laboratory of Remote Sensing and Digital Earth, Aerospace Information Research
123 Institute, Chinese Academy of Sciences, Beijing 100101, China
124 64: Ministry of Education Key Laboratory for Earth System Modeling, Department of Earth System
125 Science, Tsinghua University, Beijing 100084, China
126 65: Lawrence Berkeley National Laboratory, USA
127 66: Jet Propulsion Laboratory, California Institute of Technology, Pasadena, CA, USA
128 67: Division of Geological and Planetary Sciences, California Institute of Technology, Pasadena, CA,
129 USA
130 68: CMA Key Open Laboratory of Transforming Climate Resources to Economy, Chongqing Institute
131 of Meteorological Sciences, Chongqing 401147, China
132 69: Department of Earth System Science, Tsinghua University, Beijing, China
133 70: LOCEAN Laboratory (Sorbonne Université, CNRS, IRD, MNHN), 4 Place Jussieu, F-75005 Paris,
134 France
135 71: Department of Meteorology and National Centre for Atmospheric Science, University of Reading,
136 Reading, UK
137 72: Lamont-Doherty Earth Observatory, Columbia University, New York, NY, USA
138 73: Climate Research Division, Environment and Climate Change Canada, Victoria, BC, Canada
139 74: College of Fisheries and Ocean Sciences, University of Alaska Fairbanks, Fairbanks, Alaska 99775-
140 7220, USA
141 75: Department of Land, Air and Water Resources, University of California, Davis, CA 95616, USA
142 76: Climate Adaptation Research Center, University of California, Davis, CA 95616, USA
143 77: Carbon to Sea Initiative, Washington D.C., USA
144 78: Earth System Division, National Institute for Environmental Studies (NIES), 16-2 Onogawa,
145 Tsukuba Ibaraki, 305-8506, Japan
146 79: NORCE Research, Jahnebakken 5, 5007 Bergen, Norway

147 80: Schiller Institute of Integrated Science and Society, Department of Earth and Environmental
148 Sciences, Boston College, Chestnut Hill, MA 02467, USA
149 81: National Oceanic and Atmospheric Administration, Atlantic Oceanographic & Meteorological
150 Laboratory (NOAA/AOML), 4301 Rickenbacker Causeway, Miami, FL 33149, USA
151 82: School of Atmospheric Sciences, Sun Yat-sen University, Zhuhai 519000, China
152 83: Department of Geoscience, Environment & Society-BGEOSYS, Université Libre de Bruxelles,
153 1050 Brussels, Belgium
154 84: Leibniz Institute for Baltic Sea Research Warnemünde (IOW), Seestrasse 15, 18119 Rostock,
155 Germany
156 85: Princeton University, Department of Geosciences and Princeton Environmental Institute, Princeton,
157 NJ, USA
158 86: Max Planck Institute for Biogeochemistry, P.O. Box 600164, Hans-Knöll-Str. 10, 07745 Jena,
159 Germany
160 87: Canadian Centre for Climate Modelling and Analysis, Environment and Climate Change Canada,
161 Victoria, BC, Canada
162 88: Institute for Climate and Environmental Physics, University of Bern, Bern, Switzerland
163 89: Environnements et Paléoenvironnements Océaniques et Continentaux (EPOC) UMR CNRS 5805
164 EPOC - OASU, Université de Bordeaux, Allée Geoffroy Saint Hilaire, 33615 Pessac, France
165 90: Centre National de Recherches Météorologiques, Université de Toulouse, Météo-France, CNRS,
166 UMR 3589, Toulouse, France
167 91: Research Center for Environmental Modeling and Application, Japan Agency for Marine-Earth
168 Science and Technology, Yokohama, Japan
169 92: Advanced Institute for Marine Ecosystem Change, Japan Agency for Marine-Earth Science and
170 Technology, Yokohama, Japan
171 93: State Key Laboratory of Tibetan Plateau Earth System and Resource Environment, Institute of
172 Tibetan Plateau Research, Chinese Academy of Sciences, Beijing 100101, China
173 94: University of Chinese Academy of Sciences, Beijing 101408, China
174 95: Australian Antarctic Partnership Program, University of Tasmania, Hobart, Australia
175 96: JMA Meteorological Research Institute, Tsukuba, Ibaraki, Japan
176 97: Statistics Division, Food and Agriculture Organization of the United Nations, Via Terme di
177 Caracalla, Rome 00153, Italy
178 98: Earth Sciences New Zealand, Wellington, New Zealand
179 99: Department of Marine Science, University of Otago, Dunedin, New Zealand
180 100: Climate Change Science Institute and Environmental Sciences Division, Oak Ridge National
181 Laboratory, Oak Ridge, TN 37831, USA
182 101: Institute of Carbon Neutrality, College of Urban and Environmental Sciences, Peking University,
183 Beijing 100091, China

184 102: School of Environmental Science and Engineering, Nanjing University of Information Science and
185 Technology (NUIST), Nanjing, 210044, China
186
187 *Correspondence to:* Pierre Friedlingstein (p.friedlingstein@exeter.ac.uk)

188 **Abstract**

189 Accurate assessment of anthropogenic carbon dioxide (CO₂) emissions and their redistribution among
190 the atmosphere, ocean, and terrestrial biosphere in a changing climate is critical to better understand
191 the global carbon cycle, support the development of climate policies, and project future climate
192 change. Here we describe and synthesise datasets and methodologies to quantify the five major
193 components of the global carbon budget and their uncertainties. Fossil CO₂ emissions (E_{FOS}) are based
194 on energy and cement production data. Emissions from land-use change (E_{LUC}) are estimated by
195 bookkeeping models based on land-use data. The global atmospheric CO₂ growth rate (G_{ATM}) is
196 computed from changes in concentration, measured at surface stations. The global net uptake of CO₂
197 by the ocean (S_{OCEAN}) is estimated with global ocean biogeochemistry models and observation-based
198 fCO₂-products. The global net uptake of CO₂ by the land (S_{LAND}) is estimated with dynamic global
199 vegetation models. Additional lines of evidence are provided by atmospheric inversions, atmospheric
200 oxygen measurements, ocean interior observation-based estimates, and Earth System Models. This
201 year, we introduced corrections on the E_{LUC}, S_{OCEAN} and S_{LAND} estimates. The sum of all sources and
202 sinks results in the carbon budget imbalance (B_{IM}), a measure of imperfect data and incomplete
203 understanding of the contemporary carbon cycle. All uncertainties are reported as ±1σ.

204 For the year 2024, E_{FOS} increased by 1.1% relative to 2023, with fossil emissions at 10.3 ± 0.5 GtC yr⁻¹
205 (including the cement carbonation sink, 0.2 GtC yr⁻¹), E_{LUC} was 1.3 ± 0.7 GtC yr⁻¹, for total
206 anthropogenic CO₂ emissions of 11.6 ± 0.9 GtC yr⁻¹ (42.4 ± 3.2 GtCO₂ yr⁻¹). Also, for 2024, G_{ATM} was
207 7.9 ± 0.2 GtC yr⁻¹ (3.73 ± 0.1 ppm yr⁻¹), 2.2 GtC above the 2023 growth rate. S_{OCEAN} was 3.4 ± 0.4
208 GtC yr⁻¹ and S_{LAND} was 1.9 ± 1.1 GtC yr⁻¹, leaving a large negative B_{IM} (-1.7 GtC yr⁻¹), suggesting that
209 the total sink or G_{ATM} is strongly overestimated in 2024. The global atmospheric CO₂ concentration
210 averaged over 2024 reached 422.8 ± 0.1 ppm. Preliminary data for 2025 suggest an increase in E_{FOS}
211 relative to 2024 of +1.0% (0.2% to 1.7%) globally, and atmospheric CO₂ concentration increasing by
212 2.1 ppm reaching 425.6 ppm, 53% above the pre-industrial level (around 278 ppm in 1750). Overall,
213 the mean and trend in the components of the global carbon budget are consistently estimated over the
214 period 1959-2024, with a near-zero overall budget imbalance, although discrepancies of up to around
215 1 GtC yr⁻¹ persist for the representation of annual to decadal variability in CO₂ fluxes. Comparison of
216 estimates from multiple approaches and observations shows: (1) a persistent large uncertainty in the
217 estimate of land-use change emissions, (2) a low agreement between the different methods on the

Deleted: statistics

Deleted: and land-use change

Deleted: Atmospheric CO₂ concentration is measured at surface stations, and the global

Deleted: the annual

Deleted: .

Deleted: , called the ocean sink

Deleted: , called the land sink

Deleted: on land and ocean sinks

Deleted: /

Deleted: 1

Deleted: 2.2

Deleted: 3

Deleted: 7

Deleted: 52

233 magnitude of the land CO₂ flux in the northern extra-tropics, and (3) a discrepancy between the
234 different methods on the mean ocean sink.

235 This living data update documents changes in methods and datasets applied to this most-recent global
236 carbon budget as well as evolving community understanding of the global carbon cycle. The data
237 presented in this work are available at <https://doi.org/10.18160/GCP-2025> (Friedlingstein et al.,
238 2025c).

239

240 Executive Summary

241 **Global fossil CO₂ emissions (including cement carbonation) are expected to further increase in**
242 **2025 by 1.0% relative to 2024** (range 0.2% to 1.7%), bringing fossil emissions to an expected 10.4
243 GtC yr⁻¹ (38.1 GtCO₂ yr⁻¹)¹. Emissions from coal, oil and gas in 2025 are all expected to be above their
244 2024 levels (by 1.0%, 1.1% and 1.3% respectively). These preliminary estimates are based on available
245 data for 2025. Consolidated data confirm a growth of 1.1% in 2024 relative to 2023, with fossil CO₂
246 emissions of 10.3 ± 0.5 GtC yr⁻¹ (37.8 ± 1.8 GtCO₂ yr⁻¹) in 2024.

247 **Regionally, fossil emissions are projected to grow in 2025 in the USA and be nearly flat in the**
248 **European Union, reversing long-term decreases, and also in China and India, albeit more slowly**
249 **compared to recent trends.** The increase in fossil emissions in 2025 relative to 2024 is projected to be
250 0.4% (-0.1% to 0.9%) for China, 2.5% (2.2% to 2.8%) for the United States, 1.1% for India, 2025
251 emissions for the European Union are projected to decrease by -0.1%. Projected emissions in Japan,
252 provided this year for the first time, are for a decrease of -0.9%. Emissions are also projected to
253 increase by 6.7% for international aviation and by 2.0% for international shipping, and to increase by
254 0.9% (-1.0% to 3.0%) for the rest of the world in aggregate. The global carbon intensity of energy has
255 consistently decreased over the past decade (-0.7% yr⁻¹), indicating decarbonisation of the energy
256 system in China (-1.4% yr⁻¹), the European Union (-1.5% yr⁻¹), and the USA (-1.3% yr⁻¹), but no decline
257 in India and an increase in the rest of the world in aggregate. These trends are not sufficient to offset the
258 growth in global energy demand, which is driven by growing GDP globally and a weakening decline in
259 energy per GDP, particularly in China and the US.

260 **Fossil CO₂ emissions decreased (p<0.05) in 35 economies with growing GDP (p<0.05) during the**
261 **decade 2015–2024.** The list of decarbonising economies nearly doubled since the previous decade
262 (2005–2014; 18 countries). These 35 decarbonising economies contribute 2.7 GtC yr⁻¹ (9.7 GtCO₂)
263 fossil fuel CO₂ emissions over the last decade in aggregate, representing 27% of the world CO₂ fossil

Deleted: 1

Deleted: 2.2

Deleted: 0.8%,

Deleted: 9

Deleted: 2.

Deleted: 1.9% (-0

Deleted: 4.1

Deleted: 4% (-0.3% to 3.1%)

Deleted: , and 0.4% (-2.1% to 2.8%)

Deleted: .

Deleted: 2.2% (-8.1% to 3.7%).

Deleted: 8

Deleted: but to remain flat

Deleted: 1% (-1.1

Deleted: 3

Deleted: countries

Deleted: economies

Deleted: countries

Deleted: The

Deleted: countries

¹ All growth rates use a leap year adjustment that corrects for the extra day in 2024.

284 emissions.

285 **Global net CO₂ emissions from land use averaged 1.4 ± 0.7 GtC yr⁻¹ (5.0 ± 2.6 GtCO₂ yr⁻¹) for the**
286 **2015-2024 period.** Emissions from deforestation, the main driver of global gross emissions, remain
287 high at around 1.9 GtC yr⁻¹ over the 2015-2024 period, highlighting the strong potential of halting
288 deforestation for emissions reductions. Sequestration of 1.3 GtC yr⁻¹ through re-/afforestation and forest
289 regrowth in shifting cultivation cycles offsets two third of the deforestation emissions. In addition,
290 smaller net emissions are due to wood harvest & forest management, peat drainage and peat fire.
291 Regionally, the highest net emitters during 2015-2024 were Brazil, Indonesia, and the Democratic
292 Republic of the Congo, with these 3 countries contributing more than half of global land-use CO₂
293 emissions. Net carbon dioxide removals (CDR) from re-/afforestation were highest in China, the USA,
294 and the EU27, with combined removals of 0.3 GtC yr⁻¹ during 2015-2024.

Deleted: /

295 **Since the late-1990s, emissions from land use show a statistically significant decrease at a rate of**
296 **around 0.2 GtC per decade, with a larger drop within the most recent decade. Preliminary data**
297 **for 2025 suggest emissions decreased to around 1.1 GtC (4.1 GtCO₂ yr⁻¹), mainly attributable to**
298 **the end of the El Niño conditions.**

299 **Total anthropogenic emissions (fossil and land use, including the carbonation sink) were 11.6 GtC**
300 **yr⁻¹ (42.4 GtCO₂ yr⁻¹) in 2024, with a slightly lower preliminary estimate of 11.5 GtC yr⁻¹ (42.2**
301 **GtCO₂ yr⁻¹) for 2025.** Total anthropogenic emissions have grown more slowly over the last decade
302 (0.3% yr⁻¹ over the 2015-2024 period) compared to the previous decade (1.9% yr⁻¹ over 2005-2014).

303 **The remaining carbon budget from the beginning of 2026 for a 50% likelihood to limit warming**
304 **to 1.5°C is nearly exhausted (50 GtC, 170 GtCO₂ left, equivalent to around 4 years at the 2025**
305 **emissions levels), consistent with the warming of the planet attributed to human activities, which**
306 **reached 1.36°C in 2024.** Each additional cumulative emission of about 180 GtCO₂ will lead to
307 approximately 0.1°C of warming. The remaining carbon budgets to limit warming to 1.7°C and 2°C
308 above the 1850-1900 level have been reduced to 145 GtC (525 GtCO₂, 12 years) and 290 GtC (1055
309 GtCO₂, 25 years) respectively.

310 **The concentration of CO₂ in the atmosphere is set to reach 425.6 ppm in 2025, 53% above pre-**
311 **industrial levels.** The atmospheric CO₂ growth rate was 5.6 ± 0.02 GtC yr⁻¹ (2.6 ppm) during the
312 decade 2015-2024 (50% of total CO₂ emissions). 2024 had a record-high growth rate of 7.9 ± 0.02 GtC
313 yr⁻¹ (3.7 ppm) mainly due to the 2023/2024 El Niño conditions. The preliminary 2025 growth rate
314 estimate is 4.4 GtC (2.1 ppm).

Deleted: 7

Deleted: 52

Deleted: 9

Deleted: 3

315 **The ocean sink, the global net uptake of CO₂ by the ocean, has taken up 29% of the total**
316 **emissions in the past decade, after being re-evaluated upwards based on new evidence and**
317 **process understanding. The ocean sink has been stagnant since 2016, largely in response to**
318 **climate variability modulating the growing sink trend, but further affected by the ocean heatwave**

324 of 2023-2024 in the Northern Hemisphere. The ocean CO₂ sink was 3.2 ± 0.4 GtC yr⁻¹ during the
325 decade 2015-2024, with a preliminary estimate of 3.2 GtC yr⁻¹ for 2025, slightly below 2024 levels, due
326 to the end of the El Niño conditions in 2024 and associated reduced atmospheric CO₂ growth rate.

327 **The land sink, which is the global net uptake of CO₂ by the land excluding land use, has taken up**
328 **21% of the total emissions in the past decade, after being re-evaluated downwards based on**
329 **improved process representation. The land sink has been relatively stagnant since 2000, largely in**
330 **response to climate variability and climate change offsetting the CO₂ induced growth.** The land
331 CO₂ sink was 2.4 ± 0.8 GtC yr⁻¹ during the 2015-2024 decade, but was reduced to 1.9 GtC ± 0.8 GtC yr⁻¹
332 in 2024. The preliminary estimate for the land sink in 2025 is an increase to 3.1 GtC, recovering
333 entirely from its strong drop during the 2023-2024 El Niño conditions.

334 **The effects of climate change and climate variability act to reduce the land and ocean CO₂ sinks**
335 **by 25% and 7.1% respectively, on average for the 2015-2024 period.** The land sink is negatively
336 affected by warming with decreased tropical plant productivity and enhanced ecosystem respiration
337 globally. The ocean sink is negatively affected by altered oceanic circulation and surface warming
338 which decreases CO₂ solubility.

339 **So far in 2025, global fire CO₂ emissions have been approximately 20% lower than the 2015-2024**
340 **average due to low fire activity in Africa and the tropics, reaching 1.2-1.4 GtC globally during**
341 **January-September.** This contrasts with the above average fire emissions in 2023 (1.7-2.1 GtC yr⁻¹)
342 and 2024 (1.6-2.2 GtC yr⁻¹) due to extensive fires in Canada (2023) and Brazil and Bolivia (2024).
343 These fire emissions estimates should not be directly compared with the land-use emissions or the land
344 sink, because they represent a gross carbon flux to the atmosphere and do not account for post-fire
345 recovery. They also do not distinguish between natural, climate-driven, and land-use-related fires.

346

Deleted: 9

349 1 Introduction

350 The concentration of carbon dioxide (CO₂) in the atmosphere has increased from approximately 278
 351 parts per million (ppm) in 1750 (Gulev et al., 2021), the beginning of the Industrial Era, to 422.8 ± 0.1
 352 ppm in 2024 (Lan et al., 2025; Figure 1). The atmospheric CO₂ increase above pre-industrial levels was,
 353 initially, primarily caused by the release of carbon to the atmosphere from deforestation and other land-
 354 use change activities (Canadell et al., 2021). While emissions from fossil fuels started before the
 355 Industrial Era, they became the dominant source of anthropogenic emissions to the atmosphere from
 356 around 1950 and their relative share has continued to increase until present. Anthropogenic emissions
 357 occur on top of an active natural carbon cycle that circulates carbon between the reservoirs of the
 358 atmosphere, ocean, and terrestrial biosphere on time scales from sub-daily to millennial, while
 359 exchanges with geologic reservoirs occur on longer timescales (Archer et al., 2009).

360 The global carbon budget (GCB) presented here refers to the mean, variations, and trends in the
 361 perturbation of CO₂ in the environment, referenced to the beginning of the Industrial Era (defined here
 362 as 1750). This paper describes the components of the global carbon cycle over the historical period with
 363 a stronger focus on the recent period (since 1959, onset of robust atmospheric CO₂ measurements), the
 364 last decade (2015-2024), the last year (2024) and the current year (2025). Finally, it provides
 365 cumulative emissions from fossil fuels and land-use change since the year 1750, and since the year
 366 1850 (the reference year for historical simulations in IPCC).

367 We quantify the input of CO₂ to the atmosphere by emissions from human activities, the growth rate of
 368 atmospheric CO₂ concentration, and the resulting changes in the storage of carbon in the land and ocean
 369 reservoirs in response to increasing atmospheric CO₂ levels, climate change and variability, and other
 370 anthropogenic and natural changes (Figure 2). An understanding of this perturbation budget over time
 371 and the underlying variability and trends of the natural carbon cycle is necessary to understand the
 372 response of natural sinks to changes in climate, CO₂ and land-use change drivers, and to quantify
 373 emissions compatible with a given climate stabilisation target.

374 The components of the CO₂ budget that are reported annually in this paper include separate and
 375 independent estimates for the CO₂ emissions from (1) fossil fuel combustion and oxidation from all
 376 energy and industrial processes; also including cement production and carbonation (E_{FOS} ; GtC yr⁻¹) and
 377 (2) the emissions resulting from deliberate human activities on land, including those leading to land-use
 378 change (E_{LUC} ; GtC yr⁻¹); and their partitioning among (3) the growth rate of atmospheric CO₂
 379 concentration (G_{ATM} ; GtC yr⁻¹), and the uptake of CO₂ (the 'CO₂ sinks') in (4) the ocean (S_{OCEAN} ; GtC
 380 yr⁻¹) and (5) on land (S_{LAND} ; GtC yr⁻¹). The CO₂ sinks as defined here conceptually include the response
 381 of the land (including inland waters and estuaries) and ocean (including coastal and marginal seas) to

Formatted: Outline numbered + Level: 1 + Numbering
 Style: 1, 2, 3, ... + Start at: 1 + Alignment: Left + Aligned at:
 0 cm + Indent at: 0.76 cm

Deleted: 2025a

383 elevated CO₂ and changes in climate and other environmental conditions, although in practice not all
384 processes are fully accounted for (see Section 2.10). Note that the term sink means that the net transfer
385 of carbon is from the atmosphere to land or the ocean, but it does not imply any permanence of that sink
386 in the future.

387 Global emissions and their partitioning among the atmosphere, ocean and land are in [mass](#) balance in
388 the real world. Due to the combination of imperfect spatial and/or temporal data coverage, errors in
389 each estimate, and smaller terms not included in our budget estimate (discussed in Section 2.10), the
390 [GCB](#) independent estimates (1) to (5) above do not necessarily add up to zero. We hence estimate a
391 budget imbalance (B_{IM}), which is a measure of the mismatch between the estimated emissions and the
392 estimated changes in the atmosphere, land and ocean, as follows:

$$393 \quad B_{IM} = E_{FOS} + E_{LUC} - (G_{ATM} + S_{OCEAN} + S_{LAND}) \quad (1)$$

394 G_{ATM} is usually reported in ppm yr⁻¹, which we convert to units of carbon mass per year, GtC yr⁻¹, using
395 1 ppm = 2.124 GtC (Ballantyne et al., 2012; Table 1). Units of gigatonnes of CO₂ (or billion tonnes of
396 CO₂) used in policy are equal to 3.664 multiplied by the value in units of GtC.

397 We also assess a set of additional lines of evidence derived from global atmospheric inversion system
398 results (Section 2.7), observed changes in oxygen concentration (Section 2.8) and Earth System Models
399 (ESMs) simulations (Section 2.9), all of these methods closing the global carbon balance (zero B_{IM}).

400 We further quantify E_{FOS} and E_{LUC} by country, including both territorial and consumption-based
401 accounting for E_{FOS} (see Section 2), and discuss missing terms from sources other than the combustion
402 of fossil fuels (see Section 2.10). We also assess carbon dioxide removal (CDR) (see Sect. 2.2 and 2.3).
403 Land-based CDR is significant, but already accounted for in E_{LUC} in equation (1) (Sect 3.2.2). Other
404 CDR methods, not based on vegetation, are currently several orders of magnitude smaller than the other
405 components of the budget (Sect. 3.3), hence these are not included in equation (1), or in the global
406 carbon budget tables or figures (with the exception of Figure 2 where CDR is shown primarily for
407 illustrative purpose).

408 The global CO₂ budget has been assessed by the Intergovernmental Panel on Climate Change (IPCC) in
409 all assessment reports (Watson et al., 1990; Schimel et al., 1995; Prentice et al., 2001; Denman et al.,
410 2007; Ciais et al., 2013; Canadell et al., 2021), and by others (e.g. Ballantyne et al., 2012). The Global
411 Carbon Project (GCP, www.globalcarbonproject.org, last access: 23 October 2025) has coordinated this
412 cooperative community effort for the annual publication of global carbon budgets for the year 2005
413 (Raupach et al., 2007; including fossil emissions only), year 2006 (Canadell et al., 2007), year 2007
414 (GCP, 2008), year 2008 (Le Quéré et al., 2009), year 2009 (Friedlingstein et al., 2010), year 2010
415 (Peters et al., 2012a), year 2012 (Le Quéré et al., 2013; Peters et al., 2013), year 2013 (Le Quéré et al.,
416 2014), year 2014 (Le Quéré et al., 2015a; Friedlingstein et al., 2014), year 2015 (Jackson et al., 2016;

417 Le Quéré et al., 2015b), year 2016 (Le Quéré et al., 2016), year 2017 (Le Quéré et al., 2018a; Peters et
418 al., 2017a), year 2018 (Le Quéré et al., 2018b; Jackson et al., 2018), year 2019 (Friedlingstein et al.,
419 2019; Jackson et al., 2019; Peters et al., 2020), year 2020 (Friedlingstein et al., 2020; Le Quéré et al.,
420 2021), year 2021 (Friedlingstein et al., 2022a; Jackson et al., 2022), year 2022 (Friedlingstein et al.,
421 2022b), the year 2023 (Friedlingstein et al., 2023), and most recently the year 2024 (Friedlingstein et
422 al., 2025a). Each of these papers updated previous estimates with the latest available information for the
423 entire time series.

424 We adopt a range of ± 1 standard deviation (σ) to report the uncertainties in our global estimates,
425 representing a likelihood of 68% that the true value will be within the provided range if the errors have
426 a gaussian distribution, and no bias is assumed. Note that when less than 10 individual data are
427 available for an estimate (e.g. atmospheric inversions, f -CO₂ products), we provide the full range, as
428 opposed to the standard deviation. The choice of reporting a $\pm 1 \sigma$ r reflects the difficulty of
429 characterising the uncertainty in the CO₂ fluxes between the atmosphere and the ocean and land
430 reservoirs individually, particularly on an annual basis, as well as the difficulty of updating the CO₂
431 emissions from land-use change. A likelihood of 68% provides an indication of our current capability to
432 quantify each term and its uncertainty given the available information. The uncertainties reported here
433 combine statistical analysis of the underlying data, assessments of uncertainties in the generation of the
434 datasets, and expert judgement of the likelihood of results lying outside this range. The limitations of
435 current information are discussed in the paper and have been examined in detail elsewhere (Ballantyne
436 et al., 2015; Zscheischler et al., 2017). We also use a qualitative assessment of confidence level to
437 characterise the annual estimates from each term based on the type, amount, quality, and consistency of
438 the different lines of evidence as defined by the IPCC (Stocker et al., 2013).

439 This paper provides a detailed description of the datasets and methodology used to compute the global
440 carbon budget estimates for the industrial period, from 1750 to 2025, and in more detail for the recent
441 period since 1959. This paper is updated every year using the format of ‘living data’ to keep a record of
442 budget versions and the changes in new data, revision of data, and changes in methodology that lead to
443 changes in estimates of the carbon budget. All underlying data used to produce the budget and
444 additional materials associated with the release of each new version are available via the Global Carbon
445 Budget website (<https://globalcarbonbudget.org/>, last access: 23 October 2025), with emissions also
446 available through the Global Carbon Atlas (<http://www.globalcarbonatlas.org>, last access: 23 October
447 2025). With this approach, we aim to provide the highest transparency and traceability in the reporting
448 of CO₂, the key driver of climate change.

449 2 Methods

450 Multiple organisations and research groups around the world generated the original measurements and
451 data used to complete the global carbon budget. The effort presented here is thus mainly one of

Deleted: This choice

Formatted: Outline numbered + Level: 1 + Numbering
Style: 1, 2, 3, ... + Start at: 1 + Alignment: Left + Aligned at:
0 cm + Indent at: 0.76 cm

453 synthesis, where results from individual groups are collated, analysed, and evaluated for consistency.
454 We facilitate access to original data with the understanding that primary datasets will be referenced in
455 future work (see Table 2 for how to cite the datasets, and Section on data availability). Descriptions of
456 the measurements, models, and methodologies follow below, with more detailed descriptions of each
457 component provided as Supplementary Information (Supplement Tables S1 to S5). [In the GCB, when
458 possible, we account for adjustments and corrections to the components estimates. We refer to
459 ‘adjustments’ when accounting for known processes not included in one estimate \(ex. river
460 correction for fCO₂ products\), while we refer to ‘corrections’ when addressing know biases in
461 one estimate \(ex. replaced sinks and sources for DGVMs\).](#)

Formatted: Font: 11 pt

462 This is the 20th version of the global carbon budget and the 14th revised version in the format of a living
463 data update in Earth System Science Data. It builds on the latest published global carbon budget of
464 Friedlingstein et al. (2025a). The main changes this year are: the inclusion of (1) data to year 2024 and
465 a projection for the global carbon budget for year 2025; (2) transient carbon densities in the estimate of
466 ELUC, (3) a correction on SLAND to account for the historical changes in forest cover, (4) a correction on
467 SOCEAN to account for the underestimation of the sink by GOBMs and for the ocean temperature
468 gradients in the fCO₂-products estimate, (5) an estimate of the atmospheric CO₂ growth rate derived
469 from satellite observations, and (6) decadal estimates of change in the dissolved inorganic carbon
470 inventory in the interior ocean. Other methodological differences are summarised in Table 3 and
471 previous changes since 2006 are provided in Table [S10](#).

Deleted: S9

472 2.1 Fossil CO₂ emissions (E_{FOS})

Formatted: Outline numbered + Level: 2 + Numbering
Style: 1, 2, 3, ... + Start at: 1 + Alignment: Left + Aligned at:
0 cm + Indent at: 1.02 cm

473 2.1.1 Historical period 1850-2024

Formatted: Outline numbered + Level: 3 + Numbering
Style: 1, 2, 3, ... + Start at: 1 + Alignment: Left + Aligned at:
0 cm + Indent at: 1.27 cm

474 The estimates of global and national fossil CO₂ emissions (E_{FOS}) include the oxidation of fossil fuels
475 through both combustion (e.g., transport, heating) and chemical oxidation (e.g. carbon anode
476 decomposition in aluminium refining) activities, and the decomposition of carbonates in industrial
477 processes (e.g. the production of cement). We also include CO₂ uptake from the cement carbonation
478 process. Several emissions sources are not estimated or not fully covered: coverage of emissions from
479 lime production are not global, and decomposition of carbonates in glass and ceramic production are
480 included only for the “Annex 1” countries of the United Nations Framework Convention on Climate
481 Change (UNFCCC) for lack of activity data. These omissions are considered to be minor. Short-cycle
482 carbon emissions - for example from combustion of biomass - are not included here but are accounted
483 for in the CO₂ emissions from land use (see Section 2.2).

484 Our estimates of fossil CO₂ emissions rely on data collection by many other parties. Our goal is to
485 produce the best estimate of this flux, and we therefore use a prioritisation framework to combine data
486 from different sources that have used different methods, while being careful to avoid double counting

488 and undercounting of emissions sources. The CDIAC-FF emissions dataset, derived largely from UN
489 energy data, forms the foundation, and we extend emissions to 2024 using energy growth rates reported
490 by the Energy Institute (a dataset formerly produced by BP). We then proceed to replace estimates
491 using data from what we consider to be superior sources, for example Annex 1 countries' official
492 submissions to the UNFCCC. All data points are potentially subject to revision, not just the latest year.
493 For full details see Andrew and Peters (2025).

494 Other estimates of global fossil CO₂ emissions exist, and these are compared by Andrew (2020a). The
495 most common reason for differences in estimates of global fossil CO₂ emissions is a difference in which
496 emissions sources are included in the datasets. Datasets such as those published by the Energy Institute,
497 the US Energy Information Administration, and the International Energy Agency's 'CO₂ emissions
498 from fuel combustion' are all generally limited to emissions from combustion of fossil fuels. In
499 contrast, datasets such as PRIMAP-hist, CEDS, EDGAR, and GCP's dataset aim to include all sources
500 of fossil CO₂ emissions. See Andrew (2020a) for detailed comparisons and discussion.

501 Cement products absorb CO₂ from the atmosphere over their lifetimes, a process known as 'cement
502 carbonation'. We estimate this CO₂ sink, from 1931 onwards, as the average of two studies in the
503 literature (Cao et al., 2020; Guo et al., 2021). Both studies use the same model, developed by Xi et al.
504 (2016), with different parameterisations and input data, with the estimate of Guo and colleagues being a
505 revision of Xi et al. (2016). The trends of the two studies are very similar. Since carbonation is a
506 function of both current and previous cement production, we extend these estimates to 2024 by using
507 the growth rate derived from the smoothed cement emissions (10-year smoothing) fitted to the
508 carbonation data. In the present budget, we always include the cement carbonation carbon sink in the
509 fossil CO₂ emission component (E_{FOS}) unless explicitly stated otherwise.

510 We use the Kaya Identity for a simple decomposition of CO₂ emissions into the key drivers (Raupach et
511 al., 2007). While there are variants (Peters et al., 2017b), we focus here on a decomposition of CO₂
512 emissions into population, GDP per person, energy use per GDP, and CO₂ emissions per energy.
513 Multiplying these individual components together returns the CO₂ emissions. Using the decomposition,
514 it is possible to attribute the change in CO₂ emissions to the change in each of the drivers. This method
515 gives a first-order understanding of what causes CO₂ emissions to change each year.

516 2.1.2 2025 projection

517 We provide a projection of global fossil CO₂ emissions in 2025 by combining separate projections for
518 China, USA, EU, India, Japan, and for all other countries combined. The methods are different for each
519 of these. [For China we use growth rates from the 2026 edition of the National Bureau of Statistics'](#)
520 [Statistical Communique along with cement clinker trade data and estimated changes in lime production.](#)
521 For the USA our projection is taken directly from the Energy Information Administration's (EIA)

Formatted: Outline numbered + Level: 3 + Numbering
Style: 1, 2, 3, ... + Start at: 1 + Alignment: Left + Aligned at:
0 cm + Indent at: 1.27 cm

Deleted: For China we combine monthly fossil fuel
production data from the National Bureau of Statistics and
trade data from the Customs Administration, giving us partial
data for the growth rates to date of natural gas, petroleum,
and cement, and of the apparent consumption itself for raw
coal. We then use a regression model to project full-year
emissions based on historical observations.

529 Short-Term Energy Outlook (EIA, 2026), combined with the year-to-date growth rate of cement clinker
 530 production. For the EU we use monthly energy data from Eurostat to derive estimates of monthly CO₂
 531 emissions [through December](#) (Andrew, 2021). EU cement emissions are based on available [production](#)
 532 data [through December](#) from three of the largest producers, Germany, Poland, and Spain, [as well as](#)
 533 [production indices for Italy and France](#). India's projected emissions are derived from monthly estimates
 534 through [December](#) using the methods of Andrew (2020b). Japan's emissions are based on monthly
 535 estimates through [December](#). Emissions from international transportation (bunkers) are estimated
 536 separately for aviation and shipping. Changes in aviation emissions are derived primarily from OECD
 537 monthly estimates, extrapolated using the growth rates of global flight miles from [Airports](#), [Shipping](#)
 538 [emissions are derived from estimates of sales of bunker fuels provided by Ship and Bunker \(Ship and](#)
 539 [Bunker, 2026\)](#). Emissions for the rest of the world are derived for coal and cement using projected
 540 growth in economic production from the IMF (2025) combined with extrapolated changes in emissions
 541 intensity of economic production; for oil using a global constraint from EIA; and for natural gas using a
 542 global constraint from IEA. More details on the E_{FOS} methodology and its 2025 projection can be found
 543 in Supplement S.1.

544 We compare our 2025 projection with the Carbon Monitor (2025). Carbon Monitor is a dataset of daily
 545 emissions constructed using hourly to daily proxy data (e.g., electricity consumption, travel patterns,
 546 etc) instead of energy use data (Liu et al., 2020a; Liu et al., 2020b). [Emissions estimates from January](#)
 547 [to December are combined to give a full-year 2025 estimate.](#)

548 **2.2 CO₂ emissions from land-use, land-use change and forestry (E_{LUC})**

549 **2.2.1 Historical period 1850-2024**

550 The net CO₂ flux from land-use, land-use change and forestry (E_{LUC}, called land-use change emissions
 551 in the rest of the text) includes CO₂ fluxes from deforestation, afforestation, logging and forest
 552 degradation (including harvest activity), shifting cultivation (cycle of cutting forest for agriculture, then
 553 abandoning), regrowth of forests (following wood harvest or agriculture abandonment), peat burning,
 554 and peat drainage.

555 Updated estimates from three bookkeeping models are used to quantify gross emissions, gross removals
 556 and the resulting net E_{LUC}: BLUE (Hansis et al., 2015), LUCE (Qin et al. 2024), and OSCAR (Gasser et
 557 al., 2020). [An important improvement compared](#) to previous GCBs [is the use of transient carbon](#)
 558 [densities by all three bookkeeping models](#), i.e., they consider the effects of environmental changes, such
 559 as atmospheric CO₂ increase, on vegetation and soil carbon densities, to estimate E_{LUC} (Gasser et al.,
 560 2020; Dorgeist et al., 2024). The GCB assessments have for a long time also (and initially exclusively)
 561 used estimates from the bookkeeping model H&C2023 (Houghton and Castanho, 2023), its predecessor
 562 H&N2017 (Houghton and Nassikas, 2017), and earlier versions. However, H&C2023 does not consider

Deleted: 2025

Deleted:), with (i) coal emissions extended using a statistical relationship with reported electricity generation from coal and other factors, (ii) natural gas emissions extended using Holt-Winters, and (iii) oil emissions extended using a regression relationship between our monthly estimates and the EIA's estimates of oil consumption for Europe, which include a forecast....

Deleted: year-to-date

Deleted: .

Deleted: August/September

Deleted:) and extrapolated through December assuming seasonal patterns from before 2019.

Deleted: also projected

Deleted: July and normal seasonal patterns

Deleted: , and then the final months are projected assuming normal patterns from previous years. Shipping emissions are assumed to be unchanged in 2025, based on available sub-annual evidence from multiple sources.

Deleted: Emissions estimates from January to August are combined to a new projection for September-December to give a full-year 2025 estimate. The projections are estimated by leveraging seasonal patterns from 2019-2024 daily CO₂ emission data from Carbon Monitor. A regression model is applied separately for individual countries to obtain their respective forecast. First, the seasonality component for each month is assessed based on daily average emissions from 2019 to 2023, excluding 2020 due to the COVID-19 pandemic. Then, a linear regression model is constructed using the calculated seasonal components and the daily average emissions for the months from January to August 2025. The resulting model is used to project carbon emissions for September-December 2025. The uncertainty range is calculated by using historical monthly variance of seasonal components (See Supplement S.1.5).

Formatted: Outline numbered + Level: 2 + Numbering Style: 1, 2, 3, ... + Start at: 1 + Alignment: Left + Aligned at: 0 cm + Indent at: 1.02 cm

Formatted: Outline numbered + Level: 3 + Numbering Style: 1, 2, 3, ... + Start at: 1 + Alignment: Left + Aligned at: 0 cm + Indent at: 1.27 cm

Deleted: Different

Deleted: , all three bookkeeping models

600 transient carbon densities and only provides data up to 2020, which implies the need to extrapolate its
601 data to the time after 2020. As the model does thus not incorporate the most recent developments in
602 bookkeeping modeling, it is not used anymore in GCB2025.

603 Emissions from peat burning and peat drainage are added from external datasets (see Supplement
604 S.2.2): peat fire emissions from the Global Fire Emission Database (GFED4s; van der Werf et al.,
605 2017) and peat drainage emissions averaged from estimates of the Food Agriculture Organization
606 (Conchedda and Tubiello, 2020; FAO, 2025a) and from simulations with the DGVM ORCHIDEE-
607 PEAT (Qiu et al., 2021) and the DGVM LPX-Bern (Lienert and Joos, 2018; Müller and Joos, 2021).

608 Uncertainty estimates were derived from the Dynamic Global Vegetation Models (DGVMs) ensemble
609 for the time period prior to 1960, and using for the recent decades an uncertainty range of $\pm 0.7 \text{ GtC yr}^{-1}$,
610 which is a semi-quantitative measure for annual and decadal emissions and reflects our best value
611 judgement that there is at least 68% chance ($\pm 1\sigma$) that the true land-use change emission lies within the
612 given range, for the range of processes considered here.

613 The GCB E_{LUC} estimates follow the CO_2 flux definition of global carbon cycle models and differ from
614 IPCC definitions adopted in National GHG Inventories (NGHGI) for reporting under the UNFCCC.
615 The latter typically include terrestrial fluxes occurring on all land that countries define as managed,
616 following the IPCC managed land proxy approach (Grassi et al., 2018). This partly includes fluxes due
617 to environmental change (e.g. atmospheric CO_2 increase), which are part of S_{LAND} in our definition. As
618 a result, global emission estimates are smaller for NGHGI than for the global carbon budget definition
619 (Grassi et al., 2023). The same is the case for the FAO estimates of carbon fluxes on forest land, which
620 include both anthropogenic and natural fluxes on managed land (Tubiello et al., 2025; FAO, 2025b).
621 Using the NGHGI data collected and processed in the LULUCF data hub V3.1 (Melo et al. 2025), we
622 translate the GCB and NGHGI definitions to each other, to provide a comparison of the anthropogenic
623 carbon budget as reported in GCB to the official country reporting to the UNFCCC convention. We
624 further compare these estimates with the net atmosphere-to-land flux from atmospheric inversion
625 systems (see Section 2.7), averaged over managed land only.

626 E_{LUC} contains a range of fluxes that are related to Carbon Dioxide Removal (CDR). CDR is defined as
627 the set of anthropogenic activities that remove CO_2 from the atmosphere, in addition to the Earth's
628 natural processes (such as carbon uptake in response to atmospheric CO_2 increase), and store it in
629 durable form, such as in forest biomass, soils, long-lived products, oceans or geological reservoirs.
630 Here, we quantify vegetation-based CDR that is implicitly or explicitly captured by land-use fluxes
631 (CDR not based on vegetation is discussed in Section 2.3). We quantify CDR through re/afforestation
632 from the three bookkeeping estimates by separating permanent increases in forest cover, which counts
633 as CDR, from forest regrowth in shifting cultivation cycles (not part of CDR; see Supplement S.2.2). It
634 should be noted that the permanence of the storage under climate risks such as fire is increasingly

635 questioned. Other CDR activities related to land use but not fully accounted for in our E_{LUC} estimate
636 include the transfer of carbon to harvested wood products (HWP), bioenergy with carbon capture and
637 storage (BECCS), and biochar production (Babiker et al., 2022; Smith et al., 2024). The different
638 bookkeeping models all represent HWP but with varying details concerning product usage and their
639 lifetimes. BECCS and biochar are currently only represented in bookkeeping and DGVM models with
640 regard to the CO_2 removal through photosynthesis, without accounting for the durable storage. HWP,
641 BECCS, and biochar are typically counted as CDR once the transfer to the durable storage site occurs
642 and not when the CO_2 is removed from the atmosphere, which complicates a direct comparison to the
643 GCB approach to quantify annual fluxes to and from the atmosphere. We provide estimates for CDR
644 through HWP, BECCS, and biochar based on independent studies in Section 3.2.2. HWP and BECCS
645 estimates reflect updated 2024 data of the State of CDR report (Smith et al., 2024), while biochar
646 estimates correspond to 2023 due to unavailability of newer data. We do not add them to our E_{LUC}
647 estimate to avoid potential double-counting that arises from the partial consideration of HWP, BECCS,
648 and biochar in the bookkeeping and DGVM models and to avoid inconsistencies from the temporal
649 discrepancy between transfer to storage and removal from the atmosphere. More details on the E_{LUC}
650 methodology can be found in Supplement S.2.

651 2.2.2 2025 Projection

652 We project the 2025 land-use emissions for BLUE, OSCAR, and LUCE based on their E_{LUC} estimates
653 for 2023 and adding the anomalies in carbon emissions from peat fires in equatorial Asia and tropical
654 deforestation and degradation fires (2025 emissions relative to 2023 emissions) from GFED4s (van der
655 Werf et al., 2017) estimated using active fire data (MCD14ML; Giglio et al., 2016). 2023 is used as
656 base year since the E_{LUC} estimate for the year 2024 is informed by extrapolated land-use data
657 (Supplement S.2.1). Peat drainage is assumed to be unaltered as it has low interannual variability.

658 2.3 Carbon Dioxide Removal (CDR) not based on vegetation

659 Some CDR involves CO_2 fluxes via land use, which is included in our estimate of E_{LUC}
660 (re/afforestation) or provided separately in Section 3.2.2 (biochar, HWP, and BECCS). Other CDR
661 occurs through CO_2 fluxes directly from the air to the geosphere, which is reported in Section 3.3. The
662 majority of this derives from bio-oil storage in geological reservoirs, enhanced weathering through the
663 application of crushed rock to soils, and the production of solid mineral products with CO_2 captured
664 from the atmosphere, with smaller contributions from Direct Air Carbon Capture and Storage
665 (DACCS), sinking of terrestrial (e.g., straw) or marine (e.g., macroalgae) biomass into the deep ocean
666 through human intervention, and others like intentional ocean or river alkalinity enhancement. For these
667 methods, we use updated 2024 data (Smith et al., 2024), which compiles and harmonises reported CDR
668 from a combination of existing databases, surveys, and novel research. Currently, there are no
669 internationally agreed methods for reporting these types of CDR, implying that estimates are based on

Formatted: Outline numbered + Level: 3 + Numbering
Style: 1, 2, 3, ... + Start at: 1 + Alignment: Left + Aligned at:
0 cm + Indent at: 1.27 cm

Formatted: Outline numbered + Level: 2 + Numbering
Style: 1, 2, 3, ... + Start at: 1 + Alignment: Left + Aligned at:
0 cm + Indent at: 1.02 cm

670 self-disclosure by projects following their own protocols or protocols produced by third party registries.
671 As such, the fractional uncertainty on these numbers should be viewed as substantial, and numbers are
672 liable to change in future years as protocols are harmonised and improved.

673 2.4 Growth rate in atmospheric CO₂ concentration (G_{ATM})

674 2.4.1 Historical period 1850-2024

675 The rate of growth of the atmospheric CO₂ concentration is provided for years 1959-2024 by the US
676 National Oceanic and Atmospheric Administration Global Monitoring Laboratory (NOAA/GML; Lan
677 et al., 2025), which includes recent revisions to the calibration scale of atmospheric CO₂ measurements
678 (WMO-CO₂-X2019; Hall et al., 2021). For the 1959-1979 period, the global growth rate is based on
679 measurements of atmospheric CO₂ concentration averaged from the Mauna Loa and South Pole
680 stations, as observed by the CO₂ Program at Scripps Institution of Oceanography (SIO, Keeling et al.,
681 1976). For the 1980-2024 time period, the global growth rate is based on the average of multiple
682 stations selected from the marine boundary layer sites with well-mixed background air (Lan et al.,
683 2024), after fitting a smooth curve through the data for each station as a function of time, and averaging
684 by latitude band (Masarie and Tans, 1995). The annual growth rate is estimated by Lan et al. (2025)
685 from atmospheric CO₂ concentration by taking the average of the most recent December-January
686 months corrected for the average seasonal cycle and subtracting this same average one year earlier. To
687 obtain G_{ATM}, the observation-based growth rate in units of ppm yr⁻¹ is converted to units of GtC yr⁻¹ by
688 multiplying by a factor of 2.124 GtC per ppm, assuming instantaneous mixing of CO₂ throughout the
689 atmosphere (Ballantyne et al., 2012; Table 1). There is high confidence in the observations because
690 they are based on direct measurements from stations distributed around the world (Lan et al., 2024)
691 with all CO₂ measurements consistently measured against the same CO₂ standard scale (WMO X2019)
692 defined by a suite of gas standards (Hall et al., 2021). However, the conversion to estimates of G_{ATM} in
693 GtC_{yr}⁻¹ incurs large uncertainty on annual time scale as discussed next.

694 The uncertainty around G_{ATM} is due to three main factors. First, the network composition of the marine
695 boundary layer sites with some sites coming or going, gaps in the time series at each site, etc. This
696 uncertainty was estimated with a bootstrap method by constructing 100 "alternative" networks (Steele
697 et al., 1992; Masarie and Tans, 1995; Lan et al., 2025). Second, the analytical uncertainty that describes
698 the short- and long-term uncertainties associated with the CO₂ analyzers. A Monte Carlo method was
699 used to estimate the total analytical uncertainty by randomly selecting errors to add to each observation
700 from a normal distribution of combined short- and long-term uncertainties. Prior to the 1980s when
701 analyzers were less precise and CO₂ measurement scale was slightly less well defined, larger analytical
702 errors were assigned to account for these factors. However, the network uncertainty remains the larger
703 term of uncertainty. The first and second uncertainties are reported as 1-sigma standard deviations (i.e.,
704 68% confidence interval), and summed in quadrature to determine the global surface growth rate

Formatted: Outline numbered + Level: 2 + Numbering
Style: 1, 2, 3, ... + Start at: 1 + Alignment: Left + Aligned at:
0 cm + Indent at: 1.02 cm

Formatted: Outline numbered + Level: 3 + Numbering
Style: 1, 2, 3, ... + Start at: 1 + Alignment: Left + Aligned at:
0 cm + Indent at: 1.27 cm

Deleted: 2025a

Deleted: 2025a

Deleted: /

Deleted: 2025a

709 uncertainty, which averaged to 0.085 ppm (Lan et al., 2024). Third, the uncertainty associated with
710 using the average CO₂ concentration from a surface network to approximate the true atmospheric
711 average CO₂ concentration (mass-weighted, in 3 dimensions) as needed to assess the total atmospheric
712 CO₂ burden. In reality, CO₂ variations measured at the stations will not exactly track changes in total
713 atmospheric burden, with offsets in magnitude and phasing due to vertical and horizontal mixing
714 (Pandey et al., 2025). This effect must be very small on decadal and longer time scales, when the
715 atmosphere can be considered well mixed. The long-term CO₂ increase in the stratosphere lags the
716 increase (meaning lower concentrations) that we observe in the marine boundary layer, while the
717 continental boundary layer (where most of the emissions take place) leads the marine boundary layer
718 with higher concentrations. These effects nearly cancel each other on decadal time scales, when the
719 growth rate is nearly the same everywhere (Ballantyne et al., 2012). We therefore maintain an
720 uncertainty around the annual growth rate based on the multiple stations dataset ranges between 0.11
721 and 0.72 GtC yr⁻¹, with a mean of 0.61 GtC yr⁻¹ for 1959-1979 and 0.17 GtC yr⁻¹ for 1980-2024, when
722 more measurement sites were available (Lan et al., 2025). We estimate the uncertainty of the decadal
723 averaged growth rate after 1980 at 0.02 GtC yr⁻¹ based on the annual growth rate uncertainty but
724 stretched over a 10-year interval. For years prior to 1980, we estimate the decadal averaged uncertainty
725 to be 0.07 GtC yr⁻¹ based on a factor proportional to the annual uncertainty prior and after 1980 (0.02 *
726 [0.61/0.17] GtC yr⁻¹).

Deleted: 2024b

727 To estimate the total carbon accumulated in the atmosphere since 1750 or 1850, we use an atmospheric
728 CO₂ concentration of 278.0 ± 3 ppm or 287.7 ± 3 ppm, respectively (Gulev et al., 2021). For the
729 construction of the historical budget shown in Figure 3, we use the fitted estimates of CO₂
730 concentration from Joos and Spahni (2008) to estimate the annual atmospheric growth rate (see
731 Supplement S.7). The uncertainty of ±3 ppm (converted to ±1σ) is taken directly from the IPCC's AR5
732 assessment (Ciais et al., 2013). Typical uncertainties in the growth rate in atmospheric CO₂
733 concentration from ice core data are equivalent to ±0.1-0.15 GtC yr⁻¹ as evaluated from the Law Dome
734 data (Etheridge et al., 1996) for individual 20-year intervals over the period from 1850 to 1960 (Bruno
735 and Joos, 1997).

Deleted: 3

Deleted: 285.1

736 2.4.2 Satellite-based (2015-present)

737 Further opportunities to estimate global CO₂ growth rates are offered by space-based platforms such as
738 GOSAT (since 2010) and OCO-2 (since 2015). Their recorded short-wave infrared spectra allow
739 retrieval of column CO₂ abundances (XCO₂) over cloud-free scenes over land and ocean with footprints
740 of 80 (GOSAT) and 3 (OCO-2) km² respectively. The columns are not full integrals; the sensitivity to
741 surface and lower-tropospheric CO₂ mole fractions is much higher than to upper tropospheric and
742 stratospheric CO₂. However, for the purpose of calculating atmospheric growth rates, the sensitivity is
743 not limiting, as the pressure-weighted sensitivity is still above 0.5 in the stratosphere (Pandey et al.

Formatted: Outline numbered + Level: 3 + Numbering
Style: 1, 2, 3, ... + Start at: 1 + Alignment: Left + Aligned at:
0 cm + Indent at: 1.27 cm

748 2024) and priors used in OCO-2 account for the slow stratospheric-tropospheric exchanges using the
749 age of air (Laughner et al. 2023). Here, we use OCO-2 based whole atmosphere growth rates using the
750 Growth Rate from Satellite Observations (GRESO) approach (Pandey et al., 2024). We specifically
751 note that their retrievals are evaluated against surface-based remote sensing (Total Column Carbon
752 Observing Network) data, which in turn are tied to atmospheric observations (from aircraft and using
753 aircore) (Wunch et al., 2017). Furthermore, OCO-2 retrievals use a priori CO₂ mole fraction profiles
754 tied to NOAA GML in-situ flask records at Mauna Loa (MLO) and American Samoa (SMO)
755 measurement stations (Laughner et al., 2023). For details on evaluation, bias-correction, and
756 spatiotemporal coverage of OCO-2 we refer to O'Dell et al (2018).

757 Relative to surface observations, the GRESO product typically reflects tropical growth rate anomalies
758 earlier, and sees whole atmosphere carbon stock changes with a lower latency. The GRESO growth
759 rates presented here use both land and ocean observations of OCO-2 providing global sampling of the
760 atmosphere. We used GRESO post 2015 to present an alternative quantification of the atmospheric
761 carbon stock changes in G_{ATM}, using the reported 1-sigma uncertainty of 0.08 ppm_{yr}⁻¹. The mean
762 differences between GRESO and surface-data derived G_{ATM} is 0.05±0.26 ppm_{yr}⁻¹ over the 2015-2024
763 (n=10 years) period.

764 2.4.3 2025 projection

765 We provide an assessment of G_{ATM} for 2025 as the average of two methods. First, the GCB regression
766 method models monthly global-average atmospheric CO₂ concentrations and derives the increment and
767 annual average from these. The model uses lagged observations of concentration (Lan et al., 2025):
768 both a 12-month lag, and the lowest lag that will allow model prediction to produce an estimate for the
769 following January, recalling that the G_{ATM} increment is derived from December/January pairs. The
770 largest driver of interannual changes is the ENSO signal (Betts et al., 2016), so the monthly ENSO 3.4
771 index (Huang et al., 2023) is included in the model. Given the natural lag between sea-surface
772 temperatures and effects on the biosphere, and in turn effects on globally mixed atmospheric CO₂
773 concentration, a lagged ENSO index is used, and we use both a 5-month and a 6-month lag. The
774 combination of the two lagged ENSO values helps reduce possible effects of noise in a single month.
775 To help characterise the seasonal variation, we add month as a categorical variable. Finally, we flag the
776 period affected by the Pinatubo eruption (August 1991 - November 1993) as a categorical variable.

777 The second method uses the multi-model mean and uncertainty of the 2025 G_{ATM} estimated by the
778 ESMS prediction system (see Section 2.9). We then take the average of the GCB regression and ESMS
779 G_{ATM} estimates, with their respective uncertainty combined quadratically.

780 Similarly, the projection of the 2025 global average CO₂ concentration (in ppm), is calculated as the
781 average of the estimates from the two methods. For the GCB regression method, it is the annual average

Deleted: ,

Deleted: /

Deleted: /

Formatted: Outline numbered + Level: 3 + Numbering Style: 1, 2, 3, ... + Start at: 1 + Alignment: Left + Aligned at: 0 cm + Indent at: 1.27 cm

Deleted: 2025a

786 of global concentration over the 12 months of 2025; for the ESMs, it is the observed global average
787 CO₂ concentration for 2024 plus the annual increase in 2025 of the global average CO₂ concentration,
788 which is an average of NOAA/GML measurements from January to June (Lan et al., 2025) and
789 predictions of the ESMs multi-model mean from July to December (see Section 2.9).

790 2.5 Ocean CO₂ sink

791 2.5.1 Historical period 1850-2024

792 The reported estimate of the global ocean anthropogenic CO₂ sink S_{OCEAN} is derived as the average of
793 two estimates. The first estimate is derived as the mean over an ensemble of ten global ocean
794 biogeochemistry models (GOBMs, Table 4 and Table S2). The second estimate is obtained as the mean
795 over an ensemble of nine surface ocean fCO_2 -observation-based data-products (Table 4 and Table S3).

796 The GOBMs simulate both the natural and anthropogenic CO₂ cycles in the ocean. They constrain the
797 anthropogenic air-sea CO₂ flux (the dominant component of S_{OCEAN}) by the transport of carbon into the
798 ocean interior, which is also the controlling factor of present-day ocean carbon uptake in the real world.
799 They cover the full globe and all seasons and were evaluated against surface ocean carbon observations,
800 suggesting they are suitable to estimate the annual ocean carbon sink (Hauck et al., 2020). We derive
801 S_{OCEAN} from GOBMs by using a simulation (sim A) with historical forcing of climate and atmospheric
802 CO₂ from GCB (Section 2.4), accounting for model biases and drift from a control simulation (sim B)
803 with constant atmospheric CO₂ and normal year climate forcing. A third simulation (sim C) with
804 historical atmospheric CO₂ increase and normal year climate forcing is used to attribute the ocean sink
805 to CO₂ (sim C minus sim B) and climate (sim A minus sim C) effects. A fourth simulation (sim D;
806 historical climate forcing and constant atmospheric CO₂) is used to compare the change in
807 anthropogenic carbon inventory in the interior ocean (sim A minus sim D) to the observation-based
808 estimates of Gruber et al. (2019) and Müller et al. (2023) with the same flux components (steady state
809 and non-steady state anthropogenic carbon flux).

810 As there is accumulating evidence for a 10-20% underestimation of S_{OCEAN} by the GOBMs based on
811 ocean interior data (section 3.6.5), atmospheric oxygen (section 3.6.2), atmospheric inversions (section
812 3.8) and supported by eddy-covariance measurements (Dong et al., 2024), we scale up the global
813 GOBM multi-model mean estimates by 10% when estimating S_{OCEAN} (Friedlingstein et al., 2025b) (see
814 Supplement S3.3). Analysis of Earth System Models and GOBMs indicate that an underestimation by
815 about 10% may be due to biases in ocean carbon transport and mixing from the surface mixed layer to
816 the ocean interior (Goris et al., 2018, Terhaar et al., 2021, Bourgeois et al., 2022, Terhaar et al., 2022),
817 biases in the chemical buffer capacity (Revelle factor) of the ocean (Vaittinada Ayar et al., 2022;
818 Terhaar et al., 2022) and partly due to a late starting date of the simulations (mirrored in atmospheric
819 CO₂ chosen for the pre-industrial control simulation, Table S2, Bronselaer et al., 2017, Terhaar et al.,

Formatted: Outline numbered + Level: 2 + Numbering
Style: 1, 2, 3, ... + Start at: 1 + Alignment: Left + Aligned at:
0 cm + Indent at: 1.02 cm

Formatted: Outline numbered + Level: 3 + Numbering
Style: 1, 2, 3, ... + Start at: 1 + Alignment: Left + Aligned at:
0 cm + Indent at: 1.27 cm

Deleted: for

821 2022; 2024). GOBMs are evaluated against key metrics and their capability to reproduce various
822 statistical measures of physical and biogeochemical fields using the International Ocean Model
823 Benchmarking (IOMB) Scheme (Fu et al., 2022, Text S3.3).

824 The $f\text{CO}_2$ -products are tightly linked to observations of $f\text{CO}_2$ (fugacity of CO_2 , which equals $p\text{CO}_2$
825 corrected for the non-ideal behaviour of the gas; Pfeil et al., 2013), which carry imprints of temporal
826 and spatial variability, but are also sensitive to uncertainties in gas-exchange parameterizations and
827 data-sparsity (Fay et al., 2021, Gloege et al., 2021, Hauck et al., 2023a). Their asset is the assessment of
828 the mean spatial pattern of variability and its seasonality (Hauck et al., 2020, Gloege et al. 2021, Hauck
829 et al., 2023a). To benchmark biases and trends derived from the $f\text{CO}_2$ -products, we update a model
830 subsampling exercise following Hauck et al. (2023a, see section S3) and use independent measurements
831 from the SOCAT (Surface Ocean CO_2 Atlas) flag E dataset (uncertainty less than $10 \mu\text{atm}$) (Bakker et
832 al., 2016) and calculated $f\text{CO}_2$ from the Global Ocean Data Analysis Project GLODAP (Lauvset et al.,
833 2024). New in GCB2025, we now also include the UExp-FNN-U product in the ensemble mean, which
834 was previously shown but not included. We include it since new evidence emerged from field and
835 modelling studies, recommending ~~to adopt a temperature correction to the $f\text{CO}_2$ from measurement~~
836 ~~depth~~ to the surface skin layer where the gas exchange takes place (Dong et al., 2024, Ford et al.,
837 ~~2024a~~, Bellenger et al., 2022). Furthermore, a second $f\text{CO}_2$ -product submitted temperature ~~corrected~~
838 $f\text{CO}_2$ (JMA-MLR) this year, so we now include these corrected estimates in the ensemble mean.
839 Additionally, following Friedlingstein et al (2025b), we now also add 0.18 PgC yr^{-1} (multiplied by 7/9
840 as two products already include a temperature correction) to the multi $f\text{CO}_2$ -product average ~~when~~
841 ~~calculating~~ So_{OCEAN} to account for the warm layer and cool skin effect (See Supplement S3.1). This
842 correction is based on a recent field study (Ford et al., ~~2024a~~) and broadly consistent in magnitude with
843 a GOBM study (Bellenger et al 2022) .

Deleted: the adjustment of

Deleted: 2024

Deleted: adjusted

Deleted: in the calculation of

Formatted: Subscript

Deleted: 2024

844 The global $f\text{CO}_2$ -based flux estimates were adjusted to remove the pre-industrial natural ocean source of
845 CO_2 to the atmosphere of $0.65 \pm 0.3 \text{ GtC yr}^{-1}$, arising from the transfer of carbon from land to ocean via
846 rivers (Regnier et al., 2022), to satisfy our definition of So_{OCEAN} (Hauck et al., 2020). This CO_2
847 outgassing adjustment was distributed over the latitudinal bands using the regional distribution of
848 Lacroix et al. (2020; North: 0.14 GtC yr^{-1} , Tropics: 0.42 GtC yr^{-1} , South: 0.09 GtC yr^{-1}).
849 Acknowledging that this distribution is based on only one model, the advantage is that a gridded field is
850 available, and the adjustment can be calculated for the three latitudinal bands and the RECCAP regions
851 (REgional Carbon Cycle Assessment and Processes (RECCAP2; Ciais et al., 2020, Poulter et al., 2022,
852 DeVries et al., 2023). This dataset suggests that more of the river-induced outgassing is located in the
853 tropics than in the Southern Ocean and is thus opposed to the previously used dataset of Aumont et al.
854 (2001). Accordingly, the regional distribution is associated with an additional uncertainty in addition to
855 the large uncertainty around the global estimate (Crisp et al., 2022; Gruber et al., 2023). Anthropogenic
856 perturbations of river carbon and nutrient transport to the ocean are not represented in the process

862 models used to quantify S_{OCEAN} , but an a-posteriori correction is applied to the global S_{OCEAN} estimate
863 (see Section 2.10 and Supplement S.8.3). We calculate S_{OCEAN} as the average of the GOBM ensemble
864 mean and the fCO_2 -product ensemble mean from 1990 onwards, [including the corrections on the](#)
865 [GOBM and \$fCO_2\$ -product ensemble means as described above](#). For the 1959-1989 period, it is
866 calculated as the GOBM ensemble mean plus half of the offset between GOBMs and fCO_2 -products
867 ensemble means over 1990-2001, [also including the above corrections](#). In addition, two diagnostic
868 ocean models are used to estimate S_{OCEAN} over the industrial era (1781-1958, Khatiwala et al. (2013)
869 and DeVries (2014)).

Deleted: .

Deleted: .

870 S_{OCEAN} is evaluated against the change in the total dissolved inorganic carbon inventory in the interior
871 ocean from the observation-based estimates of Keppler et al. [\(2023\)](#) with the same flux components.

Deleted: (2023) and Ehmen et al. (2025, in review)

872 We assign an uncertainty of $\pm 0.4 \text{ GtC yr}^{-1}$ to the ocean sink based on a combination of random
873 (ensemble standard deviation) and systematic uncertainties (GOBMs bias in anthropogenic carbon
874 accumulation, previously reported uncertainties in fCO_2 -products; see Supplement S.3.4). While this
875 approach is consistent within the GCB, an independent uncertainty assessment of the fCO_2 -products
876 alone suggests a somewhat larger uncertainty of up to 0.7 GtC yr^{-1} (Ford et al. 2024). We assess a
877 medium confidence level to the annual ocean CO_2 sink and its uncertainty because it is based on
878 multiple lines of evidence, it is consistent with ocean interior carbon estimates (see Section 3.6.5) and
879 the interannual variability in the GOBMs and data-based estimates is largely consistent and can be
880 explained by climate variability. We refrain from assigning a high confidence because of the deviation
881 between the GOBM and fCO_2 -product trends between around 2002 and 2020 and the higher S_{OCEAN}
882 estimate from $O_2:N_2$ (section 2.8). More details on the S_{OCEAN} methodology can be found in Supplement
883 S.3.

884 2.5.2 2025 Projection

Formatted: Outline numbered + Level: 3 + Numbering Style: 1, 2, 3, ... + Start at: 1 + Alignment: Left + Aligned at: 0 cm + Indent at: 1.27 cm

Deleted: 2025a

885 The S_{OCEAN} forecast for the year 2025 is based on (a) the historical (Lan et al. [2025](#)) and our 2025
886 estimate of atmospheric CO_2 concentration, (b) the historical and our 2025 estimate of global fossil
887 emissions, and (c) the boreal spring (March, April, May) Oceanic Niño Index (ONI) (NCEP, 2025).
888 Using a non-linear regression approach, i.e., a feed-forward neural network, atmospheric CO_2 , ONI, and
889 the fossil emissions are used as training data to best match [the corrected](#) S_{OCEAN} from 1959 through
890 2024 from this year's carbon budget. Using this relationship, the 2025 S_{OCEAN} can then be estimated
891 from the projected 2025 input data using the non-linear relationship established during the network
892 training. To avoid overfitting, the neural network training was done using a Monte Carlo approach, with
893 a variable number of artificial neurons (varying between 2-5) and 20% of the randomly selected
894 training data were withheld for independent internal testing.

899 Based on the best output performance (tested using the 20% withheld input data), the best performing
900 number of neurons was selected. In a second step, we trained the network 10 times using the best
901 number of neurons identified in step 1 and different sets of randomly selected training data. The mean
902 of the 10 trainings is considered our best forecast, whereas the standard deviation of the 10 ensembles
903 provides a first order estimate of the forecast uncertainty. This uncertainty is then combined with the
904 SOCEAN uncertainty (0.4 GtC yr⁻¹) to estimate the overall uncertainty of the 2025 projection. As an
905 additional line of evidence, we also assess the 2025 atmosphere-ocean carbon flux from the ESM
906 prediction system (see Section 2.9).

907 2.6 Land CO₂ sink

908 2.6.1 Historical Period 1850-2024

909 The terrestrial land sink (S_{LAND}) is thought to be due to the combined effects of rising atmospheric CO₂,
910 increasing N inputs, and climate change, on plant growth and terrestrial carbon storage. S_{LAND} does not
911 include land sinks directly resulting from land-use and land-use change (e.g., regrowth of vegetation) as
912 these are part of the land-use change emissions (E_{LUC}), although system boundaries make it difficult to
913 attribute exactly CO₂ fluxes on land between S_{LAND} and E_{LUC} (Erb et al., 2013).

914 S_{LAND} is [derived](#) from the multi-model mean of 22 DGVMs (Table 4 and Table S1). DGVMs
915 simulations include all climate variability and CO₂ effects over land. In addition to the carbon cycle
916 represented in all DGVMs, 15 models also account for the nitrogen cycle and hence can include the
917 effect of N inputs on S_{LAND}. The DGVMs estimates of S_{LAND} do not explicitly include the export of
918 carbon to aquatic systems or its historical perturbation, which is discussed in Supplement S.8.3.
919 DGVMs need to meet several criteria to be included in this assessment (see Supplement S.4.2). In
920 addition, we use the International Land Model Benchmarking system (ILAMB; Collier et al., 2018) for
921 the DGVMs evaluation (see Supplement S.4.2), with an additional comparison of DGVMs with a data-
922 informed, Bayesian model-data fusion framework (CARDAMOM) (Bloom and Williams, 2015; Bloom
923 et al., 2016). The uncertainty on S_{LAND} is taken from the DGVMs standard deviation.

924 New to GCB2025 is a correction applied to the S_{LAND} [estimate](#) to account for its overestimation
925 resulting from the assumption of pre-industrial land-use in the DGVM simulations, when in reality a
926 large portion of the land surface has been converted to pasture and cropland, with a lower sink capacity.
927 This bias is termed the Replaced Sinks and Sources (RSS) (Gitz and Ciais, 2003; Sitch et al., 2005,
928 Pongratz et al., 2009; Gasser et al., 2021; Obermeier et al. 2021; Dorgeist et al., 2024). The correction
929 [which is only](#) applied [when estimating the global](#) S_{LAND}, utilises results from a subset of DGVMs that
930 were able to supply Net Biome Productivity estimates at a Plant Functional Type basis combined with
931 time-varying PFT area fractions from the simulation with land use and land use change considered
932 (O'Sullivan et al., 2025; Friedlingstein et al. 2025b), see S.4.1 for details on methodology. [The](#)

Formatted: Outline numbered + Level: 2 + Numbering
Style: 1, 2, 3, ... + Start at: 1 + Alignment: Left + Aligned at:
0 cm + Indent at: 1.02 cm

Formatted: Outline numbered + Level: 3 + Numbering
Style: 1, 2, 3, ... + Start at: 1 + Alignment: Left + Aligned at:
0 cm + Indent at: 1.27 cm

Deleted: estimated

Deleted: on

935 [corrected](#) S_{LAND} is reduced by 19% globally when accounting for the RSS. More details on the S_{LAND}
936 methodology can be found in Supplement S.4.

937 **2.6.2 2025 Projection**

938 In previous versions of the GCB, the land sink projection was similar to the ocean sink forecast, based
939 on a non-linear regression approach with a feed-forward neural network. This approach, however,
940 resulted in a large uncertainty and underestimated the land sink variability in the past. This year, we
941 update the projection and simply calculate the land sink for 2025 as the residual of the projection of the
942 other components of the carbon cycle ($S_{LAND}=E_{FOS}+E_{LUC}-G_{ATM}-S_{OCEAN}$). [Hence, by construction the](#)
943 [2025 \$B_{IM}\$ is set to zero.](#)

944

945 **2.7 Atmospheric inversion estimate**

946 The world-wide network of in-situ atmospheric measurements and satellite derived atmospheric CO_2
947 column (XCO_2) observations put a strong constraint on changes in the atmospheric abundance of CO_2 .
948 This allows atmospheric inversion methods to constrain the magnitude and location of the combined
949 total surface CO_2 fluxes from all sources, including fossil and land-use change emissions and land and
950 ocean CO_2 fluxes. The inversions assume E_{FOS} to be well known, and they solve for the spatial and
951 temporal distribution of land and ocean fluxes from the residual gradients of CO_2 between stations that
952 are not explained by fossil fuel emissions. By design, such systems thus close the carbon balance ($B_{IM} =$
953 0) and provide an additional perspective on the independent estimates of the ocean and land fluxes.

954 This year's release includes fourteen inversion systems that are described in Table S4. Each system is
955 rooted in Bayesian inversion principles but uses different methodologies. These differences concern the
956 selection of atmospheric CO_2 data or XCO_2 , and the choice of a-priori fluxes to refine. They also differ
957 in spatial and temporal resolution, assumed correlation structures, and mathematical approach of the
958 models (see references in Table S4 for details). Importantly, the systems use a variety of transport
959 models, which was demonstrated to be a driving factor behind differences in atmospheric inversion-
960 based flux estimates, and specifically their distribution across latitudinal bands (Gaubert et al., 2019;
961 Schuh et al., 2019). Six inversion systems used surface observations from the global measurement
962 network (Schuldt et al., 2024, 2025). Eight inversion systems used satellite XCO_2 retrievals from
963 GOSAT and/or OCO-2, scaled to the WMO 2019 calibration scale, of which three inversions this year
964 used these XCO_2 datasets in addition to the in-situ observational CO_2 mole fraction records.

965 The original products delivered by the inverse modellers were modified to facilitate the comparison to
966 the other elements of the budget, specifically on two accounts: (1) global total fossil emissions
967 including cement carbonation CO_2 uptake, and (2) riverine CO_2 transport. We note that with these

Formatted: Outline numbered + Level: 3 + Numbering
Style: 1, 2, 3, ... + Start at: 1 + Alignment: Left + Aligned at:
0 cm + Indent at: 1.27 cm

Formatted: Outline numbered + Level: 2 + Numbering
Style: 1, 2, 3, ... + Start at: 1 + Alignment: Left + Aligned at:
0 cm + Indent at: 1.02 cm

968 adjustments the inverse results no longer represent the net atmosphere-surface exchange over
969 land/ocean areas as sensed by atmospheric observations. Instead, for land, they become the net uptake
970 of CO₂ by vegetation and soils that is not exported by fluvial systems, similar to the DGVMs estimates.
971 For oceans, they become the net uptake of anthropogenic CO₂, similar to the GOBMs estimates.

972 The inversion systems prescribe global fossil emissions based on e.g. the GCP's Gridded Fossil
973 Emissions Dataset versions 2025.1 (GCP-GridFED; Jones et al., 2025), which are updates to GCP-
974 GridFEDv2021 presented by Jones et al. (2021b). GCP-GridFEDv2025.1 scales gridded estimates of
975 CO₂ emissions from EDGARv4.3.2 (Janssens-Maenhout et al., 2019) within national territories to
976 match national emissions estimates provided by the GCB for the years 1959-2024, which were
977 compiled following the methodology described in Section 2.1. Small differences between the systems
978 due to for instance regridding to the transport model resolution, or use of different fossil fuel emissions
979 than GCP-GridFEDv2025.1, are adjusted in the latitudinal partitioning we present, to ensure agreement
980 with the estimate of E_{FOS} in this budget. We also note that the ocean fluxes used as prior by 8 out of 14
981 inversions are part of the suite of the ocean process model or fCO₂-products listed in Section 2.5.
982 Although these fluxes are further adjusted by the atmospheric inversions (except for Jena CarboScope),
983 it makes the inversion estimates of the ocean fluxes not completely independent of S_{OCEAN} assessed
984 here.

985 To facilitate comparisons to the independent S_{OCEAN} and S_{LAND}, we used the same adjustments for
986 transport and outgassing of carbon transported from land to ocean, as done for the observation-based
987 estimates of S_{OCEAN} (see Supplement S.5.1).

988 The atmospheric inversions are evaluated using vertical profiles of atmospheric CO₂ concentrations
989 (Figure S13). More than 50 aircraft programs over the globe, either regular programs or repeated
990 surveys over at least 9 months (except for SH programs), have been used to assess system performance
991 (with space-time observational coverage sparse in the SH and tropics, and denser in NH mid-latitudes;
992 Table S9). The fourteen systems are compared to the independent aircraft CO₂ measurements between 2
993 and 7 km above sea level between 2001 and 2024. Results are shown in Figure S13 and discussed in
994 Supplement S.5.2.

995 We note that as of GCB2025, the ensemble of inverse models covering a full decade is deemed
996 sufficiently large to report the 1-sigma standard deviation as uncertainty, following the convention of
997 the other components in GCB. More details on the atmospheric inversion methodology can be found in
998 Supplement S.5.

999 2.8 Atmospheric oxygen based estimate

1000 Long-term atmospheric O₂ and CO₂ observations allow estimation of the global ocean and land carbon
1001 sinks, due to the coupling of O₂ and CO₂ with distinct exchange ratios for fossil fuel emissions and land

Deleted: S8

Formatted: Outline numbered + Level: 2 + Numbering
Style: 1, 2, 3, ... + Start at: 1 + Alignment: Left + Aligned at:
0 cm + Indent at: 1.02 cm

uptake, and uncoupled O₂ and CO₂ ocean exchange (Keeling and Manning, 2014). The global ocean and net land carbon sinks were calculated following methods and constants used in Keeling and Manning (2014) but modified to also include the effective O₂ source from metal refining (Battle et al., 2023). For the exchange ratio of the net land sink at value of 1.05 is used, following Resplandy et al. (2019). For fossil fuels, the following values are used: gas: 1.95 (+/-) 0.04, liquid: 1.44, (+/-) 0.03, solid: 1.17 (+/-) 0.03, cement: 0 (+/-) 0, gas flaring: 1.98 (+/-) 0.07 (Keeling, 1988). Atmospheric O₂ is observed as δ(O₂/N₂) and combined with CO₂ mole fraction observations into Atmospheric Potential Oxygen (APO, Stephens et al., 1998). The APO observations from 1990 to 2024 were taken from a weighted average of flask records from three stations in the Scripps O₂ program network (Alert, Canada (ALT), La Jolla, California (LJO), and Cape Grim, Australia (CGO), weighted per Keeling and Manning (2014). Observed CO₂ was taken from the globally averaged marine surface annual mean growth rate from the NOAA/GML Global Greenhouse Gas Reference Network (Lan et al., 2025). The O₂ source from ocean warming is based on ocean heat content from updated data from NOAA/NCEI (Levitus et al., 2012). The effective O₂ source from metal refining is based on production data from Bray (2020), Flanagan (2021), and Tuck (2022). Uncertainty was determined through a Monte Carlo approach with 20,000 iterations, using uncertainties prescribed in Keeling and Manning (2014), including observational uncertainties from Keeling et al. (2007) and autoregressive errors in fossil fuel emissions (Ballantyne et al., 2015). The reported uncertainty is 1 standard deviation of the ensemble. As for the atmospheric inversions, the O₂ based estimates also closes the carbon balance (B_{IM} = 0) by design and provides another independent estimate of the ocean and land fluxes. Note that the O₂ method requires a correction for global air-sea O₂ flux, which has the largest uncertainty at annual time scales, but which is still non-negligible for decadal estimates (Nevison et al., 2008).

Deleted: 2025a

2.9 Earth System Models estimate

Reconstructions and predictions from decadal prediction systems based on Earth system models (ESMs) provide a novel line of evidence in assessing the atmosphere-land and atmosphere-ocean carbon fluxes in the past decades and predicting their changes for the current year and years to come. By assimilating physical atmospheric and oceanic data products into the ESMs, the models are able to reproduce the historical variations of the atmosphere-sea CO₂ fluxes, atmosphere-land CO₂ fluxes, and atmospheric CO₂ growth rate (Li et al., 2016, 2019; Lovenduski et al., 2019a,b; Ilyina et al., 2021; Li et al., 2023). Furthermore, the ESM-based predictions have proven their skill in predicting the air-sea CO₂ fluxes for up to 6 years, the air-land CO₂ fluxes and atmospheric CO₂ growth for 2 years (Lovenduski et al., 2019a,b; Ilyina et al., 2021; Li et al., 2023). The reconstructions from the fully coupled model simulations ensure a closed budget within the Earth system, i.e., no budget imbalance term.

Six ESMs have performed the set of prediction simulations. The ensemble size of initialized prediction simulations is 10, and the ensemble mean for each individual model is used here. Each ESM uses a

Formatted: Outline numbered + Level: 2 + Numbering Style: 1, 2, 3, ... + Start at: 1 + Alignment: Left + Aligned at: 0 cm + Indent at: 1.02 cm

1039 different assimilation method and combination of data products incorporated in the system, more details
1040 on the models configuration can be found in Table 4 and Supplement Table S5. Reconstructions of
1041 atmosphere-ocean CO₂ fluxes (S_{ocean}) and atmosphere-land CO₂ fluxes (S_{land-ELUC}) for the time period
1042 from 1960-2024 are assessed here. Predictions of the atmosphere-ocean CO₂ flux, atmosphere-land CO₂
1043 flux, and atmospheric CO₂ growth for 2025 are calculated based on the predictions at lead year 1. The
1044 predictions of atmosphere-ocean CO₂ flux and atmosphere-land CO₂ flux are bias corrected by removing
1045 the climatological mean and linear trend biases from 1981-2021 referring to GCB2022 (Friedlingstein et
1046 al., 2022), the atmospheric CO₂ growth (G_{atm}) is then calculated as the residual of the CO₂ emissions
1047 subtracting the carbon sinks into the ocean and the land. With the ESMs simulations, we also compute
1048 the G_{atm} in another way based on monthly atmospheric CO₂ concentrations at 1000hPa level over the
1049 oceans to be comparable to the NOAA/GML global measurements of atmospheric CO₂ concentrations
1050 (Lan et al., 2025). The bias correction is done referring to NOAA/GML monthly CO₂ concentrations in
1051 recent 10 years from 2015-2024 regarding mean state and linear trend, a shorter period is used because a
1052 non-linear trend for the whole period is observed from both NOAA/GML measurements and model
1053 simulations. The 2025 G_{atm} is then calculated by the increment of atmospheric CO₂ concentration in
1054 December 2025 minus that in December 2024 multiplied by 2.124 to convert the unit from ppm to GtC.
1055 The prediction of 2025 atmospheric CO₂ concentration is an average of the available NOAA/GML
1056 measurements from January to June (Lan et al., 2025) and ESMs' predictions from July to December.
1057 Note that the two methods, i.e., one based on the residual of carbon sources and sinks and another based
1058 on atmospheric concentration increment, of calculation of G_{atm} result in different magnitudes, which
1059 suggests the consideration of variable ratio rather than a constant value in converting CO₂ concentration
1060 to mass. More details on methods of bias correction of decadal predictions can be found in Kharin et al.
1061 (2012), Boer et al. (2016) and Li et al. (2023). The ESMs are used here to support the assessment of
1062 S_{ocean} and net atmosphere-land CO₂ flux (S_{land - ELUC}) over the 1960-2024 period, and to provide an
1063 estimate of the 2025 prediction of G_{atm} and atmospheric CO₂ concentration.

Deleted: 2025a

1064 2.10 Processes not fully included in the global carbon budget

1065 The contribution of anthropogenic CO and CH₄ to the global carbon budget is not fully accounted for in
1066 Eq. (1) and is described in Supplement S.8.1. The contributions to CO₂ emissions of decomposition of
1067 carbonates not accounted for is described in Supplement S.8.2. The contribution of anthropogenic
1068 changes in river fluxes is conceptually included in Eq. (1) in S_{ocean} and in S_{land}, but it is not
1069 represented in the process models used to quantify these fluxes. However, a correction of -0.07 GtC_{yr}⁻¹
1070 is applied a posteriori to the S_{land} estimate for the 2015-2024 period, as proposed in Friedlingstein et
1071 al. (2025b). This effect is discussed in Supplement S.8.3. Similarly, the Replaced Sinks and Sources
1072 effect from reduced forest cover over the historical period is missing from the DGVMs used here to
1073 estimate S_{land}. However, a correction (-19%) is applied a posteriori to the S_{land} estimate from
1074 DGVMs, based on O'Sullivan et al. (2025; see Section 2.6 and Supplement S.4.1).

Formatted: Outline numbered + Level: 2 + Numbering
Style: 1, 2, 3, ... + Start at: 1 + Alignment: Left + Aligned at:
0 cm + Indent at: 1.02 cm

Deleted: /

1077 **3 Results**

1078 For each component of the global carbon budget, we present results for three different time periods: the
1079 full historical period, from 1850 to 2024, the decades in which we have atmospheric concentration
1080 records from Mauna Loa (1959-2024), a specific focus on last year (2024), and the projection for the
1081 current year (2025). Subsequently, we assess the estimates of the budget components of the last decades
1082 against the top-down constraints from inverse modelling of atmospheric observations and the
1083 land/ocean partitioning derived from the atmospheric O₂ measurements. Atmospheric inversions further
1084 allow for an assessment of the budget components with a regional breakdown of land and ocean sinks.
1085

Formatted: Indent: Left: 0 cm, First line: 0 cm, Outline numbered + Level: 1 + Numbering Style: 1, 2, 3, ... + Start at: 1 + Alignment: Left + Aligned at: 0 cm + Indent at: 0.76 cm

1086 **3.1 Fossil CO₂ Emissions**

1087 **3.1.1 Historical period 1850-2024**

1088 Cumulative fossil CO₂ emissions for 1850-2024 were 495 ± 25 GtC, including the cement carbonation
1089 sink (Table 8, with all cumulative numbers rounded to the nearest 5GtC). In this period, 46% of global
1090 fossil CO₂ emissions came from coal, 35% from oil, 15% from natural gas, 3% from decomposition of
1091 carbonates for cement production, and 1% from flaring. In 1850, the UK stood for 62% of global fossil
1092 CO₂ emissions. In 1893 the combined cumulative emissions of the current members of the European
1093 Union reached and subsequently surpassed the level of the UK. Since 1917 US cumulative emissions
1094 have been the largest. Over the entire period 1850-2024, US cumulative emissions amounted to 120
1095 GtC (24% of world total), the EU's to 80 GtC (16%), China's to 80 GtC (15%), and India's to 18 GtC
1096 (4%).

Formatted: Outline numbered + Level: 2 + Numbering Style: 1, 2, 3, ... + Start at: 1 + Alignment: Left + Aligned at: 0 cm + Indent at: 1.02 cm

Formatted: Outline numbered + Level: 3 + Numbering Style: 1, 2, 3, ... + Start at: 1 + Alignment: Left + Aligned at: 0 cm + Indent at: 1.27 cm

1097 In addition to the estimates of fossil CO₂ emissions that we provide here (see Section 2.1), there are
1098 three global datasets with long time series that include all sources of fossil CO₂ emissions: CDIAC-FF
1099 (Erb and Marland, 2025), CEDS version 2024_07_08 (Hoesly et al., 2024) and PRIMAP-hist version
1100 2.6 (Gütschow et al., 2016; Gütschow et al., 2024), although these datasets are not entirely independent
1101 from each other (Andrew, 2020a). CEDS has cumulative emissions over 1750-2022 at 480 GtC,
1102 CDIAC-FF has 481 GtC, GCP 484 GtC, PRIMAP-hist CR 490 GtC, and PRIMAP-hist TR 492 GtC.
1103 CDIAC-FF excludes emissions from lime production. CEDS estimates higher emissions from
1104 international shipping in recent years, while PRIMAP-hist has higher fugitive emissions than the other
1105 datasets. However, in general these four datasets are in relative agreement as to total historical global
1106 emissions of fossil CO₂.

1107 **3.1.2 Recent period 1959-2024**

1108 Global fossil CO₂ emissions, E_{FOS} (including the cement carbonation sink), have increased every decade
1109 from an average of 3.0 ± 0.2 GtC yr⁻¹ for the decade of the 1960s to an average of 9.8 ± 0.5 GtC yr⁻¹

Formatted: Outline numbered + Level: 3 + Numbering Style: 1, 2, 3, ... + Start at: 1 + Alignment: Left + Aligned at: 0 cm + Indent at: 1.27 cm

1110 during 2015-2024 (Table 7, Figure 2 and Figure 4). The growth rate in these emissions decreased
 1111 between the 1960s and the 1990s, from 4.3% yr⁻¹ in the 1960s (1960-1969), 3.1% yr⁻¹ in the 1970s
 1112 (1970-1979), 1.5% yr⁻¹ in the 1980s (1980-1989), to 1.0% yr⁻¹ in the 1990s (1990-1999). After this
 1113 period, the growth rate began increasing again in the 2000s at an average growth rate of 2.8% yr⁻¹,
 1114 decreasing to 1.2% yr⁻¹ in the 2010s, and 0.8% yr⁻¹ for the last decade (2015-2024). China's emissions
 1115 increased by 2.5% yr⁻¹ on average over the last 10 years dominating the global trend, and India's
 1116 emissions increased by 3.6% yr⁻¹, while emissions decreased in EU27 (-2.5% yr⁻¹), and in the USA (-
 1117 1.2% yr⁻¹) (Figure 5a). Figure 6 illustrates the spatial distribution of fossil fuel emissions for the 2015-
 1118 2024 period.

1119 E_{FOS} reported here includes the uptake of CO₂ by cement via carbonation which has increased with
 1120 increasing stocks of cement products, from an average of 20 MtC yr⁻¹ (0.02 GtC yr⁻¹) in the 1960s to an
 1121 average of 210MtC yr⁻¹ (0.21 GtC yr⁻¹) during 2015-2024 (Figure 5b).

1122 3.1.3 Final year 2024

1123 Global fossil CO₂ emissions were slightly higher, 1.1%, in 2024 than in 2023, with an increase of 0.11
 1124 GtC to reach 10.3 ± 0.5 GtC (including the 0.22 GtC cement carbonation sink) in 2024 (Figure 4),
 1125 distributed among coal (41%), oil (32%), natural gas (21%), cement (4%), flaring (1%), and others
 1126 (1%). Compared to 2023, the 2024 emissions from coal, oil, and gas increased by 0.8%, 1.3%, and
 1127 2.4% respectively, while emissions from cement decreased by 4.6%. All annual growth rates presented
 1128 are adjusted for the leap year, unless stated otherwise.

1129 In 2024, the largest absolute contributions to global fossil CO₂ emissions were from China (32%), the
 1130 USA (13%), India (8%), and the EU27 (6%). These four regions account for 59% of global fossil CO₂
 1131 emissions, while the rest of the world contributed 41%, including international aviation and marine
 1132 bunker fuels (3% of the total). Growth rates for these countries from 2023 to 2024 were 0.7% (China), -
 1133 0.6% (USA), -2.6% (EU27), and 4.0% (India), with +1.3% for the rest of the world, including
 1134 international aviation and marine bunker fuels (9.8%). The per-capita fossil CO₂ emissions in 2024
 1135 were 1.3 tC person⁻¹ yr⁻¹ for the globe, and were 3.9 (USA), 2.4 (China), 1.5 (EU27) and 0.6 (India) tC
 1136 person⁻¹ yr⁻¹ for the four highest emitters (Figure 5c).

1137 3.1.4 Year 2025 Projection

1138 Globally, we estimate that global fossil CO₂ emissions (including cement carbonation, -0.21 GtC) grew
 1139 by 1.0% in 2025 (0.2% to 1.7%) to 10.4 GtC (38.1 GtCO₂), an historical record high². The estimates of
 1140 changes in 2025 emissions per fuel types, relative to 2024, are projected to be 1.0% (range 0.2% to

² Growth rates in this section use a leap year adjustment that corrects for the extra day in 2024.

Deleted: +

Deleted: +

Deleted: by

Deleted: ,

Deleted: by

Formatted: Outline numbered + Level: 3 + Numbering
 Style: 1, 2, 3, ... + Start at: 1 + Alignment: Left + Aligned at:
 0 cm + Indent at: 1.27 cm

Deleted: +

Deleted: +

Deleted: (+

Formatted: Outline numbered + Level: 3 + Numbering
 Style: 1, 2, 3, ... + Start at: 1 + Alignment: Left + Aligned at:
 0 cm + Indent at: 1.27 cm

Deleted: will grow

Deleted: 1

Deleted: +2.2

Deleted: .8

Deleted: -

Deleted: 1

155 1.7% for coal, 1.1% (range 0.7% to 1.5%) for oil, 1.3% (range 0.1% to 2.4%) for natural gas, and -
156 0.9% (range -2.5% to 0.8%) for cement (Figure 5b).

Deleted: 9...% for coal, +...0...% (range 0.3...% to 1.8...%) for oil, +...3% (range 0.0...% to 2.5...%) for natural gas, and -0.5...% (range -1...5% to 2.6...8%) for cement (Figure 5b). (... [1])

157 The uncertainty presented for projections relates only to the estimated growth rate, and excludes the
158 uncertainty of the baseline (i.e. 2024) level. Given that our projection is effectively of what the data will
159 show when observations are first available, the uncertainty drops to zero for any country where we
160 already have data reported for all of 2025. This is the case below for both India and Japan, and also for
161 Carbon Monitor's estimates of growth in 2025, since they report data through December 2025.

162 For China, projected fossil emissions in 2025 are expected to have increased slightly by 0.4% (range -
163 0.1% to 0.9%) compared with 2024 emissions, bringing 2024 emissions for China around 3.4 GtC yr⁻¹
164 (12.3 GtCO₂ yr⁻¹). Our projected changes by fuel for China are 0.3% for coal, 3.8% for oil, 2.3% for
165 natural gas, and -7.3% for cement.

Deleted: increase...ave increased slightly by 0.4% (range -0.1% to 0.9% to 2.0...) compared with 2024 emissions, bringing 2024 emissions for China around 3.4 GtC yr⁻¹ (12.3 GtCO₂ yr⁻¹). Our projected changes by fuel for China are +...3% for coal, +2.1...8% for oil, +1...3% for natural gas, and -2.8 (... [2])

166 For the USA, using the Energy Information Administration (EIA) emissions estimate for 2025
167 combined with cement clinker data from USGS, we estimate an increase of 2.5% (range 2.2% to 2.8%)
168 compared to 2024, bringing USA 2025 emissions to around 1.4 GtC yr⁻¹ (5.0 GtCO₂ yr⁻¹). Our
169 estimated changes by fuel are 10.4% for coal, 1.1% for oil, 1.4% for natural gas, and -3.1% for cement.

Deleted: projection...estimate for 2025 combined with cement clinker data from USGS, we project...estimate an increase of 1.9...5% (range -0...2% to 4.1...8%) compared to 2024, bringing USA 2025 emissions to around 1.4 GtC yr⁻¹ (5.0 GtCO₂ yr⁻¹). Our projected...estimated changes by fuel are 7.5...0.4% for coal, 1.1% for oil, +...1...% for natural gas, and -8.0... (... [3])

170 For India, our estimate for 2025 is an increase of 1.1% over 2024, with 2025 emissions around 0.9 GtC
171 yr⁻¹ (3.2 GtCO₂ yr⁻¹). Our projected changes by fuel are 1.3% for coal, -0.5% for oil, -5.7% for natural
172 gas, and 10.5% for cement.

Deleted: projection...estimate for 2025 is an increase of 1.4% (range of -0.3% to 3.1%)...% over 2024, with 2025 emissions around 0.9 GtC yr⁻¹ (3.2 GtCO₂ yr⁻¹). Our projected changes by fuel are +...7...% for coal, +...0.1...% for oil, -6.4...7% for natural gas, and +9.9 (... [4])

173 For the European Union, our projection for 2025 is for a decrease of -0.1% (range -2.6% to 2.3%)
174 relative to 2024, with 2025 emissions around 0.7 GtC yr⁻¹ (2.4 GtCO₂ yr⁻¹). Our projected changes by
175 fuel are -2.6% for coal, -0.7% for oil, 2.8% for natural gas, and -0.8% for cement.

Deleted: an increase... decrease of -0.4...% (range -2.1...% to 2.8...%) relative to 2024, with 2025 emissions around 0.7 GtC yr⁻¹ (2.4 GtCO₂ yr⁻¹). Our projected changes by fuel are -0.3% for coal, 0...6% for coal, -0.7% for oil, +0.9...8% for natural gas, and -4.1 (... [5])

176 New this year, we provide a projection for Japan, with a 2025 decrease of 0.9%, with 2025 emissions
177 around 0.3 GtC yr⁻¹ (0.9 GtCO₂ yr⁻¹). Our projected changes by fuel are -0.7% for coal, -0.8% for oil, -
178 1.2% for natural gas, and -2.9% for cement.

Deleted: 2.2% (range of -8.1% to +3.7%),...9%, with 2025 emissions around 0.3 GtC yr⁻¹ (0.9 GtCO₂ yr⁻¹). Our projected changes by fuel are -3.1...7% for coal, -0.8% for oil, -1.2.7... for natural gas, and -3.0 (... [6])

179 International aviation and shipping are expected to have increased by 4.3% in 2025, reaching 0.3 GtC
180 yr⁻¹ (1.2 GtCO₂ yr⁻¹), with international aviation and international shipping projected to be respectively
181 6.7% and 2.0% over 2024. For the rest of the world, the expected change for 2025 is an increase of
182 0.9% (range -1.1% to 3.0%) with 2025 emissions around 3.7 GtC yr⁻¹ (13.7 GtCO₂ yr⁻¹). The fuel-
183 specific projected 2025 growth rates for the rest of the world are: 1.3% for coal, 0.3% for oil, 1.2% for
184 natural gas, 2.6% for cement.

Deleted: projected...pected to increase...ave increased by 4.3.7... in 2025, reaching 0.3 GtC yr⁻¹ (1.2 GtCO₂ yr⁻¹), with international aviation projected to be up 6.8% over 2024, and international shipping projected to be flat (0%)...espectively 6.7% and 2.0% over 2024. For the rest of the world, the expected change for 2025 is an increase of 0.9% (range -1.1.1% (range -1.1... to 3.3...%) with 2025 emissions around 3.7 GtC yr⁻¹ (13.7 GtCO₂ yr⁻¹). The fuel-specific projected 2025 growth rates for the rest of the world are: +...0...% for coal, +...5...% for oil, +...8...% for natural gas, +...4... (... [7])

185 Compared to the GCB estimate, Carbon Monitor estimates an increase in global fossil CO₂ emissions of
186 0.7% for 2025, lower than GCB but with overlapping uncertainties. In contrast to GCB, Carbon
187 Monitor projects the 2025 emissions from China to decline by -0.6%. Conversely, Carbon Monitor

Deleted: projects a
Deleted: increase ...f 0.3% (-1.8% to 2.4%)...% for 2025, lower than GCB but with overlapping uncertainties. In contrast to GCB, Carbon Monitor projects the 2025 emissions from China to decline by -2.4% (range -4.7% to -...2% (... [8])
Formatted: Not Highlight
Formatted: Not Highlight

1302 projects the 2025 emissions to increase by 1.4% for the USA, by 0.7% for India, by 0.8% for the EU27,
1303 but to decrease by -0.3% for Japan. The Carbon Monitor estimates that international aviation and
1304 shipping increased by 3.4% in 2025. For the rest of the world, the estimated change is an increase of
1305 1.3%.

1306 For traceability, Table S6 provides a comparison of annual projections from GCB since 2015 with the
1307 actual emissions assessed in the subsequent GCB annual report.

1308 3.2 Emissions from Land-Use Change

1309 3.2.1 Historical period 1850-2024

1310 Cumulative net CO₂ emissions from land-use change (E_{LUC}) for 1850-2024 are 250 ± 60 GtC (Table 8)
1311 with a large spread among individual bookkeeping estimates of 210 GtC (OSCAR), 240 GtC (LUCE)
1312 and 290 GtC (BLUE). DGVMs show a lower estimate of 160 ± 60 GtC. Vegetation biomass
1313 observations provide independent constraints on the E_{LUC} estimates over the 1901-2012 period (Li et
1314 al., 2017). Over that period, the GCB bookkeeping models' cumulative E_{LUC} amounts to 180 GtC [155
1315 to 210 GtC] and the DGVM cumulative E_{LUC} to 121 ± 45 GtC, both not significantly different from the
1316 observation-based estimate of 155 ± 50 GtC (Li et al., 2017). The substantially lower cumulative E_{LUC}
1317 estimates from DGVMs compared to GCB2024 are due to the correction for the RSS bias, which is
1318 implemented in this assessment (see Section 2.6.1; O'Sullivan et al., 2025).

1319 3.2.2 Recent period 1959-2024

1320 In contrast to growing fossil emissions, net CO₂ emissions from land use, land-use change, and forestry
1321 remained relatively constant (around 1.8 GtC yr⁻¹) over the 1959-1999 period. Since then, they have
1322 shown a statistically significant decrease of about 0.2 GtC per decade (p<0.001), reaching 1.4 ± 0.7 GtC
1323 yr⁻¹ for the 2015-2024 period (Table 7), with a spread from 1.3 to 1.6 GtC yr⁻¹ across the three
1324 bookkeeping estimates (Table 5, Figure 4b). Different from the bookkeeping average, the DGVM
1325 average grows slightly larger over the 1980-2010 period, but as bookkeeping models, DGVMs show
1326 decreasing emissions in the most recent decade, 2015-2024 (Table 5).

1327 Compared to GCB2024, the overall trends in E_{LUC} remained similar but the E_{LUC} estimates increased.
1328 The main reason for the larger estimates in this assessment is that the H&C2023 model, included up to
1329 GCB2024, is not included anymore (see Section 2.2). H&C2023 had the lowest E_{LUC} estimates among
1330 all bookkeeping models (Figure S3). Larger E_{LUC} estimates in the last few decades (compared to
1331 GCB2024) are also due to the consideration of transient, instead of constant, carbon densities by all
1332 three bookkeeping models (Section 2.2.1). The inclusion of transient carbon densities increases gross
1333 fluxes for all E_{LUC} components in the last few decades (Figure S3). Net E_{LUC} increases because
1334 emissions from deforestation are still the dominating term.

Deleted: 3.0% (0% to 6.0%)

Deleted: +

Deleted: 3% (-1.9% to +2.5%)

Deleted: 1.6% (-2

Deleted: to 5.8%)

Deleted: and

Deleted: 4% (-

Deleted: .3% to 4.0%)

Deleted: projects

Deleted: to increase

Deleted: 0.7% (-0.9% to 2.2%)

Deleted: expected

Deleted: 5% (range 0.3% to 2.7%).

Formatted: Outline numbered + Level: 2 + Numbering
Style: 1, 2, 3, ... + Start at: 1 + Alignment: Left + Aligned at:
0 cm + Indent at: 1.02 cm

Formatted: Outline numbered + Level: 3 + Numbering
Style: 1, 2, 3, ... + Start at: 1 + Alignment: Left + Aligned at:
0 cm + Indent at: 1.27 cm

Deleted: the 1901-2012

Formatted: Outline numbered + Level: 3 + Numbering
Style: 1, 2, 3, ... + Start at: 1 + Alignment: Left + Aligned at:
0 cm + Indent at: 1.27 cm

1349 We separate E_{LUC} into five component fluxes to gain further insight into the drivers of net emissions:
1350 deforestation, forest (re-)growth, wood harvest and other forest management, peat drainage and peat
1351 fires, and all other transitions, [with CO₂ emissions to the atmosphere being positive and CO₂ removals](#)
1352 [from the atmosphere being negative](#) (Figure 7b; Supplement S.2.2). We further decompose the
1353 deforestation and the forest (re-)growth term into contributions from shifting cultivation vs permanent
1354 forest cover changes (Figure 7c). Averaged over the 2015-2024 period and over the three bookkeeping
1355 estimates, fluxes from deforestation amount to [an emission of 1.9 \[1.5 to 2.3\] GtC yr⁻¹](#) (Table 5), of
1356 which 1.1 [0.9, 1.2] GtC yr⁻¹ are from permanent deforestation. Fluxes from forest (re-)growth amount
1357 to [a removal of -1.3 \[-1.5, -1.0\] GtC yr⁻¹](#) (Table 5), of which -0.6 [-0.7, -0.5] GtC yr⁻¹ ~~is~~ from
1358 re/afforestation and the remainder from forest regrowth in shifting cultivation cycles. Wood harvest and
1359 other forest management causes net emissions of 0.4 [0.1, 0.7] GtC yr⁻¹ (with substantial gross fluxes
1360 largely compensating each other; see Figure S2). Emissions from peat drainage and peat fires (0.2 [0.2,
1361 0.3] GtC yr⁻¹) and the net flux from other transitions (0.1 [0.1, 0.1] GtC yr⁻¹) are of smaller magnitude
1362 globally (Table 5).

Deleted: are

1363 The split into component fluxes clarifies the potentials for emission reduction and carbon dioxide
1364 removal: emissions from permanent deforestation - the largest of our component fluxes - could be
1365 halted (largely) without compromising carbon uptake by forests, contributing substantially to emissions
1366 reduction. By contrast, reducing wood harvesting would have limited potential to reduce net emissions
1367 as it would be associated with less forest regrowth; removals and emissions cannot be decoupled here
1368 on long timescales. A similar conclusion applies to removals and emissions from shifting cultivation,
1369 which we have therefore separated out. Carbon Dioxide Removal (CDR) in forests could instead be
1370 increased by permanently increasing the forest cover through re/afforestation, [Currently,](#)
1371 [re/afforestation creates](#) a removal of -0.6 GtC yr⁻¹ from the atmosphere averaged over 2015-2024. This
1372 value is similar to independent estimates derived from NGHGs for CDR in managed forests (through
1373 re/afforestation plus forest management) for 2013-2022 (-0.5 GtC yr⁻¹, Pongratz et al., 2024). [In](#)
1374 [contrast to NGHGs, bookkeeping estimates do not consider the impacts from natural disturbances \(like](#)
1375 [fires, windthrow, insect outbreaks\), which may lead to an overestimation of removals from](#)
1376 [re/afforestation.](#) Re/afforestation constitutes the vast majority of all current CDR (Pongratz et al., 2024).
1377 Though they cannot be compared directly to annual fluxes from the atmosphere and are thus not
1378 included in our estimate of E_{LUC} , CDR through transfers between non-atmospheric reservoirs such as in
1379 durable HWPs, biochar, or BECCS comprise much smaller amounts of carbon. 218 MtC yr⁻¹ have been
1380 estimated to be transferred to HWPs, averaged over 2013-2022 (Pongratz et al., 2024). The net flux of
1381 HWPs, considering the re-release of CO₂ through their decay, amounts to 91 MtC yr⁻¹ over that period
1382 (Pongratz et al., 2024). Note that some double-[accounting](#) between the CDR through HWPs and the
1383 CDR through re/afforestation exists if the HWPs are derived from newly forested areas. [CDR from](#)
1384 [Biochar and BECCS in 2024 amount to 0.31 MtC yr⁻¹ and 0.18 MtC yr⁻¹ respectively.](#) “Blue carbon”,
1385 i.e. coastal wetland management such as restoration of mangrove forests, saltmarshes and seagrass

Deleted: , for which we estimate

Deleted: counting

1389 meadows, though at the interface of land and ocean carbon fluxes, are counted towards the land-use
1390 sector as well. Currently, bookkeeping models do not include blue carbon; however, current CDR
1391 deployment in coastal wetlands is small globally, less than 0.003 MtC yr⁻¹ (Powis et al., 2023).

1392 The statistically significant decrease in E_{LUC} since the late-1990s, including the larger drop within the
1393 most recent decade, is due to the combination of decreasing emissions from deforestation (in particular
1394 permanent deforestation) and increasing removals from forest regrowth (with those from
1395 re/afforestation stagnating globally in the last decade). Net emissions in 2015-2024 are 23% lower than
1396 in the late-1990s (1995-2004) and 19% lower than in 2005-2014. The steep drop in E_{LUC} after 2015 is
1397 due to the combined effect from a peak in peat fire emissions in 2015 and a long-term decline in
1398 deforestation emissions in many countries over the 2010-2020 period. The processes behind gross
1399 removals, foremost forest regrowth and soil recovery, are all slow, while gross emissions include a
1400 large instantaneous component. Short-term changes in gross emissions dynamics, such as a temporary
1401 decrease in deforestation, influences E_{LUC} faster than a change in gross removals, which rather act on
1402 longer-term timescales. Component fluxes often differ more across the bookkeeping estimates than the
1403 net flux (Figure 7b), which is expected due to different process representation; in particular, the
1404 treatment of shifting cultivation, which increases both gross emissions and gross removals, differs
1405 across models, but also net and gross wood harvest fluxes show high [model spread](#) (Figure S2). By
1406 contrast, models agree relatively well for emissions from permanent deforestation.

1407 Overall, highest net land-use emissions occur in the tropical regions of all three continents. The top
1408 three emitters over 2015-2024 are Brazil (in particular the Amazon Arc of Deforestation), Indonesia,
1409 and the Democratic Republic of the Congo, with these 3 countries contributing 0.8 GtC yr⁻¹ or 57% of
1410 the global net land-use emissions (average over 2015-2024; Figure 6b, Figure 7a). This is related to
1411 massive expansion of cropland (FAO, 2025c), particularly in the last few decades in Latin America,
1412 Southeast Asia, and sub-Saharan Africa (Hong et al., 2021), to a substantial part for export of
1413 agricultural products (Pendrill et al., 2019). Emission intensity is high in many tropical countries,
1414 particularly of Southeast Asia, due to high rates of land conversion in regions of carbon-dense and often
1415 still pristine, undegraded natural forests (Hong et al., 2021). Emissions are further increased by peat
1416 fires in equatorial Asia (GFED4s, van der Werf et al., 2017), [contributing substantially to emissions in](#)
1417 [individual years, typically related to dry conditions during El Niño \(0.2 GtC in 2015; 0.03 GtC yr⁻¹](#)
1418 [averaged over 2015-2024\)](#). Uptake due to land-use change occurs in several regions of the world
1419 (Figure 6b) particularly due to re/afforestation. Highest [nature-based](#) CDR in the last decade is seen in
1420 China, the USA, and the EU27, partly related to expanding forest area as a consequence of the forest
1421 transition in the 19th and 20th century and subsequent regrowth of forest (Mather 2001; McGrath et al.,
1422 2015). Substantial uptake through re/afforestation also exists in other regions such as Brazil, Russia, or
1423 Indonesia, where, however, emissions from deforestation and other land-use changes dominate the net
1424 land-use flux. While the mentioned patterns are robust and supported by independent literature, we

Deleted:

Deleted: uncertainty

Deleted:).

1428 acknowledge that model spread is substantially larger on regional than global levels, as has been shown
1429 for bookkeeping models (Bastos et al., 2021) as well as DGVMs (Obermeier et al., 2021). [Independent](#)
1430 [assessments](#) exist for selected regions (e.g., for Europe by Petrescu et al., 2020; for Brazil by Rosan et
1431 al., 2021; for China by Zhu et al., 2025; and for 8 selected countries/regions in comparison to inventory
1432 data by Schwingshackl et al., 2022).

Deleted: Assessments for individual regions are being performed as part of the REgional Carbon Cycle Assessment and Processes 2 initiative (RECCAP2; Ciais et al., 2020, Poulter et al., 2022) or already

1433 The NGHGI data under the land-use, land-use change, and forestry (LULUCF) sector (Melo et al.
1434 2025) and the LULUCF estimates from FAOSTAT (FAO, 2025d) differ from the global models'
1435 definition of E_{LUC} (see Section 2.2.1). In the NGHGI reporting, natural land fluxes (S_{LAND}) are counted
1436 towards E_{LUC} when they occur on managed land (Grassi et al., 2018) whereas FAOSTAT LULUCF
1437 estimates generally include natural fluxes in managed and unmanaged forests (Tubiello et al., 2021). To
1438 compare our results to the NGHGI approach, we perform a translation of our E_{LUC} estimates by adding
1439 S_{LAND} in managed forest from the DGVMs simulations (1.9 GtC yr^{-1} in 2015-2024) to the bookkeeping
1440 E_{LUC} estimate (following the methodology described in Grassi et al., 2023; see Supplement S.2.4).
1441 Adding this sink changes E_{LUC} from being a source of 1.4 GtC yr^{-1} to a sink of 0.5 GtC yr^{-1} , much
1442 closer to the NGHGI estimate reporting a sink of 1.0 GtC yr^{-1} (Figure 8a, Table [S11](#)). Remaining
1443 differences in the bookkeeping and NGHGI estimates are mainly stemming from fluxes due to other
1444 transitions and permanent deforestation, whereas peat emissions and the net flux in managed forests
1445 agree well (Figure 8b,c). We further apply a mask of managed land to the net atmosphere-to-land flux
1446 estimate from atmospheric inversions to obtain inverse estimates that are comparable to the NGHGI
1447 estimates and to the translated E_{LUC} estimates from bookkeeping models (see Supplement S.2.4). The
1448 inversion-based net flux in managed land indicates a sink of 0.7 GtC yr^{-1} for 2015-2024, which is in
1449 broad agreement with the NGHGI and the translated E_{LUC} estimates (Figure 8, Table [S11](#)).
1450 Additionally, the interannual variability of the inversion estimates and the translated E_{LUC} estimates
1451 show a remarkable agreement (Pearson correlation of 0.71 in 2000-2024), which supports the suggested
1452 translation approach. Though estimates of NGHGI, FAOSTAT, and atmospheric inversions and the
1453 translated bookkeeping estimates still differ in value and need further analysis, the approach suggested
1454 by Grassi et al. (2023), which we adopt here, provides a feasible way to relate the global models' and
1455 NGHGI approach to each other and thus link the anthropogenic carbon budget estimates of land-use
1456 CO_2 fluxes directly to the Global Stocktake, as part of the UNFCCC Paris Agreement. The translation
1457 approach has been shown to be generally applicable also at the country-level (Grassi et al., 2023;
1458 Schwingshackl et al., 2022).

Deleted: S10

Deleted: S10

1459 **3.2.3 Final year 2024**

Formatted: Outline numbered + Level: 3 + Numbering Style: 1, 2, 3, ... + Start at: 1 + Alignment: Left + Aligned at: 0 cm + Indent at: 1.27 cm

1460 The global CO_2 emissions from land-use change are estimated as $1.3 \pm 0.7 \text{ GtC}$ in 2024, similar to the
1461 2023 estimate. However, confidence in the annual change remains low, as the land-use forcing
1462 underlying the E_{LUC} estimates was informed directly by data only up to and including 2023, with a trend

469 extrapolation to 2024 (see Supplement Section S.2.1). ~~The impacts of the 2023/2024 droughts linked to~~
470 ~~El Niño on the 2024 ELUC estimate, are thus not captured - while natural fires are not counted towards~~
471 ~~ELUC, deforestation, fires spreading further or drained peatlands burning more vastly because of dry~~
472 ~~conditions would be part of ELUC.~~ The extent of degradation was anomalously high in the Amazon in
1473 2024 and partly masked relatively low deforestation rates (<https://terrabrasilis.dpi.inpe.br>). However,
1474 this is not captured by our approach that is based on forest cover changes. For degradation it is currently
1475 impossible to be separated into effects of land-use activity versus effects of climate variability.

Deleted: The anomalously large fire emissions in South America in 2024 that resulted from the

Deleted: are thus not yet fully reflected in

Deleted: , even if they led to permanent

Deleted: .

476 3.2.4 Year 2025 Projection

1477 In equatorial Asia, peat fire emissions remained low (1 TgC in 2025 through October 15 2025, after 2
1478 TgC in 2024; GFED4.1s, van der Werf et al., 2017), as did deforestation and degradation fires (4 TgC
1479 in 2025; 8 TgC in 2024). South America saw a big reduction in emissions from deforestation and
480 degradation fires, from 334 TgC in 2024 to 35 TgC until October 15 2025. Pantropical 2025 fire
1481 emission estimates from deforestation and degradation through October 15 are 105 TgC, which is not
1482 just a massive drop compared to the anomalously high 2024 emissions, but also only about one third of
1483 the long-term average (1997-2024). The reduction in emissions is mainly attributable to anomalously
1484 low deforestation and degradation fire emissions in South America, likely connected to the ceasing of
1485 the El Niño conditions and their impacts on ecosystems.

Formatted: Outline numbered + Level: 3 + Numbering Style: 1, 2, 3, ... + Start at: 1 + Alignment: Left + Aligned at: 0 cm + Indent at: 1.27 cm

Deleted: up

1486 Since the ELUC estimate for the year 2024 is not informed directly by data on land-use dynamics
1487 (Section 3.2.3), we estimate the 2025 projection based on fire anomalies over the year 2023. We expect
1488 ELUC emissions of around 1.1 GtC (4.1 GtCO₂) in 2025, 0.1 GtC below the 2024 level (0.3 GtC below
1489 the 2015-2024 average). Note that the confidence in the 2025 ELUC projection remains low, as it is
1490 based on deforestation, degradation and peat fire emissions, which are only a proxy for land-use
1491 change. Projections in past GCB assessments are only partially confirmed by updated ELUC estimates
1492 based on bookkeeping models in the following GCB assessments (Figure S4). Although our
1493 extrapolation includes tropical deforestation and degradation fires, the degradation attributable to
1494 selective logging, edge-effects or fragmentation is not captured. Further, deforestation and fires in
1495 deforestation zones may become more disconnected, partly due to changes in legislation in some
1496 regions. For example, Van Wees et al. (2021) found that the contribution from fires to forest loss
1497 decreased in the Amazon and in Indonesia over the period of 2003-2018.

Formatted: Outline numbered + Level: 2 + Numbering Style: 1, 2, 3, ... + Start at: 1 + Alignment: Left + Aligned at: 0 cm + Indent at: 1.02 cm

Deleted: 0088

Deleted: /

Formatted: Not Highlight

Deleted: 002

Deleted: /

Formatted: Not Highlight

Deleted: 00022

Deleted: /

Formatted: Not Highlight

498 3.3 CDR not based on vegetation

1499 Besides the CDR through land use (Sec. 3.2), the atmosphere-to-geosphere flux of carbon resulting
500 from carbon dioxide removal (CDR) activities in 2024 is estimated at 0.011 MtC_{yr}⁻¹. This results
501 primarily from 0.0048 MtC_{yr}⁻¹ of biomass direct storage (compressing waste biomass to store
502 underground), 0.003 MtC_{yr}⁻¹ and 0.002 MtC_{yr}⁻¹ of mineralisation and enhanced weathering projects

Formatted: Not Highlight

515 respectively, and 0.0004 MtC_{yr}⁻¹ of DACCS (Pongratz et al., 2024). This represents an increase
 516 (267%) in the anthropogenic sink compared to revised estimates for 2023 (0.003 MtC yr⁻¹), although it
 517 remains roughly a million times smaller than current fossil CO₂ emissions. Note that the lower DACCS
 518 estimates, as well as revised 2023 values, reflect updated CDR tracking methodologies which include
 519 drawing on more accurate annual data from registries, indicating that operational projects are currently
 520 removing less CO₂ than their expected capacities. Similarly, reported CDR via Enhanced Rock
 521 Weathering decreased in 2024; however, this may not indicate a real decline in activity. The decline
 522 likely reflects a transition toward third party verification, with some removals not yet appearing on
 523 registries. Other novel CDR methods, including ocean and river alkalinity enhancement (0.0003 MtC_{yr}⁻¹
 524 and 0.00001 MtC_{yr}⁻¹ in 2024 respectively), and bio-oil geological storage (0.0002 MtC_{yr}⁻¹, jointly
 525 contributed just over 0.0005 MtC_{yr}⁻¹ according to updated 2024 estimates of the State of CDR report
 526 (Smith et al., 2024). CDR through intentional biomass sinking into the deep ocean was reported at
 527 0.001 MtC_{yr}⁻¹ for 2023, but no activities have been identified for 2024.

528 3.4 Total anthropogenic emissions

529 Cumulative anthropogenic CO₂ emissions (fossil, including cement carbonation, and land-use change)
 530 for 1850-2024 totalled 745 ± 65 GtC (2730 ± 240 GtCO₂), of which 71% (530 GtC) occurred since
 531 1959 and 35% (260GtC) since 2000 (Table 7 and 8). Total anthropogenic emissions more than doubled
 532 since the 1960s, from 4.9 ± 0.7 GtC yr⁻¹ for the decade of the 1960s to an average of 11.2 ± 0.9 GtC yr⁻¹
 533 during 2015-2024, and reaching 11.6 ± 0.9 GtC (42.4 ± 3.2 GtCO₂) in 2024. However, total
 534 anthropogenic CO₂ emissions have been almost stable over the last decade (0.3% yr⁻¹ average growth
 535 rate over the 2015-2024 period), much lower than the 1.9% growth rate over the previous decade
 536 (2005-2014). This slower growth is due both to the reduced growth in E_{FOS} between the two decades,
 537 and to the decrease in emissions from E_{LUC} over the past decade.

538 During the historical period 1850-2024, 67% of historical emissions were from fossil emissions and
 539 33% from land-use change. However, fossil emissions have grown significantly since the 1960s while
 540 net land-use change emissions have not, and consequently the contributions of land-use change to total
 541 anthropogenic emissions were smaller during recent periods, 21% during the period 1959-2024 and
 542 down to 12% over the last decade (2015-2024).

543 For 2025 we project global total anthropogenic CO₂ emissions from fossil and land-use changes to be
 544 around 11.5 GtC (42.2 GtCO₂), marginally below the 2024 level due to lower net land-use emissions (-
 545 0.13 GtC) compensating the growth in fossil emission (+0.09 GtC).

Deleted: 0.003 MtC/yr of bio-oil geological storage,

Deleted: /

Deleted: a decrease of 20%

Formatted: Not Highlight

Deleted: the 0.011 MtC/yr estimate

Deleted: , and

Deleted: reflect

Deleted: 0002

Deleted: /

Deleted: /

Deleted: biomass direct

Deleted: compressing waste biomass to store underground,

Deleted: 0008

Deleted: /

Deleted:),

Formatted: Not Highlight

Formatted: Not Highlight

Formatted: Not Highlight

Deleted: under

Deleted: 004

Deleted: /

Formatted: Not Highlight

Deleted: /

Formatted: Not Highlight

Formatted: Outline numbered + Level: 2 + Numbering Style: 1, 2, 3, ... + Start at: 1 + Alignment: Left + Aligned at: 0 cm + Indent at: 1.02 cm

Deleted:

1565 **3.5 Atmospheric CO₂**

1566 **3.5.1 Historical period 1850-2024**

1567 Atmospheric CO₂ concentration was approximately 278 parts per million (ppm) in 1750, reaching 300
1568 ppm in the late 1900s, 350 ppm in the late 1980s, and reaching 422.80 ± 0.1 ppm in 2024 (Lan et al.,
1569 [2025](#); Figure 1). The mass of carbon in the atmosphere increased by [52%](#) from 590 GtC in 1750 to 898
1570 GtC in 2024. Current CO₂ concentrations in the atmosphere are unprecedented in the last 2 million
1571 years and the current rate of atmospheric CO₂ increase is at least 10 times faster than at any other time
1572 during the last 800,000 years (Canadell et al., 2021).

Formatted: Indent: Left: 0 cm, First line: 0 cm, Outline numbered + Level: 2 + Numbering Style: 1, 2, 3, ... + Start at: 1 + Alignment: Left + Aligned at: 0 cm + Indent at: 1.02 cm

Formatted: Outline numbered + Level: 3 + Numbering Style: 1, 2, 3, ... + Start at: 1 + Alignment: Left + Aligned at: 0 cm + Indent at: 1.27 cm

Deleted: 2025a

Deleted: 51

1573 **3.5.2 Recent period 1959-2024**

1574 The growth rate in atmospheric CO₂ level increased from 1.7 ± 0.07 GtC yr⁻¹ in the 1960s to 5.6 ± 0.02
1575 GtC yr⁻¹ during 2015-2024 with important decadal variations (Table 7, Figure 3 and Figure 4c). During
1576 the last decade (2015-2024), the growth rate in atmospheric CO₂ concentration continued to increase,
1577 albeit with large interannual variability (Figure 9). This interannual variability is highly consistent
1578 between the surface-based CO₂ growth rate and GRESO, the XCO₂-based growth rate ([Pearson
1579 correlation of 0.84](#)), but substantial differences are seen in 2019 and 2022-2024. These reflect
1580 differences in the total atmospheric carbon stock seen within the set boundaries of Jan-1 and Dec-31
1581 used to create an annual growth rate, as discussed in Section 2.4.2. Especially with large anomalies in
1582 tropical regions and close to January 1st, the calculation becomes sensitive to when the change is
1583 detected. This affected the 2023 and 2024 growth rates most strongly as they originated from tropical
1584 regions, and late in the calendar year (see next section). Figure 9 also shows the total annual fluxes (in
1585 GtC yr⁻¹) from the inverse models, which are derived to match the observed atmospheric increase while
1586 numerically accounting for the atmospheric transport-related delay in detection. The inversely modeled
1587 values generally match the GRESO growth rate better than the surface observations-based growth rate,
1588 indicating that the latter is more strongly influenced by the delay between the fluxes occurring and the
1589 actual observation of these signals. Note that this effect is mainly important on the annual timescale,
1590 and not over longer periods.

Formatted: Outline numbered + Level: 3 + Numbering Style: 1, 2, 3, ... + Start at: 1 + Alignment: Left + Aligned at: 0 cm + Indent at: 1.27 cm

Deleted: r=

1591 **3.5.3 Final year 2024**

1592 The growth rate in the surface based atmospheric CO₂ concentration was 7.9 ± 0.2 GtC (3.73 ± 0.08
1593 ppm) in 2024 (Figure 4c; Lan et al., [2025](#)), well above the 2023 growth rate (5.7 ± 0.2 GtC, 2.7 ± 0.08
1594 ppm) or the 2015-2024 average (5.6 ± 0.02 GtC, 2.6 ± 0.008 ppm), as to be expected during an El Niño
1595 year. The 2024 atmospheric CO₂ growth rate was the largest over the 1959-2024 atmospheric
1596 observational record, more than 1.5 GtC above the growth rates of 1998, 2015, and 2016 and 1998, all
1597 strong El Niño years.

Formatted: Outline numbered + Level: 3 + Numbering Style: 1, 2, 3, ... + Start at: 1 + Alignment: Left + Aligned at: 0 cm + Indent at: 1.27 cm

Deleted: 2025a

1602 In contrast, the satellite-based GRESO growth rate was $6.8 \pm 0.2 \text{ GtC}_{\text{yr}^{-1}}$ ($3.20 \pm 0.09 \text{ ppm}_{\text{yr}^{-1}}$) for 2024
 1603 which was also above its 2023 growth rate ($6.5 \pm 0.2 \text{ GtC}_{\text{yr}^{-1}}$, $3.06 \pm 0.07 \text{ ppm}_{\text{yr}^{-1}}$) and the highest on its
 1604 10-year record. But it shows a more equal split of the anomaly between both years (2023-2024). This
 1605 likely reflects more accurately that a substantial fraction of the flux anomaly occurred in 2023, but this
 1606 was only detected by the surface network in 2024. For the interpretation of the annual global budget
 1607 this has strong implications, as 2024 surface fluxes would need to add up to a smaller anomaly (by 1.1
 1608 $\text{GtC}_{\text{yr}^{-1}}$) than when using the surface-based annual growth rate. Hence the budget imbalance in 2024
 1609 (Table 7) would be reduced from -1.7 GtC to -0.6 GtC if the GRESO growth rate was used for the
 1610 budget estimate.

1611 [As the the satellite-based GRESO growth rate is more evenly split between 2023 and 2024, so would be](#)
 1612 [the \$B_{\text{IM}}\$, \$-0.3 \text{ GtC}\$ in 2023 and \$-0.6 \text{ GtC}\$ in 2024 with GRESO, compared to \$+0.4 \text{ GtC}\$ in 2023 and \$-1.7\$](#)
 1613 [GtC in 2024 with the GATM from the surface based network.](#)

1614 3.5.4 Year 2025 Projection

1615 [The 2025 atmospheric \$\text{CO}_2\$ concentration, averaged over the year reached the level of \$425.64 \text{ ppm}\$,](#)
 1616 [53% over the pre-industrial level \(Lan et al., 2025\). We estimate the annual growth in atmospheric \$\text{CO}_2\$](#)
 1617 [\(\$G_{\text{ATM}}\$ \) to be about \$4.4 \text{ GtC}\$ \(equivalent to a \$2.1 \text{ ppm}\$ increase in the global mean concentration\), in line](#)
 1618 [with a neutral ENSO year \(ENSO 3.4 Index between \$-0.5\$ and \$0.5\$ \). The projected growth rate estimated](#)
 1619 [by the ESMS multi-model mean is slightly larger \(\$5.5 \text{ GtC}\$, \$2.6 \text{ ppm}\$ \).](#)

1620 [For traceability, Table S7 provides a comparison of annual projections of the \$G_{\text{ATM}}\$, \$S_{\text{OCEAN}}\$ and \$S_{\text{LAND}}\$](#)
 1621 [from GCB since 2021 with the actual estimate assessed in the subsequent GCB annual report.](#)

1622 3.6 Ocean Sink

1623 3.6.1 Historical period 1850-2024

1624 Cumulated since 1850, the ocean sink S_{OCEAN} adds up to $200 \pm 35 \text{ GtC}$, with more than 70% of this
 1625 amount ($145 \pm 25 \text{ GtC}$) being taken up by the global ocean since 1959. Over the historical period, the
 1626 ocean sink increased in pace with the anthropogenic emissions exponential increase (Figure 3). Since
 1627 1850, the ocean has removed 27% of total anthropogenic emissions.

1628 3.6.2 Recent period 1959-2024

1629 S_{OCEAN} increased from $1.3 \pm 0.4 \text{ GtC yr}^{-1}$ in the 1960s to $3.2 \pm 0.4 \text{ GtC yr}^{-1}$ during 2015-2024 (Table 7),
 1630 with interannual variations of the order of a few tenths of GtC yr^{-1} (Figure 4d, Figure 10b). [As](#)
 1631 [described in section 2.5.1, \$S_{\text{OCEAN}}\$ is now corrected for identified biases in the GOBMs and \$f_{\text{CO}_2}\$](#)

Deleted: /

Deleted: /

Deleted: /

Deleted: /

Deleted: >

Deleted: /

Formatted: Outline numbered + Level: 3 + Numbering Style: 1, 2, 3, ... + Start at: 1 + Alignment: Left + Aligned at: 0 cm + Indent at: 1.27 cm

Deleted: Based on a projection of the 2025 surface fluxes, we

Deleted: 9

Deleted: 3

Deleted: . This is the average of the GCB regression method (4...

Deleted: GtC, 2.1 ppm)

Deleted: the

Deleted: The 2025 atmospheric CO_2 concentration, averaged over the year, is expected to reach the level of 425.7 ppm , 53% over the pre-industrial level (278 ppm).

Formatted: Indent: Left: 0 cm, First line: 0 cm, Outline numbered + Level: 2 + Numbering Style: 1, 2, 3, ... + Start at: 1 + Alignment: Left + Aligned at: 0 cm + Indent at: 1.02 cm

Formatted: Outline numbered + Level: 3 + Numbering Style: 1, 2, 3, ... + Start at: 1 + Alignment: Left + Aligned at: 0 cm + Indent at: 1.27 cm

Formatted: Outline numbered + Level: 3 + Numbering Style: 1, 2, 3, ... + Start at: 1 + Alignment: Left + Aligned at: 0 cm + Indent at: 1.27 cm

1648 [products estimates. Compared to the uncorrected estimate, SO_{CEAN} is increased by 0.2 GtC yr⁻¹ for the](#)
1649 [2015-2024 period.](#)

1650 The ocean-borne fraction (SO_{CEAN}/(E_{FOS}+E_{LUC})) has been remarkably constant around 27% on average,
1651 with variations around this mean illustrating the decadal variability of the ocean carbon sink. So far,
1652 there is no evidence of a sustained decrease in the ocean-borne fraction from 1959 to 2024 (Figure
1653 S16).

1654 The increase of the ocean sink is primarily driven by the increased atmospheric CO₂ concentration, with
1655 the strongest CO₂ induced signal in the North Atlantic and the Southern Ocean (Figure 12a, Figure
1656 S10). The effect of climate change is much weaker, reducing the ocean sink globally by 0.20 ± 0.05
1657 GtC yr⁻¹ (~~7.1% relative to the simulation that only accounts for the effect of atmospheric CO₂ increase~~)
1658 during 2015-2024 (all models simulate a weakening of the ocean sink by climate change, range -4.2 to -
1659 ~~10.7%~~). The climate change effect leading to a reduced ocean sink is evident in all large-scale
1660 latitudinal bands (north, tropics, south, Figure 12b, Figure S10). This is the combined effect of change
1661 and variability in all atmospheric forcing fields, previously attributed to wind and temperature changes
1662 (Le Quéré et al., 2010, Bunsen et al., 2024). The effect of warming is smaller than expected from
1663 offline calculation due to a stabilising feedback from limited exchange between surface and deep waters
1664 (Bunsen et al., 2024; Müller et al., 2025).

1665 The global net air-sea CO₂ flux is a residual of large natural and anthropogenic CO₂ fluxes into and out
1666 of the ocean with distinct regional and seasonal variations (Figure 6c and Figure S5). Natural fluxes
1667 dominate on regional scales, but largely cancel out when integrated globally (Gruber et al., 2009;
1668 DeVries et al., 2023). Mid-latitudes in all basins and the high-latitude North Atlantic dominate the
1669 ocean CO₂ uptake where low temperatures and high wind speeds facilitate CO₂ uptake at the surface
1670 (Takahashi et al., 2009). In these regions, formation of mode, intermediate and deep-water masses
1671 transport anthropogenic carbon into the ocean interior, thus allowing for continued CO₂ uptake at the
1672 surface. Outgassing of natural CO₂ occurs mostly in the tropics, especially in the equatorial upwelling
1673 region, and to a lesser extent in the North Pacific and polar Southern Ocean, mirroring a well-
1674 established understanding of regional patterns of air-sea CO₂ exchange (e.g., Takahashi et al., 2009,
1675 Gruber et al., 2009; DeVries et al., 2023). These patterns are also noticeable in the Surface Ocean CO₂
1676 Atlas dataset, where an ocean *f*CO₂ value above the atmospheric level indicates outgassing (Figure S5).
1677 This map further illustrates the data-sparsity in the Indian Ocean and the Southern Hemisphere in
1678 general.

1679 The largest variability in the ocean sink occurs on decadal time-scales (Figure 10b). The ensemble
1680 means of GOBMs and *f*CO₂-products show the same patterns of decadal variability, although with a
1681 larger amplitude of variability in the *f*CO₂-products than in the GOBMs. The ocean sink stagnated in
1682 the 1990s and strengthened between the early 2000s and the mid-2010s (Figure 10b; Le Quéré et al.,

Deleted: 6.2%

Deleted: SO_{CEAN}

Deleted: 6

Deleted: 12.2

1687 2007; Landschützer et al., 2015, 2016; DeVries et al., 2017; Hauck et al., 2020; McKinley et al., 2020,
1688 Gruber et al., 2023). Different explanations have been proposed for the decadal variability in the 1990s
1689 and 2000s, ranging from the ocean's response to changes in atmospheric wind systems (e.g., Le Quéré
1690 et al., 2007, Keppler and Landschützer, 2019), including variations in upper ocean overturning
1691 circulation (DeVries et al., 2017) to the eruption of Mount Pinatubo in the 1990s (McKinley et al.,
1692 2020, Fay et al., 2023). The main origin of the decadal variability is a matter of debate with a number of
1693 studies initially pointing to the Southern Ocean (see review in Canadell et al., 2021 and Gruber et al.,
1694 2023), but also contributions from the North Atlantic and North Pacific (Landschützer et al., 2016,
1695 DeVries et al., 2019), or a global signal (McKinley et al., 2020) were proposed. The GOBM
1696 decomposition into climate and CO₂ effects emphasizes the role of the climate effect (that would
1697 include cooling signals from volcanic eruptions) for the stagnation in the 1990s until 2002, which are
1698 seemingly more pronounced in the tropics and north than in the south (Figure S10). The atmospheric
1699 pCO₂ growth rate is a spatially uniform driver that amplifies with large-scale averaging, while climate
1700 exerts spatially heterogeneous effects that cancel with averaging. Thus, climate dominates small-scale
1701 flux variability, but is matched on the global mean by the impact of the pCO₂ growth rate (Fay et al.,
1702 2024).

1703 More recently, the sink seems to have entered a phase of stagnation 2016 - 2022, largely in response to
1704 large inter-annual climate variability. The first-order effect of interannual variability stems from a
1705 stronger ocean sink during large El Niño events leading to a reduction in CO₂ outgassing from the
1706 Tropical Pacific (e.g., 1997/98, 2015/16) and a weaker sink in neutral years following El Niño (2017)
1707 and during La Niña events (2020-2022, Figure 10b; Rödenbeck et al., 2014, Hauck et al., 2020;
1708 McKinley et al. 2017). After the triple La Niña event 2020-2022, the ocean sink rebound in 2023 linked
1709 to the onset of an El Niño event. Warming in the extratropics, in particular in the Northern Hemisphere,
1710 however, weakened the overall increase in the ocean carbon sink (Müller et al., 2025). In the GOBMs,
1711 the ocean sink stagnation 2016-2022 is associated with a period of a stronger climate effect reducing
1712 the ocean sink, mostly stemming from the tropics, in line with the expected patterns from El Niño and
1713 La Niña (Figure S10). The CO₂ effect has also shown a lower growth rate since around 2016.

1714 The ensemble means of GOBMs, and fCO₂-products (adjusted for the riverine flux) show a mean offset
1715 increasing from 0.28 GtC yr⁻¹ in the 1990s (first decade available) to 0.59 GtC yr⁻¹ in the decade 2015-
1716 2024. The offset is larger than in previous GCB versions, because two fCO₂-products (UEXP-FNN-U,
1717 JMA-MLR), that use an adjusted version of the Surface Ocean CO₂ Atlas data to represent the sea
1718 surface fCO₂ within the surface skin layer where gas exchange takes place (Ford et al., 2025), are now
1719 included in the fCO₂-product mean. Additionally, an update in the SOCAT dataset with regards to
1720 Southern Ocean data led to an increase in the sink strength in three of the fCO₂-products (VLIZ-
1721 SOMFFN, LDEO-HPD, CMEMS-LSCE-FFNN - see section S3.1, Fay et al., 2025). In this version of
1722 the GCB, the positive trends in the ocean sink estimated by the GOBMs and the fCO₂-products diverges

Deleted: .(

Deleted: unscaled

Deleted: SOCEAN

Deleted: trend between

1727 over time by a factor of 1.6 since 2002 (GOBMs: 0.27 ± 0.05 GtC yr⁻¹ per decade, *f*CO₂-products: 0.46
1728 GtC yr⁻¹ per decade [0.22 to 0.81 GtC yr⁻¹ per decade], [corrected](#) SO_{CEAN}: 0.38 GtC yr⁻¹ per decade), but
1729 the uncertainty ranges overlap. A hybrid approach recently constrained the trend for 2000 to 2022 to
1730 0.42 ± 0.06 GtC yr⁻¹ decade⁻¹ (Mayot et al., 2024), which aligns with the updated trend of SO_{CEAN}
1731 (0.46 GtC yr⁻¹ decade⁻¹), while the *f*CO₂-products exhibit a larger (0.54 [0.29, 0.85] GtC yr⁻¹
1732 decade⁻¹) and the GOBMs a lower trend (0.34 ± 0.05 GtC yr⁻¹ per decade) over the same period.

1733 In the current budget, the discrepancy between the two types of estimates stems from a persistently
1734 larger ocean sink in the *f*CO₂-products in the northern and southern extra-tropics since around 2002
1735 (Figure 14). Note that the discrepancy in the mean flux, which was located in the Southern Ocean in
1736 GCB2022 and earlier, was reduced due to the choice of the regional river flux adjustment (Lacroix et
1737 al., 2020 instead of Aumont et al., 2001). This comes at the expense of a discrepancy in the mean
1738 SO_{CEAN} of about 0.2-0.3 GtC yr⁻¹ in the tropics. Likely explanations for the discrepancy in the trends and
1739 decadal variability in the high latitudes are data sparsity and uneven data distribution (Bushinsky et al.,
1740 2019, Gloege et al., 2021, Hauck et al., 2023a, Mayot et al., 2024). In particular, two *f*CO₂-products
1741 were shown to overestimate the Southern Ocean CO₂ flux trend by 50 and 130% based on current
1742 sampling in a model subsampling experiment (Hauck et al., 2023a) and the largest trends in the *f*CO₂-
1743 products occurred in a data devoid region in the North Pacific (Mayot et al., 2024). In Supplement S3
1744 we show that the strength of the trends in *f*CO₂ products [may be](#) linked to reconstruction biases of the
1745 true trend signal. In this respect it is highly worrisome that the coverage of *f*CO₂ observations has
1746 declined since 2016/17 (Dong et al., 2022, 2024; Bakker et al., 2025b) and is now down to that of the
1747 mid-2000s (Figure 10b). The temperature correction applied in two products further worsens the
1748 agreement in trends between GOBMs and *f*CO₂-products. Similarly, model biases likely contribute to
1749 the discrepancy between GOBMs and *f*CO₂-products (as indicated by the comparison with Mayot et al.,
1750 2024, and by the large model spread in the South, Figure 14).

1751 The [SO_{CEAN} estimate](#) is 2.9 ± 0.4 GtC yr⁻¹ over the period 2004 to 2019, which agrees within the ranges
1752 of uncertainty with the ocean interior estimate of 3.2 ± 0.7 GtC yr⁻¹ obtained with the MOBO-DIC
1753 approach (Keppeler et al., 2023). [The carbon flux components of the observation-based ocean interior](#)
1754 [estimate](#) match the definition of SO_{CEAN} used here (Hauck et al., 2020). [Furthermore](#), the decadal SO_{CEAN}
1755 estimates agree well with the corresponding ocean interior estimates for all decades from the 1960s to
1756 the 2010s, which represent a composite estimate of [three](#) observation-based products (Table 6).

1757 The SO_{CEAN} estimate agrees within uncertainties with other lines of evidence from atmospheric oxygen
1758 based estimates, atmospheric inversions, and ocean interior observation-based constraints (Table 6).
1759 The atmospheric oxygen-based estimate shows a [lower estimate than SO_{CEAN} in the 1990s, but a larger](#)
1760 [estimate over the 2015-2024 period, indicating a](#) strong growth of >1.5 GtC yr⁻¹ [over that period](#). ESMs
1761 with data assimilation result in lower estimates of the ocean sink than all other estimates (Table 6).

Deleted: -

Deleted: is

Deleted: adjusted

Deleted: The SO_{CEAN} estimate of 2.7 ± 0.4 GtC yr⁻¹ over the period 1990 to 2022 is further in excellent agreement with another recent ocean interior estimate of 2.6 ± 0.4 GtC yr⁻¹ obtained with the ResNet-DIC method (Ehmen et al., 2025, in review). ...

Deleted: both

Deleted: estimates

Deleted: Finally

Deleted: four

Deleted: from the 1990s to the recent decade 2015-2024

1775 Also, the atmospheric inversion estimates of the ocean sink are generally lower than S_{OCEAN} on average,
1776 but are within the uncertainties of the GOBMs and fCO_2 products.

Deleted: inversions

Deleted: and cover a similar range as the adjusted

1777 3.6.3 Final year 2024

Formatted: Outline numbered + Level: 3 + Numbering
Style: 1, 2, 3, ... + Start at: 1 + Alignment: Left + Aligned at:
0 cm + Indent at: 1.27 cm

1778 The estimated ocean CO_2 sink is 3.4 ± 0.4 GtC for 2024. This is an increase of 0.1 GtC compared to
1779 2023 (Figure 4d). The sink strengthening was expected from the atmospheric CO_2 growth and El Niño
1780 conditions in the beginning of the year (January to April). However, the continuation of the anomalous
1781 warm conditions in the extratropics, especially of the Atlantic Ocean, led to a weaker than expected
1782 increase in the sink (Figure 11c). The GOBMs suggest that the increase is driven by the anomalously
1783 high atmospheric CO_2 growth rate and dampened by climate effects, thus suggesting that warming
1784 overcompensated the effect from El Niño (Figure S10). GOBMs and fCO_2 -products largely agree on
1785 patterns of ocean sink anomalies with a reduced sink in parts of the subtropical and subpolar North
1786 Atlantic and North Pacific that coincides with regions of anomalously warm sea surface temperatures
1787 (Figure S9). GOBM and fCO_2 -product ensemble mean estimates consistently result in an ocean sink
1788 increase in 2024 (GOBMs: 0.13 ± 0.14 GtC, fCO_2 -products: $0.08 [-0.34, 0.43]$ GtC). Eight GOBMs and
1789 six fCO_2 -products show an increase in S_{OCEAN} , while only two GOBMs and three fCO_2 -products show a
1790 decrease in S_{OCEAN} . The fCO_2 -products have a larger uncertainty at the end of the reconstructed time
1791 series, potentially linked to uncertainties related to fewer available observations in the final year (see
1792 e.g. Watson et al 2020, Pérez et al 2024). Specifically, the fCO_2 -products' estimate of the last year is
1793 regularly adjusted in the following release owing to the tail effect and an incrementally increasing data
1794 availability. While the monthly grid cells covered may have a lag of only about a year (Figure 10b
1795 inset), the values within grid cells may change with 1-5 years lag (see absolute number of observations
1796 plotted in previous GCB releases), potentially resulting in annual changes in the flux magnitude from
1797 fCO_2 -products.

1798 3.6.4 Year 2025 projection

Formatted: Outline numbered + Level: 3 + Numbering
Style: 1, 2, 3, ... + Start at: 1 + Alignment: Left + Aligned at:
0 cm + Indent at: 1.27 cm

1799 Using a feed-forward neural network method (see Section 2.5.2) we project an ocean sink of 3.3 ± 0.4
1800 GtC for 2025, which is a declining sink of -0.1 GtC compared to 2024, and can be explained by the
1801 generally lower ocean CO_2 uptake following the El Niño event ending in 2024, consistent with the
1802 projected recovery of the atmospheric CO_2 growth rate after a record high in 2024. The set of ESMs
1803 predictions support this estimate with a 2025 ocean sink of around 3.1 [3.0, 3.2] GtC. Taking the
1804 average of both estimates, we project an ocean sink of 3.2 ± 0.4 GtC for 2025.

Deleted: ,

1805 3.6.5 Evaluation of ocean models and fCO_2 -products

Formatted: Outline numbered + Level: 3 + Numbering
Style: 1, 2, 3, ... + Start at: 1 + Alignment: Left + Aligned at:
0 cm + Indent at: 1.27 cm

1806 The process-based model evaluation draws a generally positive picture with GOBMs scattered around
1807 the observational values for Southern Ocean sea-surface salinity, Southern Ocean stratification index,

Deleted: and surface ocean Revelle factor

1812 albeit outliers exist (Section S3.3 and Table S12). The Revelle factor is high in most GOBMs when
1813 compared to GLODAP, but appears less biased when compared to OceanSODA. However, the Atlantic
1814 Meridional Overturning Circulation at 26°N is underestimated by 8 out of 10 GOBMs and
1815 overestimated by one GOBM. IOMB summarizes the GOBMs' performance across physical and
1816 biogeochemical data sets and various statistics relative to the GOBM ensemble (Figure S6). All
1817 GOBMs perform better in some variables compared to the other models, and worse in other variables.
1818 Despite the indication that GOBMs underestimate the ocean sink, low sink models do not perform
1819 generally worse than the other models; and similarly, high sink models do not perform better than the
1820 others.

Deleted: S11).

1821 The model simulations allow to separate the anthropogenic carbon component and to compare the
1822 GOBMs DIC inventory change directly to the interior ocean estimates of Gruber et al. (2019), Müller et
1823 al. (2023) and the GOBM anthropogenic surface fluxes to DeVries (2022) without further assumptions
1824 (Table S12). The GOBMs ensemble average of anthropogenic carbon inventory changes 1994-2007
1825 amounts to 2.3 GtC yr⁻¹ and is thus 10.5% lower than the 2.6 ± 0.3 GtC yr⁻¹ estimated by Gruber et al.
1826 (2019) although within the uncertainty. Five models fall within the range reported by Gruber et al.
1827 (2019). Comparison to the decadal estimates of anthropogenic carbon accumulation (Müller et al.,
1828 2023) are close to the interior ocean data based estimate for the decade 2004-2014 (GOBMs sim D
1829 minus sim A, 2.6 ± 0.4 GtC yr⁻¹, Müller et al. 2.7 ± 0.3 GtC yr⁻¹), but do not reproduce the supposedly
1830 higher anthropogenic carbon accumulation in the earlier period 1994-2004 (GOBMs sim D minus sim
1831 A, 2.2 ± 0.3 GtC yr⁻¹, Müller et al. 2.9 ± 0.3 GtC yr⁻¹). Finally, the mean anthropogenic carbon uptake
1832 in GOBMs from 1985 to 2018 amounts to 2.3 GtC yr⁻¹, slightly lower than the corresponding
1833 observation-based uptake rate of 2.4 ± 0.2 Gt yr⁻¹ based on OCIM (DeVries, 2022; DeVries et al.,
1834 2023). The underestimation of anthropogenic carbon accumulation by 10% in the period 1994 to 2007,
1835 in the 1990s and 2000s (Table 6) and by 15% in the 2010s (Table 6) justifies the correction of GOBMs
1836 by 10% (Friedlingstein et al., 2025a, section 2.5.1). Interestingly, and in contrast to the uncertainties in
1837 the surface CO₂ flux, we find the largest mismatch in interior ocean carbon accumulation in the tropics,
1838 with smaller contributions from the north and the south (Table S12). The large discrepancy in
1839 accumulation in the tropics highlights the role of interior ocean carbon redistribution for those
1840 inventories (Khatiwala et al., 2009, DeVries et al., 2023).

Deleted: S11

Deleted: Taken together, the comparison to observation-based estimates suggests that the majority

Deleted: the GOBMs may underestimate

Deleted: uptake

Deleted: -20%

Deleted: some models even more

Deleted: are one line of evidence that supports

Deleted: upscaling

Deleted: S11

1841 Additional benchmarking of the *f*CO₂-products with independent data generally shows low and
1842 consistent biases and RMSEs, with the exception of the comparison with SOCAT flag E data in the
1843 tropics where the biases range from -6.6 µatm in JMA-MLR to -10.29 µatm in OceanSODA_ETHv2,
1844 (Figure S7) and the Northern Hemisphere, where biases range from -2.68 µatm in VLIZ-SOMFFN to -
1845 40.47 µatm in UExp-FNN-U (Figure S7), although with few measurements covering the latter area.
1846 Furthermore, we evaluate the trends derived from a subset of *f*CO₂-products by subsampling five
1847 GOBMs used in Friedlingstein et al. (2023; covering the period up to the year 2022) following the

1859 approach of Hauck et al. (2023a) and evaluating the air-sea CO₂ flux trend for the 2001-2021 period,
1860 i.e. the period of strong divergence in the air-sea CO₂ exchange excluding the tail effect, against trend
1861 biases identified by the GOBM reconstruction. The results indicate a relationship between
1862 reconstruction bias and strength of the decadal trends (Figure S8), indicating a tendency of the f_{CO_2} -
1863 products ensemble to overestimate the air-sea CO₂ flux trends in agreement with Mayot et al. (2024).
1864 [This relationship, however, remains uncertain and its sensitivity to the GOBM used needs further](#)
1865 [investigation.](#)

1866 3.7 Land Sink

1867 3.7.1 Historical period 1850-2024

1868 Cumulated since 1850, the terrestrial carbon sink S_{LAND} amounts to 175 ± 50 GtC, 24% of total
1869 anthropogenic emissions, with more than two thirds of this amount (120 ± 40 GtC) being taken up by
1870 the terrestrial ecosystems since 1959. Over the historical period, the land sink increased in pace with the
1871 anthropogenic emissions exponential increase (Figure 3). As described in section 2, S_{LAND} estimate now
1872 includes the RSS correction.

1873 3.7.2 Recent period 1959-2024

1874 S_{LAND} increased from 0.9 ± 0.3 GtC yr⁻¹ in the 1960s to 2.4 ± 0.8 GtC yr⁻¹ during 2015-2024, with
1875 important interannual variations of up to 2 GtC yr⁻¹ generally showing a decreased land sink during El
1876 Niño events (Figure 10a), responsible for the corresponding enhanced growth rate in atmospheric CO₂
1877 concentration. The larger land CO₂ sink during 2015-2024 compared to the 1960s is reproduced by all
1878 the DGVMs in response to the increase in both atmospheric CO₂, nitrogen deposition, and the changes
1879 in climate, and is broadly consistent with the residual estimated from the other budget terms, [that is](#)
1880 [E_{FOS}+E_{LUC}-G_{ATM}-S_{OCEAN} which amounts to 2.4 GtC for the last decade \(See Table 5\). As described in](#)
1881 [section 2.6.1, S_{LAND} is now corrected for the Replaced Sinks and Sources \(RSS\) bias. Compared to the](#)
1882 [uncorrected estimate, S_{LAND} is reduced by 0.6 GtC yr⁻¹ for the 2015-2024 period.](#)

1883 Over the historical period, the increase in the global terrestrial CO₂ sink is largely attributed to the CO₂
1884 fertilisation effect (Prentice et al., 2001, Piao et al., 2009, Schimel et al., 2015) and increased nitrogen
1885 deposition (Huntzinger et al., 2017, O'Sullivan et al., 2019), directly stimulating plant photosynthesis
1886 and increased plant water use in water limited systems, with a smaller negative contribution of climate
1887 change (Figure 12). There is a range of evidence to support a positive terrestrial carbon sink in response
1888 to increasing atmospheric CO₂ (Walker et al., 2021), including a new synthesis of free-air CO₂-
1889 enrichment experiments across forests and ages, which concluded that Net Primary Productivity
1890 increased by 22% for a common 41% CO₂ enrichment (Norby 2025). As expected from theory, the
1891 greatest CO₂ effect is simulated in the tropical forest regions, associated with warm temperatures and

Formatted: Outline numbered + Level: 2 + Numbering
Style: 1, 2, 3, ... + Start at: 1 + Alignment: Left + Aligned at:
0 cm + Indent at: 1.02 cm

Formatted: Outline numbered + Level: 3 + Numbering
Style: 1, 2, 3, ... + Start at: 1 + Alignment: Left + Aligned at:
0 cm + Indent at: 1.27 cm

Formatted: Outline numbered + Level: 3 + Numbering
Style: 1, 2, 3, ... + Start at: 1 + Alignment: Left + Aligned at:
0 cm + Indent at: 1.27 cm

Deleted: (E_{FOS}+E_{LUC}-G_{ATM}-S_{OCEAN}, Table 5).

1893 long growing seasons (Hickler et al., 2008) (Figure 12a). However, evidence from tropical intact forest
1894 plots indicate an overall decline in the land sink across Amazonia (1985-2011), attributed to enhanced
1895 mortality offsetting productivity gains (Brienen et al., 2015, Hubau et al., 2020). During 2015-2024 the
1896 land sink is positive in all regions (Figure 6d) with the exception of eastern Brazil, Bolivia, northern
1897 Venezuela, Southwest USA, central Europe and Central Asia, North and South Africa, and eastern
1898 Australia, where the negative effects of climate variability and change (i.e. reduced rainfall and/or
1899 increased temperature) counterbalance CO₂ effects. This is clearly visible in Figure 12 where the effects
1900 of CO₂ (Figure 12a) and climate (Figure 12b) as simulated by the DGVMs are isolated (see also Figure
1901 S12). The negative effect of climate can be seen across the globe, and is particularly strong in most of
1902 South America, Central America, Southwest US, Central Europe, western Sahel, southern Africa,
1903 Southeast Asia and southern China, and eastern Australia (Figure 12b, Figure S12). Globally, over the
1904 2015-2024 period, climate change reduces the land sink by 0.8 ± 0.7 GtC yr⁻¹ (25% of the CO₂ effect,
1905 which is 3.2 ± 1.1 GtC yr⁻¹ for the corresponding period, see Supplement S4.1).

1906 Most DGVMs have similar S_{LAND} averaged over 2015-2024, and 14/22 models fall within the 1σ range
1907 of the residual land sink [1.4 to 3.3 GtC yr⁻¹] (see Table 5), and all models but one are within the 2σ
1908 range [0.5 to 4.3 GtC yr⁻¹]. The ED model is an outlier, with a land sink estimate of 4.9 GtC yr⁻¹ for the
1909 2015-2024 period (accounting for the RSS correction), driven by a strong CO₂ fertilisation effect (6.4
1910 GtC yr⁻¹ in the CO₂ only (S1) simulation). There are no direct global observations of the land sink
1911 (S_{LAND}), or the CO₂ fertilisation effect, and so we are not yet in a position to rule out models based on
1912 component fluxes if their net land sink (S_{LAND}-E_{LUC}) is within the observational uncertainty provided by
1913 O₂ measurements. The important role of non-living carbon pools in carbon budgets has also been
1914 recently highlighted from an Earth-observation (EO) perspective, where contrary to DGVMs, EO
1915 products do not show an increase in biomass, thus inferring a larger role of dead carbon in land carbon
1916 cycle dynamics (Bar-On et al., 2025).

1917 Since 2020 the globe has experienced La Niña conditions which would be expected to lead to an
1918 increased land carbon sink. This 3-year long period of La Niña conditions came to an end by the second
1919 half of 2023 and transitioned to an El Niño which lasted until mid-2024. A clear transition from
1920 maximum to a minimum in the global land sink is evident in S_{LAND}, from 2022 to 2023 and we find that
1921 an El Niño-driven decrease in tropical land sink is offset by a smaller increase in the high-latitude land
1922 sink. In the past years several regions experienced record-setting fire events (see also section 3.8.3).
1923 While global burned area has declined over the past decades mostly due to declining fire activity in
1924 savannas (Andela et al., 2017), forest fire emissions are rising and have the potential to counter the
1925 negative fire trend in savannas (Zheng et al., 2021). Noteworthy extreme fire events include the 2019-
1926 2020 Black Summer event in Australia (emissions of roughly 0.2 GtC; van der Velde et al., 2021),
1927 Siberia in 2021, where emissions approached 0.4 GtC or three times the 1997-2020 average according
1928 to GFED4s, Canada in 2023 and 2024 (Byrne et al., 2024), and unprecedented wildfires in Brazil and

1929 Bolivia in 2024 (partly related to land-use activity, see Sec. 3.2.3 and 3.2.4) (Bourgoin et al., 2025),
1930 partially offset by a negative trend in wildfire over Northern Hemisphere Africa. While other regions,
1931 including Western US and Mediterranean Europe, also experienced intense fire seasons in 2021 their
1932 emissions are substantially lower.

1933 Despite these regional negative effects of climate change on S_{LAND} , the efficiency of land to remove
1934 anthropogenic CO_2 emissions has remained broadly constant over the last six decades at around 23%
1935 (including the RSS correction) (Figure S16).

1936 3.7.3 Final year 2024

1937 The terrestrial CO_2 sink from the DGVMs ensemble S_{LAND} was 1.9 ± 0.9 GtC in 2024, 37% below the
1938 2022 La Niña induced strong sink of 3.1 ± 1.0 GtC, and also below the 2015-2024 average of 2.4 ± 0.8
1939 GtC yr^{-1} (Figure 4e, Table 7). We estimate that the 2024 land sink was the lowest since 2015. The
1940 severe reduction in the land sink in 2024 is likely driven by the El Niño conditions, leading to a 66%
1941 reduction in S_{LAND} in the tropics (30N-30S) from 2.8 GtC in 2022 to 1.0 GtC in 2024. This is combined
1942 with intense wildfires in Canada, Bolivia and Brazil that led to a significant CO_2 source (see also
1943 Section 3.8.3). We note that the S_{LAND} estimate for 2024 of 1.9 ± 0.9 GtC is much larger than the $0.3 \pm$
1944 1.0 GtC yr^{-1} estimate from the residual sink from the global budget ($E_{FOS} + E_{LUC} - G_{ATM} - S_{OCEAN}$, Table 5),
1945 although the residual sink would be substantially larger (at around 1.4 GtC yr^{-1}) if using the satellite-
1946 based GRESO in this equation. A large budget imbalance is often associated with El Niño years (e.g.
1947 1986/87, 1997/98, 2005/06, 2023/24), and the possible underestimation in DGVMs of the tropical land
1948 [carbon losses](#) in response to drought, high temperature extremes, and fires. Few DGVMs have explicit
1949 representation of drought-mortality and only 8 from 22 include some form of forest demography,
1950 although recent efforts are underway to fill these critical research gaps (Eckes-Shephard et al., 2025
1951 Yao et al., 2022, 2023).

1952 ~~An overestimate in S_{LAND} in 2024 can in part be attributed to the inability in DGVMs to reproduce~~
1953 ~~extreme fire emissions in 2024. Globally fire emissions as calculated by GFED were 0.43 GtC $_{yr^{-1}}$~~
1954 ~~higher in 2024 compared to the decadal average (2015-2024), similar to the anomaly in 2023 (0.44 GtC~~
1955 ~~$_{yr^{-1}}$). This was mainly due to an increase in fire over forests in Boreal North America (0.16 GtC $_{yr^{-1}}$)~~
1956 ~~and forests, savannahs and grasslands over Southern Hemisphere South America (0.35 GtC $_{yr^{-1}}$) in~~
1957 ~~2024, partly offset by a negative trend in fires over Northern Hemisphere Africa (-0.05 GtC $_{yr^{-1}}$~~
1958 ~~anomaly). In fact, across the Amazon basin emissions from degradation fires (two thirds Brazil, one~~
1959 ~~third Bolivia) surpassed those from deforestation fires in 2024 (Bourgoin et al., 2025). In contrast~~
1960 ~~DGVMs simulate an anomaly of 0.2 GtC $_{yr^{-1}}$ in 2024, i.e. an underestimate of 0.23 GtC $_{yr^{-1}}$ in fire~~
1961 ~~emissions for 2024. [Fire enabled DGVMs do simulate a larger reduction in \$S_{LAND}\$ in 2024 compared to](#)~~
1962 ~~[non-fire models \(\$0.6\$ vs \$0.3\$ GtC\), indicating the importance of representing fire extremes when](#)~~
1963 ~~[explaining reductions in the land sink.](#)~~

Formatted: Outline numbered + Level: 3 + Numbering
Style: 1, 2, 3, ... + Start at: 1 + Alignment: Left + Aligned at:
0 cm + Indent at: 1.27 cm

Deleted: and

Deleted:

Deleted: /

Deleted: /

Deleted: /

Deleted: /

Deleted: /

Deleted: /

Deleted: /

1973 Finally, a large uncertainty relates to climate forcing datasets, particularly over the critical carbon-rich
1974 tropical forest regions with poor coverage of meteorological stations. For example, there are large
1975 differences in climate forcing (e.g. CRUJRA-3Q and ERA5) and downstream DGVM carbon
1976 simulations over the Congo basin and tropical central and northern Africa in 2024 (Ke et al., 2025).

1977 3.7.4 Year 2025 projection

1978 Calculating the land sink as the residual of the other projections for 2025, we project a land sink of 3.1
1979 GtC for 2025, 1.1 GtC larger than the 2024 estimate, consistent with an expected recovery of the land
1980 sink after an El Niño event. The ESMS do not provide an additional estimate of S_{LAND} as they only
1981 simulate the net atmosphere-land carbon flux ($S_{LAND-ELUC}$).

1982 3.7.5 Evaluation of land models

1983 The evaluation of the DGVMs shows generally higher agreement across models for runoff, and to a
1984 lesser extent for GPP, and ecosystem respiration. These conclusions are supported by a more
1985 comprehensive analysis of DGVM performance in comparison with benchmark data (Sitch et al.,
1986 2024). A relative comparison of DGVM performance (Figure S11) suggests several DGVMs (CABLE-
1987 POP, CLASSIC, OCN, ORCHIDEE) may outperform others at multiple carbon and water cycle
1988 benchmarks. However, results from Seiler et al., 2022, also show how DGVM differences are often of
1989 similar magnitude compared with the range across observational datasets. All models score high
1990 enough over the metrics tests to support their use here. There are a few anomalously low scores for
1991 individual metrics from a single model, and these can direct the effort to improve models for use in
1992 future budgets (See also Supplement S.4.2).

1993 3.8 Partitioning the carbon sinks

1994 3.8.1 Global sinks and spread of estimates

1995 In the period 2015-2024, the bottom-up view of global net ocean and land carbon sinks provided by the
1996 GCB, S_{OCEAN} for the ocean and $S_{LAND-ELUC}$ for the land, agrees closely with the top-down global
1997 carbon sinks delivered by the atmospheric inversions. This is shown in Figure 13, which visualises the
1998 individual decadal mean atmosphere-land and atmosphere-ocean fluxes from each, along with the
1999 constraints on their sum offered by the global fossil CO_2 emissions flux minus the atmospheric growth
2000 rate ($E_{FOS} - G_{ATM}$, 4.2 ± 0.5 Gt C yr⁻¹, Table 7, shown as diagonal line in Figure 13). The GCB estimate
2001 for net atmosphere-to-surface flux ($S_{OCEAN} + S_{LAND-ELUC}$) during 2015-2024 is 4.2 ± 1.1 Gt C yr⁻¹
2002 (Table 7), implying a zero budget imbalance (B_{IM}) (see Section 3.9). The atmospheric inversions
2003 estimate of the net atmosphere-to-surface flux during 2015-2024 is 4.3 Gt C yr⁻¹, with a < 0.1 Gt C yr⁻¹
2004 imbalance, and thus scatter across the diagonal, with inverse models trading land for ocean fluxes in

Formatted: Outline numbered + Level: 3 + Numbering
Style: 1, 2, 3, ... + Start at: 1 + Alignment: Left + Aligned at:
0 cm + Indent at: 1.27 cm

Formatted: Outline numbered + Level: 3 + Numbering
Style: 1, 2, 3, ... + Start at: 1 + Alignment: Left + Aligned at:
0 cm + Indent at: 1.27 cm

Formatted: Outline numbered + Level: 2 + Numbering
Style: 1, 2, 3, ... + Start at: 1 + Alignment: Left + Aligned at:
0 cm + Indent at: 1.02 cm

Formatted: Indent: Left: 0 cm, First line: 0 cm, Outline
numbered + Level: 3 + Numbering Style: 1, 2, 3, ... + Start
at: 1 + Alignment: Left + Aligned at: 0 cm + Indent at: 1.27
cm

2005 their solution. The independent constraint on the net atmosphere-to-surface flux based on atmospheric
2006 O₂ by design also closes the balance and is 4.2 ± 0.9 GtC yr⁻¹ over the 2015-2024 period (orange
2007 symbol on Figure 13), while the ESMs estimate for the net atmosphere-to-surface flux over that period
2008 is $4.8 [2.4, 6.0]$ GtC yr⁻¹ (Tables 5 and 6).

2009 The distributions based on the individual models and f CO₂-products reveal substantial spread but
2010 converge near the decadal means quoted in Tables 5 to 7. Sink estimates for S_{OCEAN} are mostly non-
2011 Gaussian, while the ensemble of DGVMs and inverse models appears more normally distributed
2012 justifying the use of a multi-model mean and standard deviation for their errors in the budget.
2013 Noteworthy is that the tails of the distributions provided by the land and ocean bottom-up estimates
2014 would not agree with the global constraint provided by the fossil fuel emissions and the observed
2015 atmospheric CO₂ growth rate. This illustrates the power of the atmospheric joint constraint from the
2016 global CO₂ observation capacity.

2017 3.8.1.1 Net atmosphere-to-land flux

2018 The GCB estimate of the net atmosphere-to-land flux (S_{LAND} – E_{LUC}), calculated as the difference
2019 between S_{LAND} from the DGVMs and E_{LUC} from the bookkeeping models, amounts to a 1.0 ± 1.0 GtC
2020 yr⁻¹ sink during 2015-2024 (Table 5). The estimate of net atmosphere-to-land flux (S_{LAND} – E_{LUC}) from
2021 the DGVMs alone (1.4 ± 0.7 GtC yr⁻¹, Table 5, green symbols on Figure 13) is slightly larger, although
2022 within the uncertainty of the GCB estimate and also within uncertainty of the global carbon budget
2023 constraint (E_{FOS} – G_{ATM} – S_{OCEAN}, 1.0 ± 0.6 GtC yr⁻¹; Table 7). Also, for 2015-2024, the inversions
2024 estimate the net atmosphere-to-land flux is a 1.3 ± 0.3 GtC yr⁻¹ sink, similar to the mean of the DGVMs
2025 estimates (purple versus grey symbols on Figure 13). The independent constraint based on atmospheric
2026 O₂ is slightly lower, 0.7 ± 0.8 GtC yr⁻¹ (orange symbol in Figure 13), although its uncertainty overlaps
2027 with the uncertainty range from other approaches. Last, the ESMs estimate for the net atmosphere-to-
2028 land flux during 2014-2023 is a $2.3 [-0.1, 3.6]$ GtC yr⁻¹ sink, larger than all other estimates (Table 5).

2029 As discussed in Section 3.5.3, the atmospheric growth rate of CO₂ derived from the NOAA surface
2030 stations was very high in 2024, 7.9 GtC (3.73 ppm) the largest on the 65 years long observational
2031 record. Both DGVMs and inversions assign this large CO₂ growth rate to a continued reduction of the
2032 net atmosphere to land flux since 2023, in particular in the tropics (Figures 11 and 14), especially
2033 pronounced in the inversions. DGVMs simulate a 2024 global net atmosphere-to-land flux of 1.1 GtC
2034 yr⁻¹, a 50% decline relative to the 2.2 GtC yr⁻¹ sink in 2022, primarily driven by the severe reduction in
2035 S_{LAND} (-37%, see Section 3.7.3). The tropics (30°N-30°S) are recording a dramatic decrease in the net
2036 atmosphere-to-land flux from a 1.3 GtC yr⁻¹ sink in 2022 to a 0.2 GtC yr⁻¹ source in 2024. The
2037 atmospheric inversions show a continued reduction with the global net atmosphere-to-land flux
2038 declining from 2.9 GtC yr⁻¹ in 2022 to 0.8 GtC yr⁻¹ in 2023 to 0.2 GtC yr⁻¹ in 2024 (-94% from 2022 to
2039 2024), with the tropics turning from a 1.3 GtC yr⁻¹ sink in 2022 to a 1.2 GtC yr⁻¹ source in 2024. [This](#)

Formatted: Indent: Left: 0 cm, First line: 0 cm, Outline numbered + Level: 4 + Numbering Style: 1, 2, 3, ... + Start at: 1 + Alignment: Left + Aligned at: 0 cm + Indent at: 1.52 cm

2040 [discrepancy between the DGVMs and inversions estimates of the tropical and hence global atmosphere-](#)
2041 [land flux largely explains the negative \$B_M\$ in 2024, \(see also Section 3.8.2.2 below\).](#)

2042 3.8.1.2 Net atmosphere-to-ocean flux

2043 For the 2015-2024 period, the GOBMs ($2.7 \pm 0.4 \text{ GtC yr}^{-1}$) produce a lower estimate [of the ocean sink](#)
2044 [than the \$f\text{CO}_2\$ -products with \$3.3 \[2.9, 3.8\] \text{ GtC yr}^{-1}\$, which shows up in Figure 13 as separate peaks in](#)
2045 [the distribution from the GOBMs \(dark blue symbols\) and from the \$f\text{CO}_2\$ -products \(light blue symbols\).](#)
2046 Atmospheric inversions ($3.0 \pm 0.3 \text{ GtC yr}^{-1}$) suggest an ocean uptake more in line with the average of
2047 the GOBMs and $f\text{CO}_2$ -products for the recent decade (Table 6). The inversions are not fully
2048 independent as 7 out of 14 inversions covering the last decade use $f\text{CO}_2$ -products as ocean priors and
2049 one uses a GOBM (Table S4). The independent constraint based on atmospheric O_2 ($3.5 \pm 0.5 \text{ GtC yr}^{-1}$)
2050 ¹) is at the high end of the distribution of the other methods. However, as mentioned in section 2.8, the
2051 O_2 method requires a correction for global air-sea O_2 flux, which induces a non-negligible uncertainty
2052 on the decadal estimates (about 0.5 GtC yr^{-1}). The large growth in the ocean carbon sink from O_2 is
2053 compatible with the GOBMs and $f\text{CO}_2$ -products estimates when accounting for their uncertainty ranges.
2054 Lastly, the ESMs estimate, $2.5 [2.2, 2.8] \text{ GtC yr}^{-1}$, suggest a lower average ocean carbon sink than the
2055 other estimates. We caution that the riverine transport of carbon taken up on land and outgassing from
2056 the ocean, accounted for here, is a substantial ($0.65 \pm 0.3 \text{ GtC yr}^{-1}$) and uncertain term (Crisp et al.,
2057 2022; Gruber et al., 2023; DeVries et al., 2023) that separates the GOBMs, ESMs and oxygen-based
2058 estimates on the one hand from the $f\text{CO}_2$ -products and atmospheric inversions on the other hand.

2059 3.8.2 Regional partitioning

2060 Figure 14 shows the latitudinal partitioning of the global atmosphere-to-ocean (S_{OCEAN}), atmosphere-to-
2061 land ($S_{\text{LAND}} - E_{\text{LUC}}$), and their sum ($S_{\text{OCEAN}} + S_{\text{LAND}} - E_{\text{LUC}}$) according to the estimates from GOBMs
2062 and ocean $f\text{CO}_2$ -products (S_{OCEAN}), DGVMs ($S_{\text{LAND}} - E_{\text{LUC}}$), and from atmospheric inversions (S_{OCEAN}
2063 and $S_{\text{LAND}} - E_{\text{LUC}}$). S_{OCEAN} estimates were not [corrected](#) for the regional analysis.

2064 3.8.2.1 North

2065 Despite being one of the most densely observed and studied regions of our globe, annual mean carbon
2066 sink estimates in the northern extra-tropics (north of 30°N) continue to differ. The atmospheric
2067 inversions suggest an atmosphere-to-surface sink ($S_{\text{OCEAN}} + S_{\text{LAND}} - E_{\text{LUC}}$) for 2015-2024 of 2.7 ± 0.4
2068 GtC yr^{-1} , which is higher than the process models' estimate of $2.0 \pm 0.4 \text{ GtC yr}^{-1}$ (Figure 14). The
2069 GOBMs ($1.1 \pm 0.2 \text{ GtC yr}^{-1}$), $f\text{CO}_2$ -products ($1.4 [1.2-1.6] \text{ GtC yr}^{-1}$), and inversion systems (1.2 ± 0.1
2070 GtC yr^{-1}) produce largely consistent estimates of the ocean sink. However, the larger flux in the $f\text{CO}_2$ -
2071 products may be related to data sparsity (Mayot et al., 2024). Thus, the difference mainly arises from

Formatted: Indent: Left: 0 cm, First line: 0 cm, Outline numbered + Level: 4 + Numbering Style: 1, 2, 3, ... + Start at: 1 + Alignment: Left + Aligned at: 0 cm + Indent at: 1.52 cm

Deleted: unadjusted

Deleted: for S_{OCEAN}

Deleted: unadjusted

Formatted: Indent: Left: 0 cm, First line: 0 cm, Outline numbered + Level: 3 + Numbering Style: 1, 2, 3, ... + Start at: 1 + Alignment: Left + Aligned at: 0 cm + Indent at: 1.27 cm

Deleted: adjusted

Formatted: Indent: Left: 0 cm, First line: 0 cm, Outline numbered + Level: 4 + Numbering Style: 1, 2, 3, ... + Start at: 1 + Alignment: Left + Aligned at: 0 cm + Indent at: 1.52 cm

2076 the net land flux ($S_{\text{LAND}} - E_{\text{LUC}}$) estimate, which is $0.9 \pm 0.3 \text{ GtC yr}^{-1}$ in the DGVMs compared to $1.5 \pm$
2077 0.4 GtC yr^{-1} in the atmospheric inversions (Figure 14, second row).

2078 Discrepancies in the northern land fluxes conform with persistent issues surrounding the quantification
2079 of the drivers of the global net land CO_2 flux (Armeth et al., 2017; Huntzinger et al., 2017; O’Sullivan et
2080 al., 2022) and the distribution of atmosphere-to-land fluxes between the tropics and high northern
2081 latitudes (Baccini et al., 2017; Schimel et al., 2015; Stephens et al., 2007; Ciais et al., 2019; Gaubert et
2082 al., 2019; O’Sullivan et al. 2024).

2083 In the northern extra-tropics, the process models, inversions, and f_{CO_2} -products consistently suggest
2084 that most of the interannual variability stems from the land (Figure 14). Inversions generally agree on
2085 the magnitude of interannual variations (IAV) over land, more so than DGVMs ($0.27\text{-}0.38$ vs $0.07\text{-}0.55$
2086 GtC yr^{-1} , averaged over 1990-2024).

2087 3.8.2.2 Tropics

2088 In the tropics ($30^\circ\text{S}\text{-}30^\circ\text{N}$), both the atmospheric inversions and process models estimate a net carbon
2089 balance ($S_{\text{OCEAN}} + S_{\text{LAND}} - E_{\text{LUC}}$) that is relatively close to neutral over the past decade (inversions: 0.05
2090 $\pm 0.5 \text{ GtC yr}^{-1}$, process models: $0.4 \pm 0.6 \text{ GtC yr}^{-1}$). The GOBMs ($-0.003 \pm 0.3 \text{ GtC yr}^{-1}$), f_{CO_2} -products
2091 ($0.3 [0.1, 0.6] \text{ GtC yr}^{-1}$), and inversion systems ($0.3 \pm 0.1 \text{ GtC yr}^{-1}$) indicate a neutral to positive tropical
2092 ocean flux (see Figure S5 for spatial patterns). DGVMs indicate a net land sink ($S_{\text{LAND}} - E_{\text{LUC}}$) of 0.4
2093 $\pm 0.5 \text{ GtC yr}^{-1}$, whereas the inversion systems indicate a small source in the net land flux although with
2094 larger model spread ($-0.2 \pm 0.6 \text{ GtC yr}^{-1}$, Figure 14, third row).

2095 A continuing conundrum is the partitioning of the global atmosphere-land flux between the Northern
2096 Hemisphere land and the tropical land (Stephens et al., 2017; Pan et al., 2011; Gaubert et al., 2019). It is
2097 of importance because each region has its own history of land-use change, climate drivers, and impact
2098 of increasing atmospheric CO_2 and nitrogen deposition. Quantifying the magnitude of each sink is a
2099 prerequisite to understanding how each individual driver impacts the tropical and mid/high-latitude
2100 carbon balance. We define the North-South (N-S) difference as net atmosphere-land flux north of 30°N
2101 minus the net atmosphere-land flux south of 30°N . For the inversions, the N-S difference is 1.7 ± 1.0
2102 GtC yr^{-1} across this year’s inversion ensemble. In the ensemble of DGVMs the N-S difference is $0.6 \pm$
2103 0.5 GtC yr^{-1} , a much narrower range than the one from atmospheric inversions. The smaller spread
2104 across DGVMs than across inversions is to be expected as there is no correlation between Northern and
2105 Tropical land sinks in the DGVMs as opposed to the inversions where the sum of the two regions being
2106 well-constrained by atmospheric observations leads to an anti-correlation between these two regions.

2107 The tropical lands are the origin of most of the atmospheric CO_2 interannual variability (Ahlström et al.,
2108 2015), consistently among the process models and inversions (Figure 14). The interannual variability in

Formatted: Indent: Left: 0 cm, First line: 0 cm, Outline numbered + Level: 4 + Numbering Style: 1, 2, 3, ... + Start at: 1 + Alignment: Left + Aligned at: 0 cm + Indent at: 1.52 cm

2109 the tropics is similar among the ocean $f\text{CO}_2$ -products (0.06-0.18 GtC yr^{-1}) and the GOBMs (0.07-0.16
2110 GtC yr^{-1}). The DGVMs and inversions indicate that atmosphere-to-land CO_2 fluxes are more variable
2111 than atmosphere-to-ocean CO_2 fluxes in the tropics, with interannual variability of 0.3 to 1.13 and 0.96
2112 GtC yr^{-1} for DGVMs and inversions, respectively for 1990-2024. The year 2024 saw the largest growth
2113 rate in the atmosphere so far, largely caused by reductions in the tropical land sink, similar to earlier
2114 extreme years, such as during the 2015-2016 El Niño period. The inversions seem to capture the
2115 response of the tropical land sink to a larger degree than the DGVMs, with a 2024 tropical land source
2116 of $1.2 \pm 0.9 \text{ GtC yr}^{-1}$ for the inversions versus a 0.2 ± 0.7 sink for the DGVMs.

2117 3.8.2.3 South

2118 In the southern extra-tropics (south of 30°S), the atmospheric inversions suggest a net atmosphere-to-
2119 surface sink ($\text{SOCEAN} + \text{SLAND-ELUC}$) for 2015-2024 of $1.6 \pm 0.2 \text{ GtC yr}^{-1}$, similar to the process models'
2120 estimate of $1.5 \pm 0.4 \text{ GtC yr}^{-1}$ (Figure 14). An approximately neutral net land flux (SLAND-ELUC) for the
2121 southern extra-tropics is estimated by both the DGVMs ($0.05 \pm 0.1 \text{ GtC yr}^{-1}$) and the inversion systems
2122 ($0.01 \pm 0.1 \text{ GtC yr}^{-1}$). This means nearly all carbon uptake is due to oceanic sinks south of 30°S . The
2123 Southern Ocean flux in the $f\text{CO}_2$ -products ($1.6 [1.5, 1.9 \text{ GtC}] \text{ yr}^{-1}$) and inversion estimates (1.6 ± 0.2
2124 GtC yr^{-1}) is marginally higher than in the GOBMs ($1.5 \pm 0.4 \text{ GtC yr}^{-1}$) (Figure 14, bottom row). This
2125 agreement is subject to the choice of the river flux adjustment (Lacroix et al., 2020, Hauck et al.,
2126 2023b). Nevertheless, the time-series of atmospheric inversions and $f\text{CO}_2$ -products diverge from the
2127 GOBMs. A substantial overestimation of the trends in the $f\text{CO}_2$ -products could be explained by sparse
2128 and unevenly distributed observations, especially in wintertime (Figure S5; Hauck et al., 2023a; Gloege
2129 et al., 2021). Model biases likely contribute as well, with biases in mode water formation, stratification,
2130 and the chemical buffer capacity known to play a role in Earth System Models (Terhaar et al., 2021,
2131 Bourgeois et al., 2022, Terhaar et al., 2022).

2132 The interannual variability in the southern extra-tropics is low because of the dominance of ocean areas
2133 with low variability compared to land areas. The split between land (SLAND-ELUC) and ocean (SOCEAN)
2134 shows a substantial contribution to variability in the south coming from the land, with no consistency
2135 between the DGVMs and the inversions or among inversions. This is expected due to the difficulty of
2136 separating exactly the land and oceanic fluxes when viewed from atmospheric observations alone. The
2137 SOCEAN interannual variability was found to be higher in the $f\text{CO}_2$ -products (0.04 - 0.18 GtC yr^{-1})
2138 compared to GOBMs (0.03 to 0.06 GtC yr^{-1}) in 1990-2024. Inversions give an interannual variability
2139 of 0.13 to 0.15 GtC yr^{-1} . Model subsampling experiments recently illustrated that $f\text{CO}_2$ -products may
2140 overestimate decadal variability in the Southern Ocean carbon sink by 30% and the trend since 2000 by
2141 50-130% due to data sparsity, based on one and two $f\text{CO}_2$ -products with strong variability (Gloege et
2142 al., 2021, Hauck et al., 2023a). The trend benchmark test using the method of Hauck et al., (2023a) and
2143 a subset of 6 $f\text{CO}_2$ -products confirms the sensitivity of the decadal trends in $f\text{CO}_2$ -products to

Formatted: Indent: Left: -0.08 cm, Hanging: 0.08 cm,
Outline numbered + Level: 4 + Numbering Style: 1, 2, 3, ...
+ Start at: 1 + Alignment: Left + Aligned at: 0 cm + Indent
at: 1.52 cm

2144 reconstruction biases, particularly in the Southern Ocean, indicating an overestimation of the ensemble
2145 mean trend (See Supplement S.3.4). However, we also find compensating positive biases in the
2146 ensemble so that the ensemble mean bias is smaller than the bias from some individual $f\text{CO}_2$ -products.

2147 3.8.2.4 RECCAP2 regions

2148 Aligning with the RECCAP-2 initiative (Ciais et al., 2022; Poulter et al., 2022; DeVries et al., 2023),
2149 we provide a breakdown of this GCB paper estimate of the E_{LUC} , S_{LAND} , Net land ($S_{\text{LAND}} - E_{\text{LUC}}$), and
2150 S_{OCEAN} fluxes over the 10 land, and 5 ocean RECCAP-2 regions, averaged over the period 2015-2024
2151 (Figure 15). The DGVMs and inversions suggest a positive net land sink in all regions, except for South
2152 America, Africa, and Southeast Asia, where the inversions indicate a small net source of respectively -
2153 $0.1 \pm 0.5 \text{ GtC yr}^{-1}$, $-0.3 \pm 0.3 \text{ GtC yr}^{-1}$, and $-0.1 \pm 0.3 \text{ GtC yr}^{-1}$ compared to a small sink of $0.1 \pm 0.3 \text{ GtC}$
2154 yr^{-1} , $0.1 \pm 0.3 \text{ GtC yr}^{-1}$, and $0.03 \pm 0.1 \text{ GtC yr}^{-1}$ for the DGVMs. The uncertainty in the sign of net
2155 tropical carbon fluxes is driven by opposing gross fluxes and relatively large uncertainty in the gross
2156 fluxes themselves. For South America, DGVMs estimate S_{LAND} of $0.4 \pm 0.4 \text{ GtC yr}^{-1}$ and E_{LUC} of
2157 $0.3 \pm 0.2 \text{ GtC yr}^{-1}$. Bookkeeping models suggest a larger E_{LUC} source of around 0.5 GtC yr^{-1} . Similarly,
2158 in Southeast Asia, the DGVMs estimate an E_{LUC} of $0.2 \pm 0.1 \text{ GtC yr}^{-1}$, compared with the bookkeeping
2159 model estimate of $0.4 \pm 0.02 \text{ GtC yr}^{-1}$. Therefore, DGVMs may underestimate E_{LUC} in these regions,
2160 which could explain the net sink discrepancy with inversions. In Africa, E_{LUC} is similar for DGVMs and
2161 bookkeeping models (-0.4 GtC yr^{-1}), and DGVMs estimate an S_{LAND} of $0.5 \pm 0.2 \text{ GtC yr}^{-1}$.

2162 The inversions suggest the largest net land sinks are located in North America ($0.4 \pm 0.3 \text{ GtC yr}^{-1}$),
2163 Russia ($0.6 \pm 0.2 \text{ GtC yr}^{-1}$), Europe ($0.3 \pm 0.2 \text{ GtC yr}^{-1}$), and East Asia ($0.2 \pm 0.3 \text{ GtC yr}^{-1}$). This agrees
2164 well with the DGVMs in North America ($0.4 \pm 0.1 \text{ GtC yr}^{-1}$), which indicate a large natural land sink
2165 (S_{LAND}) of $0.4 \pm 0.2 \text{ GtC yr}^{-1}$, and near-zero net land-use related carbon losses ($0.02 \pm 0.1 \text{ GtC yr}^{-1}$). The
2166 DGVMs suggest a smaller net land sink in Russia compared to inversions ($0.3 \pm 0.1 \text{ GtC yr}^{-1}$), and a
2167 similar net sink in East Asia ($0.2 \pm 0.1 \text{ GtC yr}^{-1}$).

2168 There is generally a higher level of agreement in the estimates of regional S_{OCEAN} between the different
2169 data streams (GOBMs, $f\text{CO}_2$ -products and atmospheric inversions) on decadal scale, compared to the
2170 agreement between the different land flux estimates. All data streams agree that the largest contribution
2171 to S_{OCEAN} stems from the Southern Ocean due to a combination of high flux density and large surface
2172 area, but with important contributions also from the Atlantic (high flux density) and Pacific (large area)
2173 basins. In the Southern Ocean, GOBMs suggest a sink of $1.1 \pm 0.4 \text{ GtC yr}^{-1}$, in line with the $f\text{CO}_2$ -
2174 products ($1.1 [1.0, 1.2] \text{ GtC yr}^{-1}$) and atmospheric inversions ($1.1 \pm 0.2 \text{ GtC yr}^{-1}$). There is similar
2175 agreement in the Pacific Ocean, with GOBMs, $f\text{CO}_2$ -products, and atmospheric inversions indicating a
2176 sink of $0.6 \pm 0.1 \text{ GtC yr}^{-1}$, $0.7 [0.6, 0.9] \text{ GtC yr}^{-1}$, and $0.6 \pm 0.2 \text{ GtC yr}^{-1}$, respectively. However, in the

Formatted: Indent: Left: 0 cm, First line: 0 cm, Outline numbered + Level: 4 + Numbering Style: 1, 2, 3, ... + Start at: 1 + Alignment: Left + Aligned at: 0 cm + Indent at: 1.52 cm

2177 Atlantic Ocean, GOBMs simulate a sink of $0.5 \pm 0.1 \text{ GtC yr}^{-1}$, noticeably lower than both the $f\text{CO}_2$ -
2178 products ($0.8 [0.7, 0.9] \text{ GtC yr}^{-1}$) and atmospheric inversions ($0.8 \pm 0.1 \text{ GtC yr}^{-1}$). It is important to note
2179 the $f\text{CO}_2$ -products and atmospheric inversions have a substantial and uncertain river flux adjustment in
2180 the Atlantic Ocean (0.3 GtC yr^{-1}) that also leads to a mean offset between GOBMs and $f\text{CO}_2$ -
2181 products/inversions in the latitude band of the tropics (Figure 14). The Indian Ocean due its smaller size
2182 and the Arctic Ocean due to its size and sea-ice cover that prevents air-sea gas-exchange are responsible
2183 for smaller but non negligible SOCEAN fluxes (Indian Ocean: $(0.3 \pm 0.1 \text{ GtC yr}^{-1}, 0.3 [0.3, 0.4] \text{ GtC yr}^{-1}$,
2184 and $0.3 \pm 0.1 \text{ GtC yr}^{-1}$ for GOBMs, $f\text{CO}_2$ -products, and atmospheric inversions, respectively, and Arctic
2185 Ocean: $(0.1 \pm 0.03 \text{ GtC yr}^{-1}, 0.2 [0.1, 0.3] \text{ GtC yr}^{-1}$, and $0.1 \pm 0.04 \text{ GtC yr}^{-1}$ for GOBMs, $f\text{CO}_2$ -products,
2186 and atmospheric inversions, respectively). Note that the SOCEAN numbers presented here deviate from
2187 numbers reported in RECCAP-2 where the net air-sea CO_2 flux is reported (i.e. without river flux
2188 adjustment for $f\text{CO}_2$ -products and inversions, and with river flux adjustment subtracted from GOBMs
2189 in most chapters, or comparing unadjusted datasets with discussion of uncertain regional riverine fluxes
2190 as major uncertainty, e.g. Sarma et al., 2023, DeVries et al., 2023).

2191 3.8.3 Fire emissions in 2025

2192 Fire emissions so far in 2025 have been below the average of recent decades, chiefly due to the lowest
2193 emissions on record since 2003 across the tropics. Figure S14 shows global and regional emissions
2194 estimates for the period 1st Jan-30th September in each year 2003-2025. Estimates derive from two
2195 global fire emissions products: the global fire emissions database (GFED, version 4.1s; van der Werf et
2196 al., 2017), and the global fire assimilation system (GFAS, operated by the Copernicus Atmosphere
2197 Service; Kaiser et al., 2012). The two products estimate that global emissions from fires were 1.2-1.4
2198 GtC (the range reflecting the difference between the two fire emission datasets, actual uncertainties are
2199 larger and estimates are likely conservative, see Chen et al. (2023)) during January-September 2025.
2200 These estimates are 19-20% below the 2015-2024 average for the same months (1.5-1.7 GtC). Both the
2201 GFED4.1s and GFAS products show the second-lowest January-September fire emissions since 2003
2202 (2022 is the lowest year in both products).

2203 Notably, the year 2025 follows two years with above-average global fire emissions (Figure S14), with
2204 global emissions through September totalling 1.7-2.1 GtC in 2023 and 1.6-2.2 GtC in 2024. These high
2205 emissions totals were caused by high emissions in North America in 2023 principally in Canada; Jones
2206 et al., 2024b), and in both North America and South America in 2024 (principally in Canada and Brazil;
2207 Kelley et al., 2025). For example, in January-September 2024, GFED4.1s suggests that global
2208 emissions totalled 2.2 GtC, the highest total on record for these months and 32% above the average for
2209 the decade prior (2014-2023); GFAS also suggests that emissions were 11% above the average for
2210 January-September).

Formatted: Indent: Left: 0 cm, First line: 0 cm, Outline numbered + Level: 3 + Numbering Style: 1, 2, 3, ... + Start at: 1 + Alignment: Left + Aligned at: 0 cm + Indent at: 1.27 cm

2211 Despite low global fire emissions so far in 2025, a pattern of extremely high fire emissions from
2212 Canada has now persisted for three consecutive years commencing with the record-breaking year in
2213 2023 (Jones et al., 2024b, Byrne et al., 2024; Kelley et al., 2025). In January-September 2025, fire
2214 emissions from Canada (0.3-0.4 GtC) were slightly greater than in the same months of 2024 (0.2-0.3
2215 GtC yr⁻¹) and around half as large as those in the same months of 2023 (0.5-0.8 GtC). The emissions
2216 totals for Canada in January-September 2025 were 2.2 times the average of January-September periods
2217 during the prior decade 2015-2024 and 4-6 times greater than the average of those months in 2003-2022
2218 [excluding the record-breaking year in 2023]; Figure S14). According to GFED4.1s, January-
2219 September fire emissions from Canada in just the past three years (1.5 GtC) exceeded the country's
2220 total January-September fire emissions throughout the 20 years prior (1.2 GtC during 2003-2022). The
2221 continued anomaly in Canada propagated to the Northern Hemisphere, where January-September 2025
2222 emissions of 0.4-0.5 GtC were 13-21% above the average of 2015-2024.

2223 Fire emissions anomalies in Africa strongly influence global fire emissions totals because the continent
2224 typically contributed near 50% of global fire emissions during 2015-2024 (average of January-
2225 September periods). For 2025, fire emissions in Africa through September were 0.4-0.6 GtC, 19-25%
2226 below the average of 2015-2024 (0.6-0.8 GtC). Synchronously, emissions through September from
2227 South America were around 0.1 GtC in both GFED4.1s and GFAS systems, less than half of the
2228 average for 2015-2024 (0.2-0.3 GtC), and emissions from Southeast Asia were around 0.05 GtC, also
2229 less than half of the average for 2015-2024 (0.1 GtC in both GFED4.1s and GFAS). Low emissions
2230 from the tropical parts of Africa, South America, and Southeast Asia contribute to low emissions across
2231 the global tropics so far in 2025 (0.7-0.9 GtC), which were only around two-thirds of the average for
2232 2015-2024 (1.1-1.3 GtC) in both GFED4.1s and GFAS.

2233 We caution that the fire emissions fluxes presented here should not be compared directly with other
2234 fluxes of the budget (e.g. S_{LAND} or E_{LUC}) due to incompatibilities between the observable fire emission
2235 fluxes and what is quantified in the S_{LAND} and E_{LUC} components of the budget. The fire emission
2236 estimates from global fire products relate to all fire types that can be observed in Earth Observations
2237 (Giglio et al., 2018; Randerson et al., 2012; Kaiser et al., 2012), including (i) fires occurring as part of
2238 natural disturbance-recovery cycles that would also have occurred in the pre-industrial period (Yue et
2239 al., 2016; Keeley and Pausas, 2019; Zou et al., 2019), (ii) fires occurring above and beyond natural
2240 disturbance-recovery cycle due to changes in climate, CO₂ and N fertilisation and to an increased
2241 frequency of extreme drought and heatwave events (Abatzoglou et al., 2019; Jones et al., 2022; Zheng
2242 et al., 2021; Burton et al., 2024), and (iii) fires occurring in relation to land use and land use change,
2243 such as deforestation fires and agricultural fires (van der Werf et al., 2010; Magi et al., 2012). In the
2244 context of the global carbon budget, fire emissions associated with (ii) should be included in the S_{LAND}
2245 component, fire emissions associated with (iii) should already be accounted for in the E_{LUC} component,
2246 while fire emissions associated with (i) should not be included in the global carbon budget as part of the

2247 natural carbon cycle. However, it is not currently possible to derive specific estimates for fluxes (i), (ii),
2248 and (iii) using global fire emission products such as GFED or GFAS. In addition, the fire emissions
2249 estimates from global fire emissions products represent a gross flux of carbon to the atmosphere,
2250 whereas the S_{LAND} component of the budget is a net flux that should also include post-fire recovery
2251 fluxes. Even if emissions from fires of type (ii) could be separated from those of type (i), these fluxes
2252 may be partially or wholly offset in subsequent years by post-fire fluxes as vegetation recovers,
2253 sequestering carbon from the atmosphere to the terrestrial biosphere (Yue et al., 2016; Jones et al.,
2254 2024c). Increases in forest fire emissions and severity (emissions per unit area) globally during the past
2255 two decades have highlighted the increasing potential for fire emissions fluxes to outweigh post-fire
2256 recovery fluxes, though long-term monitoring of vegetation recovery is required to quantify the net
2257 effect on terrestrial C storage (Jones et al., 2024c).

2258 3.9 Closing the global carbon cycle

2259 3.9.1 Partitioning of cumulative emissions and sink fluxes

2260 Emissions during the period 1850-2024 amounted to 745 ± 65 GtC and were partitioned among the
2261 atmosphere (290 ± 5 GtC; 39%), ocean (200 ± 40 GtC; 27%), and land (175 ± 50 GtC; 24%). The
2262 cumulative land sink is lower than the cumulative land-use emissions (250 ± 65 GtC), making the
2263 global land a source of 75 ± 80 GtC over the whole 1850-2024 period (Table 8).

2264 The use of nearly independent estimates for the individual terms of the global carbon budget shows a
2265 cumulative budget imbalance of 80 GtC (11% of total emissions) during 1850-2024 (Table 8), which
2266 suggests that emissions could be slightly too high by the same proportion or that the combined land and
2267 ocean sinks are underestimated (by up to 20%). A large part of the B_{IM} occurs over the first half of the
2268 20th century (Figure 3, red dashed line) and could originate from the estimation of significant increase
2269 in E_{FOS} and E_{LUC} between the mid 1920s and the mid 1960s which is unmatched by a similar growth in
2270 atmospheric CO_2 concentration as recorded in ice cores (Figure 3). Also, we now correct the S_{LAND}
2271 estimate for historical reduction in forest cover (RSS, see Section 2.6). This reduces the S_{LAND} estimate
2272 by about 40 GtC over the 1850-2024 period, contributing to the increase of the historical budget
2273 imbalance in comparison to GCB2024 (Friedlingstein et al., 2025a).

2274 For the more recent 1959-2024 period where direct atmospheric CO_2 measurements are available, total
2275 emissions ($E_{FOS} + E_{LUC}$) amounted to 530 ± 50 GtC, of which 420 ± 20 GtC (79%) were caused by
2276 fossil CO_2 emissions, and 110 ± 45 GtC (21%) by land-use change (Table 8). The total emissions were
2277 partitioned among the atmosphere (230 ± 5 GtC; 44%), ocean (145 ± 30 GtC; 27%), and the land (120
2278 ± 30 GtC; 23%), with a budget imbalance of 35 GtC (7% of total emissions). All components except
2279 land-use change emissions have significantly grown since the 1960s, with important interannual
2280 variability in the growth rate in atmospheric CO_2 concentration primarily mirrored in the land CO_2 sink

Formatted: Outline numbered + Level: 2 + Numbering Style: 1, 2, 3, ... + Start at: 1 + Alignment: Left + Aligned at: 0 cm + Indent at: 1.02 cm

Formatted: Outline numbered + Level: 3 + Numbering Style: 1, 2, 3, ... + Start at: 1 + Alignment: Left + Aligned at: 0 cm + Indent at: 1.27 cm

Formatted: Superscript

2281 (Figure 4), and some decadal variability in all terms (Table 7). Differences with previous budget
2282 releases are documented in Figure S15.

2283 The global carbon budget averaged over the last decade (2015-2024) is shown in Figure 2 and Table 7.
2284 For this period, 88% of the total emissions ($E_{\text{FOS}} + E_{\text{LUC}}$) were from fossil CO₂ emissions (E_{FOS}), and
2285 12% from land-use change (E_{LUC}). The total emissions were partitioned among the atmosphere (50%),
2286 ocean (29%) and land (21%), with a near zero budget imbalance (0.1%, $<0.1 \text{ GtC yr}^{-1}$). We note that,
2287 compared to GCB2024, ~~the corrections on S_{OCEAN} and S_{LAND} largely reduced the B_{IM} over the 2015-~~
2288 ~~2024 period, by about 0.4 GtC, but at the cost of increasing the cumulated B_{IM} over the longer 1959-~~
2289 ~~2024 period, from 17 GtC (uncorrected estimate) to 37 GtC (corrected estimate).~~

2290 For single years, the budget imbalance can be larger (Figure 4f). For 2024, the combination of our
2291 estimated anthropogenic sources ($11.6 \pm 0.9 \text{ GtC yr}^{-1}$) and partitioning in atmosphere, land and ocean
2292 ($13.3 \pm 0.9 \text{ GtC yr}^{-1}$) leads to a large negative B_{IM} of -1.7 GtC (Table 7), indicating that, despite the
2293 lower than average S_{LAND} in 2024, the land sink is still too large to explain the record-high atmospheric
2294 CO₂ growth rate of 2024. We note that using the 2024 GRESO atmospheric growth rate of $6.8 \pm 0.2 \text{ GtC}$
2295 yr^{-1} (Section 3.5.3) would reduce the 2024 B_{IM} to about -0.6 GtC.

2296 3.9.2 Trend and variability in the carbon budget imbalance

2297 The carbon budget imbalance (B_{IM} ; Eq. 1, Figure 4f) quantifies the mismatch between the estimated
2298 total emissions and the estimated changes in the atmosphere, land, and ocean reservoirs. The budget
2299 imbalance from 1959 to 2024 is small (35 GtC cumulated over the period, i.e. 0.5 GtC yr^{-1} on average)
2300 and shows no significant trend over the 1959-2024 period (Figure 4). The process models (GOBMs and
2301 DGVMs) and f_{CO_2} -products have been selected to match observational constraints in the 1990s, but no
2302 further constraints have been applied to their representation of trend and variability. Therefore, the
2303 small mean and trend in the budget imbalance can be seen as evidence of a coherent community
2304 understanding of the emissions and their partitioning on those time scales (Figure 4). However, the
2305 budget imbalance shows substantial variability of the order of $\pm 1 \text{ GtC yr}^{-1}$, particularly over semi-
2306 decadal time scales, although most of the variability is within the uncertainty of the estimates.

2307 We cannot attribute the cause of the budget imbalance with our analysis, we only note that the budget
2308 imbalance is unlikely to be explained by errors in the emissions alone because of its large semi-decadal
2309 variability component, a variability that is atypical of emissions, and also because the budget imbalance
2310 has not increased in the past 60 years despite a near tripling in anthropogenic emissions (Figure 4).
2311 Errors in S_{LAND} and S_{OCEAN} are more likely to be the main cause for the budget imbalance, especially on
2312 interannual to semi-decadal timescales. For example, underestimation of the S_{LAND} by DGVMs has
2313 been reported following the eruption of Mount Pinatubo in 1991 possibly due to missing responses to
2314 changes in diffuse radiation (Mercado et al., 2009). Although we account for aerosol effects on solar

Deleted: we

Deleted: .

Deleted: land sink

Deleted: combined

Deleted: and ocean

Formatted: Outline numbered + Level: 3 + Numbering
Style: 1, 2, 3, ... + Start at: 1 + Alignment: Left + Aligned at:
0 cm + Indent at: 1.27 cm

2320 radiation quantity and quality (diffuse vs direct), most DGVMs only used the former as input (i.e., total
2321 solar radiation) (Table S1). Thus, the ensemble mean may not capture the full effects of volcanic
2322 eruptions, i.e. associated with high light scattering sulphate aerosols, on the land carbon sink
2323 (O’Sullivan et al., 2021), potentially explaining the large positive B_{IM} in 1991-1992. DGVMs are
2324 suspected to underestimate the land sink reduction in response to El Niño events (see Section 3.7.3),
2325 which could explain the large negative B_{IM} in 1986-1987, 1997-1998 or 2023-2024). Quasi-decadal
2326 variability in the ocean sink has also been reported, with all methods agreeing on smaller than expected
2327 ocean CO₂ sink in the 1990s and a larger than expected sink in the 2000s (Figure 10b; Landschützer et
2328 al., 2016, DeVries et al., 2019, Hauck et al., 2020, McKinley et al., 2020, Gruber et al., 2023) and the
2329 climate-driven variability could be substantial but is not well constrained (DeVries et al., 2023, Müller
2330 et al., 2023). Errors in sink estimates could also be partly driven by errors in the climatic forcing data,
2331 particularly precipitation for S_{LAND} and wind for S_{OCEAN} .

2332 Although the budget imbalance is near zero for the most recent decade, it could be due to a
2333 compensation of errors. We cannot exclude an overestimation of CO₂ emissions, particularly from land-
2334 use change, given their large uncertainty, as has been suggested elsewhere (Piao et al., 2018), and/or an
2335 underestimate of the land or ocean sinks. A larger estimate of the atmosphere-land CO₂ flux (S_{LAND} -
2336 E_{LUC}) over the extra-tropics would reconcile bottom-up model results with inversion estimates (Figure
2337 14). Likewise, a larger S_{OCEAN} is also possible given the higher estimates from the fCO_2 -products and
2338 the oxygen based estimates (see Table 6 and Figure 10b), the underestimation of interior ocean
2339 anthropogenic carbon accumulation in the GOBMs (Section 3.6.5, Müller et al., 2023), or known biases
2340 of ocean models (e.g., Terhaar et al., 2022; 2024). More integrated use of observations in the global
2341 carbon budget, either on their own or for further constraining model results, should help resolve some
2342 of the budget imbalance.

2343 4 Tracking progress towards mitigation targets

2344 The average growth in global fossil CO₂ emissions peaked at nearly +3% per year during the 2000s,
2345 driven by the rapid growth in emissions in China. In the last decade, however, the global growth rate
2346 has slowly declined, reaching a low +0.8% per year over 2015-2024. While this slowdown in global
2347 fossil CO₂ emissions growth is welcome, global fossil CO₂ emissions continue to grow, far from the
2348 rapid emission decreases needed to be consistent with the temperature goals of the Paris Agreement.

2349 Since the 1990s, the average growth rate of fossil CO₂ emissions has continuously declined across the
2350 group of developed countries of the Organisation for Economic Co-operation and Development
2351 (OECD), with emissions peaking in around 2005 and declining at 1.5% yr⁻¹ in the decade 2015-2024,
2352 compared to a decline of 0.9% yr⁻¹ during the 2005-2014 period (Table 9). In the non-OECD countries,
2353 emissions rose 4.6% yr⁻¹ from 2005-2014, but growth has lowered to 2.1% yr⁻¹ from 2015-2024. In the
2354 decade 2015-2024, territorial fossil CO₂ emissions decreased significantly (at the 95% confidence level)

Formatted: Outline numbered + Level: 1 + Numbering
Style: 1, 2, 3, ... + Start at: 1 + Alignment: Left + Aligned at:
0 cm + Indent at: 0.76 cm

Deleted: .

2356 in 35 economies whose gross domestic product (GDP) grew significantly (also at the 95% confidence
2357 level): Andorra, Australia, Austria, Belgium, Bulgaria, Czechia, Denmark, Estonia, Finland, France,
2358 Germany, Greece, Hungary, Ireland, Israel, Jordan, Latvia, Luxembourg, Netherlands, New Zealand,
2359 Norway, Poland, Portugal, South Korea, Romania, Serbia, Slovakia, Slovenia, Spain, Sweden,
2360 Switzerland, Taiwan, Thailand, United Kingdom, and USA (updated from Le Quéré et al., 2019).
2361 Altogether, these 35 economies emitted 2.7 GtC yr⁻¹ (9.7 GtCO₂ yr⁻¹) on average over the last decade,
2362 about 27% of world CO₂ fossil emissions. For comparison, over the previous decade (2005-2014), 18
2363 economies showed a significant decrease in territorial fossil CO₂ emissions while significantly growing
2364 their GDP (Austria, Belgium, Bulgaria, Czechia, France, Germany, Luxembourg, North Macedonia,
2365 Netherlands, New Zealand, Romania, Serbia, Slovakia, Sweden, Switzerland, United Kingdom, USA,
2366 Uzbekistan). These 18 economies emitted an average 2.0 GtC yr⁻¹ over 2005–2014, or 20% of the
2367 global total.

2368 Decomposing emission changes into the components of growth, a Kaya decomposition, helps give an
2369 initial understanding of the drivers of emission changes (Peters et al., 2017b). The reduction in growth
2370 in global fossil CO₂ emissions in the last decade (2015-2024, 0.8% yr⁻¹) relative to the previous decade
2371 (2005-2014, 2.2% yr⁻¹) is due to slightly weaker economic growth (3.5% yr⁻¹ to 2.4% yr⁻¹), increasing
2372 declines in CO₂ emissions per unit energy (0% yr⁻¹ to 0.7% yr⁻¹), and weakening declines in energy per
2373 unit GDP (1.6% yr⁻¹ to 1.3% yr⁻¹) (Figure S17). Fossil CO₂ emission declines in the USA and the EU27
2374 are primarily driven by sustained or increasing declines in energy per GDP and CO₂ emissions per unit
2375 energy. China has seen emissions growth decline from 6.7% yr⁻¹ in the 2005-2014 decade to 2.5% yr⁻¹
2376 from 2015-2024, driven by weaker economic growth (five percentage points), offset by a considerable
2377 weakening in the rate of reduction in the energy per GDP (four percentage points), with sustained
2378 improvements in CO₂ emissions per unit energy (Figure S17). India has had strong economic growth
2379 that is not offset by declines in energy per GDP or declines in CO₂ emissions per unit energy, driving
2380 up fossil CO₂ emissions. In the rest of the world, economic growth has slowed considerably in the last
2381 decade, and carbon intensity has increased, with declines in energy per GDP unable to counteract these
2382 increases leading to growing emissions. Despite the high deployment of renewables in some countries
2383 (e.g., China, India), fossil energy sources continue to grow to meet growing energy demand (Le Quéré
2384 et al., 2019). In summary, the carbon intensity of energy has consistently decreased over the past
2385 decade globally (-0.7% yr⁻¹), indicating decarbonisation of the global energy system, with declines in
2386 China (-1.4% yr⁻¹), the European Union (-1.5% yr⁻¹), the USA (-1.3% yr⁻¹), but no change in India and
2387 increases (carbonisation) in the Rest of the World. The global decarbonation trends are not sufficient to
2388 offset the growth in global energy demand, with energy demand growing faster than expected due to
2389 weakening declines in energy per GDP in China, US, and globally.

2390 The slower growth of global fossil CO₂ emissions in the last decade is due in part to the emergence of
2391 climate policy (Eskander and Fankhauser 2020; Le Quere et al 2019; Hoppe et al., 2023) and

Deleted: countries whose

Deleted: countries

Deleted: countries

Deleted: economy

Deleted: countries

Deleted: /

Formatted: Not Highlight

2398 technological change, which is leading to a shift from coal to gas and growth in renewable energies, and
2399 reduced expansion of coal capacity. At the aggregated global level, decarbonisation shows a strong and
2400 growing signal in the last decade, with smaller contributions from lower economic growth and declines
2401 in energy per GDP. Altogether, global fossil CO₂ emissions are still growing, far from the reductions
2402 needed to meet the ambitious climate goals of the UNFCCC Paris agreement.

2403 Last, we update the remaining carbon budget (RCB) based on two studies, the IPCC AR6 (Canadell et
2404 al., 2021) and the revision of the IPCC AR6 estimates (Forster et al., 2025, Lamboll et al., 2023). We
2405 update the RCB assessed by the IPCC AR6 (Canadell et al., 2021), accounting for the 2020 to 2025
2406 GCB estimated anthropogenic emissions from fossil combustion (E_{FOS}) and land use change (E_{LUC}).
2407 From January 2026, the IPCC AR6 RCB (50% likelihood) for limiting global warming to 1.5°C, 1.7°C
2408 and 2°C is estimated to amount to 70, 165, and 300 GtC (250, 600, 1100 GtCO₂). The Forster et al.
2409 (2025) study proposed a significantly lower RCB than IPCC AR6, with the largest reduction being due
2410 to an update of the climate emulator (MAGICC) used to estimate the warming contribution of non-CO₂
2411 agents, and to the warming (i.e. emissions) that occurred over the 2020-2024 period. We update the
2412 Forster et al., budget accounting for the 2025 GCB estimated anthropogenic emissions. From January
2413 2026, the Forster et al., (2025) RCB (50% likelihood) for limiting global warming to 1.5°C, 1.7°C and
2414 2°C is estimated to amount to 25, 120, and 275 GtC (90, 450, 1010 GtCO₂), significantly smaller than
2415 the updated IPCC AR6 estimate. Both the original IPCC AR6 and Forster et al. (2025) estimates
2416 include the Earth System uncertainty on the climate response to cumulative CO₂ emissions, which is
2417 reflected through the percent likelihood of exceeding the given temperature threshold, an additional
2418 uncertainty of ± 220 GtCO₂ due to alternative non-CO₂ emission scenarios, and other sources of
2419 uncertainties (see Canadell et al., 2021). The two sets of estimates overlap when considering all
2420 uncertainties.

2421 Here, we take the average of our update of both IPCC AR6 and Forster et al. (2025) estimates, giving a
2422 remaining carbon (50% likelihood) for limiting global warming to 1.5°C, 1.7°C and 2°C of respectively
2423 45, 145, and 290 GtC (170, 525, 1055 GtCO₂) starting from January 2026. We emphasise the large
2424 uncertainties, particularly when close to the global warming limit of 1.5°C. These 1.5°C, 1.7°C and 2°C
2425 remaining carbon budgets correspond respectively to about 4, 12 and 25 years from the beginning of
2426 2026, at the 2025 level of total anthropogenic CO₂ emissions. Reaching net-zero CO₂ emissions by
2427 2050 entails cutting total anthropogenic CO₂ emissions by about 0.5 GtC (1.7 GtCO₂), 4% of 2025
2428 emissions, each year on average, comparable to the decrease in E_{FOS} observed in 2020 during the
2429 COVID-19 pandemic. However, this would lead to cumulative emissions over 2025-2050 of 140 GtC
2430 (520 GtCO₂), well above the remaining carbon budget of 50 GtC to limit global warming to 1.5°C, but
2431 still within the remaining budget of 145 GtC to limit warming to 1.7°C (in phase with the “well below
2432 2°C” ambition of the Paris Agreement).

2433 **5 Discussion**

2434 Each year when the global carbon budget is published, each flux component is updated for all previous
2435 years to consider corrections that are the result of further scrutiny and verification of the underlying
2436 data in the primary input datasets. Annual estimates may be updated with improvements in data quality
2437 and timeliness (e.g., to eliminate the need for extrapolation of forcing data such as land use). Of all
2438 terms in the global budget, only the fossil CO₂ emissions and the growth rate in atmospheric CO₂
2439 concentration are based primarily on empirical inputs supporting annual estimates in this carbon
2440 budget. The carbon budget imbalance, yet an imperfect measure, provides a strong indication of the
2441 limitations in observations, in understanding and representing processes in models, and/or in the
2442 integration of the carbon budget components.

2443 The persistent unexplained variability in the carbon budget imbalance limits our ability to verify
2444 reported emissions (Peters et al., 2017a) and suggests we do not yet have a complete understanding of
2445 the underlying carbon cycle dynamics on annual to decadal timescales. Resolving most of this
2446 unexplained variability should be possible through different and complementary approaches. First, as
2447 intended with our annual updates, the imbalance as an error term should be reduced by improvements
2448 of individual components of the global carbon budget that follow from improving the underlying data
2449 and statistics and by improving the models through the resolution of some of the key uncertainties
2450 detailed in Table 10. Second, additional clues to the origin and processes responsible for the variability
2451 in the budget imbalance could be obtained through a closer scrutiny of carbon variability in light of
2452 other Earth system data (e.g., heat balance, water balance), and the use of a wider range of
2453 biogeochemical observations to better understand the land-ocean partitioning of the carbon imbalance
2454 such as the constraint from atmospheric oxygen. Finally, additional information could also be obtained
2455 through better inclusion of process knowledge at the regional level. The limit for reducing the carbon
2456 budget imbalance is yet unclear, but most certainly not yet reached given the possibilities for
2457 improvements that lie ahead.

2458 Estimates of global fossil CO₂ emissions from different datasets are in relatively good agreement when
2459 the different system boundaries of these datasets are considered (Andrew, 2020a). While estimates of
2460 E_{FOS} are derived from reported activity data requiring much fewer complex transformations than some
2461 other components of the budget, uncertainties remain, and one reason for the apparently low variation
2462 between datasets is precisely the reliance on the same underlying reported energy data. The budget
2463 excludes some sources of fossil CO₂ emissions, which available evidence suggests are relatively small
2464 (<1%) (see Supplement S.8.2). We have added emissions from lime production in China and the US,
2465 but these are still absent in reporting from most other non-Annex I countries, and before 1990 in other
2466 Annex I countries.

Formatted: Indent: Left: 0 cm, First line: 0 cm, Outline numbered + Level: 1 + Numbering Style: 1, 2, 3, ... + Start at: 1 + Alignment: Left + Aligned at: 0 cm + Indent at: 0.76 cm

2467 Estimates of E_{LUC} suffer from a range of intertwined issues (Obermeier et al., 2025), including the poor
2468 knowledge of historical land-cover and land-use change (particularly before the 1960s when FAO
2469 reporting started), the rudimentary representation of management processes in most models, and the
2470 diversity in methodologies and boundary conditions used across methods (e.g., Armeth et al., 2017;
2471 Pongratz et al., 2014; Bastos et al., 2021). Uncertainties in current and historical carbon stocks in soils
2472 and vegetation also contribute to uncertainty in E_{LUC} estimates. Major efforts are thus necessary to
2473 resolve the different issues concerning E_{LUC} (Obermeier et al., 2025). The large uncertainty and limited
2474 reliability of E_{LUC} estimates are particularly concerning given the growing importance of E_{LUC} for
2475 climate mitigation strategies, and the large issues in the quantification of the cumulative emissions over
2476 the historical period that arise from large uncertainties in E_{LUC} .

2477 By adding the natural land sink in managed forests estimated by DGVMs (part of S_{LAND} in this budget)
2478 to the budget E_{LUC} estimate, we reconcile most of the large gap between our E_{LUC} estimate and the land-
2479 use flux estimates from NGHGs (Figure 8). This reconciliation (translation) can be used as potential
2480 adjustment in the policy context, for instance to help assess the collective countries' progress towards
2481 the goal of the Paris Agreement avoiding double-accounting for the natural sink in managed forests. In
2482 the absence of this translation, collective progress would appear better than it is (Grassi et al., 2021). A
2483 clear understanding of these implications is thus essential for policymakers for developing effective
2484 climate targets (Grassi et al., 2025). The application of this translation is also recommended in the
2485 UNFCCC Synthesis report for the first Global Stocktake (UNFCCC, 2022) whenever a comparison
2486 between LULUCF fluxes reported by countries and the global emission estimates of the IPCC is
2487 conducted. However, this translation should be seen as a short-term and pragmatic fix based on existing
2488 data, rather than a definitive solution to bridge the differences between global models and national
2489 inventories. Platforms for dataset comparisons (e.g., Melo et al., 2025) help strengthening the dialogue
2490 across communities and identify the additional steps needed to understand and reconcile the remaining
2491 differences, some of which are relevant at the country level (Grassi, et al., 2023, Schwingshackl, et al.,
2492 2022).

2493 The comparison of GOBMs, fCO_2 -products, and inversions highlights discrepancies in the temporal
2494 evolution of SO_{CEAN} in the Southern Ocean and northern high-latitudes (Figure 14, Hauck et al., 2023a)
2495 and in the mean SO_{CEAN} in the tropics. A large part of the uncertainty in the mean fluxes stems from the
2496 regional distribution of the river flux adjustment term. The current distribution simulates the largest
2497 share of the outgassing to occur in the tropics (Lacroix et al., 2020). The long-standing sparse data
2498 coverage of fCO_2 observations in the Southern compared to the Northern Hemisphere (e.g., Takahashi
2499 et al., 2009) continues to exist (Bakker et al., 2016, 2025a, Figure S5) and to lead to substantially higher
2500 uncertainty in the SO_{CEAN} estimate for the Southern Hemisphere (Watson et al., 2020, Gloege et al.,
2501 2021, Hauck et al., 2023a). This discrepancy, which also hampers model improvement, points to the
2502 need for increased high-quality fCO_2 observations especially in the Southern Ocean. At the same time,

2503 model uncertainty is illustrated by the large spread of individual GOBM estimates (indicated by
2504 shading in Figure 14) and highlights the need for model improvement, now also supported by the
2505 IOMB benchmarking. The issue of diverging trends in S_{OCEAN} from different methods remains a matter
2506 of concern. Recent and on-going work suggests that the $f\text{CO}_2$ -products may overestimate the trend
2507 although biases in the $f\text{CO}_2$ -product ensemble may partly cancel out (Supplement section S3.4). A data-
2508 constrained model approach suggests that the GOBMs underestimate the amplitude of decadal
2509 variability, but that the $f\text{CO}_2$ -products overestimate the trend (Mayot et al., 2024). The various methods,
2510 now also including ocean interior observation-based estimates, agree within uncertainties on the mean
2511 ocean sink in the last decade, although the independent estimate from atmospheric oxygen
2512 measurements still shows the largest sink estimate for the past decade and has a steeper trend (Table 6).
2513 However, the estimate is consistent within uncertainties with S_{OCEAN} , with the relatively larger ocean
2514 sink in the $f\text{CO}_2$ -products and some of the GOBMs. The assessment of the net land-atmosphere
2515 exchange from DGVMs and atmospheric inversions also shows substantial discrepancy, particularly for
2516 the estimate of the net land flux over the northern extra-tropic. This discrepancy highlights the
2517 difficulty to quantify complex processes (CO_2 fertilisation, nitrogen deposition and fertilisers, climate
2518 change and variability, land management, etc.) that collectively determine the net land CO_2 flux.
2519 Resolving the differences in the Northern Hemisphere land sink will require the consideration and
2520 inclusion of larger volumes of observations.

2521 The adjustments introduced in this budget for S_{LAND} and S_{OCEAN} to account for known biases (RSS for
2522 DGVMs, cold skin/warm layer for $f\text{CO}_2$ products, ocean sink underestimation for GOBMs) lead to a
2523 smaller net land sink ($S_{\text{LAND-ELUC}}$) and a larger ocean sink (S_{OCEAN}), more in line with the atmospheric
2524 inversions and independent oxygen based estimates (Table 7), and also consistent with a recent study
2525 based on satellite derived changes in aboveground biomass over the 2000-2019 period (Randerson et
2526 al., 2025).

2527 We provide metrics for the evaluation of the ocean and land models and the atmospheric inversions
2528 (Figure S6-S8 and S13, Table S12). These metrics expand the use of observations in the global carbon
2529 budget, helping 1) to support improvements in the ocean and land carbon models that produce the sink
2530 estimates, and 2) to constrain the representation of key underlying processes in the models and to
2531 allocate the regional partitioning of the CO_2 fluxes. The use of process-based metrics in an objective
2532 evaluation framework (IOMB) targeted to evaluate the simulation of S_{OCEAN} in the ocean
2533 biogeochemistry models is an important advance. This is another step in the endeavour to use a broader
2534 range of observations and more stringent model evaluation that we hope will support continued
2535 improvements in the models and in the annual estimates of the global carbon budget.

2536 We assessed before that a sustained decrease of -1% in global emissions could be detected at the 66%
2537 likelihood level after a decade only (Peters et al., 2017a). Similarly, a change in behaviour of the land
2538 and/or ocean carbon sink would take as long to detect, and much longer if it emerges more slowly. To

Deleted: S11

2540 continue reducing the carbon imbalance on annual to decadal time scales, regionalising the carbon
2541 budget, and integrating multiple variables are powerful ways to shorten the detection limit and ensure
2542 the research community can rapidly identify issues of concern in the evolution of the global carbon
2543 cycle under the current rapid and unprecedented changing environmental conditions.

2544 6 Conclusions

2545 The estimation of global CO₂ emissions and sinks is a major effort by the carbon cycle research
2546 community that requires a careful compilation and synthesis of measurements, statistical estimates, and
2547 model results. The delivery of an annual carbon budget serves two purposes. First, there is a large
2548 demand for up-to-date information on the state of the anthropogenic perturbation of the climate system
2549 and its underpinning causes. A broad stakeholder community relies on the datasets associated with the
2550 annual carbon budget including scientists, policy makers, businesses, journalists, and non-governmental
2551 organisations engaged in adapting to and mitigating human-driven climate change. Second, over the last
2552 decades we have seen unprecedented changes in the human and biophysical environments (e.g.,
2553 changes in the growth of fossil fuel emissions, impact of COVID-19 pandemic, Earth's warming,
2554 extreme events, and strength of the carbon sinks), which call for frequent assessments of the state of the
2555 planet, a better quantification of the causes of changes in the contemporary global carbon cycle, and an
2556 improved capacity to anticipate its evolution in the future. Building this scientific understanding to meet
2557 the extraordinary climate mitigation challenge requires frequent, robust, transparent, and traceable
2558 datasets and methods that can be scrutinised and replicated. This paper via 'living data' helps to keep
2559 track of new budget updates.

2560 7 Data availability

2561 The data presented here are made available in the belief that their wide dissemination will lead to
2562 greater understanding and new scientific insights of how the carbon cycle works, how humans are
2563 altering it, and how we can mitigate the resulting human-driven climate change. Full contact details and
2564 information on how to cite the data shown here are given at the top of each page in the accompanying
2565 database and summarised in Table 2.

2566 The accompanying database includes three Excel files organised in the following spreadsheets:

2567 File Global_Carbon_Budget_2025v1.0.xlsx includes the following:

- 2568 1. Summary
- 2569 2. The global carbon budget (1959-2024);
- 2570 3. The historical global carbon budget (1750-2024);

Formatted: Indent: Left: 0 cm, First line: 0 cm, Outline numbered + Level: 1 + Numbering Style: 1, 2, 3, ... + Start at: 1 + Alignment: Left + Aligned at: 0 cm + Indent at: 0.76 cm

Formatted: Indent: Left: 0 cm, First line: 0 cm, Outline numbered + Level: 1 + Numbering Style: 1, 2, 3, ... + Start at: 1 + Alignment: Left + Aligned at: 0 cm + Indent at: 0.76 cm

Formatted: Indent: Left: 0.12 cm, Outline numbered + Level: 4 + Numbering Style: 1, 2, 3, ... + Start at: 1 + Alignment: Left + Aligned at: 4.44 cm + Indent at: 5.08 cm

2571 4. Global CO₂ emissions from fossil fuels and cement production by fuel type, and the per-capita
2572 emissions (1850-2024);

2573 5. CO₂ emissions from land-use change from the individual bookkeeping models (1959-2024);

2574 6. Ocean CO₂ sink from the individual global ocean biogeochemistry models and f CO₂-products
2575 (1959-2024);

2576 7. Terrestrial CO₂ sink from the individual DGVMs (1959-2024);

2577 8. Cement carbonation CO₂ sink (1959-2024).

2578 File National_Fossil_Carbon_Emissions_2025v1.0.xlsx includes the following:

2579 1. Summary

2580 2. Territorial country CO₂ emissions from fossil fuels and cement production (1850-2024);

2581 3. Consumption country CO₂ emissions from fossil fuels and cement production and emissions
2582 transfer from the international trade of goods and services (1990-2020) using CDIAC/UNFCCC
2583 data as reference;

2584 4. Emissions transfers (Consumption minus territorial emissions; 1990-2020);

2585 5. Country definitions.

2586 File National_LandUseChange_Carbon_Emissions_2024v1.0.xlsx includes the following:

2587 1. Summary

2588 2. Territorial country CO₂ emissions from Land Use Change (1850-2024) from three bookkeeping
2589 models;

2590 All three spreadsheets are published by the Integrated Carbon Observation System (ICOS) Carbon
2591 Portal and are available at <https://doi.org/10.18160/GCP-2025> (Friedlingstein et al., 2025c). National
2592 emissions data are also available at <https://doi.org/10.5281/zenodo.5569234> (Andrew and Peters, 2025),
2593 from the Global Carbon Atlas (<http://www.globalcarbonatlas.org/>, last access: 23 October 2025) and
2594 from Our World in Data (<https://ourworldindata.org/co2-emissions>, last access: 23 October 2025).

2595 **Author contributions**

2596 PF, MOS, MWJ, DCEB, RMA, JH, PL, CLQ, HL, ITL, GPP, WP, JP, CSc, and SS designed the study,
2597 conducted the analysis, and wrote the paper with input from JGC and PC. RMA, GPP, JIK and TK

Formatted: Indent: Left: 0.12 cm, Outline numbered +
Level: 4 + Numbering Style: 1, 2, 3, ... + Start at: 1 +
Alignment: Left + Aligned at: 4.44 cm + Indent at: 5.08 cm

Formatted: Indent: Left: 0.12 cm, Outline numbered +
Level: 4 + Numbering Style: 1, 2, 3, ... + Start at: 1 +
Alignment: Left + Aligned at: 4.44 cm + Indent at: 5.08 cm

2598 produced the fossil CO₂ emissions and their uncertainties and analysed the emissions data. ME and GM
2599 provided fossil fuel emission data. ZL provided the Carbon Monitor fossil emission projection. JP, CSc,
2600 TG and ZQ provided the bookkeeping land-use change emissions with synthesis by JP and CSc. KH
2601 and JDM provided the estimates of non-vegetation CDR fluxes. LB, MAC, ÖG, NG, TI, TJ, LR, JS,
2602 RS, and HTs provided an update of the global ocean biogeochemical models; LD, DJF, MG, LG, YI,
2603 AJ, GMK, CR, JZ, and PC provided an update of the ocean *f*CO₂-data products, with synthesis on both
2604 streams by JH, PL and AR. SRA, LBa, NRB, AB, CFB, MC, MPE, KE, WE, RAF, TGk, CL, NM,
2605 DRM, SN, AO, AMO, DP, GR, IS, AJS, CSw, ST, BT, SJvdV, EVO, and RW provided ocean *f*CO₂
2606 measurements for the year 2024, with synthesis by DCEB and SDJ. KA, PA, THC, JHE, AFo, BG, JG,
2607 AI, AKJ, EK, JK, EM, JM, LM, TN, QS, TLS, HT, APW, WY, XYa, XYu and CK provided an update
2608 of the Dynamic Global Vegetation Models, with synthesis by SS and MOS. RB, FF, HL, VS, DS, and
2609 HiT provided estimates of land and ocean sinks from Earth System Models, as well as a projection of
2610 the atmospheric growth rate for 2025, with synthesis by HL. FC, NC, LF, ARJ, FJ, ITL, JL, LRN, YN,
2611 CR, XT, YK, and ZL provided an updated atmospheric inversion, WP, FC, and ITL developed the
2612 protocol and produced the synthesis and evaluation of the atmospheric inversions. EJM and RfK
2613 provided the atmospheric oxygen estimate of surface net carbon sinks. RMA provided projections of
2614 the 2025 fossil emissions and atmospheric CO₂ growth rate. PL provided the predictions of the 2025
2615 ocean sink. IBMB, LPC, KKG, GCH, TMR and GRvdW provided forcing data for land-use change. FT
2616 and GG provided data for the land-use change NGHGI harmonisation. XL provided the atmospheric
2617 CO₂ data. SP provided the satellite OCO-2 atmospheric CO₂ growth rate. MWJ provided the historical
2618 atmospheric CO₂ concentration and growth rate. IH provided the climate forcing data for the DGVMs.
2619 NP provided the nitrogen fertilizer forcing data for the DGVMs. MOS and NB produced the aerosol
2620 diffuse radiative forcing for the DGVMs. PCM provided the iLAMB evaluation of the DGVMs. NOC
2621 and MGS provided the iOMB evaluation of the GOBMs. PR provided the historical land carbon export
2622 estimate, MWJ provided the emissions prior for use in the inversion systems. XD provided seasonal
2623 emissions data, based on GRACED (Global gridded daily CO₂ emissions dataset), for most recent years
2624 for the emission prior. PF, MO and MWJ coordinated the effort, revised all figures, tables, text and

2625 numbers to ensure the update was clear from the 2024 edition and in line with the
2626 globalcarbonatlas.org.

2627

2628 **Competing interests.**

2629 At least one of the authors is a member of the editorial board of Earth System Science Data

2630

2631 **Acknowledgements**

2632 First, we wish to thank Richard ‘Skee’ Houghton for his tremendous contribution to the Global Carbon
2633 Budget since its inception, pioneering the estimate of land use change emissions with bookkeeping
2634 models. We thank all people and institutions who provided the data used in this global carbon budget
2635 2025 and the Global Carbon Project members for their input throughout the development of this
2636 publication. We thank Christian Ethé, Xavier Perrot, Damian Loher, Fatemeh Chegini, Fabrice Lacroix,
2637 Yangyang Zhao, Paridhi Rustogi, Sarah Berthet, Aurore Voldoire, Laurent Oziel, T. Toyoda, Y.
2638 Kitamura, K. Toyama, H. Nakano, L. S. Urakawa, Philip Townsend, Nathaniel O. Collier, Min Xu, James
2639 D. Shutler, Andrew J. Watson, T. Holding, I.G.C. Ashton, D. K. Woolf, Lonneke Goddijn-Murphy,
2640 Richard Sims, Stefanie Falk, Pengyue Du, Peter Lawrence, Sean Swenson, Daniel Kennedy, Sam Levis,
2641 Erik Kluzek, Lachlan Whyborn, Drew Holzworth, Ian Harman, Naiqing Pan, Shufen Pan for their
2642 involvement in the development, use, and analysis of the models and data products used here. We thank
2643 Kim Currie, Hannelore Theetaert, and Coraline Leseurre who contributed to the provision of surface
2644 ocean CO₂ observations for the year 2024 (see Table S8). We also thank Kevin O’Brien and Eugene
2645 Burger of NOAA’s Pacific Marine Environmental Laboratory and Alex Kozyr of NOAA’s National
2646 Centers for Environmental Information, for their contribution to surface ocean CO₂ data and metadata
2647 management. We thank the scientists, institutions, and funding agencies responsible for the collection
2648 and quality control of the data in SOCAT as well as the International Ocean Carbon Coordination Project
2649 (IOCCP) and the Surface Ocean Lower Atmosphere Study (SOLAS) program for their support. ITL and
2650 WP thank the CarbonTracker Europe team at Wageningen University, including Remco de Kok, Joram
2651 Hooghiem and Auke van der Woude. The inverse modelling team thanks all data providers of
2652 atmospheric CO₂ data provided through multiple ObsPack products. HL thanks Tatiana Ilyina for
2653 supporting the coordination of ESMs’ contributions to GCBs, and Sebastian Brune and Kristina Frölich
2654 for helping with the MPI-ESM1-2-LR assimilation. Zhangeai Qin thanks Ziwang Fu and Dr. Yakun Zhu
2655 for contributing to LUCE modeling. We thank Ram Alkama and Simone Rossi for helping in filtering
2656 S_{LAND} data from DGVMs with managed forest area and Joana Melo for extracting and processing data

Deleted: A5

2658 from NGHGs. FT acknowledges support of member countries to the FAO regular budget and
2659 FAOSTAT. The conclusions in this paper are the authors' only and do not represent FAO views and
2660 position on the subject matter. This is PMEL contribution 5802. MC thanks Tobias Steinhoff (MACID),
2661 Lukasz Pawlikowski, Ian Murphy and Gordon Furey (P&O Maritime Services), and Aodhan Fitzgerald
2662 (Marine Institute) for their support. TG and the VLIZ team are thankful to the management group and
2663 crew of the research vessels Simon Stevin, Skagerak and Neil Armstrong for all the support and help they
2664 provided. pCO₂ measurements on the Marion Dufresne were collected in the frame of the French
2665 COOL/OISO long-term monitoring program with support from the National Institute of Sciences of the
2666 Universe (INSU), the French Polar Institute (IPEV) and the French Oceanographic Fleet (FOF). AMO
2667 thanks the captain and crew on the Sea-Cargo Express for their help. DP would like to thank Kevin
2668 Sullivan for processing and quality controlling AOML data and facilitating submission to SOCATv2025.
2669 GR thanks the "Finnmaid science and tech-teams" at IOW and SYKE for their support, and is indebted
2670 to the crew of the ship and the people involved at Finnlines. IS thanks the captain and crew on the G. O.
2671 Sars for their help. BT and EvO thank Australia's Integrated Marine Observing System (IMOS) for
2672 sourcing CO₂ data. IMOS is enabled by the National Collaborative Research Infrastructure Strategy
2673 (NCRIS). SJV thanks Andrew Marriner for maintaining the pCO₂ underway system on the RV Tangaroa.
2674 PCM thanks Tristan Quaife, Eddy Robertson, Emily Black and Anthony Walker for support. FC thanks
2675 Adrien Martinez who maintained the atmospheric transport model for the CAMS inversion. We
2676 acknowledge the contributions of Jeongmin Yun, Anthony Bloom, and Kevin Bowman to the CMS-Flux
2677 inversion submission. YN thanks Suman Maity who performed the NISMON-GOSAT inversion. LF
2678 thanks Paul I. Palmer and acknowledges ongoing support from the National Centre for Earth Observation.
2679 Xiangjun Tian thanks Zhe Jin, Yilong Wang, Hongqin Zhang, Min Zhao, Tao Wang, Jinzhi Ding, and
2680 Shilong Piao for their contributions to the GONGGA inversion system. We thank Ning Zeng, Yun Liu,
2681 Eugenia Kalnay, and Gassem Asrar for their contributions to the COLA system. CarbonTracker CT2025
2682 results provided by NOAA GML, Boulder, Colorado, USA from the website at
2683 <http://carbontracker.noaa.gov>. FJ thanks Weimin Ju for running the BEPS model. LN thanks Shamil
2684 Maksyutov, Rajesh Janardanan and Tsuneo Matsunaga for contributing to NTFVAR inverse model study.
2685 YK acknowledges Bo Zheng from Tsinghua University for his contribution to the THU inversion system.
2686 RSA thanks William Merryfield, Woosung Lee, Jason Cole for their help to set up and produce the model
2687 runs. The IPSL contribution was achieved thanks to the valuable contributions of Patricia Cadule, Juliette
2688 Mignot and Olivier Torres. GAM acknowledges contributions from Amanda Fay to updating the LDEO-
2689 HPD fCO₂ product. JRM thanks Gesa Meyer for assistance setting up the DGVM simulations. LMD
2690 thanks Pedro. M. S. Monteiro (SCS-SU) and Sandy Thomalla (SOCCO-CSIR) for their continued support
2691 to make the CSIR-ML6 fCO₂-product up-to-date. CFB is grateful to the technicians and crew of the
2692 research vessel Victor Angelescu for all the support and assistance they provided. This is INIDEP
2693 contribution 2460.

2694

2695 **Financial and computing support**

2696 This research was supported by the following sources of funding: Instituto Nacional de Investigación y
2697 Desarrollo Pesquero (INIDEP) (Argentina); Joint Technical Commission of the Maritime Front
2698 (CTMFM, Argentina-Uruguay) (Argentina); Integrated Marine Observing System (IMOS) (Australia);
2699 National Environmental Science Program (NESP) (Australia); Research Foundation Flanders (grant no.
2700 I001821N) (Belgium); ICOS (Integrated Carbon Observing System) Belgium (Belgium); Tula
2701 Foundation (Canada); National Key Research and Development Program of China (grant no.
2702 [2023YFF0805400](#)) (China); [Copernicus Atmosphere Monitoring Service, implemented by ECMWF on](#)
2703 [behalf of the European Commission \(Grant no. CAMS2 55 bis\) \(EC\); European Research Council \(ERC-](#)
2704 [2022-STG OceanPeak, grant 101077209\) \(EC\)](#); Horizon Europe (NextGenCarbon: grant no. 101184989)
2705 (EC); Horizon Europe (RESCUE: grant no. 101056939) (EC); Horizon 2020 (ESM2025: grant no.
2706 101003536) (EC); Horizon Europe (TRICUSO: grant no. 101199028) (EC); Horizon Europe
2707 (GreenFeedBack: grant no. 101056921) (EC); H2020 (JERICO-S3: grant no. 871153) (EC); Horizon
2708 Europe (GEORGE: grant no. 101094716) (EC); [Horizon Europe \(AI4PEX; grant no. 101137682\) \(EC\); ;](#)
2709 MOB TAC project of the European Copernicus Marine Environment Monitoring Service (EC); Horizon
2710 Europe (TipESM: grant no. 101137673) (EC); [European Union under grant agreement no. 101083922](#)
2711 [\(OceanICU\) and UK Research and Innovation \(UKRI\) under the UK government's Horizon Europe](#)
2712 [funding guarantee \[grant number 10054454, 10063673, 10064020, 10059241, 10079684, 10059012,](#)
2713 [10048179\]. Views and opinions expressed are however those of the author\(s\) only and do not necessarily](#)
2714 [reflect those of the European Union or European Research Executive Agency. Neither the European](#)
2715 [Union nor the granting authority can be held responsible for them; Climate Space RECCAP-2 \(grant no.](#)
2716 [4000144908/24/1-LR\) \(European Space Agency\); EO-LINCS \(European Space Agency\); Ocean Carbon](#)
2717 [for Climate \(grant no. 3-18399/24/I-NB\) \(European Space Agency\); Satellite-based observations of](#)
2718 [Carbon in the Ocean: Pools, Fluxes and Exchanges \(grant no. 4000142532/23/I-DT\) \(European Space](#)
2719 [Agency\); THRAC3E \(grant no. 4000149569/25/I-AG\) \(European Space Agency\); ; ICOS Germany](#)
2720 [\(Germany\); Federal Ministry of Education and Research \(BMBF\) \(STEPSEC: grant no. 01LS2102A\)](#)
2721 [\(Germany\); Marine Institute \(Ireland\); Japan Meteorological Agency \(Japan\); Global Environmental](#)
2722 [Research Coordination System, Ministry of the Environment \(grant nos. E2152 and E2252\) \(Japan\);](#)
2723 [NIES GOSAT Project \(Japan\); the Environment Research and Technology Development Fund](#)
2724 [\(JPMEERF24S12200\) of the Environmental Restoration and Conservation Agency provided by Ministry](#)
2725 [of the Environment of Japan \(Japan\); Environment Research and Technology Development Fund \(grant](#)
2726 [no. JPMEERF24S12205, Co-PI: P. K. Patra\) of the Environmental Restoration and Conservation Agency](#)
2727 [of Japan, and the Arctic Challenge for Sustainability phase III project \(ArCS-3; grant no.](#)
2728 [JPMXD1720251001; Co-PI: P. K. Patra\) \(Japan\); Environment Research and Technology Development](#)
2729 [Fund \(grant no. JPMEERF24S12206\) of the Environmental Restoration and Conservation Agency of](#)
2730 [Japan \(Japan\); Ministry of Business, Innovation and Employment \(Strategic Science Investment Fund](#)
2731 [via the NIWA Ocean-Climate Interaction programme\) \(New Zealand\); Research Council of Norway](#)

Deleted: 2023YFF0805400) (China

Deleted: Copernicus Atmosphere Monitoring Service, implemented by ECMWF on behalf of the European Commission (Grant...

Deleted: CAMS2 55 bis

Deleted: Horizon Europe (OceanICU: grant no. 101083922) (EC); Climate Space RECCAP-2 (grant no.

2739 (ICOS-3, grant no. 350341) (Norway); Research Council of Norway (grant no. 352474) (Norway);
2740 Research Council of Norway (grant no. 352204) (Norway); South African Department of Science,
2741 Technology and Innovation (grant no. DSI/CON C3184/2023) (South Africa); UK Research and
2742 Innovation (Horizon Europe GreenFeedBack: grant no. 10040851) (UK); NCAS at the University of
2743 Reading (UK); NERC NE/V011103/1 “Frontiers of instability in marine ecosystems and carbon
2744 export”UK Natural Environment Research Council (NE/V01417X/1) (UK); Department of Energy,
2745 Office of Science, Office of Biological and Environmental Research (USA); NOAA (Global Ocean
2746 Monitoring and Observing Program: Open Funder Registry no. 100018302) (USA); NOAA (Ocean
2747 Acidification Program: Open Funder Registry no. 100018228) (USA); NOAA (Cooperative Agreement
2748 NA20OAR4320472) (USA); NOAA (Cooperative Agreement NA-03-AR4320179) (USA); Alaska
2749 Ocean Observing System (USA); NASA Carbon Monitoring System (grant no. 80NSSC25K7221)
2750 (USA); NASA Early Career Investigator Program in Earth Science (grant no. 80NSSC24K1632) (USA);
2751 NASA Land Cover and Land Use Change Program (Grants: 80NSSC24K0920 and 80NSSC25K7497)
2752 (USA); NSF (Cooperative Agreement No. 1852977) (USA); NASA Orbiting Carbon Observatory
2753 Science Team Program (grant no. NNH23ZDA001N-OCOST) (USA); NASA Carbon Monitoring
2754 System (grant no. NNH22ZDA001N-CMS) (USA); Work of J.L. and S.P. was conducted at the Jet
2755 Propulsion Laboratory, California Institute of Technology, under a contract with the National Aeronautics
2756 and Space Administration (80NM0018D0004) (USA); NOAA (Cooperative Institute for Marine, Earth
2757 and Atmospheric Systems, Award No. NA25NMF432C0003-T1-01) (USA); NSF (OPP-2329254)
2758 (USA); ORNL is managed by UT-Battelle, LLC, for the DOE (grant no. DE-AC05-1008 00OR22725)
2759 (USA); Schmidt Sciences (VESRI CALIPSO) (USA); Schmidt Sciences (OBVI InMOS) (USA); NSF
2760 (OPP-1922922) (USA); NOAA grant NA24NESX432C0001 (Cooperative Institute for Satellite Earth
2761 System Studies - CISESS) (USA); NOAA cooperative agreement NA22OAR4320151 (CIRES: Andrew
2762 Jacobson and Xin Lan) (USA); Schmidt Sciences (CLARiTy project, part of the Virtual Institute for the
2763 Carbon Cycle) (USA); Schmidt Sciences (COCO2 project, part of the Virtual Institute for the Carbon
2764 Cycle) (USA); NSF (LEAP STC Award no 2019625) (USA); NASA (grant no. 80NSSC22K0150)
2765 (USA); NOAA (GOMO, grant no. NA24OARX431G0151-T1-01) (USA).

2766 The US National Science Foundation (grant nos. OPP-1922922, OPP-2329254), a NOAA cooperative
2767 agreement, the Cooperative Institute for Marine, Earth and Atmospheric Systems (CIMEAS, grant nos.
2768 NA20OAR4320278-T1-01 and NA25NMF432C0003-T3-01S022); although NSF grants 1922922 and
2769 2329254 and NOAA grants NA20OAR4320278-T1-01 and NA25NMF432C0003-T3-01S022 have
2770 been identified for conflict of interest management based on the overall scope of the project and its
2771 potential benefit to the Keeling Curve Foundation, the research findings included in this particular
2772 publication may not necessarily relate to the interests of Keeling Curve Foundation. The terms of this
2773 arrangement have been reviewed and approved by the University of California, San Diego in accordance
2774 with its conflict of interest policies.

2775 We also acknowledge support from the following computing facilities: Australian Community Climate
2776 and Earth System Simulator – National Research Infrastructure (ACCESS-NRI) (Australia); National
2777 Computational Infrastructure (NCI) (Australia); High-Performance Computing Center (HPCC) of
2778 Nanjing University for doing the inversions on its blade cluster system (China); HPC computing and
2779 storage resources by GENCI at IDRIS and TGCC thanks to the grant 2024-2201 on the supercomputers
2780 Jean Zay's V100 and Joliot Curie's SKL and V100 partitions. (France); The ORCHIDEE simulations
2781 were performed using HPC resources from GENCI-TGCC on grant 2024-00006328 (France); IPSL
2782 Climate Modelling Centre (<https://mesocentre.ipsl.fr>) (France); HPC resources from GENCI - TGCC
2783 (Grant A005-017403) (France); Deutsches Klimarechenzentrum (DKRZ) (Projects: bm0891, bm1124
2784 and bg1446) (Germany); NIES Supercomputer system, GOSAT Supercomputing Facility (GOFC)
2785 (Japan); NEC SX-Aurora TSUBASA at NIES (Japan);Fugaku provided by the RIKEN Center for
2786 Computational Science (Project ID: hp250024) (Japan); JAMSTEC's ES4 Super Computer system
2787 (Japan); Sigma2 - the National Infrastructure for High-Performance Computing and Data Storage in
2788 Norway (Norway); NICIS Centre for High-Performance Computing (South Africa); UK CEDA JASMIN
2789 supercomputer (UK); Compute and Data Environment for Science (CADES) at the Oak Ridge National
2790 Laboratory (USA); LEAP Pangeo cloud platform (USA);NASA Ames Supercomputers (USA).

Deleted: ¶

- 2793 Andela, N., Morton, D. C., Giglio, L., Chen, Y., van der Werf, G. R., Kasibhatla, P. S., DeFries, R. S., Collatz, G.
2794 J., Hantson, S., Kloster, S., Bachelet, D., Forrest, M., Lasslop, G., Li, F., Mangeon, S., Melton, J. R., Yue, C., and
2795 Randerson, J. T.: A human-driven decline in global burned area, *Science*, 356, 1356–1362,
2796 <https://doi.org/10.1126/science.aal4108>, 2017.
- 2797 Andrew, R. M.: A comparison of estimates of global carbon dioxide emissions from fossil carbon sources, *Earth*
2798 *Syst. Sci. Data*, 12, 1437–1465, <https://doi.org/10.5194/essd-12-1437-2020>, 2020a.
- 2799 Andrew, R. M.: Timely estimates of India's annual and monthly fossil CO₂ emissions, *Earth Syst. Sci. Data*, 12,
2800 2411–2421, <https://doi.org/10.5194/essd-12-2411-2020>, 2020b.
- 2801 Andrew, R. M.: Towards near real-time, monthly fossil CO₂ emissions estimates for the European Union with
2802 current-year projections, *Atmospheric Pollution Research*, 12, 101229, <https://doi.org/10.1016/j.apr.2021.101229>,
2803 2021.
- 2804 Andrew, R. M., & Peters, G. P.: The Global Carbon Project's fossil CO₂ emissions dataset (Version 251022) [Data
2805 set]. Zenodo. <https://doi.org/10.5281/zenodo.5569234>, 2025.
- 2806 Aragão, L. E. O. C., Anderson, L. O., Fonseca, M. G., Rosan, T. M., Vedovato, L. B., Wagner, F. H., Silva, C. V.
2807 J., Silva Junior, C. H. L., Arai, E., Aguiar, A. P., Barlow, J., Berenguer, E., Deeter, M. N., Domingues, L. G., Gatti,
2808 L., Gloor, M., Malhi, Y., Marengo, J. A., Miller, J. B., Phillips, O. L., and Saatchi, S.: 21st Century drought-related
2809 fires counteract the decline of Amazon deforestation carbon emissions, *Nat Commun*, 9, 536,
2810 <https://doi.org/10.1038/s41467-017-02771-y>, 2018.
- 2811 Archer, D., Eby, M., Brovkin, V., Ridgwell, A., Cao, L., Mikolajewicz, U., Caldeira, K., Matsumoto, K.,
2812 Munhoven, G., Montenegro, A., and Tokos, K.: Atmospheric Lifetime of Fossil Fuel Carbon Dioxide, *Annu. Rev.*
2813 *Earth Planet. Sci.*, 37, 117–134, <https://doi.org/10.1146/annurev.earth.031208.100206>, 2009.
- 2814 Arneth, A., Sitch, S., Pongratz, J., Stocker, B. D., Ciais, P., Poulter, B., Bayer, A. D., Bondeau, A., Calle, L., Chini,
2815 L. P., Gasser, T., Fader, M., Friedlingstein, P., Kato, E., Li, W., Lindeskog, M., Nabel, J. E. M. S., Pugh, T. A. M.,
2816 Robertson, E., Viovy, N., Yue, C., and Zaehle, S.: Historical carbon dioxide emissions caused by land-use changes
2817 are possibly larger than assumed, *Nature Geosci*, 10, 79–84, <https://doi.org/10.1038/ngeo2882>, 2017.
- 2818 Asaadi, A., Arora, V. K., Melton, J. R., and Bartlett, P.: An improved parameterization of leaf area index (LAI)
2819 seasonality in the Canadian Land Surface Scheme (CLASS) and Canadian Terrestrial Ecosystem Model (CTEM)
2820 modelling framework, 15, 6885–6907, <https://doi.org/10.5194/bg-15-6885-2018>, 2018.
- 2821 Aumont, O., Orr, J. C., Monfray, P., Ludwig, W., Amiotte-Suchet, P., and Probst, J.-L.: Riverine-driven
2822 interhemispheric transport of carbon, *Global Biogeochem. Cycles*, 15, 393–405,
2823 <https://doi.org/10.1029/1999GB001238>, 2001.
- 2824 Aumont, O., Ethé, C., Tagliabue, A., Bopp, L., and Gehlen, M.: PISCES-v2: an ocean biogeochemical model for
2825 carbon and ecosystem studies, 8, 2465–2513, <https://doi.org/10.5194/gmd-8-2465-2015>, 2015.
- 2826 Babiker, M., G. Berndes, K. Blok, B. Cohen, A. Cowie, O. Geden, V. Ginzburg, A. Leip, P. Smith, M. Sugiyama,
2827 F. Yamba, Al Khourdajie, A., Arneth, A., Lima de Azevedo, I. M., Bataille, C., Beerling, D., Bezner Kerr, R.,
2828 Bradley, J., Buck, H. J., Cabeza, L. F., Calvin, K., Campbell, D., Carnicer Cols, J., Daioglou, V., Harmsen, M.,
2829 Höglund-Isaksson, L., House, J. I., Keller, D., de Kleijne, K., Kugelberg, S., Makarov, I., Meza, F., Minx, J. C.,
2830 Morecroft, M., Nabuurs, G. J., Neufeldt, H., Novikova, A., Nugroho, S. B., Oeschlies, A., Parmesan, C., Peters, G.
2831 P., Poore, J., Portugal-Pereira, J., Postigo, J. C., Pradhan, P., Renforth, P., Rivera-Ferre, M. G., Roe, S., Singh, P.
2832 K., Slade, R., Smith, S. M., Tirado von der Pahlen, M. C., and Toribio Ramirez, D.: Cross sectoral perspectives. In:
2833 *Climate Change 2022: Mitigation of Climate Change. Contribution of Working Group III to the Sixth Assessment*
2834 *Report of the Intergovernmental Panel on Climate Change* [P.R. Shukla, J. Skea, R. Slade, A. Al Khourdajie, R.
2835 van Diemen, D. McCollum, M. Pathak, S. Some, P. Vyas, R. Fradera, M. Belkacemi, A. Hasija, G. Lisboa, S. Luz,
2836 J. Malley, (eds.)]. Cambridge University Press, Cambridge, UK and New York, NY, USA. doi:
2837 10.1017/9781009157926.014, 2022.

2838 Baccini, A., Walker, W., Carvalho, L., Farina, M., Sulla-Menashe, D., and Houghton, R. A.: Tropical forests are a
2839 net carbon source based on aboveground measurements of gain and loss, *Science*, 358, 230–234,
2840 <https://doi.org/10.1126/science.aam5962>, 2017.

2841 Bakker, D. C. E., Pfeil, B., Landa, C. S., Metzl, N., O'Brien, K. M., Olsen, A., Smith, K., Cosca, C., Harasawa, S.,
2842 Jones, S. D., Nakaoka, S., Nojiri, Y., Schuster, U., Steinhoff, T., Sweeney, C., Takahashi, T., Tilbrook, B., Wada,
2843 C., Wanninkhof, R., Alin, S. R., Balestrini, C. F., Barbero, L., Bates, N. R., Bianchi, A. A., Bonou, F., Boutin, J.,
2844 Bozec, Y., Burger, E. F., Cai, W.-J., Castle, R. D., Chen, L., Chierici, M., Currie, K., Evans, W., Featherstone, C.,
2845 Feely, R. A., Fransson, A., Goyet, C., Greenwood, N., Gregor, L., Hankin, S., Hardman-Mountford, N. J., Harlay,
2846 J., Hauck, J., Hoppema, M., Humphreys, M. P., Hunt, C. W., Huss, B., Ibáñez, J. S. P., Johannessen, T., Keeling,
2847 R., Kitidis, V., Körtzinger, A., Kozyr, A., Krasakopoulou, E., Kuwata, A., Landschützer, P., Lauvset, S. K.,
2848 Lefèvre, N., Lo Monaco, C., Manke, A., Mathis, J. T., Merlivat, L., Millero, F. J., Monteiro, P. M. S., Munro, D.
2849 R., Murata, A., Newberger, T., Omar, A. M., Ono, T., Paterson, K., Pearce, D., Pierrot, D., Robbins, L. L., Saito,
2850 S., Salisbury, J., Schlitzer, R., Schneider, B., Schweitzer, R., Sieger, R., Skjelvan, I., Sullivan, K. F., Sutherland, S.
2851 C., Sutton, A. J., Tadokoro, K., Telszewski, M., Tuma, M., van Heuven, S. M. A. C., Vandemark, D., Ward, B.,
2852 Watson, A. J., and Xu, S.: A multi-decade record of high-quality CO₂ data in version 3 of the Surface Ocean CO₂
2853 Atlas (SOCAT), *Earth Syst. Sci. Data*, 8, 383–413, <https://doi.org/10.5194/essd-8-383-2016>, 2016.

2854 Bakker, D. C. E., Alin, S. R., Aramaki, T., Barbero, L., Bates, N. R., Gkritzalis, T., Jones, S. D., Kozyr, A.,
2855 Lauvset, S. K., Macovei, V., Metzl, N., Munro, D. R., Nakaoka, S.-i., O'Brien, K. M., Olsen, A., Pierrot, D.,
2856 Steinhoff, T., Sullivan, K. F., Sutton, A. J., Sweeney, C., Wada, C., Wanninkhof, R., Akl, J., Arbilla, L. A., Azetsu-
2857 Scott, K., Battisti, R., Beatty, C. M., Becker, M., Benoit-Cattin, A., Berghoff, C. F., Bittig, H. C., Bonin, J. A.,
2858 Bott, R., Bozzano, R., Burger, E. F., Brunetti, F., Cantoni, C., Castelli, G., Chambers, D. P., Chierici, M., Corbo,
2859 A., Cronin, M., Cross, J. N., Currie, K. I., Dentico, C., Emerson, S. R., Enochs, I., Enright, M. P., Enyo, K.,
2860 Ericson, Y., Evans, W., Fay, A. R., Feely, R. A., Fragiaco, E., Fransson, A., Gehrung, M., Giani, M., Glockzin,
2861 M., Hamna, S., Holodkov, N., Hoppema, M., Ibáñez, J. S. P., Kadono, K., Kamb, L., Kralj, M., Kristensin, T. O.,
2862 Laudicella, V. A., Lefèvre, N., Leseurre, C., Lo Monaco, C., Maenner Jones, S. M., Maenza, R. A., McAuliffe, A.
2863 M., Mdokwana, B. W., Monacci, N. M., Musielewicz, S., Neill, C., Newberger, T., Nojiri, Y., Ohman, M. D.,
2864 Ólafsdóttir, S. R., Olivier, L., Omar, A., Osborne, J., Pensieri, S., Petersen, W., Plueddemann, A. J., Rehder, G.,
2865 Roden, N. P., Rutgersson, A., Sallée, J.-B., Sanders, R., Sarpe, D., Schirnik, C., Schlitzer, R., Send, U., Skjelvan,
2866 I., Sutherland, S. C., T'Jampens, M., Tamsitt, V., Telszewski, M., Theetaert, H., Tilbrook, B., Trull, T., Tsanwani,
2867 M., Van de Velde, S., Van Heuven, S. M. A. C., Vecchia, M. H., Voynova, Y. G., Weller, R. A., Williams, N. L.:
2868 Surface Ocean CO₂ Atlas Database Version 2025 (SOCATv2025) (NCEI Accession 0304549), NOAA National
2869 Centers for Environmental Information, Dataset, <https://doi.org/10.25921/648f-fv35>, 2025a.

2870 Bakker, D. C. E., Alin, S. R., Aramaki, T., Barbero, L., Bates, N. R., Gkritzalis, T., Jones, S. D., Kozyr, A.,
2871 Lauvset, S. K., Macovei, V. A., Metzl, N., Munro, D. R., Nakaoka, S.-i., O'Brien, K. M., Olsen, A., Pierrot, D.,
2872 Steinhoff, T., Sullivan, K. F., Sutton, A. J., Sweeney, C., Wada, C., Wanninkhof, R.: SOCAT version 2025: Open
2873 ocean CO₂ data submissions stabilise, <https://socat.info/index.php/posters/>, Poster published on 05/06/2025. Last
2874 access 23 October 2025, 2025b.

2875 Ballantyne, A. P., Alden, C. B., Miller, J. B., Tans, P. P., and White, J. W. C.: Increase in observed net carbon
2876 dioxide uptake by land and oceans during the past 50 years, *Nature*, 488, 70–72,
2877 <https://doi.org/10.1038/nature11299>, 2012.

2878 Ballantyne, A. P., Andres, R., Houghton, R., Stocker, B. D., Wanninkhof, R., Anderegg, W., Cooper, L. A.,
2879 DeGrandpre, M., Tans, P. P., Miller, J. B., Alden, C., and White, J. W. C.: Audit of the global carbon budget:
2880 estimate errors and their impact on uptake uncertainty, *Biogeosciences*, 12, 2565–2584, <https://doi.org/10.5194/bg-12-2565-2015>, 2015.

2882 Bar-On, Y. M., Li, X., O'Sullivan, M., Wigneron, J.-P., Sitch, S., Ciais, P., Frankenberg, C., Fischer, W. W.: Recent
2883 gains in global terrestrial carbon stocks are mostly stored in nonliving pools, *Science* 387, 1291–1295, 2025.

2884 Bastos, A., Hartung, K., Nützel, T. B., Nabel, J. E. M. S., Houghton, R. A., and Pongratz, J.: Comparison of
2885 uncertainties in land-use change fluxes from bookkeeping model parameterisation, 12, 745–762,
2886 <https://doi.org/10.5194/esd-12-745-2021>, 2021.

2887 Battle, M. O., Raynor, R., Kesler, S., and Keeling, R.: Technical Note: The impact of industrial activity on the
2888 amount of atmospheric O₂, *Atmospheric Chem. Phys. Discuss.*, 1–17, <https://doi.org/10.5194/acp-2022-765>, 2023.

Deleted: <https://doi.org/10.25921/648f-fv35>

- 2890 Bellenger, H., Bopp, L., Ethé, C., Ho, D., Duvel, J. P., Flavoni, S., Guez, L., Kataoka, T., Perrot, X., Parc, L., and
2891 Watanabe, M.: Sensitivity of the Global Ocean Carbon Sink to the Ocean Skin in a Climate Model, *J. Geophys.*
2892 *Res. Oceans*, 128, e2022JC019479, <https://doi.org/10.1029/2022JC019479>, 2023.
- 2893 Bennington, V., Gloege, L., and McKinley, G. A.: Variability in the Global Ocean Carbon Sink From 1959 to 2020
2894 by Correcting Models with Observations, *Geophys. Res. Lett.*, 49, e2022GL098632,
2895 <https://doi.org/10.1029/2022GL098632>, 2022.
- 2896 Bernardello, R., Sicardi, V., Lapin, V., Ortega, P., Ruprich-Robert, Y., Tourigny, E. and Ferrer, E.: Ocean
2897 biogeochemical reconstructions to estimate historical ocean CO₂ uptake. *Earth System Dynamics*, 15(5), pp.1255-
2898 1275, <https://doi.org/10.5194/esd-15-1255-2024>, 2024.
- 2899 Berthet, S., Sférian, R., Bricaud, C., Chevallier, M., Voldoire, A., and Ethé, C.: Evaluation of an Online Grid-
2900 Coarsening Algorithm in a Global Eddy-Admitting Ocean Biogeochemical Model, *J. Adv. Model Earth Syst.*, 11,
2901 1759–1783, <https://doi.org/10.1029/2019MS001644>, 2019.
- 2902 Bethke, I., Wang, Y., Counillon, F., Keenlyside, N., Kimmritz, M., Fransner, F., Samuelsen, A., Langehaug, H.,
2903 Svendsen, L., Chiu, P.-G., Passos, L., Bentsen, M., Guo, C., Gupta, A., Tjiputra, J., Kirkevåg, A., Olivie, D.,
2904 Seland, Ø., Solsvik Vågane, J., Fan, Y., and Eldevik, T.: NorCPM1 and its contribution to CMIP6 DCCP, *Geosci.*
2905 *Model Dev.*, 14, 7073–7116, <https://doi.org/10.5194/gmd-14-7073-2021>, 2021.
- 2906 Betts, R. A., Jones, C. D., Knight, J. R., Keeling, R. F., and Kennedy, J. J.: El Niño and a record CO₂ rise, *Nat.*
2907 *Clim. Change*, 6, 806–810, <https://doi.org/10.1038/nclimate3063>, 2016.
- 2908 Bilbao, R., Wild, S., Ortega, P., Acosta-Navarro, J., Arsouze, T., Bretonnière, P.A., Caron, L.P., Castrillo, M.,
2909 Cruz-García, R., Cvijanovic, I. and Doblas-Reyes, F.J.: Assessment of a full-field initialised decadal climate
2910 prediction system with the CMIP6 version of EC-Earth. *Earth System Dynamics Discussions*, 2020, pp.1-30,
2911 <https://doi.org/10.5194/esd-12-173-2021>, 2020.
- 2912 Bloom, A. A. and Williams, M.: Constraining ecosystem carbon dynamics in a data-limited world: integrating
2913 ecological “common sense” in a model–data fusion framework, *Biogeosciences*, 12, 1299–1315,
2914 <https://doi.org/10.5194/bg-12-1299-2015>, 2015.
- 2915 Bloom, A. A., Exbrayat, J.-F., van der Velde, I. R., Feng, L., and Williams, M.: The decadal state of the terrestrial
2916 carbon cycle: Global retrievals of terrestrial carbon allocation, pools, and residence times, *Proc. Natl. Acad. Sci.*,
2917 113, 1285–1290, <https://doi.org/10.1073/pnas.1515160113>, 2016.
- 2918 Boer, G. J., Smith, D. M., Cassou, C., Doblas-Reyes, F., Danabasoglu, G., Kirtman, B., Kushnir, Y., Kimoto, M.,
2919 Meehl, G. A., Msadek, R., Mueller, W. A., Taylor, K. E., Zwiers, F., Rixen, M., Ruprich-Robert, Y., and Eade, R.:
2920 The Decadal Climate Prediction Project (DCPP) contribution to CMIP6, *Geosci. Model Dev.*, 9, 3751–3777,
2921 <https://doi.org/10.5194/gmd-9-3751-2016>, 2016.
- 2922 Boucher, O., Servonnat, J., Albright, A. L., Aumont, O., Balkanski, Y., Bastrikov, V., Bekki, S., Bonnet, R., Bony,
2923 S., Bopp, L., Braconnot, P., Brockmann, P., Cadule, P., Caubel, A., Cheruy, F., Codron, F., Cozic, A., Cugnet, D.,
2924 D’Andrea, F., Davini, P., de Lavergne, C., Denvil, S., Deshayes, J., Devilliers, M., Ducharne, A., Dufresne, J.-L.,
2925 Dupont, E., Ethé, C., Fairhead, L., Falletti, L., Flavoni, S., Foujols, M.-A., Gardoll, S., Gastineau, G., Ghattas, J.,
2926 Grandpeix, J.-Y., Guenet, B., Guez, E., Lionel, Guilyardi, E., Guimberteau, M., Hauglustaine, D., Hourdin, F.,
2927 Idelkadi, A., Joussaume, S., Kageyama, M., Khodri, M., Krinner, G., Lebas, N., Levvasseur, G., Lévy, C., Li, L.,
2928 Lott, F., Lurton, T., Luyssaert, S., Madec, G., Madeleine, J.-B., Maignan, F., Marchand, M., Marti, O., Mellul, L.,
2929 Meurdesoif, Y., Mignot, J., Musat, I., Ottlé, C., Peylin, P., Planton, Y., Polcher, J., Rio, C., Rochetin, N., Rousset,
2930 C., Sepulchre, P., Sima, A., Swingedouw, D., Thiéblemont, R., Traore, A. K., Vancoppenolle, M., Vial, J., Vialard,
2931 J., Viovy, N., and Vuichard, N.: Presentation and Evaluation of the IPSL-CM6A-LR Climate Model, *J. Adv.*
2932 *Model. Earth Syst.*, 12, e2019MS002010, <https://doi.org/10.1029/2019MS002010>, 2020.
- 2933 Bourgeois, T., Goris, N., Schwinger, J., and Tjiputra, J. F.: Stratification constrains future heat and carbon uptake
2934 in the Southern Ocean between 30°S and 55°S, *Nat. Commun.*, 13, 340, <https://doi.org/10.1038/s41467-022-27979-5>, 2022.
- 2936 Bourgoin, C., Beuchle, R., Branco, A., Carreiras, J., Ceccherini, G., Oom, D., San-Miguel-Ayanz, J., and Sedano,
2937 F.: Extensive fire-driven degradation in 2024 marks worst Amazon forest disturbance in over 2 decades,
2938 *Biogeosciences*, 22, 5247–5256, <https://doi.org/10.5194/bg-22-5247-2025>, 2025.

Deleted: <https://doi.org/10.5194/gmd-14-7073-2021>

- 2940 Bray, E.: 2017 Minerals Yearbook: Aluminum [Advance Release], Tech. rep., U.S. Geological Survey, <https://d9-wret.s3-us-west-2.amazonaws.com/assets/palladium/production/atoms/files/myb1-2017-alumi.pdf>, 2020.
- 2941
- 2942 Brienen, R. J. W., Caldwell, L., Duchesne, L., Voelker, S., Barichivich, J., Baliva, M., Ceccantini, G., Di Filippo, A., Helama, S., Locosselli, G. M., Lopez, L., Piovesan, G., Schöngart, J., Villalba, R., and Gloor, E.: Forest carbon sink neutralized by pervasive growth-lifespan trade-offs, *Nat. Commun.*, 11, 4241, <https://doi.org/10.1038/s41467-020-17966-z>, 2020.
- 2943
- 2944
- 2945
- 2946 Brienen, R. J. W., Phillips, O. L., Feldpausch, T. R., Gloor, E., Baker, T. R., Lloyd, J., Lopez-Gonzalez, G., Monteagudo-Mendoza, A., Malhi, Y., Lewis, S. L., Vásquez Martínez, R., Alexiades, M., Álvarez Dávila, E., Alvarez-Loayza, P., Andrade, A., Aragão, L. E. O. C., Araujo-Murakami, A., Arets, E. J. M. M., Arroyo, L., Aymard C., G. A., Bánki, O. S., Baraloto, C., Barroso, J., Bonal, D., Boot, R. G. A., Camargo, J. L. C., Castilho, C. V., Chama, V., Chao, K. J., Chave, J., Comiskey, J. A., Cornejo Valverde, F., da Costa, L., de Oliveira, E. A., Di Fiore, A., Erwin, T. L., Fauset, S., Forsthofer, M., Galbraith, D. R., Grahame, E. S., Groot, N., Hérault, B., Higuchi, N., Honorio Coronado, E. N., Keeling, H., Killeen, T. J., Laurance, W. F., Laurance, S., Licona, J., Magnussen, W. E., Marimon, B. S., Marimon-Junior, B. H., Mendoza, C., Neill, D. A., Nogueira, E. M., Núñez, P., Pallqui Camacho, N. C., Parada, A., Pardo-Molina, G., Peacock, J., Peña-Claros, M., Pickavance, G. C., Pitman, N. C. A., Poorter, L., Prieto, A., Quesada, C. A., Ramirez, F., Ramirez-Angulo, H., Restrepo, Z., Roopsind, A., Rudas, A., Salomão, R. P., Schwarz, M., Silva, N., Silva-Espejo, J. E., Silveira, M., Stropp, J., Talbot, J., ter Steege, H., Teran-Aguilar, J., Terborgh, J., Thomas-Caesar, R., Toledo, M., Torello-Raventos, M., Umetzu, R. K., van der Heijden, G. M. F., van der Hout, P., Guimarães Vieira, I. C., Vieira, S. A., Vilanova, E., Vos, V. A., and Zagt, R. J.: Long-term decline of the Amazon carbon sink, 519, 344–348, <https://doi.org/10.1038/nature14283>, 2015.
- 2947
- 2948
- 2949
- 2950
- 2951
- 2952
- 2953
- 2954
- 2955
- 2956
- 2957
- 2958
- 2959
- 2960 Bronselaer, B., Winton, M., Russell, J., Sabine, C. L., and Khatiwala, S.: Agreement of CMIP5 Simulated and Observed Ocean Anthropogenic CO₂ Uptake, *Geophys. Res. Lett.*, 44, 12,298–12,305, <https://doi.org/10.1002/2017GL074435>, 2017.
- 2961
- 2962
- 2963 Bruno, M. and Joos, F.: Terrestrial carbon storage during the past 200 years: A Monte Carlo Analysis of CO₂ data from ice core and atmospheric measurements, *Global Biogeochem. Cycles*, 11, 111–124, <https://doi.org/10.1029/96GB03611>, 1997.
- 2964
- 2965
- 2966 Burrows, S. M., Maltrud, M., Yang, X., Zhu, Q., Jeffery, N., Shi, X., Ricciuto, D., Wang, S., Bisht, G., Tang, J., Wolfe, J., Harrop, B. E., Singh, B., Brent, L., Baldwin, S., Zhou, T., Cameron-Smith, P., Keen, N., Collier, N., Xu, M., Hunke, E. C., Elliott, S. M., Turner, A. K., Li, H., Wang, H., Golaz, J.-C., Bond-Lamberty, B., Hoffman, F. M., Riley, W. J., Thornton, P. E., Calvin, K., and Leung, L. R.: The DOE E3SM v1.1 Biogeochemistry Configuration: Description and Simulated Ecosystem-Climate Responses to Historical Changes in Forcing, *J. Adv. Model. Earth Syst.*, 12, e2019MS001766, <https://doi.org/10.1029/2019MS001766>, 2020.
- 2967
- 2968
- 2969
- 2970
- 2971
- 2972 Bunsen, F., Nissen, C., and Hauck, J.: The Impact of Recent Climate Change on the Global Ocean Carbon Sink. *Geophysical Research Letters*, 51(4), e2023GL107030, <https://doi.org/10.1029/2023GL107030>, 2024.
- 2973
- 2974 Burton, C., Betts, R., Cardoso, M., Feldpausch, T. R., Harper, A., Jones, C. D., Kelley, D. I., Robertson, E., and Wiltshire, A.: Representation of fire, land-use change and vegetation dynamics in the Joint UK Land Environment Simulator vn4.9 (JULES), *Geosci. Model Dev.*, 12, 179–193, <https://doi.org/10.5194/gmd-12-179-2019>, 2019.
- 2975
- 2976
- 2977 Burton, C., Lampe, S., Kelley, D. I., Thiery, W., Hantson, S., Christidis, N., Gudmundsson, L., Forrest, M., Burke, E., Chang, J., Huang, H., Ito, A., Kou-Giesbrecht, S., Lasslop, G., Li, W., Nieradzki, L., Li, F., Chen, Y., Randerson, J., Reyer, C. P. O., and Mengel, M.: Global burned area increasingly explained by climate change, *Nature Climate Change*, <https://doi.org/10.1038/s41558-024-02140-w>, 2024.
- 2978
- 2979
- 2980
- 2981 Bushinsky, S. M., Landschützer, P., Rödenbeck, C., Gray, A. R., Baker, D., Mazloff, M. R., Resplandy, L., Johnson, K. S., and Sarmiento, J. L.: Reassessing Southern Ocean Air-Sea CO₂ Flux Estimates With the Addition of Biogeochemical Float Observations, *Global Biogeochem. Cycles*, 33, 1370–1388, <https://doi.org/10.1029/2019GB006176>, 2019.
- 2982
- 2983
- 2984
- 2985 Byrne, B., Liu, J., Bowman, K.W., Pascolini-Campbell, M., Chatterjee, A., Pandey, S., Miyazaki, K., van der Werf, G.R., Wunch, D., Wennberg, P.O., Roehl, C.M., and Sinha, S.: Carbon emissions from the 2023 Canadian wildfires. *Nature*, 633, 835–839, <https://doi.org/10.1038/s41586-024-07878-z>, 2024.
- 2986
- 2987
- 2988 Canadell, J. G., Le Quere, C., Raupach, M. R., Field, C. B., Buitenhuis, E. T., Ciais, P., Conway, T. J., Gillett, N. P., Houghton, R. A., and Marland, G.: Contributions to accelerating atmospheric CO₂ growth from economic
- 2989

2990 activity, carbon intensity, and efficiency of natural sinks, *Proceedings of the National Academy of Sciences*, 104,
2991 18866–18870, <https://doi.org/10.1073/pnas.0702737104>, 2007.

2992 Canadell, J. G., Monteiro, P. M. S., Costa, M. H., Cotrim da Cunha, L., Cox, P. M., Eliseev, A. V., Henson, S.,
2993 Ishii, M., Jaccard, S., Koven, C., Lohila, A., Patra, P. K., Piao, S., Rogelj, J., Syampungani, S., Zaehle, S., and
2994 Zickfeld, K.: Global Carbon and other Biogeochemical Cycles and Feedbacks. In: *Climate Change 2021: The
2995 Physical Science Basis. Contribution of Working Group I to the Sixth Assessment Report of the Intergovernmental
2996 Panel on Climate Change* [Masson-Delmotte, V., P. Zhai, A. Pirani, S. L. Connors, C. Péan, S. Berger, N. Caud, Y.
2997 Chen, L. Goldfarb, M. I. Gomis, M. Huang, K. Leitzell, E. Lonnoy, J.B.R. Matthews, T. K. Maycock, T.
2998 Waterfield, O. Yelekçi, R. Yu and B. Zhou (eds.)]. Cambridge University Press, Cambridge, United Kingdom and
2999 New York, NY, USA, pp. 673–816, <https://doi.org/10.1017/9781009157896.007>, 2021.

3000 Cao, Z., Myers, R. J., Lupton, R. C., Duan, H., Sacchi, R., Zhou, N., Reed Miller, T., Cullen, J. M., Ge, Q., and
3001 Liu, G.: The sponge effect and carbon emission mitigation potentials of the global cement cycle, *Nat Commun*, 11,
3002 3777, <https://doi.org/10.1038/s41467-020-17583-w>, 2020.

3003 Carbon Monitor: Year in Review: Global carbon emissions and decarbonization in 2024, available at:
3004 <https://carbonmonitor.org/>, last access: 23 October 2025, 2025.

3005 Centro Nacional de Monitoramento e Alertas de Desastres Naturais (CEMADEN): Monitoramento de secas e
3006 impactos no Brasil - Agosto 2024, available at: [https://www.gov.br/cemaden/pt-
3007 br/assuntos/monitoramento/monitoramento-de-seca-para-o-brasil/monitoramento-de-secas-e-impactos-no-brasil-
3008 agosto-2024](https://www.gov.br/cemaden/pt-br/assuntos/monitoramento/monitoramento-de-seca-para-o-brasil/monitoramento-de-secas-e-impactos-no-brasil-agosto-2024), last access: 23 October 2025.

3009 Céspedes, J., Sylvester, J. M., Pérez-Marulanda, L., Paz-García, P., Reymondin, L., Khodadadi, M., Tello, J. J., and
3010 Castro-Nunez, A.: Has global deforestation accelerated due to the COVID-19 pandemic?, *J. For. Res.*, 34, 1153–
3011 1165, <https://doi.org/10.1007/s11676-022-01561-7>, 2023.

3012 Chandra, N., Patra, P. K., Niwa, Y., Ito, A., Iida, Y., Goto, D., Morimoto, S., Kondo, M., Takigawa, M., Hajima,
3013 T., and Watanabe, M.: Estimated regional CO₂ flux and uncertainty based on an ensemble of atmospheric CO₂
3014 inversions, *Atmospheric Chem. Phys.*, 22, 9215–9243, <https://doi.org/10.5194/acp-22-9215-2022>, 2022.

3015 Chatfield, C.: The Holt-Winters Forecasting Procedure, *J. Roy. Stat. Soc. C.*, 27, 264–279,
3016 <https://doi.org/10.2307/2347162>, 1978.

3017 Chau, T. T. T., Gehlen, M., and Chevallier, F.: A seamless ensemble-based reconstruction of surface ocean pCO₂
3018 and air–sea CO₂ fluxes over the global coastal and open oceans, *Biogeosciences*, 19, 1087–1109,
3019 <https://doi.org/10.5194/bg-19-1087-2022>, 2022.

3020 Chen, Y., Hall, J., Van Wees, D., Andela, N., Hantson, S., Giglio, L., Van Der Werf, G. R., Morton, D. C., and
3021 Randerson, J. T.: Multi-decadal trends and variability in burned area from the fifth version of the Global Fire
3022 Emissions Database (GFED5), *Earth Syst. Sci. Data*, 15, 5227–5259, <https://doi.org/10.5194/essd-15-5227-2023>,
3023 2023.

3024 Chevallier, F., Fisher, M., Peylin, P., Serrar, S., Bousquet, P., Bréon, F.-M., Chédin, A., and Ciais, P.: Inferring CO₂
3025 2 sources and sinks from satellite observations: Method and application to TOVS data, *J. Geophys. Res.*, 110,
3026 D24309, <https://doi.org/10.1029/2005JD006390>, 2005.

3027 Chevallier, F., Martínez, A., Lloret, Z., Takache, S., and Cozic, A.: Offline Atmospheric Transport on a Global
3028 Mesh of Hexagons, *JGR Atmospheres*, 130, e2025JD043579, <https://doi.org/10.1029/2025JD043579>, 2025.

3029 Ciais, P., Sabine, C., Bala, G., Bopp, L., Brovkin, V., Canadell, J. G., Chhabra, A., DeFries, R., Galloway, J.,
3030 Heimann, M., Jones, C., Le Quéré, C., Myneni, R., Piao, S., Thornton, P., Willem, J., Friedlingstein, P., and
3031 Munhoven, G.: Carbon and Other Biogeochemical Cycles, in *Climate Change 2013: The Physical Science Basis,
3032 Contribution of Working Group I to the Fifth Assessment Report of the Intergovernmental Panel on Climate
3033 Change*, edited by: Intergovernmental Panel on Climate Change, Cambridge University Press, Cambridge, United
3034 Kingdom and New York, NY, USA, <https://doi.org/10.1017/CBO9781107415324.015>, 2013.

3035 Ciais, P., Tan, J., Wang, X., Roedenbeck, C., Chevallier, F., Piao, S.-L., Moriarty, R., Broquet, G., Le Quéré, C.,
3036 Canadell, J. G., Peng, S., Poulter, B., Liu, Z., and Tans, P.: Five decades of northern land carbon uptake revealed
3037 by the interhemispheric CO₂ gradient, *Nature*, 568, 221–225, <https://doi.org/10.1038/s41586-019-1078-6>, 2019.

Deleted: Data, 15, 5227–5259, <https://doi.org/10.5194/essd-15-5227-2023>

Deleted: <https://doi.org/10.1029/2025JD043579>

- 3041 Ciais, P., Bastos, A., Chevallier, F., Lauerwald, R., Poulter, B., Canadell, P., Hugelius, G., Jackson, R. B., Jain, A.,
3042 Jones, M., Kondo, M., Luijkx, I. T., Patra, P. K., Peters, W., Pongratz, J., Petrescu, A. M. R., Piao, S., Qiu, C., Von
3043 Randow, C., Regnier, P., Saunois, M., Scholes, R., Shvidenko, A., Tian, H., Yang, H., Wang, X., and Zheng, B.:
3044 Definitions and methods to estimate regional land carbon fluxes for the second phase of the REgional Carbon
3045 Cycle Assessment and Processes Project (RECCAP-2), *Geosci. Model Dev.*, 15, 1289–1316,
3046 <https://doi.org/10.5194/gmd-15-1289-2022>, 2022.
- 3047 Ciais, P., Ke, P., Yao, Y., Sitch, S., Li, W., Xu, Y., Du, X., Gui, X., Bastos, A., Zaehle, S., Poulter, B., Colligan, T.,
3048 van der Woude, A. M., Peters, W., Liu, Z., Jin, Z., Tian, X., Wang, Y., Liu, J., Pandey, S., O'Dell, C., Bian, J.,
3049 Zhou, C., Miller, J., Lan, X., Goncalves De Souza, J., O'Sullivan, M., Friedlingstein, P., van der Werf, G. R.,
3050 Peters, G. P., and Chevallier, F.: Low latency global carbon budget indicates reduced land carbon sink in the year
3051 2024, *National Science Review*, submitted.
- 3052 Collier, N., Hoffman, F. M., Lawrence, D. M., Keppel-Aleks, G., Koven, C. D., Riley, W. J., Mu, M., and
3053 Randerson, J. T.: The International Land Model Benchmarking (ILAMB) System: Design, Theory, and
3054 Implementation, *J. Adv. Model. Earth Syst.*, 10, 2731–2754, <https://doi.org/10.1029/2018MS001354>, 2018.
- 3055 Conchedda, G. and Tubiello, F. N.: Drainage of organic soils and GHG emissions: Validation with country data,
3056 *Biosphere – Biogeosciences*, <https://doi.org/10.5194/essd-2020-202>, 2020.
- 3057 Cox, P. M., Pearson, D., Booth, B. B., Friedlingstein, P., Huntingford, C., Jones, C. D., and Luke, C. M.:
3058 Sensitivity of tropical carbon to climate change constrained by carbon dioxide variability, *Nature*, 494, 341–344,
3059 <https://doi.org/10.1038/nature11882>, 2013.
- 3060 De Kauwe, M. G., Medlyn, B. E., Zaehle, S., Walker, A. P., Dietze, M. C., Wang, Y.-P., Luo, Y., Jain, A. K., El-
3061 Masri, B., Hickler, T., Wärlind, D., Weng, E., Parton, W. J., Thornton, P. E., Wang, S., Prentice, I. C., Asao, S.,
3062 Smith, B., McCarthy, H. R., Iversen, C. M., Hanson, P. J., Warren, J. M., Oren, R., and Norby, R. J.: Where does
3063 the carbon go? A model–data intercomparison of vegetation carbon allocation and turnover processes at two
3064 temperate forest free-air CO₂ enrichment sites, *New Phytol.*, 203, 883–899, <https://doi.org/10.1111/nph.12847>,
3065 2014.
- 3066 Delire, C., Séférian, R., Decharme, B., Alkama, R., Calvet, J.-C., Carrer, D., Gibelin, A.-L., Joetzjer, E., Morel, X.,
3067 Rocher, M., and Tzanos, D.: The Global Land Carbon Cycle Simulated With ISBA-CTRIP: Improvements Over
3068 the Last Decade, *J. Adv. Model. Earth Syst.*, 12, e2019MS001886, <https://doi.org/10.1029/2019MS001886>, 2020.
- 3069 Denman, K. L., Brasseur, G., Chidthaisong, A., Ciais, P., Cox, P. M., Dickinson, R. E., Hauglustaine, D., Heinze,
3070 C., Holland, E., Jacob, D., Lohmann, U., Ramachandran, S., Leite da Silva Dias, P., Wofsy, S. C., and Zhang, X.:
3071 Couplings Between Changes in the Climate System and Biogeochemistry, in: *Climate Change 2007: The Physical
3072 Science Basis. Contribution of Working Group I to the Fourth Assessment Report of the Intergovernmental Panel
3073 on Climate Change*, edited by: Solomon, S., Qin, D., Manning, M., Marquis, M., Averyt, K., Tignor, M. M. B.,
3074 Miller, H. L., and Chen, Z. L., Cambridge University Press, Cambridge, UK and New York, USA, 499–587, ISBN:
3075 9780521705967, 2007.
- 3076 Denvil-Sommer, A., Gehlen, M., and Vrac, M.: Observation system simulation experiments in the Atlantic Ocean
3077 for enhanced surface ocean pCO₂ reconstructions, *Ocean Sci.*, 17, 1011–1030, <https://doi.org/10.5194/os-17-1011-2021>,
3078 2021.
- 3079 DeVries, T., Holzer, M., and Primeau, F.: Recent increase in oceanic carbon uptake driven by weaker upper-ocean
3080 overturning, *Nature*, 542, 215–218, <https://doi.org/10.1038/nature21068>, 2017.
- 3081 DeVries, T.: The oceanic anthropogenic CO₂ sink: Storage, air-sea fluxes, and transports over the industrial era,
3082 *Global Biogeochem. Cycles*, 28, 631–647, <https://doi.org/10.1002/2013GB004739>, 2014.
- 3083 DeVries, T., Quéré, C. L., Andrews, O., Berthet, S., Hauck, J., Ilyina, T., Landschützer, P., Lenton, A., Lima, I. D.,
3084 Nowicki, M., Schwinger, J., and Séférian, R.: Decadal trends in the ocean carbon sink, *PNAS*, 116, 11646–11651,
3085 <https://doi.org/10.1073/pnas.1900371116>, 2019.
- 3086 DeVries, T.: Atmospheric CO₂ and Sea Surface Temperature Variability Cannot Explain Recent Decadal
3087 Variability of the Ocean CO₂ Sink, *Geophysical Research Letters*, 49, e2021GL096018, <https://doi.org/10.1029/2021GL096018>,
3088 <https://doi.org/10.1029/2021GL096018>, 2022.

Deleted: <https://doi.org/10.1029/2021GL096018>

3090 DeVries, T., Yamamoto, K., Wanninkhof, R., Gruber, N., Hauck, J., Müller, J. D., Bopp, L., Carroll, D., Carter, B.,
3091 Chau, T.-T., Doney, S. C., Gehlen, M., Gloege, L., Gregor, L., Henson, S., Kim, J. H., Iida, Y., Ilyina, T.,
3092 Landschützer, P., Le Quéré, C., Munro, D., Nissen, C., Patara, L., Pérez, F. F., Resplandy, L., Rodgers, K. B.,
3093 Schwinger, J., Séférian, R., Sicardi, V., Terhaar, J., Triñanes, J., Tsujino, H., Watson, A., Yasunaka, S., and Zeng,
3094 J.: Magnitude, trends, and variability of the global ocean carbon sink from 1985-2018, *Glob. Biogeochem. Cycles*,
3095 n/a, e2023GB007780, <https://doi.org/10.1029/2023GB007780>, 2023.

3096 Döscher, R., Acosta, M., Alessandri, A., Anthoni, P., Arneeth, A., Arsouze, T., Bergmann, T., Bernadello, R.,
3097 Bouseetta, S., Caron, L.P. and Carver, G.: The EC-earth3 Earth system model for the climate model intercomparison
3098 project 6. *Geoscientific Model Development Discussions*, 2021, pp.1-90, [https://doi.org/10.5194/gmd-15-2973-](https://doi.org/10.5194/gmd-15-2973-2022)
3099 2022, 2021.

3100 Doney, S. C., Lima, I., Feely, R. A., Glover, D. M., Lindsay, K., Mahowald, N., Moore, J. K., and Wanninkhof, R.:
3101 Mechanisms governing interannual variability in upper-ocean inorganic carbon system and air-sea CO₂ fluxes:
3102 Physical climate and atmospheric dust, *Deep Sea Research Part II: Topical Studies in Oceanography*, 56, 640–655,
3103 <https://doi.org/10.1016/j.dsr2.2008.12.006>, 2009.

3104 Dong, Y., Bakker, D. C. E., Bell, T. G., Huang, B., Landschützer, P., Liss, P. S., and Yang, M.: Update on the
3105 Temperature Corrections of Global Air-Sea CO₂ Flux Estimates, *Glob. Biogeochem. Cycles*, 36, e2022GB007360,
3106 <https://doi.org/10.1029/2022GB007360>, 2022.

3107 Dong, Y., Bakker, D. C. E., Bell, T. G., Yang, M., Landschützer, P., Hauck, J., Rödenbeck, C., Kitidis, V.,
3108 Bushinsky, S. M., and Liss, P. S. (2024). Direct observational evidence of strong CO₂ uptake in the Southern
3109 Ocean. *Science Advances*, 10(30), eadn5781, <https://doi.org/10.1126/sciadv.adn5781>, 2024a.

3110 Dong, Y., Bakker, D. C. E., and Landschützer, P.: Accuracy of ocean CO₂ uptake estimates at a risk by a reduction
3111 in the data collection. *Geophysical Research Letters*, 51, e2024GL108502, <https://doi.org/10.1029/2024GL108502>,
3112 2024b.

3113 Dorgeist, L., Schwingshackl, C., Bultan, S., and Pongratz, J.: A consistent budgeting of terrestrial carbon fluxes.
3114 *Nature Communications*, 15(1), 7426, <https://doi.org/10.1038/s41467-024-51126-x>, 2024.

3115 Dou, X., Wang, Y., Ciais, P., Chevallier, F., Davis, S. J., Crippa, M., Janssens-Maenhout, G., Guizzardi, D.,
3116 Solazzo, E., Yan, F., Huo, D., Zheng, B., Zhu, B., Cui, D., Ke, P., Sun, T., Wang, H., Zhang, Q., Gentile, P., Deng,
3117 Z., and Liu, Z.: Near-real-time global gridded daily CO₂ emissions, *The Innovation*, 3, 100182,
3118 <https://doi.org/10.1016/j.xinn.2021.100182>, 2022.

3119 Eckes-Shephard, A. H., Argles, A. P. K., Brzeziecki, B., Cox, P. M., De Kauwe, M. G., Esquivel-Muelbert, A.,
3120 Fisher, R. A., Hurtt, G. C., Knauer, J., Koven, C. D., Lehtonen, A., Luysaert, S., Marqués, L., Ma, L., Marie, G.,
3121 Moore, J. R., Needham, J. F., Olin, S., Peltoniemi, M., Piltz, K., Sato, H., Sitch, S., Stocker, B. D., Weng, E.,
3122 Zuleta, D., and Pugh, T. A. M. Pugh: Demography, dynamics and data: building confidence for simulating changes
3123 in the world's forests, *New Phytologist*, doi: 10.1111/nph.70643, 2025.

3124 Edson, J. B., Jampana, V., Weller, R. A., Bigorre, S. P., Plueddemann, A. J., Fairall, C. W., Miller, S. D., Mahrt,
3125 L., Vickers, D., and Hersbach, H.: On the Exchange of Momentum over the Open Ocean, *J. Phys. Oceanogr.*, 43,
3126 1589–1610, <https://doi.org/10.1175/JPO-D-12-0173.1>, 2013.

3127 EIA: Short-Term Energy Outlook: [March 2026](https://www.eia.gov/forecasts/steo/outlook.cfm). U.S. Energy Information Administration [Data set]. Available at:
3128 <http://www.eia.gov/forecasts/steo/outlook.cfm>, last access: 23 [March 2026](https://www.eia.gov/forecasts/steo/outlook.cfm), 2023.

3129 Embury, O., Merchant, C.J., Good, S.A., Rayner, N.A., Hoyer, J.L., Atkinson, C., Block, T., Alerskans, E.,
3130 Pearson, K.J., Worsfold, M. and McCarroll, N. and Donlon, C.: Satellite-based time-series of sea-surface
3131 temperature since 1980 for climate applications. *Scientific Data*, 11(1), 326, [https://doi.org/10.1038/s41597-024-](https://doi.org/10.1038/s41597-024-03147-w)
3132 03147-w, 2024.

3133 Erb, K.-H., Kastner, T., Luysaert, S., Houghton, R. A., Kuemmerle, T., Olofsson, P., and Haberl, H.: Bias in the
3134 attribution of forest carbon sinks, *Nature Clim Change*, 3, 854–856, <https://doi.org/10.1038/nclimate2004>, 2013.

3135 Erb, K.-H., Kastner, T., Plutzer, C., Bais, A. L. S., Carvalhais, N., Fetzel, T., Gingrich, S., Haberl, H., Lauk, C.,
3136 Niederscheider, M., Pongratz, J., Thurner, M., and Luysaert, S.: Unexpectedly large impact of forest management
3137 and grazing on global vegetation biomass, *Nature*, 553, 73–76, <https://doi.org/10.1038/nature25138>, 2018.

Deleted: October 2025

Deleted: October 2025

Deleted: Ehmen, T. F., Mackay, N. S., and Watson, A.: The Spatiotemporal Distribution of Dissolved Inorganic Carbon in the Global Ocean Interior: Reconstructed through Machine Learning, ESS Open Archive, id. essoar.173687460.04244614/v1, available at: <https://doi.org/10.22541/essoar.173687460.04244614/v1>, last access: 23 October 2025, 2025.

3147 Erb, M. and Marland G.: Global, Regional, and National Fossil-Fuel CO₂ Emissions: 1751-2022 CDIAC-FF,
3148 Research Institute for Environment, Energy, and Economics, Appalachian State University.
3149 <https://rieee.appstate.edu/projects-programs/cdiac/>, last access: 23 October 2025, 2025.

3150 Eskander, S. M. S. U. and Fankhauser, S.: Reduction in greenhouse gas emissions from national climate legislation,
3151 *Nat. Clim. Chang.*, 10, 750–756, <https://doi.org/10.1038/s41558-020-0831-z>, 2020.

3152 Etheridge, D. M., Steele, L. P., Langenfelds, R. L., Francey, R. J., Barnola, J.-M., and Morgan, V. I.: Natural and
3153 anthropogenic changes in atmospheric CO₂ over the last 1000 years from air in Antarctic ice and firn, *J. Geophys.*
3154 *Res.*, 101, 4115–4128, <https://doi.org/10.1029/95JD03410>, 1996.

3155 FAO, Food and Agriculture Organization of the United Nations (FAO): Impact of the Ukraine-Russia conflict on
3156 global food security and related matters under the mandate of the Food and Agriculture Organization of the United
3157 Nations (FAO), Hundred and Seventieth Session of the Council, <https://www.fao.org/3/nj164en/nj164en.pdf>, last
3158 access: 23 October 2025, 2023.

3159 FAO: FAOSTAT Emissions from drained organic soils. Available at <http://www.fao.org/faostat/en/#data/GV>, last
3160 access: 23 October 2025, 2025a.

3161 FAO: Forest emissions and removals – Global, regional and country trends 1990–2025.FAOSTAT Analytical
3162 Briefs, No. 114. Rome., available at: <https://doi.org/10.4060/cd7163en>, last access: 23 October 2025, 2025b.

3163 FAO: Land statistics 2001–2023 – Global, regional and country trends. FAOSTAT Analytical Briefs, No.107.
3164 Rome, available at: <https://doi.org/10.4060/cd5765en>, last access: 23 October 2025, 2025c.

3165 FAO: FAOSTAT Emissions totals database, available at: <https://faostat.fao.org/internal/en/#data/GT>, FAO, Rome,
3166 , last access: 23 October 2025, 2025d.

3167 Fay, A. R., Gregor, L., Landschützer, P., McKinley, G. A., Gruber, N., Gehlen, M., Iida, Y., Laruelle, G. G.,
3168 Rödenbeck, C., Roobaert, A., and Zeng, J.: SeaFlux: harmonization of air–sea CO₂ fluxes from surface pCO₂ data
3169 products using a standardized approach, *Earth System Science Data*, 13, 4693–4710, [https://doi.org/10.5194/essd-](https://doi.org/10.5194/essd-13-4693-2021)
3170 13-4693-2021, 2021.

3171 Fay, A. R., McKinley, G. A., Lovenduski, N. S., Eddebar, Y., Levy, M. N., Long, M. C., Olivarez, H. C., and
3172 Rustagi, R. R.: Immediate and Long-Lasting Impacts of the Mt. Pinatubo Eruption on Ocean Oxygen and Carbon
3173 Inventories. *Global Biogeochemical Cycles*, 37(2). <https://doi.org/10.1029/2022gb007513>, 2023.

3174 Fay, A. R., Carroll, D., McKinley, G. A., Menemenlis, D., and Zhang, H.: Scale-Dependent Drivers of Air-Sea
3175 CO₂ Flux Variability, *Geophysical Research Letters*, 51, e2024GL111911, <https://doi.org/10.1029/2024GL111911>,
3176 2024.

3177 Fay, A. R., Heimdal, T. H., Acquaviva, V., Shaum, A. P., and McKinley, G. A.: Sensitivity of Ocean Carbon Sink
3178 Estimates to Rare Observations, *Geophysical Research Letters*, 52, e2025GL117961,
3179 <https://doi.org/10.1029/2025GL117961>, 2025.

3180 Felzer, B. S.: Carbon, nitrogen, and water response to climate and land use changes in Pennsylvania during the
3181 20th and 21st centuries, *Ecological Modelling*, 240, 49–63, <https://doi.org/10.1016/j.ecolmodel.2012.05.003>, 2012.

3182 Felzer, B. S. and Jiang, M.: Effect of Land Use and Land Cover Change in Context of Growth Enhancements in the
3183 United States Since 1700: Net Source or Sink?, *JGR Biogeosciences*, 123, 3439–3457,
3184 <https://doi.org/10.1029/2017JG004378>, 2018.

3185 Felzer, B. S., Cronin, T. W., Melillo, J. M., Kicklighter, D. W., and Schlosser, C. A.: Importance of carbon-
3186 nitrogen interactions and ozone on ecosystem hydrology during the 21st century, *J. Geophys. Res.*, 114,
3187 2008JG000826, <https://doi.org/10.1029/2008JG000826>, 2009.

3188 Felzer, B. S., Cronin, T. W., Melillo, J. M., Kicklighter, D. W., Schlosser, C. A., and Dangal, S. R. S.: Nitrogen
3189 effect on carbon-water coupling in forests, grasslands, and shrublands in the arid western United States, *J.*
3190 *Geophys. Res.*, 116, G03023, <https://doi.org/10.1029/2010JG001621>, 2011.

3191 Feng, L., Palmer, P. I., Bösch, H., and Dance, S.: Estimating surface CO₂ fluxes from space-borne CO₂ dry air
3192 mole fraction observations using an ensemble Kalman Filter, *Atmospheric Chem. Phys.*, 9, 2619–2633,
3193 <https://doi.org/10.5194/acp-9-2619-2009>, 2009.

Deleted: <https://doi.org/10.1016/j.ecolmodel.2012.05.003>

Deleted:

Deleted: <https://doi.org/10.1029/2017JG004378>

Deleted:

Deleted: <https://doi.org/10.1029/2008JG000826>

Deleted:

Deleted: <https://doi.org/10.1029/2010JG001621>

3201 Feng, L., Palmer, P. I., Parker, R. J., Deutscher, N. M., Feist, D. G., Kivi, R., Morino, I., and Sussmann, R.:
3202 Estimates of European uptake of CO₂ inferred from GOSAT XCO₂ retrievals: sensitivity to measurement bias
3203 inside and outside Europe, *Atmos. Chem. Phys.*, 16, 1289–1302, <https://doi.org/10.5194/acp-16-1289-2016>, 2016.

3204 Fisher, R. A., Muszala, S., Versteinstein, M., Lawrence, P., Xu, C., McDowell, N. G., Knox, R. G., Koven, C.,
3205 Holm, J., Rogers, B. M., Spessa, A., Lawrence, D., and Bonan, G.: Taking off the training wheels: the properties of
3206 a dynamic vegetation model without climate envelopes, *CLM4.5(ED)*, *Geosci. Model Dev.*, 8, 3593–3619,
3207 <https://doi.org/10.5194/gmd-8-3593-2015>, 2015.

3208 Flanagan, D.: 2017 Minerals Yearbook: Copper [Advance Release], Tech. rep., U.S. Geological Survey,
3209 <https://pubs.usgs.gov/myb/vol11/2017/myb1-2017-copper.pdf>, 2021.

3210 Ford, D. J., Blannin, J., Watts, J., Watson, A. J., Landschützer, P., Jersild, A., and Shutler, J. D.: A Comprehensive
3211 Analysis of Air-Sea CO₂ Flux Uncertainties Constructed From Surface Ocean Data Products, *Global*
3212 *Biogeochemical Cycles*, 38, e2024GB008188, <https://doi.org/10.1029/2024GB008188>, 2024.

3213 [Ford, D.J., Shutler, J.D., Blanco-Sacristán, J. et al. Enhanced ocean CO₂ uptake due to near-surface temperature
3214 gradients. *Nat. Geosci.* 17, 1135–1140. <https://doi.org/10.1038/s41561-024-01570-7>, 2024a](https://doi.org/10.1038/s41561-024-01570-7)

3215 Ford, D. J., Shutler, J. D., Ashton, I., Sims, R. P., and Holding, T.: Recalculated (depth and temperature consistent)
3216 surface ocean CO₂ atlas (SOCAT) version 2025 (v0-1), <https://doi.org/10.5281/ZENODO.15656803>, 2025.

3217 Forster, P. M., Smith, C., Walsh, T., Lamb, W. F., Lamboll, R., Cassou, C., Hauser, M., Hausfather, Z., Lee, J.-Y.,
3218 Palmer, M. D., Von Schuckmann, K., Slangen, A. B. A., Szopa, S., Trewin, B., Yun, J., Gillett, N. P., Jenkins, S.,
3219 Matthews, H. D., Raghavan, K., Ribes, A., Rogelj, J., Rosen, D., Zhang, X., Allen, M., Aleluia Reis, L., Andrew,
3220 R. M., Betts, R. A., Borge, A., Broersma, J. A., Burgess, S. N., Cheng, L., Friedlingstein, P., Domingues, C. M.,
3221 Gambarini, M., Gasser, T., Gütschow, J., Ishii, M., Kadow, C., Kennedy, J., Killick, R. E., Krummel, P. B., Liné,
3222 A., Monselesan, D. P., Morice, C., Mühlle, J., Naik, V., Peters, G. P., Pirani, A., Pongratz, J., Minx, J. C., Rigby,
3223 M., Rohde, R., Savita, A., Seneviratne, S. I., Thorne, P., Wells, C., Western, L. M., Van Der Werf, G. R., Wijffels,
3224 S. E., Masson-Delmotte, V., and Zhai, P.: Indicators of Global Climate Change 2024: annual update of key
3225 indicators of the state of the climate system and human influence, *Earth Syst. Sci. Data*, 17, 2641–2680,
3226 <https://doi.org/10.5194/essd-17-2641-2025>, 2025.

3227 Friedlingstein, P., Houghton, R. A., Marland, G., Hackler, J., Boden, T. A., Conway, T. J., Canadell, J. G.,
3228 Raupach, M. R., Ciais, P., and Le Quéré, C.: Update on CO₂ emissions, *Nature Geosci*, 3, 811–812,
3229 <https://doi.org/10.1038/ngeo1022>, 2010.

3230 Friedlingstein, P., Andrew, R. M., Rogelj, J., Peters, G. P., Canadell, J. G., Knutti, R., Luderer, G., Raupach, M. R.,
3231 Schaeffer, M., van Vuuren, D. P., and Le Quéré, C.: Persistent growth of CO₂ emissions and implications for
3232 reaching climate targets, *Nature Geosci*, 7, 709–715, <https://doi.org/10.1038/ngeo2248>, 2014.

3233 Friedlingstein, P., Jones, M. W., O’Sullivan, M., Andrew, R. M., Hauck, J., Peters, G. P., Peters, W., Pongratz, J.,
3234 Sitch, S., Le Quéré, C., Bakker, D. C. E., Canadell, J. G., Ciais, P., Jackson, R. B., Anthoni, P., Barbero, L., Bastos,
3235 A., Bastrikov, V., Becker, M., Bopp, L., Buitenhuis, E., Chandra, N., Chevallier, F., Chini, L. P., Currie, K. I.,
3236 Feely, R. A., Gehlen, M., Gilfillan, D., Gkritzalis, T., Goll, D. S., Gruber, N., Gutekunst, S., Harris, I., Haverd, V.,
3237 Houghton, R. A., Hurtt, G., Ilyina, T., Jain, A. K., Joetzjer, E., Kaplan, J. O., Kato, E., Klein Goldewijk, K.,
3238 Korsbakken, J. I., Landschützer, P., Lauvset, S. K., Lefèvre, N., Lenton, A., Lienert, S., Lombardozzi, D., Marland,
3239 G., McGuire, P. C., Melton, J. R., Metz, N., Munro, D. R., Nabel, J. E. M. S., Nakaoka, S.-I., Neill, C., Omar, A.
3240 M., Ono, T., Peregion, A., Pierrot, D., Poulter, B., Rehder, G., Resplandy, L., Robertson, E., Rödenbeck, C.,
3241 Séférian, R., Schwinger, J., Smith, N., Tans, P. P., Tian, H., Tilbrook, B., Tubiello, F. N., van der Werf, G. R.,
3242 Wiltshire, A. J., and Zaehle, S.: Global Carbon Budget 2019, *Earth Syst. Sci. Data*, 11, 1783–1838,
3243 <https://doi.org/10.5194/essd-11-1783-2019>, 2019.

3244 Friedlingstein, P., O’Sullivan, M., Jones, M. W., Andrew, R. M., Hauck, J., Olsen, A., Peters, G. P., Peters, W.,
3245 Pongratz, J., Sitch, S., Le Quéré, C., Canadell, J. G., Ciais, P., Jackson, R. B., Alin, S., Aragão, L. E. O. C., Armeth,
3246 A., Arora, V., Bates, N. R., Becker, M., Benoit-Cattin, A., Bittig, H. C., Bopp, L., Bultan, S., Chandra, N.,
3247 Chevallier, F., Chini, L. P., Evans, W., Florentie, L., Forster, P. M., Gasser, T., Gehlen, M., Gilfillan, D.,
3248 Gkritzalis, T., Gregor, L., Gruber, N., Harris, I., Hartung, K., Haverd, V., Houghton, R. A., Ilyina, T., Jain, A. K.,
3249 Joetzjer, E., Kadono, K., Kato, E., Kitidis, V., Korsbakken, J. I., Landschützer, P., Lefèvre, N., Lenton, A., Lienert,
3250 S., Liu, Z., Lombardozzi, D., Marland, G., Metz, N., Munro, D. R., Nabel, J. E. M. S., Nakaoka, S.-I., Niwa, Y.,
3251 O’Brien, K., Ono, T., Palmer, P. I., Pierrot, D., Poulter, B., Resplandy, L., Robertson, E., Rödenbeck, C.,
3252 Schwinger, J., Séférian, R., Skjelvan, I., Smith, A. J. P., Sutton, A. J., Tanhua, T., Tans, P. P., Tian, H., Tilbrook,

Deleted: <https://doi.org/10.5194/gmd-8-3593-2015>

Deleted: [Data, 17, 2641–2680, https://doi.org/10.5194/essd-17-2641-2025](https://doi.org/10.5194/essd-17-2641-2025)

3256 B., van der Werf, G., Vuichard, N., Walker, A. P., Wanninkhof, R., Watson, A. J., Willis, D., Wiltshire, A. J.,
3257 Yuan, W., Yue, X., and Zaehe, S.: Global Carbon Budget 2020, *Earth Syst. Sci. Data*, 12, 3269–3340,
3258 <https://doi.org/10.5194/essd-12-3269-2020>, 2020.

3259 Friedlingstein, P., Jones, M. W., O'Sullivan, M., Andrew, R. M., Bakker, D. C. E., Hauck, J., Le Quéré, C., Peters,
3260 G. P., Peters, W., Pongratz, J., Sitch, S., Canadell, J. G., Ciais, P., Jackson, R. B., Alin, S. R., Anthoni, P., Bates, N.
3261 R., Becker, M., Bellouin, N., Bopp, L., Chau, T. T. T., Chevallier, F., Chini, L. P., Cronin, M., Currie, K. I.,
3262 Decharme, B., Djeutchouang, L. M., Dou, X., Evans, W., Feely, R. A., Feng, L., Gasser, T., Gilfillan, D.,
3263 Gkritzalis, T., Grassi, G., Gregor, L., Gruber, N., Gürses, Ö., Harris, I., Houghton, R. A., Hurtt, G. C., Iida, Y.,
3264 Ilyina, T., Luijckx, I. T., Jain, A., Jones, S. D., Kato, E., Kennedy, D., Klein Goldewijk, K., Knauer, J., Korsbakken,
3265 J. I., Körtzinger, A., Landschützer, P., Lauvset, S. K., Lefèvre, N., Lienert, S., Liu, J., Marland, G., McGuire, P. C.,
3266 Melton, J. R., Munro, D. R., Nabel, J. E. M. S., Nakaoka, S.-I., Niwa, Y., Ono, T., Pierrot, D., Poulter, B., Rehder,
3267 G., Resplandy, L., Robertson, E., Rödenbeck, C., Rosan, T. M., Schwinger, J., Schwingshackl, C., Séférian, R.,
3268 Sutton, A. J., Sweeney, C., Tanhua, T., Tans, P. P., Tian, H., Tilbrook, B., Tubiello, F., van der Werf, G. R.,
3269 Vuichard, N., Wada, G., Wanninkhof, R., Watson, A. J., Willis, D., Wiltshire, A. J., Yuan, W., Yue, C., Yue, X.,
3270 Zaehe, S., and Zeng, J.: Global Carbon Budget 2021, *Earth Syst. Sci. Data*, 14, 1917–2005,
3271 <https://doi.org/10.5194/essd-14-1917-2022>, 2022a.

3272 Friedlingstein, P., O'Sullivan, M., Jones, M. W., Andrew, R. M., Gregor, L., Hauck, J., Le Quéré, C., Luijckx, I. T.,
3273 Olsen, A., Peters, G. P., Peters, W., Pongratz, J., Schwingshackl, C., Sitch, S., Canadell, J. G., Ciais, P., Jackson, R.
3274 B., Alin, S. R., Alkama, R., Arneth, A., Arora, V. K., Bates, N. R., Becker, M., Bellouin, N., Bittig, H. C., Bopp,
3275 L., Chevallier, F., Chini, L. P., Cronin, M., Evans, W., Falk, S., Feely, R. A., Gasser, T., Gehlen, M., Gkritzalis, T.,
3276 Gloege, L., Grassi, G., Gruber, N., Gürses, Ö., Harris, I., Hefner, M., Houghton, R. A., Hurtt, G. C., Iida, Y., Ilyina,
3277 T., Jain, A. K., Jersild, A., Kadono, K., Kato, E., Kennedy, D., Klein Goldewijk, K., Knauer, J., Korsbakken, J. I.,
3278 Landschützer, P., Lefèvre, N., Lindsay, K., Liu, J., Liu, Z., Marland, G., Mayot, N., McGrath, M. J., Metzl, N.,
3279 Monacci, N. M., Munro, D. R., Nakaoka, S., Niwa, Y., O'Brien, K., Ono, T., Palmer, P. I., Pan, N., Pierrot, D.,
3280 Pockock, K., Poulter, B., Resplandy, L., Robertson, E., Rödenbeck, C., Rodriguez, C., Rosan, T. M., Schwinger, J.,
3281 Séférian, R., Shutler, J. D., Skjelvan, I., Steinhoff, T., Sun, Q., Sutton, A. J., Sweeney, C., Takao, S., Tanhua, T.,
3282 Tans, P. P., Tian, X., Tian, H., Tilbrook, B., Tsujino, H., Tubiello, F., van der Werf, G. R., Walker, A. P.,
3283 Wanninkhof, R., Whitehead, C., Willstrand Wranne, A., Wright, R., Yuan, W., Yue, C., Yue, X., Zaehe, S., Zeng,
3284 J., and Zheng, B.: Global Carbon Budget 2022, *Earth Syst. Sci. Data*, 14, 4811–4900, <https://doi.org/10.5194/essd-14-4811-2022>, 2022b.

3286 Friedlingstein, P., O'Sullivan, M., Jones, M. W., Andrew, R. M., Bakker, D. C. E., Hauck, J., Landschützer, P., Le
3287 Quéré, C., Luijckx, I. T., Peters, G. P., Peters, W., Pongratz, J., Schwingshackl, C., Sitch, S., Canadell, J. G., Ciais,
3288 P., Jackson, R. B., Alin, S. R., Anthoni, P., Barbero, L., Bates, N. R., Becker, M., Bellouin, N., Decharme, B.,
3289 Bopp, L., Brasika, I. B. M., Cadule, P., Chamberlain, M. A., Chandra, N., Chau, T.-T.-T., Chevallier, F., Chini, L.
3290 P., Cronin, M., Dou, X., Enyo, K., Evans, W., Falk, S., Feely, R. A., Feng, L., Ford, D. J., Gasser, T., Ghattas, J.,
3291 Gkritzalis, T., Grassi, G., Gregor, L., Gruber, N., Gürses, Ö., Harris, I., Hefner, M., Heinke, J., Houghton, R. A.,
3292 Hurtt, G. C., Iida, Y., Ilyina, T., Jacobson, A. R., Jain, A. K., Jarníková, T., Jersild, A., Jiang, F., Jin, Z., Joos, F.,
3293 Kato, E., Keeling, R. F., Kennedy, D., Klein Goldewijk, K., Knauer, J., Korsbakken, J. I., Körtzinger, A., Lan, X.,
3294 Lefèvre, N., Li, H., Liu, J., Liu, Z., Ma, L., Marland, G., Mayot, N., McGuire, P. C., McKinley, G. A., Meyer, G.,
3295 Morgan, E. J., Munro, D. R., Nakaoka, S., Niwa, Y., O'Brien, K. M., Olsen, A., Omar, A. M., Ono, T., Paulsen, M.,
3296 Pierrot, D., Pockock, K., Poulter, B., Powis, C. M., Rehder, G., Resplandy, L., Robertson, E., Rödenbeck, C., Rosan,
3297 T. M., Schwinger, J., Séférian, R., Smallman, T. L., Smith, S. M., Sospedra-Alfonso, R., Sun, Q., Sutton, A. J.,
3298 Sweeney, C., Takao, S., Tans, P. P., Tian, H., Tilbrook, B., Tsujino, H., Tubiello, F., van der Werf, G. R., van
3299 Ooijen, E., Wanninkhof, R., Watanabe, M., Wilmart-Rousseau, C., Yang, D., Yang, X., Yuan, W., Yue, X., Zaehe,
3300 S., Zeng, J., and Zheng, B.: Global Carbon Budget 2023, *Earth Syst. Sci. Data*, 15, 5301–5369,
3301 <https://doi.org/10.5194/essd-15-5301-2023>, 2023.

3302 Friedlingstein, P., O'Sullivan, M., Jones, M. W., Andrew, R. M., Hauck, J., Landschützer, P., Le Quéré, C., Li, H.,
3303 Luijckx, I. T., Olsen, A., Peters, G. P., Peters, W., Pongratz, J., Schwingshackl, C., Sitch, S., Canadell, J. G., Ciais,
3304 P., Jackson, R. B., Alin, S. R., Arneth, A., Arora, V., Bates, N. R., Becker, M., Bellouin, N., Berghoff, C. F., Bittig,
3305 H. C., Bopp, L., Cadule, P., Campbell, K., Chamberlain, M. A., Chandra, N., Chevallier, F., Chini, L. P., Colligan,
3306 T., Decayeux, J., Djeutchouang, L. M., Dou, X., Duran Rojas, C., Enyo, K., Evans, W., Fay, A. R., Feely, R. A.,
3307 Ford, D. J., Foster, A., Gasser, T., Gehlen, M., Gkritzalis, T., Grassi, G., Gregor, L., Gruber, N., Gürses, Ö., Harris,
3308 I., Hefner, M., Heinke, J., Hurtt, G. C., Iida, Y., Ilyina, T., Jacobson, A. R., Jain, A. K., Jarníková, T., Jersild, A.,
3309 Jiang, F., Jin, Z., Kato, E., Keeling, R. F., Klein Goldewijk, K., Knauer, J., Korsbakken, J. I., Lan, X., Lauvset, S.
3310 K., Lefèvre, N., Liu, Z., Liu, J., Ma, L., Maksyutov, S., Marland, G., Mayot, N., McGuire, P. C., Metzl, N.,
3311 Monacci, N. M., Morgan, E. J., Nakaoka, S.-I., Neill, C., Niwa, Y., Nützel, T., Olivier, L., Ono, T., Palmer, P. I.,
3312 Pierrot, D., Qin, Z., Resplandy, L., Roobaert, A., Rosan, T. M., Rödenbeck, C., Schwinger, J., Smallman, T. L.,
3313 Smith, S. M., Sospedra-Alfonso, R., Steinhoff, T., Sun, Q., Sutton, A. J., Séférian, R., Takao, S., Tatebe, H., Tian,

3314 H., Tilbrook, B., Torres, O., Tourigny, E., Tsujino, H., Tubiello, F., van der Werf, G., Wanninkhof, R., Wang, X.,
3315 Yang, D., Yang, X., Yu, Z., Yuan, W., Yue, X., Zaehle, S., Zeng, N., and Zeng, J.: Global Carbon Budget 2024,
3316 Earth Syst. Sci. [Data, 17, 965–1039](https://doi.org/10.5194/essd-17-965-2025), <https://doi.org/10.5194/essd-17-965-2025>, 2025a.

3317 Friedlingstein, P., Le Quéré, C., O'Sullivan, M., Hauck, J., Landschützer, P., Luijckx, I.T., Li, H., van der Woude,
3318 A., Schwingshackl, C., Pongratz, P., Regnier, P., Andrew, R.M., Bakker, D.C.E., Canadell, J.G., Ciais, P., Gasser,
3319 T., Jones, M.W., Lan, X., Morgan, E., Olsen, A., Peters, G.P., Peters, W., Sitch, S., and Tian, H.: Emerging climate
3320 impact on carbon sinks in a consolidated carbon budget, *Nature*, <https://doi.org/10.1038/s41586-025-09802-5>,
3321 2025b.

3322 Friedlingstein, P., O'Sullivan, M., Jones, M. W., Andrew, R. M., Bakker, D. C. E., Hauck, J., Landschützer, P., Le
3323 Quéré, C., Li, H., Luijckx, I. T., Peters, G. P., Peters, W., Pongratz, J., Schwingshackl, C., Sitch, S., Canadell, J. G.,
3324 Ciais, P., Aas, K., Alin, S. R., Anthoni, P., Barbero, L., Bates, N. R., Bellouin, N., Benoit-Cattin, A., Berghoff, C.
3325 F., Bernardello, R., Bopp, L., Brasika, I. B. M., Chamberlain, M. A., Chandra, N., Chevallier, F., Chini, L. P.,
3326 Collier, N. O., Colligan, T. H., Cronin, M., Djeutchouang, L. M., Dou, X., Enright, M. P., Enyo, K., Erb, M.,
3327 Evans, W., Feely, R. A., Feng, L., Ford, D. J., Foster, A., Fransner, F., Gasser, T., Gehlen, M., Gkritzalis, T.,
3328 Goncalves De Souza, J., Grassi, G., Gregor, L., Gruber, N., Guenet, B., Gürses, Ö., Harrington, K., Harris, I.,
3329 Heinke, J., Hurtt, G. C., Iida, Y., Ilyina, T., Ito, A., Jacobson, A. R., Jain, A. K., Jarníková, T., Jersild, A., Jiang, F.,
3330 Jones, S. D., Kato, E., Keeling, R. F., Klein Goldewijk, K., Knauer, J., Kong, Y., Korsbakken, J. I., Koven, C.,
3331 Kunimitsu, T., Lan, X., Liu, J., Liu, Z., Liu, Z., Lo Monaco, C., Ma, L., Marland, G., McGuire, P. C., McKinley,
3332 G. A., Melton, J. R., Monacci, N., Monier, E., Morgan, E. J., Munro, D. R., Müller, J. D., Nakaoka, S., Nayagam,
3333 L. R., Niwa, Y., Nutzel, T., Olsen, A., Omar, A. M., Pan, N., Pandey, S., Pierrot, D., Qin, Z., Regnier, P., Rehder,
3334 G., Resplandy, L., Roobaert, A., Rosan, T. M., Rödenbeck, C., Schwinger, J., Skjelvan, I., Smallman, T. L., Spada,
3335 V., Sreesh, M. G., Sun, Q., Sutton, A. J., Sweeney, C., Swingedouw, D., Séférian, R., Takao, S., Tatebe, H., Tian,
3336 H., Tian, X., Tilbrook, B., Tsujino, H., Tubiello, F., van Ooijen, E., van der Werf, G. R., van de Velde, S. J.,
3337 Walker, A. P., Wanninkhof, R., Yang, X., Yuan, W., Yue, X., and Zeng, J.: Supplemental data of the Global
3338 Carbon Budget 2025, ICOS-ERIC Carbon Portal, <https://doi.org/10.18160/GCP-2025>, 2025c.

3339 Fu, W., Moore, J. K., Primeau, F., Collier, N., Ogunro, O. O., Hoffman, F. M., and Randerson, J. T.: Evaluation of
3340 Ocean Biogeochemistry and Carbon Cycling in CMIP Earth System Models With the International Ocean Model
3341 Benchmarking (IOMB) Software System, *JGR Oceans*, 127, e2022JC018965, <https://doi.org/10.1029/2022JC018965>, 2022.

3343 Ganzenmüller, R., Bultan, S., Winkler, K., Fuchs, R., Zabel, F., and Pongratz, J.: Land-use change emissions based
3344 on high-resolution activity data substantially lower than previously estimated, *Environ. Res. Lett.*, 17, 064050,
3345 <https://doi.org/10.1088/1748-9326/ac70d8>, 2022.

3346 Gasser, T., Crepin, L., Quilcaille, Y., Houghton, R. A., Ciais, P., and Obersteiner, M.: Historical CO₂ emissions
3347 from land use and land cover change and their uncertainty, *Biogeosciences*, 17, 4075–4101,
3348 <https://doi.org/10.5194/bg-17-4075-2020>, 2020.

3349 Gaubert, B., Stephens, B. B., Basu, S., Chevallier, F., Deng, F., Kort, E. A., Patra, P. K., Peters, W., Rödenbeck,
3350 C., Saeki, T., Schimel, D., Van der Laan-Luijckx, I., Wofsy, S., and Yin, Y.: Global atmospheric CO₂ inverse
3351 models converging on neutral tropical land exchange, but disagreeing on fossil fuel and atmospheric growth rate,
3352 *Biogeosciences*, 16, 117–134, <https://doi.org/10.5194/bg-16-117-2019>, 2019.

3353 Gauthier, C. B., Melton, J. R., Meyer, G., Raj Deepak, S. N., and Sonnentag, O.: Parameter Optimization for
3354 Global Soil Carbon Simulations: Not a Simple Problem, *J Adv Model Earth Syst*, 17, e2024MS004577,
3355 <https://doi.org/10.1029/2024MS004577>, 2025.

3356 GCP: The Global Carbon Budget 2007, available at: <http://www.globalcarbonproject.org/carbonbudget/archive.htm>, last access: 23 October 2025, 2007.

3358 Giglio, L., Schroeder, W., and Justice, C. O.: The collection 6 MODIS active fire detection algorithm and fire
3359 products, *Remote Sensing of Environment*, 178, 31–41, <https://doi.org/10.1016/j.rse.2016.02.054>, 2016.

3360 Gitz V, Ciais P. Amplifying effects of land-use change on future atmospheric CO₂ levels. *Global Biogeochemical*
3361 *Cycles*. <https://doi.org/10.1029/2002GB001963>, 2003.

3362 Gloege, L., McKinley, G. A., Landschützer, P., Fay, A. R., Frölicher, T. L., Fyfe, J. C., Ilyina, T., Jones, S.,
3363 Lovenduski, N. S., Rodgers, K. B., Schlunegger, S., and Takano, Y.: Quantifying Errors in Observationally Based

Deleted: Data, 17, 965–1039, <https://doi.org/10.5194/essd-17-965-2025>

Deleted: <https://doi.org/10.1029/2024MS004577>

- 3367 Estimates of Ocean Carbon Sink Variability, *Global Biogeochem. Cy.*, 35, e2020GB006788,
3368 <https://doi.org/10.1029/2020GB006788>, 2021.
- 3369 Gloege, L., Yan, M., Zheng, T., and McKinley, G. A.: Improved Quantification of Ocean Carbon Uptake by Using
3370 Machine Learning to Merge Global Models and pCO₂ Data, *J. Adv. Model. Earth Syst.*, 14, e2021MS002620,
3371 <https://doi.org/10.1029/2021MS002620>, 2022.
- 3372 Golar, G., Malik, A., Muis, H., Herman, A., Nurudin, N., and Lukman, L.: The social-economic impact of COVID-
3373 19 pandemic: implications for potential forest degradation, *Heliyon*, 6, e05354,
3374 <https://doi.org/10.1016/j.heliyon.2020.e05354>, 2020.
- 3375 Goris, N., Tjiputra, J. F., Olsen, A., Schwinger, J., Lauvset, S. K., and Jeansson, E.: Constraining Projection-Based
3376 Estimates of the Future North Atlantic Carbon Uptake, *J. Clim.*, 31, 3959–3978, <https://doi.org/10.1175/JCLI-D-17-0564.1>, 2018.
- 3378 Grassi, G., House, J., Kurz, W. A., Cescatti, A., Houghton, R. A., Peters, G. P., Sanz, M. J., Viñas, R. A., Alkama,
3379 R., Arneeth, A., Bondeau, A., Dentener, F., Fader, M., Federici, S., Friedlingstein, P., Jain, A. K., Kato, E., Koven,
3380 C. D., Lee, D., Nabel, J. E. M. S., Nassikas, A. A., Perugini, L., Rossi, S., Sitch, S., Viovy, N., Wiltshire, A., and
3381 Zaehele, S.: Reconciling global-model estimates and country reporting of anthropogenic forest CO₂ sinks, *Nature
3382 Clim Change*, 8, 914–920, <https://doi.org/10.1038/s41558-018-0283-x>, 2018.
- 3383 Grassi, G., Stehfest, E., Rogelj, J., van Vuuren, D., Cescatti, A., House, J., Nabuurs, G.-J., Rossi, S., Alkama, R.,
3384 Viñas, R. A., Calvin, K., Ceccherini, G., Federici, S., Fujimori, S., Gusti, M., Hasegawa, T., Havlik, P.,
3385 Humpenöder, F., Korosuo, A., Perugini, L., Tubiello, F. N., and Popp, A.: Critical adjustment of land mitigation
3386 pathways for assessing countries' climate progress, *Nat. Clim. Chang.*, 11, 425–434,
3387 <https://doi.org/10.1038/s41558-021-01033-6>, 2021.
- 3388 Grassi, G., Schwingshackl, C., Gasser, T., Houghton, R. A., Sitch, S., Canadell, J. G., Cescatti, A., Ciais, P.,
3389 Federici, S., Friedlingstein, P., Kurz, W. A., Sanz Sanchez, M. J., Abad Viñas, R., Alkama, R., Bultan, S.,
3390 Ceccherini, G., Falk, S., Kato, E., Kennedy, D., Knauer, J., Korosuo, A., Melo, J., McGrath, M. J., Nabel, J. E. M.
3391 S., Poulter, B., Romanovskaya, A. A., Rossi, S., Tian, H., Walker, A. P., Yuan, W., Yue, X., and Pongratz, J.:
3392 Harmonising the land-use flux estimates of global models and national inventories for 2000–2020, *Earth Syst. Sci.
3393 Data*, 15, 1093–1114, <https://doi.org/10.5194/essd-15-1093-2023>, 2023.
- 3394 Grassi, G., Peters, G. P., Canadell, J. G., Cescatti, A., Federici, S., Gidden, M. J., Harris, N., Herold, M., Krug, T.,
3395 O'Sullivan, M., Pongratz, J., Sanz, M. J., Schwingshackl, C., and Van Vuuren, D.: Improving land-use emission
3396 estimates under the Paris Agreement, *Nat Sustain*, 8, 579–581, <https://doi.org/10.1038/s41893-025-01565-1>, 2025.
- 3397 Gregor, L., Lebehoh, A. D., Kok, S., and Scheel Monteiro, P. M.: A comparative assessment of the uncertainties of
3398 global surface ocean CO₂ estimates using a machine-learning ensemble (CSIR-ML6 version 2019a)—have we hit
3399 the wall?. *Geoscientific Model Development*, 12(12), 5113–5136, <https://doi.org/10.5194/gmd-12-5113-2019>,
3400 2019.
- 3401 Gregor, L., Shutler, J., and Gruber, N.: High-resolution variability of the ocean carbon sink. *Global
3402 Biogeochemical Cycles*, 38(8), e2024GB008127, <https://doi.org/10.1029/2024GB008127>, 2024.
- 3403 Gruber, N., Bakker, D. C. E., DeVries, T., Gregor, L., Hauck, J., Landschützer, P., McKinley, G. A., and Müller, J.
3404 D.: Trends and variability in the ocean carbon sink, *Nat. Rev. Earth Environ.*, 4, 119–134,
3405 <https://doi.org/10.1038/s43017-022-00381-x>, 2023.
- 3406 Gruber, N., Clement, D., Carter, B. R., Feely, R. A., van Heuven, S., Hoppema, M., Ishii, M., Key, R. M., Kozyr,
3407 A., Lauvset, S. K., Lo Monaco, C., Mathis, J. T., Murata, A., Olsen, A., Perez, F. F., Sabine, C. L., Tanhua, T., and
3408 Wanninkhof, R.: The oceanic sink for anthropogenic CO₂ from 1994 to 2007, 363, 1193–1199,
3409 <https://doi.org/10.1126/science.aau5153>, 2019.
- 3410 Guan, D., Liu, Z., Geng, Y., Lindner, S., and Hubacek, K.: The gigatonne gap in China's carbon dioxide
3411 inventories, *Nature Clim Change*, 2, 672–675, <https://doi.org/10.1038/nclimate1560>, 2012.
- 3412 Gulev, S. K., Thorne, P. W., Ahn, J., Dentener, F. J., Domingues, C. M., Gerland, S., Gong, D. S., Kaufman, S.,
3413 Nnamchi, H. C., Quaas, J., Rivera, J. A., Sathyendranath, S., Smith, S. L., Trewin, B., von Shuckmann, K., and
3414 Vose, R. S.: Changing State of the Climate System. In: *Climate Change 2021: The Physical Science Basis.*
3415 Contribution of Working Group I to the Sixth Assessment Report of the Intergovernmental Panel on Climate

Deleted: <https://doi.org/10.1038/s41893-025-01565-1>

- 3417 Change [Masson-Delmotte, V., Zhai, P., Pirani, A., Connors, S. L., Péan, C., Berger, S., Caud, N., Chen, Y.,
3418 Goldfarb, L., Gomis, M. I., Huang, M., Leitzell, K., Lonnoy, E., Matthews, J.B.R., Maycock, T.K., Waterfield, T.,
3419 Yelekçi, O., Yu, R. and Zhou, B. (eds.)]. Cambridge University Press, Cambridge, United Kingdom and New
3420 York, NY, USA, pp. 287–422, <https://doi.org/10.1017/9781009157896.004>, 2021.
- 3421 Guo, R., Wang, J., Bing, L., Tong, D., Ciais, P., Davis, S. J., Andrew, R. M., Xi, F., and Liu, Z.: Global CO₂
3422 uptake by cement from 1930 to 2019, 13, 1791–1805, <https://doi.org/10.5194/essd-13-1791-2021>, 2021.
- 3423 Gürses, Ö., Orziel, L., Karakuş, O., Sidorenko, D., Völker, C., Ye, Y., Zeising, M., Butzin, M., and Hauck, J.:
3424 Ocean biogeochemistry in the coupled ocean–sea ice–biogeochemistry model FESOM2.1–REcoM3, *Geosci.
3425 Model Dev.*, 16, 4883–4936, <https://doi.org/10.5194/gmd-16-4883-2023>, 2023.
- 3426 Gütschow, J., Jeffery, M. L., Gieseke, R., Gebel, R., Stevens, D., Krapp, M., and Rocha, M.: The PRIMAP-hist
3427 national historical emissions time series, 8, 571–603, <https://doi.org/10.5194/essd-8-571-2016>, 2016.
- 3428 Gütschow, J., Busch, D. and Pflüger, M.: The PRIMAP-hist national historical emissions time series (1750-2023)
3429 v2.6, Zenodo [Data set], <https://doi.org/10.5281/zenodo.13752654>, 2023.
- 3430 Hall, B. D., Crotwell, A. M., Kitzis, D. R., Mefford, T., Miller, B. R., Schibig, M. F., and Tans, P. P.: Revision of
3431 the World Meteorological Organization Global Atmosphere Watch (WMO/GAW) CO₂ calibration scale, 14,
3432 3015–3032, <https://doi.org/10.5194/amt-14-3015-2021>, 2021.
- 3433 Hansis, E., Davis, S. J., and Pongratz, J.: Relevance of methodological choices for accounting of land use change
3434 carbon fluxes, *Global Biogeochem. Cycles*, 29, 1230–1246, <https://doi.org/10.1002/2014GB004997>, 2015.
- 3435 Hauck, J., Nissen, C., Landschützer, P., Rödenbeck, C., Bushinsky, S., and Olsen, A.: Sparse observations induce
3436 large biases in estimates of the global ocean CO₂ sink: an ocean model subsampling experiment, *Philos. Trans. R.
3437 Soc. Math. Phys. Eng. Sci.*, 381, 20220063, <https://doi.org/10.1098/rsta.2022.0063>, 2023a.
- 3438 Hauck, J., Gregor, L., Nissen, C., Patara, L., Hague, M., Mongwe, P., Bushinsky, S., Doney, S. C., Gruber, N., Le
3439 Quéré, C., Manizza, M., Mazloff, M., Monteiro, P. M. S., and Terhaar, J.: The Southern Ocean Carbon Cycle
3440 1985–2018: Mean, Seasonal Cycle, Trends, and Storage. *Global Biogeochemical Cycles*, 37(11), e2023GB007848,
3441 <https://doi.org/10.1029/2023GB007848>, 2023b.
- 3442 Hauck, J., Zeising, M., Le Quéré, C., Gruber, N., Bakker, D. C. E., Bopp, L., Chau, T. T. T., Gürses, Ö., Ilyina, T.,
3443 Landschützer, P., Lenton, A., Resplandy, L., Rödenbeck, C., Schwinger, J., and Séférian, R.: Consistency and
3444 Challenges in the Ocean Carbon Sink Estimate for the Global Carbon Budget, *Front. Mar. Sci.*, 7, 571720,
3445 <https://doi.org/10.3389/fmars.2020.571720>, 2020.
- 3446 Haverd, V., Smith, B., Nieradzki, L., Briggs, P. R., Woodgate, W., Trudinger, C. M., Canadell, J. G., and Cuntz,
3447 M.: A new version of the CABLE land surface model (Subversion revision r4601) incorporating land use and land
3448 cover change, woody vegetation demography, and a novel optimisation-based approach to plant coordination of
3449 photosynthesis, *Geosci. Model Dev.*, 11, 2995–3026, <https://doi.org/10.5194/gmd-11-2995-2018>, 2018.
- 3450 Heinke, J., Rolinski, S., and Müller, C.: Modelling the role of livestock grazing in C and N cycling in grasslands
3451 with LPJmL5.0-grazing, *Geosci. Model Dev.*, 16, 2455–2475, <https://doi.org/10.5194/gmd-16-2455-2023>, 2023.
- 3452 Hickler, T., Smith, B., Prentice, I. C., Mjöfors, K., Miller, P., Arneth, A., and Sykes, M. T.: CO₂ fertilization in
3453 temperate FACE experiments not representative of boreal and tropical forests, *Glob. Change Biol.*, 14, 1531–1542,
3454 <https://doi.org/10.1111/j.1365-2486.2008.01598.x>, 2008.
- 3455 Hoesly, R. M., Smith, S. J., Feng, L., Klimont, Z., Janssens-Maenhout, G., Pitkanen, T., Seibert, J. J., Vu, L.,
3456 Andres, R. J., Bolt, R. M., Bond, T. C., Dawidowski, L., Kholod, N., Kurokawa, J., Li, M., Liu, L., Lu, Z., Moura,
3457 M. C. P., O'Rourke, P. R., and Zhang, Q.: Historical (1750–2014) anthropogenic emissions of reactive gases and
3458 aerosols from the Community Emissions Data System (CEDS), *Geosci. Model Dev.*, 11, 369–408,
3459 <https://doi.org/10.5194/gmd-11-369-2018>, 2018.
- 3460 Hoesly, R., Smith, S. J., Prime, N., Ahsan, H., Suchyta, H., O'Rourke, P., Crippa, M., Klimont, Z., Guizzardi, D.,
3461 Behrendt, J., Feng, L., Harkins, C., McDonald, B., Mott, A., McDuffie, A., Nicholson, M. and Wang, S.: CEDS
3462 v_2024_07_08 Release Emission Data, Zenodo [Data set], <https://doi.org/10.5281/zenodo.12803196>, 2024.

3463 Hong, C., Burney, J. A., Pongratz, J., Nabel, J. E. M. S., Mueller, N. D., Jackson, R. B., and Davis, S. J.: Global
3464 and regional drivers of land-use emissions in 1961–2017, *Nature*, 589, 554–561, [https://doi.org/10.1038/s41586-](https://doi.org/10.1038/s41586-020-03138-y)
3465 020-03138-y, 2021.

3466 Holding, T., Ashton, I. G., Shutler, J. D., Land, P. E., Nightingale, P. D., Rees, A. P., Brown, I., Piolle, J.-F., Kock,
3467 A., Bange, H. W., Woolf, D. K., Goddijn-Murphy, L., Pereira, R., Paul, F., Girard-Arduin, F., Chapron, B.,
3468 Rehder, G., Arduin, F., and Donlon, C. J.: The FluxEngine air–sea gas flux toolbox: simplified interface and
3469 extensions for in situ analyses and multiple sparingly soluble gases, *Ocean Sci.*, 15, 1707–1728,
3470 <https://doi.org/10.5194/os-15-1707-2019>, 2019.

3471 Hoppe, J., Hinder, B., Rafaty, R., Patt, A., and Grubb, M.: Three Decades of Climate Mitigation Policy: What Has
3472 It Delivered?, *Annu. Rev. Environ. Resour.*, 48, 615–650, [https://doi.org/10.1146/annurev-environ-112321-](https://doi.org/10.1146/annurev-environ-112321-103821)
3473 103821, 2023.

3474 Houghton, R. A. and Castanho, A.: Annual emissions of carbon from land use, land-use change, and forestry from
3475 1850 to 2020, *Earth Syst. Sci. Data*, 15, 2025–2054, <https://doi.org/10.5194/essd-15-2025-2023>, 2023.

3476 Houghton, R. A., House, J. I., Pongratz, J., van der Werf, G. R., DeFries, R. S., Hansen, M. C., Le Quééré, C., and
3477 Ramankutty, N.: Carbon emissions from land use and land-cover change, *Biogeosciences*, 9, 5125–5142,
3478 <https://doi.org/10.5194/bg-9-5125-2012>, 2012.

3479 Houghton, R. A. and Nassikas, A. A.: Global and regional fluxes of carbon from land use and land cover change
3480 1850–2015: Carbon Emissions From Land Use, *Global Biogeochem. Cycles*, 31, 456–472,
3481 <https://doi.org/10.1002/2016GB005546>, 2017.

3482 Huang, B., Thorne, P. W., Banzon, V. F., Boyer, T., Chepurin, G., Lawrimore, J. H., Menne, M. J., Smith, T. M.,
3483 Vose, R. S., and Zhang, H.-M.: NOAA Extended Reconstructed Sea Surface Temperature (ERSST), Version 5,
3484 <https://doi.org/10.7289/V5T72FNM>, 2017.

3485 Hubau, W., Lewis, S.L., Phillips, O.L., Affum-Baffoe, K., Beeckman, H., Cuni-Sanchez, A., Daniels, A.K.,
3486 Ewango, C.E.N., Fauset, S., Mukinzi, J.M., Sheil, D., Sonké, B., Sullivan, M.J.P., Sunderland, T.C.H., Taedoung,
3487 H., Thomas, S.C., White, L.J.T., Abernethy, K.A., Adu-Bredu, S., Amani, C.A., Baker, T.R., Banin, L.F., Baya, F.,
3488 Begne, S.K., Bennett, A.C., Benedet, F., Bitariho, R., Bocko, Y.E., Boeckx, P., Boundja, P., Brienen, R.J.W.,
3489 Brncic, T., Chezeaux, E., Chuyong, G.B., Clark, C.J., Collins, M., Comiskey, J.A., Coomes, D.A., Dargie, G.C., de
3490 Haulleville, T., Kamdem, M.N.D., Doucet, J.-L., Esquivel-Muelbert, A., Feldpausch, T.R., Fofanah, A., Foli, E.G.,
3491 Gilpin, M., Gloor, E., Gonmadje, C., Gourlet-Fleury, S., Hall, J.S., Hamilton, A.C., Harris, D.J., Hart, T.B.,
3492 Hockemba, M.B.N., Hladik, A., Ifo, S.A., Jeffery, K.J., Jucker, T., Yakusu, E.K., Kearsley, E., Kenfack, D., Koch,
3493 A., Leal, M.E., Levesley, A., Lindsell, J.A., Lisingo, J., Lopez-Gonzalez, G., Lovett, J.C., Makana, J.-R., Malhi,
3494 Y., Marshall, A.R., Martin, J., Martin, E.H., Mbayu, F.M., Medjibe, V.P., Mihindou, V., Mitchard, E.T.A., Moore,
3495 S., Munishi, P.K.T., Bengone, N.N., Ojo, L., Ondo, F.E., Peh, K.S.-H., Pickavance, G.C., Poulsen, A.D., Poulsen,
3496 J.R., Qie, L., Reitsma, J., Rovero, F., Swaine, M.D., Talbot, J., Taplin, J., Taylor, D.M., Thomas, D.W., Toirambe,
3497 B., Mukendi, J.T., Tuagben, D., Umunay, P.M., van der Heijden, G.M.F., Verbeeck, H., Vleminckx, J., Willcock,
3498 S., Wöll, H., Woods, J.T., Zemagho, L.: Asynchronous carbon sink saturation in African and Amazonian tropical
3499 forests, *Nature*, 579, 80–87, <https://doi.org/10.1038/s41586-020-2035-0>, 2020.

3500 Humphrey, V., Zscheischler, J., Ciais, P., Gudmundsson, L., Sitch, S., and Seneviratne, S. I.: Sensitivity of
3501 atmospheric CO₂ growth rate to observed changes in terrestrial water storage, *Nature*, 560, 628–631,
3502 <https://doi.org/10.1038/s41586-018-0424-4>, 2018.

3503 Humphrey, V., Berg, A., Ciais, P., Gentile, P., Jung, M., Reichstein, M., Seneviratne, S. I., and Frankenberg, C.:
3504 Soil moisture–atmosphere feedback dominates land carbon uptake variability, *Nature*, 592, 65–69,
3505 <https://doi.org/10.1038/s41586-021-03325-5>, 2021.

3506 Huntzinger, D. N., Michalak, A. M., Schwalm, C., Ciais, P., King, A. W., Fang, Y., Schaefer, K., Wei, Y., Cook,
3507 R. B., Fisher, J. B., Hayes, D., Huang, M., Ito, A., Jain, A. K., Lei, H., Lu, C., Maignan, F., Mao, J., Parazoo, N.,
3508 Peng, S., Poulter, B., Ricciuto, D., Shi, X., Tian, H., Wang, W., Zeng, N., and Zhao, F.: Uncertainty in the response
3509 of terrestrial carbon sink to environmental drivers undermines carbon-climate feedback predictions, *Sci Rep.*, 7,
3510 4765, <https://doi.org/10.1038/s41598-017-03818-2>, 2017.

3511 Iida, Y., Takatani, Y., Kojima, A., and Ishii, M.: Global trends of ocean CO₂ sink and ocean acidification: an
3512 observation-based reconstruction of surface ocean inorganic carbon variables, *J Oceanogr.*, 77, 323–358,
3513 <https://doi.org/10.1007/s10872-020-00571-5>, 2021.

Deleted: Resour., 48, 615–650,
<https://doi.org/10.1146/annurev-environ-112321-103821>

3516 Ilyina, T., Li, H., Spring, A., Müller, W. A., Bopp, L., Chikamoto, M. O., Danabasoglu, G., Dobrynin, M., Dunne,
3517 J., Fransner, F., Friedlingstein, P., Lee, W., Lovenduski, N. S., Merryfield, W. J., Mignot, J., Park, J. Y., Séférian,
3518 R., Sospedra-Alfonso, R., Watanabe, M., and Yeager, S.: Predictable Variations of the Carbon Sinks and
3519 Atmospheric CO₂ Growth in a Multi-Model Framework, *Geophys. Res. Lett.*, 48, e2020GL090695,
3520 <https://doi.org/10.1029/2020GL090695>, 2021.

3521 IMF: International Monetary Fund: World Economic Outlook, available at: <http://www.imf.org>, last access: 23
3522 October 2025, 2025.

3523 Instituto Nacional de Pesquisas Espaciais (INPE): Portal TerraBrasilis, available at:
3524 <http://terrabrasilis.dpi.inpe.br/en/home-page/>, last access: 23 October 2025.

3525 Ito, A.: Disequilibrium of terrestrial ecosystem CO₂ budget caused by disturbance-induced emissions and non-CO₂
3526 carbon export flows: a global model assessment, *Earth Syst. Dynam.*, 10, 685–709, [https://doi.org/10.5194/esd-10-
3527 685-2019](https://doi.org/10.5194/esd-10-685-2019), 2019.

3528 Ito, A. and Inatomi, M.: Use of a process-based model for assessing the methane budgets of global terrestrial
3529 ecosystems and evaluation of uncertainty, 9, 759–773, <https://doi.org/10.5194/bg-9-759-2012>, 2012.

3530 Jackson, R. B., Canadell, J. G., Le Quéré, C., Andrew, R. M., Korsbakken, J. I., Peters, G. P., and Nakicenovic, N.:
3531 Reaching peak emissions, *Nature Clim Change*, 6, 7–10, <https://doi.org/10.1038/nclimate2892>, 2016.

3532 Jackson, R. B., Le Quéré, C., Andrew, R. M., Canadell, J. G., Korsbakken, J. I., Liu, Z., Peters, G. P., and Zheng,
3533 B.: Global energy growth is outpacing decarbonization, *Environ. Res. Lett.*, 13, 120401,
3534 <https://doi.org/10.1088/1748-9326/aaf303>, 2018.

3535 Jackson, R. B., Friedlingstein, P., Andrew, R. M., Canadell, J. G., Le Quéré, C., and Peters, G. P.: Persistent fossil
3536 fuel growth threatens the Paris Agreement and planetary health, *Environ. Res. Lett.*, 14, 121001,
3537 <https://doi.org/10.1088/1748-9326/ab57b3>, 2019.

3538 Jackson, R. B., Friedlingstein, P., Quéré, C. L., Abernethy, S., Andrew, R. M., Canadell, J. G., Ciais, P., Davis, S.
3539 J., Deng, Z., Liu, Z., Korsbakken, J. I., and Peters, G. P.: Global fossil carbon emissions rebound near pre-COVID-
3540 19 levels, *Environ. Res. Lett.*, 17, 031001, <https://doi.org/10.1088/1748-9326/ac55b6>, 2022.

3541 Jacobson, A. R., Schuldt, K. N., Tans, P., Andrews, A., Miller, J. B., Oda, T., Basu, S., Mund, J., Weir, B., Ott, L.,
3542 Aalto, T., Abshire, J. B., Aikin, K., Aoki, S., Apadula, F., Arnold, S., Baier, B., Bartyzel, J., Beyersdorf, A.,
3543 Biermann, T., Biraud, S. C., Boenisch, H., Brailsford, G., Brand, W. A., Chen, G., Chen, H., Chmura, L., Clark, S.,
3544 Colomb, A., Commane, R., Conil, S., Couret, C., Cox, A., Cristofanelli, P., Cuevas, E., Curcoll, R., Daube, B.,
3545 Davis, K. J., De Wekker, S., Della Coletta, J., Delmotte, M., DiGangi, E., DiGangi, J. P., di Sarra, A. G.,
3546 Dlugokencky, E., Elkins, J. W., Emmenegger, L., Fang, S., Fischer, M. L., Forster, G., Frumau, A., Galkowski, M.,
3547 Gatti, L. V., Gehrlein, T., Gerbig, C., Gheusi, F., Gloor, E., Gomez-Trueba, V., Goto, D., Griffis, T., Hammer, S.,
3548 Hanson, C., Haszpra, L., Hatakka, J., Heimann, M., Heliasz, M., Hensen, A., Hermansen, O., Hintsa, E., Holst, J.,
3549 Ivakhov, V., Jaffe, D. A., Jordan, A., Joubert, W., Karion, A., Kawa, S. R., Kazan, V., Keeling, R. F., Kerónen, P.,
3550 Kneuer, T., Kolari, P., Kominková, K., Kort, E., Kozlova, E., Krummel, P., Kubistin, D., Labuschagne, C., Lam,
3551 D. H. Y., Lan, X., Langenfelds, R. L., Laurent, O., Laurila, T., Lauvaux, T., Lavric, J., Law, B. E., Lee, J., Lee, O.
3552 S. M., Lehner, I., Lehtinen, K., Leppert, R., Leskinen, A., Leuenberger, M., Levin, I., Levula, J., Lin, J., Lindauer,
3553 M., Loh, Z., Lopez, M., Lujikx, I. T., Lunder, C. R., Machida, T., Mammarella, I., Manca, G., Manning, A.,
3554 Manning, A., Marek, M. V., Martin, M. Y., Matsueda, H., McKain, K., Meijer, H., Meinhardt, F., Merchant, L.,
3555 Mihalopoulos, N., Miles, N. L., Miller, C. E., Mitchell, L., Mölder, M., Montzka, S., Moore, F., Moossen, H.,
3556 Morgan, E., Morgui, J.-A., Morimoto, S., Müller-Williams, J., Munger, J. W., Munro, D., Myhre, C. L., Nakaoka,
3557 S.-I., Necki, J., Newman, S., Nichol, S., Niwa, Y., Obersteiner, F., O'Doherty, S., Paplawsky, B., Peischl, J.,
3558 Peltola, O., Piacentino, S., Pichon, J.-M., Pickers, P., Piper, S., Pitt, J., Plass-Dülmer, C., Platt, S. M., Prinzivalli,
3559 S., Ramonet, M., Ramos, R., Reyes-Sanchez, E., Richardson, S. J., Riris, H., Rivas, P. P., Ryerson, T., Saito, K.,
3560 Sargent, M., Sasakawa, M., Scheeren, B., Schuck, T., Schumacher, M., Seifert, T., Sha, M. K., Shepson, P., Shook,
3561 M., Sloop, C. D., Smith, P., Stanley, K., Steinbacher, M., Stephens, B., Sweeney, C., Thoning, K., Timas, H., Torn,
3562 M., Tørseth, K., Trisolino, P., Turnbull, J., van den Bulk, P., van Dinter, D., Vermeulen, A., Viner, B., Vitkova,
3563 G., Walker, S., Watson, A., Wofsy, S. C., Worsley, J., Worthy, D., Young, D., Zaehe, S., Zahn, A., and Zimnoch,
3564 M.: CarbonTracker CT2022, NOAA GML [Data set], <https://doi.org/10.25925/Z1GJ-3254>, 2023a.

3565 Jacobson, A. R., Schuldt, K. N., Tans, P., Andrews, A., Miller, J. B., Oda, T., Basu, S., Mund, J., Weir, B., Ott, L.,
3566 Aalto, T., Abshire, J. B., Aikin, K., Aoki, S., Apadula, F., Arnold, S., Baier, B., Bartyzel, J., Beyersdorf, A.,
3567 Biermann, T., Biraud, S. C., Boenisch, H., Brailsford, G., Brand, W. A., Chen, G., Chen, H., Chmura, L., Clark, S.,

Deleted: <https://doi.org/10.5194/esd-10-685-2019>

3569 Colomb, A., Commane, R., Conil, S., Couret, C., Cox, A., Cristofanelli, P., Cuevas, E., Curcoll, R., Daube, B.,
3570 Davis, K. J., De Wekker, S., Della Coletta, J., Delmotte, M., DiGangi, E., DiGangi, J. P., di Sarra, A. G.,
3571 Dlugokencky, E., Elkins, J. W., Emmenegger, L., Fang, S., Fischer, M. L., Forster, G., Frumau, A., Galkowski, M.,
3572 Gatti, L. V., Gehrlein, T., Gerbig, C., Gheusi, F., Gloor, E., Gomez-Trueba, V., Goto, D., Griffis, T., Hammer, S.,
3573 Hanson, C., Haszpra, L., Hatakka, J., Heimann, M., Heliasz, M., Hensen, A., Hermansen, O., Hints, E., Holst, J.,
3574 Ivakhov, V., Jaffe, D. A., Jordan, A., Joubert, W., Karion, A., Kawa, S. R., Kazan, V., Keeling, R. F., Keronen, P.,
3575 Kneuer, T., Kolari, P., Kominková, K., Kort, E., Kozlova, E., Krummel, P., Kubistin, D., Labuschagne, C., Lam,
3576 D. H. Y., Lan, X., Langenfelds, R. L., Laurent, O., Laurila, T., Lauvoux, T., Lavric, J., Law, B. E., Lee, J., Lee, O.
3577 S. M., Lehner, I., Lehtinen, K., Leppert, R., Leskinen, A., Leuenberger, M., Levin, I., Levula, J., Lin, J., Lindauer,
3578 M., Loh, Z., Lopez, M., Luijkx, I. T., Lunder, C. R., Machida, T., Mammarella, I., Manca, G., Manning, A.,
3579 Manning, A., Marek, M. V., Martin, M. Y., Matsueda, H., McKain, K., Meijer, H., Meinhardt, F., Merchant, L.,
3580 Mihalopoulos, N., Miles, N. L., Miller, C. E., Mitchell, L., Mölder, M., Montzka, S., Moore, F., Moossen, H.,
3581 Morgan, E., Morgui, J.-A., Morimoto, S., Müller-Williams, J., Munger, J. W., Munro, D., Myhre, C. L., Nakaoka,
3582 S.-I., Necki, J., Newman, S., Nichol, S., Niwa, Y., Obersteiner, F., O'Doherty, S., Paplawsky, B., Peischl, J.,
3583 Peltola, O., Piacentino, S., Pichon, J.-M., Pickers, P., Piper, S., Pitt, J., Plass-Dülmer, C., Platt, S. M., Prinzivalli,
3584 S., Ramonet, M., Ramos, R., Reyes-Sanchez, E., Richardson, S. J., Riris, H., Rivas, P. P., Ryerson, T., Saito, K.,
3585 Sargent, M., Sasakawa, M., Scheeren, B., Schuck, T., Schumacher, M., Seifert, T., Sha, M. K., Shepson, P., Shook,
3586 M., Sloop, C. D., Smith, P., Stanley, K., Steinbacher, M., Stephens, B., Sweeney, C., Thoning, K., Timas, H., Tom,
3587 M., Tørseth, K., Trisolino, P., Turnbull, J., van den Bulk, P., van Dinter, D., Vermeulen, A., Viner, B., Vitkova,
3588 G., Walker, S., Watson, A., Wofsy, S. C., Worsley, J., Worthy, D., Young, D., Zaehle, S., Zahn, A., and Zimnoch,
3589 M.: CarbonTracker CT-NRT.v2023-3, NOAA GML [Data set], https://doi.org/10.25925/TTAF-J322_2023b.

3590 Jain, A. K., Meiyappan, P., Song, Y., and House, J. I.: CO₂ emissions from land-use change affected more by
3591 nitrogen cycle, than by the choice of land-cover data, *Global Change Biology*, 19, 2893–2906,
3592 <https://doi.org/10.1111/gcb.12207>, 2013.

3593 Jain, P., Barber, Q. E., Taylor, S. W., Whitman, E., Castellanos Acuna, D., Boulanger, Y., Chavardès, R. D., Chen,
3594 J., Englefield, P., Flannigan, M., Girardin, M. P., Hanes, C. C., Little, J., Morrison, K., Skakun, R. S., Thompson,
3595 D. K., Wang, X., Parisien, M.-A.: Drivers and Impacts of the Record-Breaking 2023 Wildfire Season in Canada.
3596 *Nature Communications*, 15(1), p.6764, <https://doi.org/10.1038/s41467-024-51154-7>, 2024.

3597 Janssens-Maenhout, G., Crippa, M., Guizzardi, D., Muntean, M., Schaaf, E., Dentener, F., Bergamaschi, P.,
3598 Pagliari, V., Olivier, J. G. J., Peters, J. A. H. W., van Aardenne, J. A., Monni, S., Doering, U., Petrescu, A. M. R.,
3599 Solazzo, E., and Oreggioni, G. D.: EDGAR v4.3.2 Global Atlas of the three major greenhouse gas emissions for
3600 the period 1970–2012, *Earth Syst. Sci. Data*, 11, 959–1002, <https://doi.org/10.5194/essd-11-959-2019>.

3601 Jean-Michel, L., Eric, G., Romain, B.-B., Gilles, G., Angélique, M., Marie, D., Clément, B., Mathieu, H., Olivier,
3602 L. G., Charly, R., Tony, C., Charles-Emmanuel, T., Florent, G., Giovanni, R., Mounir, B., Yann, D., and Pierre-
3603 Yves, L. T.: The Copernicus Global 1/12° Oceanic and Sea Ice GLORYS12 Reanalysis, *Front. Earth Sci.*, 9, 2021.

3604 Jiang, F., Ju, W., He, W., Wu, M., Wang, H., Wang, J., Jia, M., Feng, S., Zhang, L., and Chen, J. M.: A 10-year
3605 global monthly averaged terrestrial net ecosystem exchange dataset inferred from the ACOS GOSAT v9 XCO₂
3606 retrievals (GCAS2021), *Earth Syst. Sci. Data*, 14, 3013–3037, <https://doi.org/10.5194/essd-14-3013-2022>, 2022.

3607 Jiang, F., Wang, H., Chen, J. M., Ju, W., Tian, X., Feng, S., Li, G., Chen, Z., Zhang, S., Lu, X., Liu, J., Wang, H.,
3608 Wang, J., He, W., and Wu, M.: Regional CO₂ fluxes from 2010 to 2015 inferred from GOSAT XCO₂ retrievals
3609 using a new version of the Global Carbon Assimilation System, *Atmospheric Chem. Phys.*, 21, 1963–1985,
3610 <https://doi.org/10.5194/acp-21-1963-2021>, 2021.

3611 Jin, Y., Keeling, R. F., Stephens, B. B., Long, M. C., Patra, P. K., Rödenbeck, C., Morgan, E. J., Kort, E. A., and
3612 Sweeney, C.: Improved atmospheric constraints on Southern Ocean CO₂ exchange. *Proceedings of the National
3613 Academy of Sciences*, 121(6), e2309333121, <https://doi.org/10.1073/pnas.2309333121>, 2024.

3614 Jin, Z., Wang, T., Zhang, H., Wang, Y., Ding, J., and Tian, X.: Constraint of satellite CO₂ retrieval on the global
3615 carbon cycle from a Chinese atmospheric inversion system, *Sci. China Earth Sci.*, 66, 609–618,
3616 <https://doi.org/10.1007/s11430-022-1036-7>, 2023.

3617 Joos, F. and Spahni, R.: Rates of change in natural and anthropogenic radiative forcing over the past 20,000 years,
3618 *Proceedings of the National Academy of Sciences*, 105, 1425–1430, <https://doi.org/10.1073/pnas.0707386105>,
3619 2008.

Deleted: <https://doi.org/10.1111/gcb.12207>

- 3621 Jones, C. D., Hickman, J. E., Rumbold, S. T., Walton, J., Lamboll, R. D., Skeie, R. B., Fiedler, S., Forster, P. M.,
3622 Rogelj, J., Abe, M., Botzet, M., Calvin, K., Cassou, C., Cole, J. N. S., Davini, P., Deushi, M., Dix, M., Fyfe, J. C.,
3623 Gillett, N. P., Ilyina, T., Kawamiya, M., Kelley, M., Kharin, S., Koshiro, T., Li, H., Mackallah, C., Müller, W. A.,
3624 Nabat, P., van Noije, T., Nolan, P., Ohgaito, R., Olivié, D., Oshima, N., Parodi, J., Reerink, T. J., Ren, L.,
3625 Romanou, A., Séférian, R., Tang, Y., Timmreck, C., Tjiputra, J., Tourigny, E., Tsigaridis, K., Wang, H., Wu, M.,
3626 Wyser, K., Yang, S., Yang, Y., and Ziehn, T.: The Climate Response to Emissions Reductions Due to COVID-19:
3627 Initial Results From CovidMIP, *Geophys. Res. Lett.*, 48, e2020GL091883, <https://doi.org/10.1029/2020GL091883>,
3628 2021a.
- 3629 Jones, M. W., Abatzoglou, J. T., Veraverbeke, S., Andela, N., Lasslop, G., Forkel, M., Smith, A. J. P., Burton, C.,
3630 Betts, R. A., van der Werf, G. R., Sitch, S., Canadell, J. G., Santin, C., Kolden, C., Doerr, S. H., and Le Quéré, C.:
3631 Global and Regional Trends and Drivers of Fire Under Climate Change, *Rev. Geophys.*, 60, e2020RG000726,
3632 <https://doi.org/10.1029/2020RG000726>, 2022.
- 3633 Jones, M. W., Andrew, R. M., Peters, G. P., Janssens-Maenhout, G., De-Gol, A. J., Ciais, P., Patra, P. K.,
3634 Chevallier, F., and Le Quéré, C.: Gridded fossil CO₂ emissions and related O₂ combustion consistent with national
3635 inventories 1959–2018, *Sci Data*, 8, 2, <https://doi.org/10.1038/s41597-020-00779-6>, 2021b.
- 3636 Jones, M. W., Andrew, R. M., Peters, G. P., Janssens-Maenhout, G., De-Gol, A. J., Dou, X., Liu, Z., Pickers, P.,
3637 Ciais, P., Patra, P. K., Chevallier, F., and Le Quéré, C.: Gridded fossil CO₂ emissions and related O₂ combustion
3638 consistent with national inventories, Zenodo [Data set], <https://doi.org/10.5281/zenodo.17467681>, 2025.
- 3639 Jones, M. W., Kelley, D. I., Burton, C. A., Di Giuseppe, F., Barbosa, M. L. F., Brambleby, E., Hartley, A. J.,
3640 Lombardi, A., Matalavi, G., McNorton, J. R., Spuler, F. R., Wessel, J. B., Abatzoglou, J. T., Anderson, L. O.,
3641 Andela, N., Archibald, S., Armenteras, D., Burke, E., Carmenta, R., Chuvieco, E., Clarke, H., Doerr, S. H.,
3642 Fernandes, P. M., Giglio, L., Hamilton, D. S., Hantson, S., Harris, S., Jain, P., Kolden, C. A., Kurvits, T., Lampe,
3643 S., Meier, S., New, S., Parrington, M., Perron, M. M. G., Qu, Y., Ribeiro, N. S., Saharjo, B. H., San-Miguel-Ayanz,
3644 J., Shuman, J. K., Tanpipat, V., van der Werf, G. R., Veraverbeke, S., and Xanthopoulos, G.: State of Wildfires
3645 2023–2024, *Earth System Science Data*, 16, 3601–3685, <https://doi.org/10.5194/essd-16-3601-2024>, 2024b.
- 3646 Jones, M.W., Veraverbeke, S., Andela, N., Doerr, S.H., Kolden, C., Matalavi, G., Pettinari, M.L., Le Quéré, C.,
3647 Rosan, T.M., van der Werf, G.R. and van Wees, D.: Global rise in forest fire emissions linked to climate change in
3648 the extratropics. *Science*, 386(6719), p.ead15889, 2024c.
- 3649 Jung, M., Reichstein, M., Schwalm, C. R., Huntingford, C., Sitch, S., Ahlström, A., Arneeth, A., Camps-Valls, G.,
3650 Ciais, P., Friedlingstein, P., Gans, F., Ichii, K., Jain, A. K., Kato, E., Papale, D., Poulter, B., Raduly, B.,
3651 Rödenbeck, C., Tramontana, G., Viovy, N., Wang, Y.-P., Weber, U., Zaehle, S., and Zeng, N.: Compensatory
3652 water effects link yearly global land CO₂ sink changes to temperature, *Nature*, 541, 516–520,
3653 <https://doi.org/10.1038/nature20780>, 2017.
- 3654 Kaiser, J. W., Heil, A., Andreae, M. O., Benedetti, A., Chubarova, N., Jones, L., Morcrette, J.-J., Razinger, M.,
3655 Schultz, M. G., Suttie, M., and van der Werf, G. R.: Biomass burning emissions estimated with a global fire
3656 assimilation system based on observed fire radiative power, *Biogeosciences*, 9, 527–554,
3657 <https://doi.org/10.5194/bg-9-527-2012>, 2012.
- 3658 Kato, E., Kinoshita, T., Ito, A., Kawamiya, M., and Yamagata, Y.: Evaluation of spatially explicit emission
3659 scenario of land-use change and biomass burning using a process-based biogeochemical model, *J. Land Use Sci.*, 8,
3660 104–122, <https://doi.org/10.1080/1747423X.2011.628705>, 2013.
- 3661 Kawasaki, T., Hasumi, H., and Tanaka, Y.: Role of tide-induced vertical mixing in the deep Pacific Ocean
3662 circulation, *J. Oceanogr.*, 77, 173–184, <https://doi.org/10.1007/s10872-020-00584-0>, 2021.
- 3663 Ke, P., Ciais, P., Sitch, S., Li, W., Bastos, A., Liu, Z., Xu, Y., Gui, X., Bian, J., Goll, D. S., Xi, Y., Li, W.,
3664 O'Sullivan, M., Goncalves de Souza, J., Friedlingstein, P., Chevallier, F.: Low latency carbon budget analysis
3665 reveals a large decline of the land carbon sink in 2023. *National Science Review*, p.nwae367,
3666 <https://doi.org/10.1093/nsr/nwae367>, 2024.
- 3667 Keeley, J. E. and Pausas, J. G.: Distinguishing disturbance from perturbations in fire-prone ecosystems, *Int. J.*
3668 *Wildland Fire*, 28, 282–287, <https://doi.org/10.1071/WF18203>, 2019.

3669 Keeling, C. D., Bacastow, R. B., Bainbridge, A. E., Ekdahl, C. A., Guenther, P. R., Waterman, L. S., and Chin, J.
3670 F. S.: Atmospheric carbon dioxide variations at Mauna Loa Observatory, Hawaii, *Tellus A*, 28, 538–551,
3671 <https://doi.org/10.1111/j.2153-3490.1976.tb00701.x>, 1976.

3672 Keeling R.F.: Development of an Interferometric Oxygen Analyzer for Precise Measurement of the Atmospheric
3673 O₂ Mole Fraction, PhD thesis, Harvard University, Cambridge, Massachusetts, available at:
3674 https://bluemoon.ucsd.edu/publications/ralph/34_PhDthesis.pdf, last access: 23 October 2025, 1988.

3675 Keeling, R. F., Manning, A. C., Paplawsky, W. J., and Cox, A. C.: On the long-term stability of reference gases for
3676 atmospheric O₂/N₂ and CO₂ measurements, *Tellus B Chem. Phys. Meteorol.*, 59, 3–14,
3677 <https://doi.org/10.1111/j.1600-0889.2006.00196.x>, 2007.

3678 Keeling, R. F. and Manning, A. C.: 5.15 - Studies of Recent Changes in Atmospheric O₂ Content, in: *Treatise on
3679 Geochemistry (Second Edition)*, edited by: Holland, H. D. and Turekian, K. K., Elsevier, Oxford, 385–404,
3680 <https://doi.org/10.1016/B978-0-08-095975-7.00420-4>, 2014.

3681 Kelley, D. I., Burton, C., Di Giuseppe, F., Jones, M. W., Barbosa, M. L. F., Brambleby, E., McNorton, J. R., Liu,
3682 Z., Bradley, A. S. I., Blackford, K., Burke, E., Ciavarella, A., Di Tomaso, E., Eden, J., Ferreira, I. J. M., Fiedler, L.,
3683 Hartley, A. J., Keeping, T. R., Lampe, S., Lombardi, A., Matalveli, G., Qu, Y., Silva, P. S., Spuler, F. R.,
3684 Steinmann, C. B., Torres-Vázquez, M. Á., Veiga, R., Van Wees, D., Wessel, J. B., Wright, E., Bilbao, B.,
3685 Bourbonnais, M., Gao, C., Di Bella, C. M., Dintwe, K., Donovan, V. M., Harris, S., Kukavskaya, E. A., N'Dri, A.
3686 B., Santin, C., Selaya, G., Sjöström, J., Abatzoglou, J. T., Andela, N., Carmenta, R., Chuvieco, E., Giglio, L.,
3687 Hamilton, D. S., Hantson, S., Meier, S., Parrington, M., Sadegh, M., San-Miguel-Ayanz, J., Sedano, F., Turco, M.,
3688 Van Der Werf, G. R., Veraverbeke, S., Anderson, L. O., Clarke, H., Fernandes, P. M., and Kolden, C. A.: State of
3689 Wildfires 2024–2025, *Earth Syst. Sci. Data*, 17, 5377–5488, <https://doi.org/10.5194/essd-17-5377-2025>, 2025.

3690 Keppler, L. and Landschützer, P.: Regional Wind Variability Modulates the Southern Ocean Carbon Sink, *Sci Rep*,
3691 9, 7384, <https://doi.org/10.1038/s41598-019-43826-y>, 2019.

3692 Kharin, V. V., Boer, G. J., Merryfield, W. J., Scinocca, J. F., and Lee, W. -S.: Statistical adjustment of decadal
3693 predictions in a changing climate, *Geophysical Research Letters*, 39, 2012GL052647,
3694 <https://doi.org/10.1029/2012GL052647>, 2012.

3695 Khatiwala, S., Primeau, F., and Hall, T.: Reconstruction of the history of anthropogenic CO₂ concentrations in the
3696 ocean, *Nature*, 462, 346–349, <https://doi.org/10.1038/nature08526>, 2009.

3697 Khatiwala, S., Tanhua, T., Mikaloff Fletcher, S., Gerber, M., Doney, S. C., Graven, H. D., Gruber, N., McKinley,
3698 G. A., Murata, A., Ríos, A. F., and Sabine, C. L.: Global ocean storage of anthropogenic carbon, *Biogeosciences*,
3699 10, 2169–2191, <https://doi.org/10.5194/bg-10-2169-2013>, 2013.

3700 Kong, Y., Zheng, B., Zhang, Q., and He, K.: Global and regional carbon budget for 2015–2020 inferred from
3701 OCO-2 based on an ensemble Kalman filter coupled with GEOS-Chem, *Atmospheric Chem. Phys.*, 22, 10769–
3702 10788, <https://doi.org/10.5194/acp-22-10769-2022>, 2022.

3703 Kou-Giesbrecht, S. and Arora, V. K.: Representing the Dynamic Response of Vegetation to Nitrogen Limitation
3704 via Biological Nitrogen Fixation in the CLASSIC Land Model, *Global Biogeochemical Cycles*, 36,
3705 e2022GB007341, <https://doi.org/10.1029/2022GB007341>, 2022.

3706 Korsbakken, J. I., Peters, G. P., and Andrew, R. M.: Uncertainties around reductions in China's coal use and CO₂
3707 emissions, *Nature Clim Change*, 6, 687–690, <https://doi.org/10.1038/nclimate2963>, 2016.

3708 Koven, C. D., Knox, R. G., Fisher, R. A., Chambers, J. Q., Christoffersen, B. O., Davies, S. J., Detto, M., Dietze,
3709 M. C., Faybishenko, B., Holm, J., Huang, M., Kovenock, M., Kueppers, L. M., Lemieux, G., Massoud, E.,
3710 McDowell, N. G., Muller-Landau, H. C., Needham, J. F., Norby, R. J., Powell, T., Rogers, A., Serbin, S. P.,
3711 Shuman, J. K., Swann, A. L. S., Varadharajan, C., Walker, A. P., Wright, S. J., and Xu, C.: Benchmarking and
3712 parameter sensitivity of physiological and vegetation dynamics using the Functionally Assembled Terrestrial
3713 Ecosystem Simulator (FATES) at Barro Colorado Island, Panama, *Biogeosciences*, 17, 3017–3044,
3714 <https://doi.org/10.5194/bg-17-3017-2020>, 2020.

3715 Krinner, G., Viovy, N., de Noblet-Ducoudré, N., Ogée, J., Polcher, J., Friedlingstein, P., Ciais, P., Sitch, S., and
3716 Prentice, I. C.: A dynamic global vegetation model for studies of the coupled atmosphere-biosphere system:

Deleted: Data, 17, 5377–5488, <https://doi.org/10.5194/essd-17-5377-2025>

Deleted: <https://doi.org/10.1029/2022GB007341>

Deleted: <https://doi.org/10.5194/bg-17-3017-2020>

3721 DVGM for coupled climate studies, *Global Biogeochem. Cycles*, 19, GB1015,
3722 <https://doi.org/10.1029/2003GB002199>, 2005.

3723 Lacroix, F., Ilyina, T., and Hartmann, J.: Oceanic CO₂ outgassing and biological production hotspots induced by
3724 pre-industrial river loads of nutrients and carbon in a global modeling approach, *Biogeosciences*, 17, 55–88,
3725 <https://doi.org/10.5194/bg-17-55-2020>, 2020.

3726 Lacroix, F., Ilyina, T., Mathis, M., Laruelle, G. G., and Regnier, P.: Historical increases in land-derived nutrient
3727 inputs may alleviate effects of a changing physical climate on the oceanic carbon cycle, *Glob Change Biol*, 27,
3728 5491–5513, <https://doi.org/10.1111/gcb.15822>, 2021.

3729 Lamboll, R. D., Nicholls, Z. R. J., Smith, C. J., Kikstra, J. S., Byers, E., and Rogelj, J.: Assessing the size and
3730 uncertainty of remaining carbon budgets, *Nat. Clim. Change*, <https://doi.org/10.1038/s41558-023-01848-5>, 2023.

3731 Lamboll, R. D., Jones, C. D., Skeie, R. B., Fiedler, S., Samset, B. H., Gillett, N. P., Rogelj, J., Forster, P. M., 2021:
3732 Modifying emissions scenario projections to account for the effects of COVID-19: protocol for CovidMIP, *Geosci.
3733 Model Dev.*, 14, 3683–3695, <https://doi.org/10.5194/gmd-14-3683-2021>, 2021.

3734 Lan, X., Tans, P. and Thoning, K.: NOAA Greenhouse Gas Marine Boundary Layer Reference - CO₂ [Data set].
3735 NOAA Global Monitoring Laboratory, <https://doi.org/10.15138/DVNP-F961>, 2024.

3736 Lan, X., Tans, P. and Thoning, K. W.: Trends in globally-averaged CO₂ determined from NOAA Global
3737 Monitoring Laboratory measurements, <https://doi.org/10.15138/9N0H-ZH07>, 2025.

3738 Landschützer, P., Gruber, N., Haumann, F. A., Rödenbeck, C., Bakker, D. C. E., van Heuven, S., Hoppema, M.,
3739 Metz, N., Sweeney, C., Takahashi, T., Tilbrook, B., and Wanninkhof, R.: The reinvigoration of the Southern
3740 Ocean carbon sink, *Science*, 349, 1221–1224, <https://doi.org/10.1126/science.aab2620>, 2015.

3741 Landschützer, P., Gruber, N., and Bakker, D. C. E.: Decadal variations and trends of the global ocean carbon sink:
3742 decadal air-sea CO₂ flux variability, *Global Biogeochem. Cycles*, 30, 1396–1417,
3743 <https://doi.org/10.1002/2015GB005359>, 2016.


3744 Lapola, D. M., Pinho, P., Barlow, J., Aragão, L. E. O. C., Berenguer, E., Carmenta, R., Liddy, H. M., Seixas, H.,
3745 Silva, C. V. J., Silva-Junior, C. H. L., Alencar, A. A. C., Anderson, L. O., Armenteras, D., Brovkin, V., Calders,
3746 K., Chambers, J., Chini, L., Costa, M. H., Faria, B. L., Fearnside, P. M., Ferreira, J., Gatti, L., Gutierrez-Velez, V.
3747 H., Han, Z., Hibbard, K., Koven, C., Lawrence, P., Pongratz, J., Portela, B. T. T., Rounsevell, M., Ruane, A. C.,
3748 Schaldach, R., da Silva, S. S., von Randow, C., Walker, W. S.: The drivers and impacts of Amazon forest
3749 degradation. *Science*, 379(6630), p.eabp8622, <https://doi.org/10.1126/science.abp8622>, 2023.

3750 Law, R. M., Ziehn, T., Matear, R. J., Lenton, A., Chamberlain, M. A., Stevens, L. E., Wang, Y.-P., Srbnovsky, J.,
3751 Bi, D., Yan, H., and Vohralik, P. F.: The carbon cycle in the Australian Community Climate and Earth System
3752 Simulator (ACCESS-ESM1) – Part 1: Model description and pre-industrial simulation, *Geosci. Model Dev.*, 10,
3753 2567–2590, <https://doi.org/10.5194/gmd-10-2567-2017>, 2017.

3754 Laughner, J. L., Roche, S., Kiel, M., Toon, G. C., Wunch, D., Baier, B. C., Biraud, S., Chen, H., Kivi, R.,
3755 Laemmle, T., McKain, K., Quéhé, P.-Y., Rousogonous, C., Stephens, B. B., Walker, K., and Wennberg, P. O.: A
3756 new algorithm to generate a priori trace gas profiles for the GGG2020 retrieval algorithm, *Atmos. Meas. Tech.*, 16,
3757 1121–1146, <https://doi.org/10.5194/amt-16-1121-2023>, 2023.

3758 Lauvset, S. K., Lange, N., Tanhua, T., Bittig, H. C., Olsen, A., Kozyr, A., Álvarez, M., Azetsu-Scott, K., Brown, P.
3759 J., Carter, B. R., Cotrim Da Cunha, L., Hoppema, M., Humphreys, M. P., Ishii, M., Jeansson, E., Murata, A.,
3760 Müller, J. D., Pérez, F. F., Schirnick, C., Steinfeldt, R., Suzuki, T., Ulfssbo, A., Velo, A., Woosley, R. J., and Key,
3761 R. M.: The annual update GLODAPv2.2023: the global interior ocean biogeochemical data product, *Earth Syst.
3762 Sci. Data*, 16, 2047–2072, <https://doi.org/10.5194/essd-16-2047-2024>, 2024.

3763 Lawrence, D. M., Fisher, R. A., Koven, C. D., Oleson, K. W., Swenson, S. C., Bonan, G., Collier, N., Ghimire, B.,
3764 van Kampenhout, L., Kennedy, D., Kluzek, E., Lawrence, P. J., Li, F., Li, H., Lombardozzi, D., Riley, W. J.,
3765 Sacks, W. J., Shi, M., Verstein, M., Wieder, W. R., Xu, C., Ali, A. A., Badger, A. M., Bisht, G., van den
3766 Broeke, M., Brunke, M. A., Burns, S. P., Buzan, J., Clark, M., Craig, A., Dahlin, K., Drewniak, B., Fisher, J. B.,
3767 Flanner, M., Fox, A. M., Gentine, P., Hoffman, F., Keppel-Aleks, G., Knox, R., Kumar, S., Lenaerts, J., Leung, L.
3768 R., Lipscomb, W. H., Lu, Y., Pandey, A., Pelletier, J. D., Perket, J., Randerson, J. T., Ricciuto, D. M., Sanderson,
3769 B. M., Slater, A., Subin, Z. M., Tang, J., Thomas, R. Q., Val Martin, M., and Zeng, X.: The Community Land

Deleted: and K.W. Thoning: Trends in globally-averaged CO₂ determined from NOAA Global Monitoring Laboratory measurements. Version Friday, 05-Sep-2025 12:12:59 MDT, <https://doi.org/10.15138/9N0H-ZH07>, 2025. 

Deleted: 2024b

Deleted: <https://doi.org/10.5194/amt-16-1121-2023>

- 3777 Model Version 5: Description of New Features, Benchmarking, and Impact of Forcing Uncertainty, *J. Adv. Model Earth, Sy.*, 11, 4245–4287, <https://doi.org/10.1029/2018MS001583>, 2019.
- 3779 Le Quéré, C., Rödenbeck, C., Buitenhuis, E. T., Conway, T. J., Langenfelds, R., Gomez, A., Labuschagne, C.,
3780 Ramonet, M., Nakazawa, T., Metzl, N., Gillett, N., and Heimann, M.: Saturation of the Southern Ocean CO₂ Sink
3781 Due to Recent Climate Change, *Science*, 316, 1735–1738, <https://doi.org/10.1126/science.1136188>, 2007.
- 3782 Le Quéré, C., Raupach, M. R., Canadell, J. G., Marland, G., Bopp, L., Ciais, P., Conway, T. J., Doney, S. C., Feely,
3783 R. A., Foster, P., Friedlingstein, P., Gurney, K., Houghton, R. A., House, J. I., Huntingford, C., Levy, P. E., Lomas,
3784 M. R., Majkut, J., Metzl, N., Ometto, J. P., Peters, G. P., Prentice, I. C., Randerson, J. T., Running, S. W.,
3785 Sarmiento, J. L., Schuster, U., Sitch, S., Takahashi, T., Viovy, N., van der Werf, G. R., and Woodward, F. I.:
3786 Trends in the sources and sinks of carbon dioxide, *Nature Geosci*, 2, 831–836, <https://doi.org/10.1038/ngeo689>,
3787 2009.
- 3788 Le Quéré, C., Andres, R. J., Boden, T., Conway, T., Houghton, R. A., House, J. I., Marland, G., Peters, G. P., van
3789 der Werf, G. R., Ahlström, A., Andrew, R. M., Bopp, L., Canadell, J. G., Ciais, P., Doney, S. C., Enright, C.,
3790 Friedlingstein, P., Huntingford, C., Jain, A. K., Jourdain, C., Kato, E., Keeling, R. F., Klein Goldewijk, K., Levis,
3791 S., Levy, P., Lomas, M., Poulter, B., Raupach, M. R., Schwinger, J., Sitch, S., Stocker, B. D., Viovy, N., Zaehle,
3792 S., and Zeng, N.: The global carbon budget 1959–2011, *Earth Syst. Sci. Data*, 5, 165–185,
3793 <https://doi.org/10.5194/essd-5-165-2013>, 2013.
- 3794 Le Quéré, C., Peters, G. P., Andres, R. J., Andrew, R. M., Boden, T. A., Ciais, P., Friedlingstein, P., Houghton, R.
3795 A., Marland, G., Moriarty, R., Sitch, S., Tans, P., Armeth, A., Arvanitis, A., Bakker, D. C. E., Bopp, L., Canadell, J.
3796 G., Chini, L. P., Doney, S. C., Harper, A., Harris, I., House, J. I., Jain, A. K., Jones, S. D., Kato, E., Keeling, R. F.,
3797 Klein Goldewijk, K., Körtzinger, A., Koven, C., Lefèvre, N., Maignan, F., Omar, A., Ono, T., Park, G.-H., Pfeil,
3798 B., Poulter, B., Raupach, M. R., Regnier, P., Rödenbeck, C., Saito, S., Schwinger, J., Segsneider, J., Stocker, B.
3799 D., Takahashi, T., Tilbrook, B., van Heuven, S., Viovy, N., Wanninkhof, R., Wiltshire, A., and Zaehle, S.: Global
3800 carbon budget 2013, *Earth Syst. Sci. Data*, 6, 235–263, <https://doi.org/10.5194/essd-6-235-2014>, 2014.
- 3801 Le Quéré, C., Moriarty, R., Andrew, R. M., Peters, G. P., Ciais, P., Friedlingstein, P., Jones, S. D., Sitch, S., Tans,
3802 P., Armeth, A., Boden, T. A., Bopp, L., Bozec, Y., Canadell, J. G., Chini, L. P., Chevallier, F., Cosca, C. E., Harris,
3803 I., Hoppema, M., Houghton, R. A., House, J. I., Jain, A. K., Johannessen, T., Kato, E., Keeling, R. F., Kitidis, V.,
3804 Klein Goldewijk, K., Koven, C., Landa, C. S., Landschützer, P., Lenton, A., Lima, I. D., Marland, G., Mathis, J. T.,
3805 Metzl, N., Nojiri, Y., Olsen, A., Ono, T., Peng, S., Peters, W., Pfeil, B., Poulter, B., Raupach, M. R., Regnier, P.,
3806 Rödenbeck, C., Saito, S., Salisbury, J. E., Schuster, U., Schwinger, J., Séférian, R., Segsneider, J., Steinhoff, T.,
3807 Stocker, B. D., Sutton, A. J., Takahashi, T., Tilbrook, B., van der Werf, G. R., Viovy, N., Wang, Y.-P.,
3808 Wanninkhof, R., Wiltshire, A., and Zeng, N.: Global carbon budget 2014, *Earth Syst. Sci. Data*, 7, 47–85,
3809 <https://doi.org/10.5194/essd-7-47-2015>, 2015a.
- 3810 Le Quéré, C., Moriarty, R., Andrew, R. M., Canadell, J. G., Sitch, S., Korsbakken, J. I., Friedlingstein, P., Peters,
3811 G. P., Andres, R. J., Boden, T. A., Houghton, R. A., House, J. I., Keeling, R. F., Tans, P., Armeth, A., Bakker, D. C.
3812 E., Barbero, L., Bopp, L., Chang, J., Chevallier, F., Chini, L. P., Ciais, P., Fader, M., Feely, R. A., Gkritzalis, T.,
3813 Harris, I., Hauck, J., Ilyina, T., Jain, A. K., Kato, E., Kitidis, V., Klein Goldewijk, K., Koven, C., Landschützer, P.,
3814 Lauvset, S. K., Lefèvre, N., Lenton, A., Lima, I. D., Metzl, N., Millero, F., Munro, D. R., Murata, A., Nabel, J. E.
3815 M. S., Nakaoka, S., Nojiri, Y., O'Brien, K., Olsen, A., Ono, T., Pérez, F. F., Pfeil, B., Pierrot, D., Poulter, B.,
3816 Rehder, G., Rödenbeck, C., Saito, S., Schuster, U., Schwinger, J., Séférian, R., Steinhoff, T., Stocker, B. D.,
3817 Sutton, A. J., Takahashi, T., Tilbrook, B., van der Laan-Luijkx, I. T., van der Werf, G. R., van Heuven, S.,
3818 Vandemark, D., Viovy, N., Wiltshire, A., Zaehle, S., and Zeng, N.: Global Carbon Budget 2015, *Earth Syst. Sci.*
3819 *Data*, 7, 349–396, <https://doi.org/10.5194/essd-7-349-2015>, 2015b.
- 3820 Le Quéré, C., Andrew, R. M., Canadell, J. G., Sitch, S., Korsbakken, J. I., Peters, G. P., Manning, A. C., Boden, T.
3821 A., Tans, P. P., Houghton, R. A., Keeling, R. F., Alin, S., Andrews, O. D., Anthoni, P., Barbero, L., Bopp, L.,
3822 Chevallier, F., Chini, L. P., Ciais, P., Currie, K., Delire, C., Doney, S. C., Friedlingstein, P., Gkritzalis, T., Harris,
3823 I., Hauck, J., Haverd, V., Hoppema, M., Klein Goldewijk, K., Jain, A. K., Kato, E., Körtzinger, A., Landschützer,
3824 P., Lefèvre, N., Lenton, A., Lienert, S., Lombardozzi, D., Melton, J. R., Metzl, N., Millero, F., Monteiro, P. M. S.,
3825 Munro, D. R., Nabel, J. E. M. S., Nakaoka, S., O'Brien, K., Olsen, A., Omar, A. M., Ono, T., Pierrot, D., Poulter,
3826 B., Rödenbeck, C., Salisbury, J., Schuster, U., Schwinger, J., Séférian, R., Skjelvan, I., Stocker, B. D., Sutton, A. J.,
3827 Takahashi, T., Tian, H., Tilbrook, B., van der Laan-Luijkx, I. T., van der Werf, G. R., Viovy, N., Walker, A. P.,
3828 Wiltshire, A. J., and Zaehle, S.: Global Carbon Budget 2016, *Earth Syst. Sci. Data*, 8, 605–649,
3829 <https://doi.org/10.5194/essd-8-605-2016>, 2016.

3830 Le Quéré, C., Andrew, R. M., Friedlingstein, P., Sitch, S., Pongratz, J., Manning, A. C., Korsbakken, J. I., Peters,
3831 G. P., Canadell, J. G., Jackson, R. B., Boden, T. A., Tans, P. P., Andrews, O. D., Arora, V. K., Bakker, D. C. E.,
3832 Barbero, L., Becker, M., Betts, R. A., Bopp, L., Chevallier, F., Chini, L. P., Ciais, P., Cosca, C. E., Cross, J.,
3833 Currie, K., Gasser, T., Harris, I., Hauck, J., Haverd, V., Houghton, R. A., Hunt, C. W., Hurtt, G., Ilyina, T., Jain, A.
3834 K., Kato, E., Kautz, M., Keeling, R. F., Klein Goldewijk, K., Körtzinger, A., Landschützer, P., Lefèvre, N., Lenton,
3835 A., Lienert, S., Lima, I., Lombardozi, D., Metzl, N., Millero, F., Monteiro, P. M. S., Munro, D. R., Nabel, J. E. M.
3836 S., Nakaoka, S., Nojiri, Y., Padin, X. A., Peregón, A., Pfeil, B., Pierrot, D., Poulter, B., Rehder, G., Reimer, J.,
3837 Rödenbeck, C., Schwinger, J., Séférian, R., Skjelvan, I., Stocker, B. D., Tian, H., Tilbrook, B., Tubiello, F. N., van
3838 der Laan-Luijkx, I. T., van der Werf, G. R., van Heuven, S., Viovy, N., Vuichard, N., Walker, A. P., Watson, A. J.,
3839 Wiltshire, A. J., Zaehle, S., and Zhu, D.: Global Carbon Budget 2017, *Earth Syst. Sci. Data*, 10, 405–448,
3840 <https://doi.org/10.5194/essd-10-405-2018>, 2018a.

3841 Le Quéré, C., Andrew, R. M., Friedlingstein, P., Sitch, S., Hauck, J., Pongratz, J., Pickers, P. A., Korsbakken, J. I.,
3842 Peters, G. P., Canadell, J. G., Armeth, A., Arora, V. K., Barbero, L., Bastos, A., Bopp, L., Chevallier, F., Chini, L.
3843 P., Ciais, P., Doney, S. C., Gkritzalis, T., Goll, D. S., Harris, I., Haverd, V., Hoffman, F. M., Hoppema, M.,
3844 Houghton, R. A., Hurtt, G., Ilyina, T., Jain, A. K., Johannessen, T., Jones, C. D., Kato, E., Keeling, R. F., Klein
3845 Goldewijk, K., Landschützer, P., Lefèvre, N., Lienert, S., Liu, Z., Lombardozi, D., Metzl, N., Munro, D. R.,
3846 Nabel, J. E. M. S., Nakaoka, S., Neill, C., Olsen, A., Ono, T., Patra, P., Peregón, A., Peters, W., Peylin, P., Pfeil,
3847 B., Pierrot, D., Poulter, B., Rehder, G., Resplandy, L., Robertson, E., Rocher, M., Rödenbeck, C., Schuster, U.,
3848 Schwinger, J., Séférian, R., Skjelvan, I., Steinhoff, T., Sutton, A., Tans, P. P., Tian, H., Tilbrook, B., Tubiello, F.
3849 N., van der Laan-Luijkx, I. T., van der Werf, G. R., Viovy, N., Walker, A. P., Wiltshire, A. J., Wright, R., Zaehle,
3850 S., and Zheng, B.: Global Carbon Budget 2018, *Earth Syst. Sci. Data*, 10, 2141–2194, <https://doi.org/10.5194/essd-10-2141-2018>, 2018b.

3852 Le Quéré, C., Korsbakken, J. I., Wilson, C., Tosun, J., Andrew, R., Andres, R. J., Canadell, J. G., Jordan, A.,
3853 Peters, G. P., and van Vuuren, D. P.: Drivers of declining CO₂ emissions in 18 developed economies, *Nat. Clim.
3854 Chang.*, 9, 213–217, <https://doi.org/10.1038/s41558-019-0419-7>, 2019.

3855 Le Quéré, C., Peters, G. P., Friedlingstein, P., Andrew, R. M., Canadell, J. G., Davis, S. J., Jackson, R. B., and
3856 Jones, M. W.: Fossil CO₂ emissions in the post-COVID-19 era, *Nat. Clim. Chang.*, 11, 197–199,
3857 <https://doi.org/10.1038/s41558-021-01001-0>, 2021.

3858 Levitus, S., Antonov, J. I., Boyer, T. P., Baranova, O. K., Garcia, H. E., Locarnini, R. A., Mishonov, A. V.,
3859 Reagan, J. R., Seidov, D., Yarosh, E. S., and Zweng, M. M.: World ocean heat content and thermosteric sea level
3860 change (0–2000 m), 1955–2010, *Geophys. Res. Lett.*, 39, <https://doi.org/10.1029/2012GL051106>, 2012.

3861 Li, H., Ilyina, T., Müller, W. A., and Sienz, F.: Decadal predictions of the North Atlantic CO₂ uptake, *Nat.
3862 Commun.*, 7, 11076, <https://doi.org/10.1038/ncomms11076>, 2016.

3863 Li, H., Ilyina, T., Müller, W. A., and Landschützer, P.: Predicting the variable ocean carbon sink, *Sci. Adv.*, 5,
3864 eaav6471, <https://doi.org/10.1126/sciadv.aav6471>, 2019.

3865 Li, H., Ilyina, T., Loughran, T., Spring, A., and Pongratz, J.: Reconstructions and predictions of the global carbon
3866 budget with an emission-driven Earth system model, *Earth Syst. Dyn.*, 14, 101–119, <https://doi.org/10.5194/esd-14-101-2023>, 2023.

3868 Li, W., Ciais, P., Peng, S., Yue, C., Wang, Y., Thurner, M., Saatchi, S. S., Armeth, A., Avitabile, V., Carvalhais, N.,
3869 Harper, A. B., Kato, E., Koven, C., Liu, Y. Y., Nabel, J. E. M. S., Pan, Y., Pongratz, J., Poulter, B., Pugh, T. A. M.,
3870 Santoro, M., Sitch, S., Stocker, B. D., Viovy, N., Wiltshire, A., Yousefpour, R., and Zaehle, S.: Land-use and land-
3871 cover change carbon emissions between 1901 and 2012 constrained by biomass observations, *Biogeosciences*, 14,
3872 5053–5067, <https://doi.org/10.5194/bg-14-5053-2017>, 2017.

3873 Liao, E., Resplandy, L., Liu, J., and Bowman, K. W.: Amplification of the Ocean Carbon Sink During El Niños:
3874 Role of Poleward Ekman Transport and Influence on Atmospheric CO₂, *Global Biogeochem. Cy.*, 34,
3875 e2020GB006574, <https://doi.org/10.1029/2020GB006574>, 2020.

3876 Lienert, S. and Joos, F.: A Bayesian ensemble data assimilation to constrain model parameters and land-use carbon
3877 emissions, *Biogeosciences*, 15, 2909–2930, <https://doi.org/10.5194/bg-15-2909-2018>, 2018.

3878 Liu, J., Baskaran, L., Bowman, K., Schimel, D., Bloom, A. A., Parazoo, N. C., Oda, T., Carroll, D., Menemenlis,
3879 D., Joiner, J., Commancin, R., Daube, B., Gatti, L. V., McKain, K., Miller, J., Stephens, B. B., Sweeney, C., and

3880 Wofsy, S.: Carbon Monitoring System Flux Net Biosphere Exchange 2020 (CMS-Flux NBE 2020), 13, 299–330,
3881 <https://doi.org/10.5194/essd-13-299-2021>, 2021.

3882 Liu, Z., Guan, D., Wei, W., Davis, S. J., Ciais, P., Bai, J., Peng, S., Zhang, Q., Hubacek, K., Marland, G., Andres,
3883 R. J., Crawford-Brown, D., Lin, J., Zhao, H., Hong, C., Boden, T. A., Feng, K., Peters, G. P., Xi, F., Liu, J., Li, Y.,
3884 Zhao, Y., Zeng, N., and He, K.: Reduced carbon emission estimates from fossil fuel combustion and cement
3885 production in China, *Nature*, 524, 335–338, <https://doi.org/10.1038/nature14677>, 2015.

3886 Liu, Z., Zeng, N., Liu, Y., Kalnay, E., Asrar, G., Wu, B., Cai, Q., Liu, D., and Han, P.: Improving the joint
3887 estimation of CO₂ and surface carbon fluxes using a constrained ensemble Kalman filter in COLA (v1.0), *Geosci.
3888 Model Dev.*, 15, 5511–5528, <https://doi.org/10.5194/gmd-15-5511-2022>, 2022.

3889 Liu, Z., Ciais, P., Deng, Z., Lei, R., Davis, S. J., Feng, S., Zheng, B., Cui, D., Dou, X., Zhu, B., Guo, R., Ke, P.,
3890 Sun, T., Lu, C., He, P., Wang, Y., Yue, X., Wang, Y., Lei, Y., Zhou, H., Cai, Z., Wu, Y., Guo, R., Han, T., Xue, J.,
3891 Boucher, O., Boucher, E., Chevallier, F., Tanaka, K., Wei, Y., Zhong, H., Kang, C., Zhang, N., Chen, B., Xi, F.,
3892 Liu, M., Bréon, F.-M., Lu, Y., Zhang, Q., Guan, D., Gong, P., Kammen, D. M., He, K., and Schellnhuber, H. J.:
3893 Near-real-time monitoring of global CO₂ emissions reveals the effects of the COVID-19 pandemic, *Nat Commun*,
3894 11, 5172, <https://doi.org/10.1038/s41467-020-18922-7>, 2020a.

3895 Liu, Z., Ciais, P., Deng, Z., Davis, S. J., Zheng, B., Wang, Y., Cui, D., Zhu, B., Dou, X., Ke, P., Sun, T., Guo, R.,
3896 Zhong, H., Boucher, O., Bréon, F.-M., Lu, C., Guo, R., Xue, J., Boucher, E., Tanaka, K., and Chevallier, F.:
3897 Carbon Monitor, a near-real-time daily dataset of global CO₂ emission from fossil fuel and cement production, *Sci
3898 Data*, 7, 392, <https://doi.org/10.1038/s41597-020-00708-7>, 2020b.

3899 Long, M. C., Stephens, B. B., McKain, K., Sweeney, C., Keeling, R. F., Kort, E. A., Morgan, E. J., Bent, J. D.,
3900 Chandra, N., Chevallier, F., Commane, R., Daube, B. C., Krummel, P. B., Loh, Z., Luijkx, I. T., Munro, D., Patra,
3901 P., Peters, W., Ramonet, M., Rödenbeck, C., Stavert, A., Tans, P., Wofsy, S. C.: Strong Southern Ocean carbon
3902 uptake evident in airborne observations. *Science*, 374(6572), 1275–1280, <https://doi.org/10.1126/science.abi4355>,
3903 2021.

3904 Lovenduski, N. S., Bonan, G. B., Yeager, S. G., Lindsay, K., and Lombardozzi, D. L.: High predictability of
3905 terrestrial carbon fluxes from an initialized decadal prediction system, *Environ. Res. Lett.*, 14, 124074,
3906 <https://doi.org/10.1088/1748-9326/ab5c55>, 2019a.

3907 Lovenduski, N. S., Yeager, S. G., Lindsay, K., and Long, M. C.: Predicting near-term variability in ocean carbon
3908 uptake, *Earth Syst. Dyn.*, 10, 45–57, <https://doi.org/10.5194/esd-10-45-2019>, 2019b.

3909 Lutz, F., Herzfeld, T., Heinke, J., Rolinski, S., Schaphoff, S., von Bloh, W., Stoorvogel, J. J., and Müller, C.:
3910 Simulating the effect of tillage practices with the global ecosystem model LPJmL (version 5.0-tillage), *Geosci.
3911 Model Dev.*, 12, 2419–2440, <https://doi.org/10.5194/gmd-12-2419-2019>, 2019.

3912 Ma, L., Hurtt, G., Ott, L., Sahajpal, R., Fisk, J., Lamb, R., Tang, H., Flanagan, S., Chini, L., Chatterjee, A., and
3913 Sullivan, J.: Global evaluation of the Ecosystem Demography model (ED v3.0), *Geosci. Model Dev.*, 15, 1971–
3914 1994, <https://doi.org/10.5194/gmd-15-1971-2022>, 2022.

3915 Magi, B. I., Rabin, S., Shevliakova, E., and Pacala, S.: Separating agricultural and non-agricultural fire seasonality
3916 at regional scales, *Biogeosciences*, 9, 3003–3012, <https://doi.org/10.5194/bg-9-3003-2012>, 2012.

3917 Maksyutov, S., Oda, T., Saito, M., Janardanan, R., Belikov, D., Kaiser, J. W., Zhuravlev, R., Ganshin, A., Valsala,
3918 V. K., Andrews, A., Chmura, L., Dlugokencky, E., Haszpra, L., Langenfelds, R. L., Machida, T., Nakazawa, T.,
3919 Ramonet, M., Sweeney, C., and Worthy, D.: Technical note: A high-resolution inverse modelling technique for
3920 estimating surface CO₂ fluxes based on the NIES-TM-FLEXPART coupled transport model and its adjoint,
3921 *Atmos. Chem. Phys.*, 21, 1245–1266, <https://doi.org/10.5194/acp-21-1245-2021>, 2021.

3922 Masarie, K. A. and Tans, P. P.: Extension and integration of atmospheric carbon dioxide data into a globally
3923 consistent measurement record, *J. Geophys. Res.*, 100, 11593, <https://doi.org/10.1029/95JD00859>, 1995.

3924 Mataveli, G., Jones, M.W., Carmenta, R., Sanchez, A., Dutra, D.J., Chaves, M., de Oliveira, G., Anderson, L.O.
3925 and Aragão, L.E.: Deforestation falls but rise of wildfires continues degrading Brazilian Amazon forests. *Global
3926 Change Biology*, 30(2), p.e17202, <https://doi.org/10.1111/gcb.17202>, 2024.

Deleted: <https://doi.org/10.1038/s41467-020-18922-7>

Deleted:

Deleted: <https://doi.org/10.1038/s41597-020-00708-7>

- 3930 Mather, A. S.: The transition from deforestation to reforestation in Europe, in: *Agricultural technologies and*
3931 *tropical deforestation* (eds. Angelsen, A.; Kaimowitz, D.), CABI in association with centre for international
3932 *Forestry Research*, 35–52, 2001.
- 3933 Mauritsen, T., Bader, J., Becker, T., Behrens, J., Bittner, M., Brokopf, R., Brovkin, V., Claussen, M., Crueger, T.,
3934 Esch, M., Fast, I., Fiedler, S., Fläschner, D., Gayler, V., Giorgetta, M., Goll, D. S., Haak, H., Hagemann, S.,
3935 Hedemann, C., Hohenegger, C., Ilyina, T., Jahns, T., Jimenez-de-la-Cuesta, D., Jungclaus, J., Kleinen, T., Kloster,
3936 S., Kracher, D., Kinne, S., Kleberg, D., Lasslop, G., Kornbluh, L., Marotzke, J., Matei, D., Meraner, K.,
3937 Mikolajewicz, U., Modali, K., Möbis, B., Müller, W. A., Nabel, J. E. M. S., Nam, C. C. W., Notz, D., Nyawira, S.-
3938 S., Paulsen, H., Peters, K., Pincus, R., Pohlmann, H., Pongratz, J., Popp, M., Raddatz, T. J., Rast, S., Redler, R.,
3939 Reick, C. H., Rohrschneider, T., Schemann, V., Schmidt, H., Schnur, R., Schulzweida, U., Six, K. D., Stein, L.,
3940 Stemmler, I., Stevens, B., von Storch, J.-S., Tian, F., Voigt, A., Vrese, P., Wieners, K.-H., Wilkenskjaeld, S.,
3941 Winkler, A., and Roeckner, E.: Developments in the MPI-M Earth System Model version 1.2 (MPI-ESM1.2) and
3942 Its Response to Increasing CO₂, *J. Adv. Model Earth Sy.*, 11, 998–1038, <https://doi.org/10.1029/2018MS001400>,
3943 2019.
- 3944 Mayot, N., Buitenhuis, E. T., Wright, R. M., Hauck, J., Bakker, D. C. E., and Le Quéré, C.: Constraining the trend
3945 in the ocean CO₂ sink during 2000–2022. *Nat Commun* 15, 8429, <https://doi.org/10.1038/s41467-024-52641-7>,
3946 2024.
- 3947 McGrath, M. J., Luyssaert, S., Meyfroidt, P., Kaplan, J. O., Bürgi, M., Chen, Y., Erb, K., Gimmi, U., McInerney,
3948 D., Naudts, K., Otto, J., Pasztor, F., Ryder, J., Schelhaas, M.-J., and Valade, A.: Reconstructing European forest
3949 management from 1600 to 2010, *12*, 4291–4316, <https://doi.org/10.5194/bg-12-4291-2015>, 2015.
- 3950 McKinley, G. A., Fay, A. R., Eddebbar, Y. A., Gloege, L., and Lovenduski, N. S.: External Forcing Explains
3951 Recent Decadal Variability of the Ocean Carbon Sink, *AGU Advances*, 1, e2019AV000149,
3952 <https://doi.org/10.1029/2019AV000149>, 2020.
- 3953 McKinley, G. A., Fay, A. R., Lovenduski, N. S., and Pilcher, D. J.: Natural Variability and Anthropogenic Trends
3954 in the Ocean Carbon Sink, *Annu. Rev. Mar. Sci.*, 9, 125–150, <https://doi.org/10.1146/annurev-marine-010816-060529>, 2017.
- 3956 Meiyappan, P., Jain, A. K., and House, J. I.: Increased influence of nitrogen limitation on CO₂ emissions from
3957 future land use and land use change, *Global Biogeochem. Cycles*, 29, 1524–1548,
3958 <https://doi.org/10.1002/2015GB005086>, 2015.
- 3959 Melo, J., Rossi, S., Achard, F., Alkama, R., Canadell, J. G., Federici, S., Friedlingstein, P., Gibbs, D., Harris, N.,
3960 Heinrich, V., O’Sullivan, M., Peters, G., Pongratz, J., Rose, M., Roman-Cuesta, R., Sanz Sanchez, M. J.,
3961 Schwingshackl, C., Sitch, S., and Grassi, G.: The LULUCF Data Hub: translating global land use emissions
3962 estimates into the national GHG inventory framework (Version 3.0, 2025 NGHGI release) (3.0)★,
3963 <https://doi.org/10.5281/ZENODO.17140775>, 2025.
- 3964 Melton, J. R., Arora, V. K., Wisemig-Cojoc, E., Seiler, C., Fortier, M., Chan, E., and Teckentrup, L.: CLASSIC
3965 v1.0: the open-source community successor to the Canadian Land Surface Scheme (CLASS) and the Canadian
3966 Terrestrial Ecosystem Model (CTEM) – Part 1: Model framework and site-level performance, *Geosci. Model Dev.*,
3967 13, 2825–2850, <https://doi.org/10.5194/gmd-13-2825-2020>, 2020.
- 3968 Mercado, L. M., Bellouin, N., Sitch, S., Boucher, O., Huntingford, C., Wild, M., and Cox, P. M.: Impact of
3969 changes in diffuse radiation on the global land carbon sink, *Nature*, 458, 1014–1017,
3970 <https://doi.org/10.1038/nature07949>, 2009.
- 3971 Merchant, C. J., Embury, O., Bulgin, C. E., Block, T., Corlett, G. K., Fiedler, E., Good, S. A., Mittaz, J., Rayner,
3972 N. A., Berry, D., Eastwood, S., Taylor, M., Tsushima, Y., Waterfall, A., Wilson, R., and Donlon, C.: Satellite-
3973 based time-series of sea-surface temperature since 1981 for climate applications, *Sci. Data*, 6, 223,
3974 <https://doi.org/10.1038/s41597-019-0236-x>, 2019.
- 3975 Moorcroft, P. R., Hurtt, G. C., and Pacala, S. W.: A Method for Scaling Vegetation Dynamics: The Ecosystem
3976 Demography Model (ed), *Ecol. Monogr.*, 71, 557–586, [https://doi.org/10.1890/0012-9615\(2001\)071\[0557:AMFSVD\]2.0.CO;2](https://doi.org/10.1890/0012-9615(2001)071[0557:AMFSVD]2.0.CO;2), 2001.

Deleted: <https://doi.org/10.5281/ZENODO.17140775>

3979 Müller, J. D., Gruber, N., Carter, B., Feely, R., Ishii, M., Lange, N., Lauvset, S. K., Murata, A., Olsen, A., Pérez, F.
3980 F., Sabine, C., Tanhua, T., Wanninkhof, R., and Zhu, D.: Decadal Trends in the Oceanic Storage of Anthropogenic
3981 Carbon From 1994 to 2014, *AGU Adv.*, 4, e2023AV000875, <https://doi.org/10.1029/2023AV000875>, 2023.

3982 Müller, J. D., Gruber, N., Schneuwly, A., Bakker, D. C. E., Gehlen, M., Gregor, L., Hauck, J., Landschützer, P.,
3983 and McKinley, G. A.: Unexpected decline in the ocean carbon sink under record-high sea surface temperatures in
3984 2023, *Nat. Clim. Chang.*, 15, 978–985, <https://doi.org/10.1038/s41558-025-02380-4>, 2025.

3985 Müller, J. and Joos, F.: Committed and projected future changes in global peatlands – continued transient model
3986 simulations since the Last Glacial Maximum, *Biogeosciences*, 18, 3657–3687, [https://doi.org/10.5194/bg-18-3657-](https://doi.org/10.5194/bg-18-3657-2021)
3987 2021, 2021.

3988 Nayagam, L., Maksyutov, S., Oda, T., Janardanan, R., Trisolino, P., Zeng J., Kaiser, J.W. and Matsunaga, T.: A
3989 top-down estimation of subnational CO2 budget using a global high-resolution inverse model with data from
3990 regional surface networks, *Environ. Res. Lett.*, 19, 0140312024, <https://doi.org/10.1088/1748-9326/ad0f74>, 2024.

3991 NCEP: National Centers for Environmental Prediction. ONI Index. Cold & Warm Episodes by Season [Data set],
3992 available at: https://www.cpc.ncep.noaa.gov/products/analysis_monitoring/ensostuff/ONI_v5.php, last access: 23
3993 October 2025, 2025.

3994 Nayagam, L., Maksyutov, S., Janardanan, R., Oda, T., Tiwari, Y. K., Sreenivas, G., Datye, A., Jain, C. D., Ratnam,
3995 M. V., Sinha, V., Hakkim, H., Terao, Y., Naja, M., Ahmed, Md. K., Mukai, H., Zeng, J., Kaiser, J. W., Someya,
3996 Y., Yoshida, Y., and Matsunaga, T.: Indian Land Carbon Sink Estimated from Surface and GOSAT Observations,
3997 *Remote Sensing*, 17, 450, <https://doi.org/10.3390/rs17030450>, 2025.

3998 Nevison, C.D., Mahowald, N.M., Doney, S.C., Lima, I.D. and Cassar, N.: Impact of variable air-sea O₂ and CO₂
3999 fluxes on atmospheric potential oxygen (APO) and land-ocean carbon sink partitioning, *Biogeosciences*, 5(3),
4000 pp.875-889, <https://doi.org/10.5194/bg-5-875-2008>, 2008.

4001 Niu, G.-Y., Yang, Z.-L., Mitchell, K. E., Chen, F., Ek, M. B., Barlage, M., Kumar, A., Manning, K., Niyogi, D.,
4002 Rosero, E., Tewari, M., and Xia, Y.: The community Noah land surface model with multiparameterization options
4003 (Noah-MP): 1. Model description and evaluation with local-scale measurements, *J. Geophys. Res. Atmospheres*,
4004 116, <https://doi.org/10.1029/2010JD015139>, 2011.

4005 Niwa, Y., Ishijima, K., Ito, A., and Iida, Y.: Toward a long-term atmospheric CO₂ inversion for elucidating natural
4006 carbon fluxes: technical notes of NISMON-CO₂ v2021.1, *Prog. Earth Planet Sci.*, 9, 42,
4007 <https://doi.org/10.1186/s40645-022-00502-6>, 2022.

4008 Niwa, Y., Fujii, Y., Sawa, Y., Iida, Y., Ito, A., Satoh, M., Imasu, R., Tsuboi, K., Matsueda, H., and Saigusa, N.: A
4009 4D-Var inversion system based on the icosahedral grid model (NICAM-TM 4D-Var v1.0) – Part 2: Optimization
4010 scheme and identical twin experiment of atmospheric CO₂ inversion, *Geosci. Model Dev.*,
4011 10, 2201–2219, <https://doi.org/10.5194/gmd-10-2201-2017>, 2017.

4012 Niwa, Y., Langenfelds, R., Krummel, P., Loh, Z., Worthy, Doug, Hatakka, Juha, Aalto, Tuula, Ramonet, Michel,
4013 Delmotte, Marc, Schmidt, Martina, Gheusi, Francois, Mihalopoulos, N., Morgui, J.A., Andrews, Arlyn,
4014 Dlugokencky, Ed, Lee, John, Sweeney, Colm, Thoning, Kirk, Tans, Pieter, De Wekker, Stephan, Fischer, Marc L.,
4015 Jaffe, Dan, McKain, Kathryn, Viner, Brian, Miller, John B., Karion, Anna, Miller, Charles, Sloop, Christopher D.,
4016 Saito, Kazuyuki, Aoki, Shuji, Morimoto, Shinji, Goto, Daisuke, Steinbacher, Martin, Myhre, Cathrine Lund,
4017 Hermanssen, Ove, Stephens, Britton, Keeling, Ralph, Afshar, Sara, Paplawsky, Bill, Cox, Adam, Walker, Stephen,
4018 Schuldt, Kenneth, Mukai, Hitoshi, Machida, Toshinobu, Sasakawa, Motoki, Nomura, Shohei, Ito, Akihiko, Iida,
4019 Yosuke, and Jones, Matthew W.: Long-term global CO₂ fluxes estimated by NICAM-based Inverse Simulation for
4020 Monitoring CO₂ (NISMON-CO₂) (ver.2022.1), National Institute for Environmental Studies Japan [Data set],
4021 <https://doi.org/10.17595/20201127.001>, 2020.

4022 Norby, R.J.: Forest productivity response to elevated CO₂ in free-air CO₂ enrichment experiments: the 23 percent
4023 solution, revisited, *New Phytologist*, <https://doi.org/10.1111/nph.70162>, 2025.

4024 Obermeier, W. A., Nabel, J. E. M. S., Loughran, T., Hartung, K., Bastos, A., Havermann, F., Anthoni, P., Arneth,
4025 A., Goll, D. S., Lienert, S., Lombardozzi, D., Luyssaert, S., McGuire, P. C., Melton, J. R., Poulter, B., Sitch, S.,
4026 Sullivan, M. O., Tian, H., Walker, A. P., Wiltshire, A. J., Zaehle, S., and Pongratz, J.: Modelled land use and land
4027 cover change emissions – a spatio-temporal comparison of different approaches, *ESD*, 12, 635–670,
4028 <https://doi.org/10.5194/esd-12-635-2021>, 2021.

Deleted: <https://doi.org/10.3390/rs17030450>

Deleted: <https://doi.org/10.5194/gmd-10-2201-2017>

4031 Obermeier, W. A., Schwingshackl, C., Ganzenmüller, R., Grassi, G., Heinrich, V., Luijkx, I. T., Bastos, A., Ciais, P., Sitch, S., and Pongratz, J.: Differences and uncertainties in land-use CO₂ flux estimates, *Nat Rev Earth Environ*, <https://doi.org/10.1038/s43017-025-00730-6>, 2025.

4034 O'Dell, C. W., Eldering, A., Wennberg, P. O., Crisp, D., Gunson, M. R., Fisher, B., Frankenberg, C., Kiel, M., Lindqvist, H., Mandrake, L., Merrelli, A., Natraj, V., Nelson, R. R., Osterman, G. B., Payne, V. H., Taylor, T. E., Wunch, D., Drouin, B. J., Oyafuso, F., Chang, A., McDuffie, J., Smyth, M., Baker, D. F., Basu, S., Chevallier, F., Crowell, S. M. R., Feng, L., Palmer, P. I., Dubey, M., Garcia, O. E., Griffith, D. W. T., Hase, F., Iraci, L. T., Kivi, R., Morino, I., Notholt, J., Ohyama, H., Petri, C., Roehl, C. M., Sha, M. K., Strong, K., Sussmann, R., Te, Y., Uchino, O., and Velasco, V. A.: Improved retrievals of carbon dioxide from Orbiting Carbon Observatory-2 with the version 8 ACOS algorithm, *Atmos. Meas. Tech.*, 11, 6539–6576, <https://doi.org/10.5194/amt-11-6539-2018>, 2018.

4042 O'Rourke, P. R., Smith, S. J., Mott, A., Ahsan, H., McDuffie, E. E., Crippa, M., Klimont, Z., McDonald, B., Wang, S., Nicholson, M. B., Feng, L., and Hoesly, R. M.: CEDS v_2021_04_21 Release Emission Data, Zenodo [Data set], <https://doi.org/10.5281/zenodo.4741285>, 2021.

4045 O'Sullivan, M., Zhang, Y., Bellouin, N., Harris, I., Mercado, L. M., Sitch, S., Ciais, P., and Friedlingstein, P.: Aerosol–light interactions reduce the carbon budget imbalance, *Environ. Res. Lett.*, 16, 124072, <https://doi.org/10.1088/1748-9326/ac3b77>, 2021.

4048 O'Sullivan, M., Friedlingstein, P., Sitch, S., Anthoni, P., Armeth, A., Arora, V. K., Bastrikov, V., Delire, C., Goll, D. S., Jain, A., Kato, E., Kennedy, D., Knauer, J., Lienert, S., Lombardozzi, D., McGuire, P. C., Melton, J. R., Nabel, J. E. M. S., Pongratz, J., Poulter, B., Séférian, R., Tian, H., Vuichard, N., Walker, A. P., Yuan, W., Yue, X., and Zaehle, S.: Process-oriented analysis of dominant sources of uncertainty in the land carbon sink, *Nat. Commun.*, 13, 4781, <https://doi.org/10.1038/s41467-022-32416-8>, 2022.

4053 O'Sullivan, M., Spracklen, D. V., Batterman, S. A., Arnold, S. R., Gloor, M., and Buermann, W.: Have Synergies Between Nitrogen Deposition and Atmospheric CO₂ Driven the Recent Enhancement of the Terrestrial Carbon Sink?, *Glob. Biogeochem. Cycles*, 33, 163–180, <https://doi.org/10.1029/2018GB005922>, 2019.

4056 O'Sullivan, M., Sitch, S., Friedlingstein, P., Luijkx, I. T., Peters, W., Rosan, T. M., Armeth, A., Arora, V. K., Chandra, N., Chevallier, F., Ciais, P., Falk, S., Feng, L., Gasser, T., Houghton, R. A., Jain, A. K., Kato, E., Kennedy, D., Knauer, J., McGrath, M. J., Niwa, Y., Palmer, P. I., Patra, P. K., Pongratz, J., Poulter, B., Rödenbeck, C., Schwingshackl, C., Sun, Q., Tian, H., Walker, A. P., Yang, D., Yuan, W., Yue, X., and Zaehle, S.: The key role of forest disturbance in reconciling estimates of the northern carbon sink. *Commun Earth Environ* 5, 705, <https://doi.org/10.1038/s43247-024-01827-4>, 2024.

4062 O'Sullivan, M., Friedlingstein, P., Sitch, S., Pongratz, J., Schwingshackl, C., Gasser, T., Ciais, P., Arora, V., Kato, E., Knauer, J., Nützel, T., Sun, Q., Yuan, W., and Zaehle, S.: An improved approach to estimate the natural land carbon sink, 27 July 2025, PREPRINT (Version 1) available at Research Square [<https://doi.org/10.21203/rs.3.rs-7207206/v1>], 2025.

4066 Palmer, P. I., Feng, L., Baker, D., Chevallier, F., Bösch, H., and Somkuti, P.: Net carbon emissions from African biosphere dominate pan-tropical atmospheric CO₂ signal, *Nat Commun*, 10, 3344, <https://doi.org/10.1038/s41467-019-11097-w>, 2019.

4069 Pan, Y., Birdsey, R. A., Fang, J., Houghton, R., Kauppi, P. E., Kurz, W. A., Phillips, O. L., Shvidenko, A., Lewis, S. L., Canadell, J. G., Ciais, P., Jackson, R. B., Pacala, S. W., McGuire, A. D., Piao, S., Rautiainen, A., Sitch, S., and Hayes, D.: A Large and Persistent Carbon Sink in the World's Forests, *Science*, 333, 988–993, <https://doi.org/10.1126/science.1201609>, 2011.

4073 Pandey, S., Miller, J. B., Basu, S., Liu, J., Weir, B., Byrne, B., Chevallier, F., Bowman, K. W., Liu, Z., Deng, F., O'Dell, C. W., and Chatterjee, A.: Toward Low-Latency Estimation of Atmospheric CO₂ Growth Rates Using Satellite Observations: Evaluating Sampling Errors of Satellite and In Situ Observing Approaches, *AGU Advances*, 5, e2023AV001145, <https://doi.org/10.1029/2023AV001145>, 2024.

4077 Pandey, S., Chevallier, F., Rödenbeck, C., Byrne, B., Chatterjee, A., Liu, J., and Frankenberg, C.: Reduction in Earth's carbon budget imbalance, *Nat Commun*, 16, 6818, <https://doi.org/10.1038/s41467-025-61588-2>, 2025.

Deleted: <https://doi.org/10.5194/amt-11-6539-2018>

Deleted: <https://doi.org/10.1029/2023AV001145>

Deleted: <https://doi.org/10.1038/s41467-025-61588-2>

4082 Patra, P. K., Takigawa, M., Watanabe, S., Chandra, N., Ishijima, K., and Yamashita, Y.: Improved Chemical
4083 Tracer Simulation by MIROC4.0-based Atmospheric Chemistry-Transport Model (MIROC4-ACTM), SOLA, 14,
4084 91–96, <https://doi.org/10.2151/sola.2018-016>, 2018.

4085 Pendrill, F., Persson, U. M., Godar, J., Kastner, T., Moran, D., Schmidt, S., and Wood, R.: Agricultural and
4086 forestry trade drives large share of tropical deforestation emissions, *Global Environmental Change*, 56, 1–10,
4087 <https://doi.org/10.1016/j.gloenvcha.2019.03.002>, 2019.

4088 Pérez, F. F., Becker, M., Goris, N., Gehlen, M., López-Mozos, M., Tjiputra, J., Olsen, A., Müller, J. D., Huertas, I.
4089 E., Chau, T. T. T., Cainzos, V., Velo, A., Benard, G., Hauck, J., Gruber, N., and Wanninkhof, R.: An Assessment
4090 of CO₂ Storage and Sea-Air Fluxes for the Atlantic Ocean and Mediterranean Sea Between 1985 and 2018. *Global
4091 Biogeochemical Cycles*, 38(4), e2023GB007862, <https://doi.org/10.1029/2023GB007862>, 2024.

4092 Peters, G. P., Minx, J. C., Weber, C. L., and Edenhofer, O.: Growth in emission transfers via international trade
4093 from 1990 to 2008, *Proceedings of the National Academy of Sciences*, 108, 8903–8908,
4094 <https://doi.org/10.1073/pnas.1006388108>, 2011a.

4095 Peters, G. P., Marland, G., Le Quéré, C., Boden, T., Canadell, J. G., and Raupach, M. R.: Rapid growth in CO₂
4096 emissions after the 2008–2009 global financial crisis, *Nature Clim Change*, 2, 2–4,
4097 <https://doi.org/10.1038/nclimate1332>, 2012a.

4098 Peters, G. P., Andrew, R. M., Boden, T., Canadell, J. G., Ciais, P., Le Quéré, C., Marland, G., Raupach, M. R., and
4099 Wilson, C.: The challenge to keep global warming below 2 °C, *Nature Clim Change*, 3, 4–6,
4100 <https://doi.org/10.1038/nclimate1783>, 2013.

4101 Peters, G. P., Le Quéré, C., Andrew, R. M., Canadell, J. G., Friedlingstein, P., Ilyina, T., Jackson, R. B., Joos, F.,
4102 Korsbakken, J. I., McKinley, G. A., Sitch, S., and Tans, P.: Towards real-time verification of CO₂ emissions,
4103 *Nature Clim Change*, 7, 848–850, <https://doi.org/10.1038/s41558-017-0013-9>, 2017a.

4104 Peters, G. P., Andrew, R. M., Canadell, J. G., Fuss, S., Jackson, R. B., Korsbakken, J. I., Le Quéré, C. and
4105 Nakicenovic, N.: Key indicators to track current progress and future ambition of the Paris Agreement, 7, 118–122,
4106 <https://doi.org/10.1038/nclimate3202>, 2017b.

4107 Peters, G. P., Andrew, R. M., Canadell, J. G., Friedlingstein, P., Jackson, R. B., Korsbakken, J. I., Le Quéré, C.,
4108 and Peregon, A.: Carbon dioxide emissions continue to grow amidst slowly emerging climate policies, *Nat. Clim.
4109 Chang.*, 10, 3–6, <https://doi.org/10.1038/s41558-019-0659-6>, 2020.

4110 Peters, W., Miller, J. B., Whitaker, J., Denning, A. S., Hirsch, A., Krol, M. C., Zupanski, D., Bruhwiler, L., and
4111 Tans, P. P.: An ensemble data assimilation system to estimate CO₂ surface fluxes from atmospheric trace gas
4112 observations, *J. Geophys. Res. Atmospheres*, 110, <https://doi.org/10.1029/2005JD006157>, 2005.

4113 Petrescu, A. M. R., Peters, G. P., Janssens-Maenhout, G., Ciais, P., Tubiello, F. N., Grassi, G., Nabuurs, G.-J.,
4114 Leip, A., Carmona-García, G., Winiwarter, W., Höglund-Isaksson, L., Günther, D., Solazzo, E., Kiesow, A.,
4115 Bastos, A., Pongratz, J., Nabel, J. E. M. S., Conchedda, G., Pilli, R., Andrew, R. M., Schelhaas, M.-J., and Dolman,
4116 A. J.: European anthropogenic AFOLU greenhouse gas emissions: a review and benchmark data, *Earth Syst. Sci.
4117 Data*, 12, 961–1001, <https://doi.org/10.5194/essd-12-961-2020>, 2020.

4118 Pfeil, B., Olsen, A., Bakker, D. C. E., Hankin, S., Koyuk, H., Kozyr, A., Malczyk, J., Manke, A., Metzl, N., Sabine,
4119 C. L., Akl, J., Alin, S. R., Bates, N., Bellerby, R. G. J., Borges, A., Boutin, J., Brown, P. J., Cai, W.-J., Chavez, F.
4120 P., Chen, A., Cosca, C., Fassbender, A. J., Feely, R. A., González-Dávila, M., Goyet, C., Hales, B., Hardman-
4121 Mountford, N., Heinze, C., Hood, M., Hoppema, M., Hunt, C. W., Hydes, D., Ishii, M., Johannessen, T., Jones, S.
4122 D., Key, R. M., Körtzinger, A., Landschützer, P., Lauvset, S. K., Lefèvre, N., Lenton, A., Lourdantou, A., Merlivat,
4123 L., Midorikawa, T., Mintrop, L., Miyazaki, C., Murata, A., Nakadate, A., Nakano, Y., Nakaoka, S., Nojiri, Y.,
4124 Omar, A. M., Padin, X. A., Park, G.-H., Paterson, K., Perez, F. F., Pierrot, D., Poisson, A., Ríos, A. F., Santana-
4125 Casiano, J. M., Salisbury, J., Sarma, V. V. S. S., Schlitzer, R., Schneider, B., Schuster, U., Sieger, R., Skjelvan, I.,
4126 Steinhoff, T., Suzuki, T., Takahashi, T., Tedesco, K., Telszewski, M., Thomas, H., Tilbrook, B., Tjiputra, J.,
4127 Vandemark, D., Veness, T., Wanninkhof, R., Watson, A. J., Weiss, R., Wong, C. S., and Yoshikawa-Inoue, H.: A
4128 uniform, quality controlled Surface Ocean CO₂ Atlas (SOCAT), *Earth Syst. Sci. Data*, 5, 125–143,
4129 <https://doi.org/10.5194/essd-5-125-2013>, 2013.

Deleted: <https://doi.org/10.2151/sola.2018-016>

- 4131 Piao, S., Ciais, P., Friedlingstein, P., de Noblet-Ducoudré, N., Cadule, P., Viovy, N., and Wang, T.: Spatiotemporal
4132 patterns of terrestrial carbon cycle during the 20th century, *Global Biogeochem. Cy.*, 23, GB4026,
4133 <https://doi.org/10.1029/2008GB003339>, 2009.
- 4134 Piao, S., Huang, M., Liu, Z., Wang, X., Ciais, P., Canadell, J. G., Wang, K., Bastos, A., Friedlingstein, P.,
4135 Houghton, R. A., Le Quééré, C., Liu, Y., Myneni, R. B., Peng, S., Pongratz, J., Sitch, S., Yan, T., Wang, Y., Zhu, Z.,
4136 Wu, D., and Wang, T.: Lower land-use emissions responsible for increased net land carbon sink during the slow
4137 warming period, *Nature Geosci.*, 11, 739–743, <https://doi.org/10.1038/s41561-018-0204-7>, 2018.
- 4138 Pongratz, J., Reick, C.H., Raddatz, T. and Claussen, M.: Effects of anthropogenic land cover change on the carbon
4139 cycle of the last millennium. *Global Biogeochemical Cycles*, 23(4), doi:10.1029/2009GB003488, 2009.
- 4140 Pongratz, J., Reick, C. H., Houghton, R. A., and House, J. I.: Terminology as a key uncertainty in net land use and
4141 land cover change carbon flux estimates, *Earth Syst. Dynam.*, 5, 177–195, <https://doi.org/10.5194/esd-5-177-2014>,
4142 2014.
- 4143 Pongratz, J., Smith, S. M., Schwingshackl, C., Dayathilake, L., Gasser, T., Grassi, G. and Pilli, R.: Chapter 7:
4144 Current levels of CDR. in *The State of Carbon Dioxide Removal 2024 – 2nd Edition*,
4145 <https://doi.org/10.17605/OSF.IOZXSKB>, 2024.
- 4146 Poulter, B., Bastos, A., Canadell, J., Ciais, P., Gruber, N., Hauck, J., Jackson, R., Ishii, M., Müller, J., Patra, P., and
4147 Tian, H.: Inventorying Earth's Land and Ocean Greenhouse Gases, *Eos*, 103,
4148 <https://doi.org/10.1029/2022EO179084>, 2022.
- 4149 Poulter, B., Frank, D. C., Hodson, E. L., and Zimmermann, N. E.: Impacts of land cover and climate data selection
4150 on understanding terrestrial carbon dynamics and the CO2 airborne fraction, *Biogeosciences*, 8, 2027–2036,
4151 <https://doi.org/10.5194/bg-8-2027-2011>, 2011.
- 4152 Poulter, B., Freeborn, P. H., Jolly, W. M., and Varner, J. M.: COVID-19 lockdowns drive decline in active fires in
4153 southeastern United States, *PNAS*, 118, e2105666118, <https://doi.org/10.1073/pnas.2105666118>, 2021.
- 4154 Powis, C. M., Smith, S. M., Minx, J. C., and Gasser, T.: Quantifying global carbon dioxide removal deployment,
4155 *Environ. Res. Lett.*, 18, 024022, <https://doi.org/10.1088/1748-9326/acb450>, 2023.
- 4156 Prentice, I. C., Farquhar, G. D., Fasham, M. J. R., Goulden, M. L., Heimann, M., Jaramillo, V. J., Khashgi, H. S.,
4157 Le Quééré, C., Scholes, R. J., and Wallace, D. W. R.: The Carbon Cycle and Atmospheric Carbon Dioxide, in
4158 *Climate Change 2001: The Scientific Basis. Contribution of Working Group I to the Third Assessment Report of*
4159 *the Intergovernmental Panel on Climate Change*, edited by: Houghton, J. T., Ding, Y., Griggs, D. J., Noguer, M.,
4160 van der Linden, P. J., Dai, X., Maskell, K., and Johnson, C. A., Cambridge University Press, Cambridge, United
4161 Kingdom and New York, NY, USA, 183–237, ISBN: 978-0521014953, 2001.
- 4162 Price, J. T. and Warren, R.: Literature Review of the Potential of “Blue Carbon” Activities to Reduce Emissions,
4163 available at: <https://avoid-net-uk.cc.ic.ac.uk/wp-content/uploads/delightful-downloads/2016/03/Literature-review-of-the-potential-of-blue-carbon-activities-to-reduce-emissions-AVOID2-WPE2.pdf>, last access: 23 October 2025,
4164 2016.
4165
- 4166 Qin, Y., Xiao, X., Wigneron, J.-P., Ciais, P., Brandt, M., Fan, L., Li, X., Crowell, S., Wu, X., Doughty, R., Zhang,
4167 Y., Liu, F., Sitch, S., and Moore, B.: Carbon loss from forest degradation exceeds that from deforestation in the
4168 Brazilian Amazon, *Nat. Clim. Chang.*, 11, 442–448, <https://doi.org/10.1038/s41558-021-01026-5>, 2021.
- 4169 Qin, Z., Zhu, Y., Canadell, J.G., Chen, M., Li, T., Mishra, U. and Yuan, W.: Global spatially explicit carbon
4170 emissions from land-use change over the past six decades (1961–2020). *One Earth*, 7(5), pp.835-847,
4171 <https://doi.org/10.1016/j.oneear.2024.04.002>, 2024.
- 4172 Qiu, C., Ciais, P., Zhu, D., Guenet, B., Peng, S., Petrescu, A. M. R., Lauerwald, R., Makowski, D., Gallego-Sala,
4173 A. V., Charman, D. J., and Brewer, S. C.: Large historical carbon emissions from cultivated northern peatlands,
4174 *Sci. Adv.*, 7, eabf1332, <https://doi.org/10.1126/sciadv.abf1332>, 2021.
- 4175 Randerson, J. T., Chen, Y., van der Werf, G. R., Rogers, B. M., and Morton, D. C.: Global burned area and
4176 biomass burning emissions from small fires: BURNED AREA FROM SMALL FIRES, *J. Geophys. Res.*
4177 *Biogeosciences*, 117, n/a-n/a, <https://doi.org/10.1029/2012JG002128>, 2012.

- 4178 Randerson, J. T., Li, Y., Fu, W., Primeau, F., Kim, J. E., Mu, M., Hoffman, F. M., Trugman, A. T., Yang, L., Wu,
4179 C., Wang, J. A., Anderegg, W. R. L., Baccini, A., Friedl, M. A., Saatchi, S. S., Denning, A. S., and Goulden, M. L.:
4180 The weak land carbon sink hypothesis, *Sci. Adv.*, 11, eadr5489, <https://doi.org/10.1126/sciadv.adr5489>, 2025.
- 4181 Raupach, M. R., Marland, G., Ciais, P., Le Quere, C., Canadell, J. G., Klepper, G., and Field, C. B.: Global and
4182 regional drivers of accelerating CO₂ emissions, *Proceedings of the National Academy of Sciences*, 104, 10288–
4183 10293, <https://doi.org/10.1073/pnas.0700609104>, 2007.
- 4184 Regnier, P., Resplandy, L., Najjar, R. G., and Ciais, P.: The land-to-ocean loops of the global carbon cycle, *Nature*,
4185 603, 401–410, <https://doi.org/10.1038/s41586-021-04339-9>, 2022.
- 4186 Reick, C. H., Gayler, V., Goll, D., Hagemann, S., Heidkamp, M., Nabel, J. E. M. S., Raddatz, T., Roeckner, E.,
4187 Schnur, R., 110 and Wilkenskjaeld, S.: JSBACH 3 – The land component of the MPI Earth System Model:
4188 documentation of version 3.2, available at: <https://doi.org/10.17617/2.3279802>, 2021.
- 4189 Remaud, M., Chevallier, F., Cozic, A., Lin, X., and Bousquet, P.: On the impact of recent developments of the
4190 LMDz atmospheric general circulation model on the simulation of CO₂ transport, 11, 4489,
4191 <https://doi.org/10.5194/gmd-11-4489-2018>, 2018.
- 4192 Resplandy, L., Keeling, R. F., Rödenbeck, C., Stephens, B. B., Khatiwala, S., Rodgers, K. B., Long, M. C., Bopp,
4193 L., and Tans, P. P.: Revision of global carbon fluxes based on a reassessment of oceanic and riverine carbon
4194 transport, *Nature Geosci.*, 11, 504–509, <https://doi.org/10.1038/s41561-018-0151-3>, 2018.
- 4195 Resplandy, L., Keeling, R. F., Edebbbar, Y., Brooks, M., Wang, R., Bopp, L., Long, M. C., Dunne, J. P., Koeve,
4196 W., and Oschlies, A.: Quantification of ocean heat uptake from changes in atmospheric O₂ and CO₂ composition,
4197 *Scientific Reports*, 9, 20244, <https://doi.org/10.1038/s41598-019-56490-z>, 2019.
- 4198 Rödenbeck, C., Houweling, S., Gloor, M., and Heimann, M.: CO₂ flux history 1982–2001 inferred from
4199 atmospheric data using a global inversion of atmospheric transport, *Atmos Chem Phys*, 3, 1919–1964, 2003.
- 4200 Rödenbeck, C., Bakker, D. C. E., Metzl, N., Olsen, A., Sabine, C., Cassar, N., Reum, F., Keeling, R. F., and
4201 Heimann, M.: Interannual sea–air CO₂ flux variability from an observation-driven ocean mixed-layer scheme, 11,
4202 4599–4613, <https://doi.org/10.5194/bg-11-4599-2014>, 2014.
- 4203 Rödenbeck, C., Zaehle, S., Keeling, R., and Heimann, M.: History of El Niño impacts on the global carbon cycle
4204 1957–2017: a quantification from atmospheric CO₂ data, 373, 20170303, <https://doi.org/10.1098/rstb.2017.0303>,
4205 2018.
- 4206 Rödenbeck, C., DeVries, T., Hauck, J., Le Quéré, C., and Keeling, R. F.: Data-based estimates of interannual sea–
4207 air CO₂ flux variations 1957–2020 and their relation to environmental drivers, *Biogeosciences*, 19, 2627–2652,
4208 <https://doi.org/10.5194/bg-19-2627-2022>, 2022.
- 4209 Rosan, T. M., Klein Goldewijk, K., Ganzenmüller, R., O’Sullivan, M., Pongratz, J., Mercado, L. M., Aragao, L. E.
4210 O. C., Heinrich, V., Randow, C. V., Wiltshire, A., Tubiello, F. N., Bastos, A., Friedlingstein, P., and Sitch, S.: A
4211 multi-data assessment of land use and land cover emissions from Brazil during 2000–2019, *Environ. Res. Lett.*, 16,
4212 074004, <https://doi.org/10.1088/1748-9326/ac08c3>, 2021.
- 4213 Rosan, T. M., Sitch, S., O’Sullivan, M., Basso, L. S., Wilson, C., Silva, C., Gloor, E., Fawcett, D., Heinrich, V.,
4214 Souza, J. G. and Bezerra, F.G.S.: Synthesis of the land carbon fluxes of the Amazon region between 2010 and
4215 2020. *Communications Earth & Environment*, 5(1), p.46. <https://doi.org/10.1038/s43247-024-01205-0>, 2024.
- 4216 Sakamoto, K., H. Nakano, S. Urakawa, T. Toyoda, Y. Kawakami, H. Tsujino, G. Yamanaka, 2023: Reference
4217 manual for the Meteorological Research Institute Community Ocean Model version 5 (MRI.COMv5), Technical
4218 Reports of the Meteorological Research Institute, No.87, <https://doi.org/10.11483/mritechrepo.87>.
- 4219 Sarma, V. V. S. S., Sridevi, B., Metzl, N., Patra, P. K., Lachkar, Z., Chakraborty, K., Goyet, C., Levy, M., Mehari,
4220 M., and Chandra, N.: Air–Sea Fluxes of CO₂ in the Indian Ocean Between 1985 and 2018: A Synthesis Based on
4221 Observation-Based Surface CO₂, Hindcast and Atmospheric Inversion Models, *Glob. Biogeochem. Cycles*, 37,
4222 e2023GB007694, <https://doi.org/10.1029/2023GB007694>, 2023.
- 4223 Schaphoff, S., von Bloh, W., Rammig, A., Thonicke, K., Biemans, H., Forkel, M., Gerten, D., Heinke, J.,
4224 Jägermeyr, J., Knauer, J., Langerwisch, F., Lucht, W., Müller, C., Rolinski, S., and Waha, K.: LPJmL4 – a dynamic

- 4225 global vegetation model with managed land – Part 1: Model description, *Geosci. Model Dev.*, 11, 1343–1375,
4226 <https://doi.org/10.5194/gmd-11-1343-2018>, 2018.
- 4227 Schimel, D., Alves, D., Enting, I. G., Heimann, M., Joos, F., Raynaud, D., Wigley, T., Prater, M., Derwent, R.,
4228 Ehhalt, D., Fraser, P., Sanhueza, E., Zhou, X., Jonas, P., Charlson, R., Rodhe, H., Sadasivan, S., Shine, K. P.,
4229 Fouquart, Y., Ramaswamy, V., Solomon, S., Srinivasan, J., Albritton, D., Derwent, R., Isaksen, I., Lal, M., and
4230 Wuebbles, D.: Radiative Forcing of Climate Change, in: *Climate Change 1995: The Science of Climate Change*,
4231 Contribution of Working Group I to the Second Assessment Report of the Intergovernmental Panel on Climate
4232 Change [Houghton, J. T., Meira Rilho, L. G., Callander, B. A., Harris, N., Kattenberg, A., and Maskell, K. (eds.)],
4233 Cambridge University Press, Cambridge, United Kingdom and New York, NY, USA, ISBN: 978-0521559621,
4234 1995.
- 4235 Schimel, D., Stephens, B. B., and Fisher, J. B.: Effect of increasing CO₂ on the terrestrial carbon cycle, *Proc Natl*
4236 *Acad Sci USA*, 112, 436–441, <https://doi.org/10.1073/pnas.1407302112>, 2015.
- 4237 Schuh, A. E., Jacobson, A. R., Basu, S., Weir, B., Baker, D., Bowman, K., Chevallier, F., Crowell, S., Davis, K. J.,
4238 Deng, F., Denning, S., Feng, L., Jones, D., Liu, J., and Palmer, P. I.: Quantifying the Impact of Atmospheric
4239 Transport Uncertainty on CO₂ Surface Flux Estimates, *Global Biogeochem. Cycles*, 33, 484–500,
4240 <https://doi.org/10.1029/2018GB006086>, 2019.
- 4241 Schuldt, K. N., Mund, J., Aalto, T., Abshire, J. B., Aikin, K., Allen, G., Andrade, M., Andrews, A., Apadula, F.,
4242 Arnold, S., Baier, B., Bakwin, P., Bartyzel, J., Bentz, G., Bergamaschi, P., Beyersdorf, A., Biermann, T., Biraud, S.
4243 C., Blanc, P.-E., Boenisch, H., Bowling, D., Brailsford, G., Brand, W. A., Brunner, D., Bui, T. P., Burban, B.,
4244 Băni, L., Calzolari, F., Chang, C. S., Chen, H., Chen, G., Chmura, L., Clark, S., Climadat, S., Colomb, A.,
4245 Commane, R., Condori, L., Conen, F., Conil, S., Couret, C., Cristofanelli, P., Cuevas, E., Curcoll, R., Daube, B.,
4246 Davis, K. J., De Mazière, M., De Wekker, S., Dean-Day, J. M., Della Coletta, J., Delmotte, M., Di Iorio, T.,
4247 DiGangi, E., DiGangi, J. P., Dickerson, R., Elsasser, M., Emmenegger, L., Fang, S., Forster, G., France, J.,
4248 Frumau, A., Fuente-Lastra, M., Galkowski, M., Gatti, L. V., Gehrlein, T., Gerbig, C., Gheusi, F., Gloor, E., Goto,
4249 D., Griffis, T., Hammer, S., Hanisco, T. F., Hanson, C., Haszpra, L., Hatakka, J., Heimann, M., Heliasz, M., Heltai,
4250 D., Henne, S., Hensen, A., Hermans, C., Hermansen, O., Hints, E., Hoheisel, A., Holst, J., Iraci, L. T., Ivakhov,
4251 V., Jaffe, D. A., Jordan, A., Joubert, W., Kang, H.-Y., Karion, A., Kawa, S. R., Kazan, V., Keeling, R. F., Keronen,
4252 P., Kim, J., Klausen, J., Kneuer, T., Ko, M.-Y., Kolari, P., Kominkova, K., Kort, E., Kozlova, E., Krummel, P. B.,
4253 Kubistin, D., Kulawik, S. S., Kumps, N., Labuschagne, C., Lam, D. H., Lan, X., Langenfelds, R. L., Lanza, A.,
4254 Laurent, O., Laurila, T., Lauvaux, T., Lavric, J., Law, B. E., Lee, C.-H., Lee, J., Lehner, I., Lehtinen, K., Leppert,
4255 R., Leskinen, A., Leuenberger, M., Leung, W. H., Levin, I., Levula, J., Lin, J., Lindauer, M., Lindroth, A., Loh, Z.
4256 M., Lopez, M., Lunder, C. R., Löfvenius, M. O., Machida, T., Mammarella, I., Manca, G., Manning, A., Manning,
4257 A., Marek, M. V., Marklund, P., Marrero, J. E., Martin, M. Y., Martin, D., Martins, G. A., Matsueda, H., McKain,
4258 K., Meijer, H., Meinhardt, F., Merchant, L., Metzger, J.-M., Mihalopoulos, N., Miles, N. L., Miller, C. E., Miller, J.
4259 B., Mitchell, L., Monteiro, V., Montzka, S., Moossen, H., Moreno, C., Morgan, E., Morgui, J.-A., Morimoto, S.,
4260 Munger, J. W., Munro, D., Mutuku, M., Myhre, C. L., Mölder, M., Müller-Williams, J., Nakaoka, S.-I., Necki, J.,
4261 Newman, S., Nichol, S., Nisbet, E., Niwa, Y., Njiru, D. M., Noe, S. M., Nojiri, Y., O'Doherty, S., Obersteiner, F.,
4262 Paplawsky, B., Parworth, C. L., Peischl, J., Peltola, O., Peters, W., Philippon, C., Piacentino, S., Pichon, J. M.,
4263 Pickers, P., Piper, S., Pitt, J., Plass-Dülmer, C., Platt, S. M., Prinzivalli, S., Ramonet, M., Ramos, R., Ren, X.,
4264 Reyes-Sanchez, E., Richardson, S. J., Rigoulet, L.-J., Riris, H., Rivas, P. P., Rothe, M., Roulet, Y.-A., Ryerson,
4265 T., Ryoo, J.-M., Sargent, M., Sasaki, M., Schaefer, H., Scheeren, B., Schmidt, M., Schuck, T., Schumacher, M.,
4266 Seibel, J., Seifert, T., Sha, M. K., Shepson, P., Shin, D., Shook, M., Sloop, C. D., Smale, D., Smith, P. D., Spain,
4267 G., St. Clair, J. M., Steger, D., Steinbacher, M., Stephens, B., Sweeney, C., Sørensen, L. L., Taipale, R., Takatsuki,
4268 S., Tans, P., Thoning, K., Timas, H., Torn, M., Trisolino, P., Turnbull, J., Vermeulen, A., Viner, B., Vitkova, G.,
4269 Walker, S., Watson, A., Weiss, R., Weyrauch, D., Wofsy, S. C., Worsley, J., Worthy, D., Xueref-Remy, I., Yates,
4270 E. L., Young, D., Yver-Kwok, C., Zaehle, S., Zahn, A., Zellweger, C., Zimnoch, M., de Souza, R. A., di Sarra, A.
4271 G., van Dinter, D., van den Bulk, P.: Multi-laboratory compilation of atmospheric carbon dioxide data for the
4272 period 1957-2023; obspack_co2_1_GLOBALVIEWplus_v10.1_2024-11-13, <https://doi.org/10.25925/20241101>,
4273 2024.
- 4274 Schuldt, K. N., Jacobson, A. R., Aalto, T., Aaltonen, H., Andrews, A., Apadula, F., Arnold, S., Bakwin, P.,
4275 Bartyzel, J., Bergamaschi, P., Biermann, T., Biraud, S. C., Blanc, P.-E., Brunner, D., Băni, L., Calzolari, F., Chen,
4276 H., Chmura, L., Colomb, A., Condori, L., Conen, F., Conil, S., Couret, C., Cristofanelli, P., Cuevas, E., De
4277 Mazière, M., De Wekker, S., Della Coletta, J., Delmotte, M., Di Iorio, T., Elsasser, M., Emmenegger, L., Forster,
4278 G., Frumau, A., Fuente-Lastra, M., Galkowski, M., Gheusi, F., Hammer, S., Haszpra, L., Hatakka, J., Heliasz, M.,
4279 Heltai, D., Henne, S., Hensen, A., Hermans, C., Hermansen, O., Hoheisel, A., Holst, J., Jaffe, D. A., Karion, A.,
4280 Kazan, V., Keronen, P., Kneuer, T., Kolari, P., Kominkova, K., Krummel, P. B., Kubistin, D., Kumps, N., Lan, X.,
4281 Langenfelds, R. L., Lanza, A., Laurent, O., Lee, J., Lehner, I., Lehtinen, K., Leskinen, A., Leuenberger, M., Levin,

Deleted: <https://doi.org/10.25925/20241101>

4283 I., Levula, J., Lindauer, M., Lindroth, A., Loh, Z. M., Lopez, M., Lunder, C. R., Löfvenius, M. O., Mammarella, I.,
4284 Manca, G., Manning, A., Manning, A., Marek, M. V., Marklund, P., McKain, K., Meijer, H., Meinhardt, F.,
4285 Metzger, J.-M., Müller, J. B., Müller, C. E., Myhre, C. L., Mölder, M., Müller-Williams, J., Necki, J., Noe, S. M.,
4286 O'Doherty, S., Peltola, O., Philippon, C., Piacentino, S., Pichon, J. M., Pickers, P., Pitt, J., Plass-Dülmer, C., Platt,
4287 S. M., Ramonet, M., Ramos, R., Reyes-Sanchez, E., Rigouleau, L.-J., Rivas, P. P., Roulet, Y.-A., Scheeren, B.,
4288 Schmidt, M., Schumacher, M., Sha, M. K., Sloop, C. D., Smith, P. D., Steger, D., Steinbacher, M., Sweeney, C.,
4289 Sørensen, L. L., Taipale, R., Tans, P., Thoning, K., Trisolino, P., Vermeulen, A., Viner, B., Vitkova, G., Weyrauch,
4290 D., Worthy, D., Xueref-Remy, I., Young, D., Yver-Kwok, C., Zimnoch, M., di Sarra, A. G., van den Bulk, P.:
4291 Multi-laboratory compilation of atmospheric carbon dioxide data for the year 2024;
4292 obspack_co2_1_NRT_v10.1_2025-02-07, <https://doi.org/10.25925/20250101>, 2025.

4293 Schwinger, J., Goris, N., Tjiputra, J. F., Kriest, I., Bentsen, M., Bethke, I., Ilicak, M., Assmann, K. M., and Heinze,
4294 C.: Evaluation of NorESM-OC (versions 1 and 1.2), the ocean carbon-cycle stand-alone configuration of the
4295 Norwegian Earth System Model (NorESM1), *Geosci. Model Dev.*, 9, 2589–2622, [https://doi.org/10.5194/gmd-9-](https://doi.org/10.5194/gmd-9-2589-2016)
4296 2589-2016, 2016.

4297 Schwingshackl, C., Obermeier, W. A., Bultan, S., Grassi, G., Canadell, J. G., Friedlingstein, P., Gasser, T.,
4298 Houghton, R. A., Kurz, W. A., Sitch, S., and Pongratz, J.: Differences in land-based mitigation estimates
4299 reconciled by separating natural and land-use CO2 fluxes at the country level, *One Earth*, 5, 1367–1376,
4300 <https://doi.org/10.1016/j.oneear.2022.11.009>, 2022.

4301 Séférian, R., Nabat, P., Michou, M., Saint-Martin, D., Voltaire, A., Colin, J., Decharme, B., Delire, C., Berthet, S.,
4302 Chevallier, M., Sénéci, S., Franchisteguy, L., Vial, J., Mallet, M., Joetzjer, E., Geoffroy, O., Guérémy, J.-F., Moine,
4303 M.-P., Msadek, R., Ribes, A., Rocher, M., Roehrig, R., Salas-y-Mérida, D., Sanchez, E., Terray, L., Valcke, S.,
4304 Waldman, R., Aumont, O., Bopp, L., Deshayes, J., Ethé, C., and Madec, G.: Evaluation of CNRM Earth System
4305 Model, CNRM-ESM2-1: Role of Earth System Processes in Present-Day and Future Climate, *Journal of Advances*
4306 *in Modeling Earth Systems*, 11, 4182–4227, <https://doi.org/10.1029/2019MS001791>, 2019.

4307 Seiler, C., Melton, J. R., Arora, V. K., Sitch, S., Friedlingstein, P., Anthoni, P., Goll, D., Jain, A. K., Joetzjer, E.,
4308 Lienert, S., Lombardozzi, D., Luyssaert, S., Nabel, J. E. M. S., Tian, H., Vuichard, N., Walker, A. P., Yuan, W.,
4309 and Zaehle, S.: Are Terrestrial Biosphere Models Fit for Simulating the Global Land Carbon Sink?, *J. Adv. Model.*
4310 *Earth Syst.*, 14, e2021MS002946, <https://doi.org/10.1029/2021MS002946>, 2022.

4311 Sellar, A. A., Jones, C. G., Mulcahy, J. P., Tang, Y., Yool, A., Wiltshire, A., O'Connor, F. M., Stringer, M., Hill,
4312 R., Palmieri, J., Woodward, S., Mora, L., Kuhlbrodt, T., Rumbold, S. T., Kelley, D. I., Ellis, R., Johnson, C. E.,
4313 Walton, J., Abraham, N. L., Andrews, M. B., Andrews, T., Archibald, A. T., Berthou, S., Burke, E., Blockley, E.,
4314 Carslaw, K., Dalvi, M., Edwards, J., Folberth, G. A., Gedney, N., Griffiths, P. T., Harper, A. B., Hendry, M. A.,
4315 Hewitt, A. J., Johnson, B., Jones, A., Jones, C. D., Keeble, J., Liddicoat, S., Morgenstern, O., Parker, R. J.,
4316 Predoi, V., Robertson, E., Siahhaan, A., Smith, R. S., Swaminathan, R., Woodhouse, M. T., Zeng, G.,
4317 and Zerroukat, M.: UKESM1: Description and Evaluation of the U.K. Earth System Model, *J. Adv.*
4318 *Model. Earth Syst.*, 11, 4513–4558, <https://doi.org/10.1029/2019MS001739>, 2019.

4319 [Ship and Bunker. 2026. Bunker demand change, Q3 2025, at key global bunkering locations. Available](https://shipandbunker.com/bi/bunker-volumes)
4320 [at: https://shipandbunker.com/bi/bunker-volumes](https://shipandbunker.com/bi/bunker-volumes), last access: 23 March 2026.

4321 Shu, S., Jain, A. K., Koven, C. D., and Mishra, U.: Estimation of Permafrost SOC Stock and Turnover Time
4322 Using a Land Surface Model With Vertical Heterogeneity of Permafrost Soils, *Global Biogeochem. Cy.*, 34,
4323 e2020GB006585, <https://doi.org/10.1029/2020GB006585>, 2020.

4324 Shutler, J. D., Land, P. E., Piolle, J.-F., Woolf, D. K., Goddijn-Murphy, L., Paul, F., Girard-Arduin, F., Chapron,
4325 B., and Donlon, C. J.: FluxEngine: A Flexible Processing System for Calculating Atmosphere–Ocean Carbon
4326 Dioxide Gas Fluxes and Climatologies, *J. Atmospheric Ocean. Technol.*, 33, 741–756,
4327 <https://doi.org/10.1175/JTECH-D-14-00204.1>, 2016.

4328 Silva Junior, C.H., Anderson, L.O., Silva, A.L., Almeida, C.T., Dalagnol, R., Pletsch, M.A., Penha, T.V., Paloschi,
4329 R.A. and Aragão, L.E.: Fire responses to the 2010 and 2015/2016 Amazonian droughts. *Frontiers in Earth Science*,
4330 7, p.97, <https://doi.org/10.3389/feart.2019.00097>, 2019.

4331 Sitch, S., V. Brovkin, W. von Bloh, D. Van Vuuren, B. Eickhout, and Ganopolski, A.: Impacts of future land cover
4332 on atmospheric CO2 and climate. *Global Biogeochemical Cycles*, 19, GB2013. doi:10.1029/2004GB002311, 2005.

Deleted: <https://doi.org/10.25925/20250101>

Formatted: Font: 10 pt

Formatted: Font: 10 pt

- 4334 Sitch, S., Huntingford, C., Gedney, N., Levy, P. E., Lomas, M., Piao, S. L., Betts, R., Ciais, P., Cox, P.,
 4335 Friedlingstein, P., Jones, C. D., Prentice, I. C., and Woodward, F. I.: Evaluation of the terrestrial carbon cycle,
 4336 future plant geography and climate-carbon cycle feedbacks using five Dynamic Global Vegetation Models
 4337 (DGVMs): Uncertainty In Land Carbon Cycle Feedbacks, *Glob. Change Biol.*, 14, 2015–2039,
 4338 <https://doi.org/10.1111/j.1365-2486.2008.01626.x>, 2008.
- 4339 Sitch, S., O’Sullivan, M., Robertson, E., Friedlingstein, P., Albergel, C., Anthoni, P., Arneth, A., Arora, V. K.,
 4340 Bastos, A., Bastrikov, V., Bellouin, N., Canadell, J. G., Chini, L., Ciais, P., Falk, S., Harris, I., Hurtt, G., Ito, A.,
 4341 Jain, A. K., Jones, M. W., Joos, F., Kato, E., Kennedy, D., Klein Goldewijk, K., Kluzek, E., Knauer, J., Lawrence,
 4342 P. J., Lombardozzi, D., Melton, J. R., Nabel, J. E. M. S., Pan, N., Peylin, P., Pongratz, J., Poulter, B., Rosan, T. M.,
 4343 Sun, Q., Tian, H., Walker, A. P., Weber, U., Yuan, W., Yue, X., Zaehle, S.: Trends and Drivers of Terrestrial
 4344 Sources and Sinks of Carbon Dioxide: An Overview of the TRENDY Project, *Global Biogeochemical Cycles*,
 4345 38(7), e2024GB008102, <https://doi.org/10.1029/2024GB008102>, 2024.
- 4346 Smallman, T. L., Milodowski, D. T., Neto, E. S., Koren, G., Ometto, J., and Williams, M.: Parameter uncertainty
 4347 dominates C-cycle forecast errors over most of Brazil for the 21st century, *Earth Syst. Dyn.*, 12, 1191–1237,
 4348 <https://doi.org/10.5194/esd-12-1191-2021>, 2021.
- 4349 Smith, B., Wärlind, D., Arneth, A., Hickler, T., Leadley, P., Siltberg, J., and Zaehle, S.: Implications of
 4350 incorporating N cycling and N limitations on primary production in an individual-based dynamic vegetation model,
 4351 *Biogeosciences*, 11, 2027–2054, <https://doi.org/10.5194/bg-11-2027-2014>, 2014.
- 4352 Smith, S. M., Geden, O., Gidden, M. J., Lamb, W. F., Nemet, G. F., Minx, J. C., Buck, H., Burke, J., Cox, E.,
 4353 Edwards, M. R., Fuss, S., Johnstone, I., Müller-Hansen, F., Pongratz, J., Probst, B. S., Roe, S., Schenuit, F.,
 4354 Schulte, I., and Vaughan, N. E. The State of Carbon Dioxide Removal 2024 - 2nd Edition,
 4355 <http://dx.doi.org/10.17605/OSF.IO/F85QJ>, 2024.
- 4356 Sospedra-Alfonso, R., Merryfield, W. J., Boer, G. J., Kharin, V. V., Lee, W.-S., Seiler, C., and Christian, J. R.:
 4357 Decadal climate predictions with the Canadian Earth System Model version 5 (CanESM5), *Geosci. Model Dev.*,
 4358 14, 6863–6891, <https://doi.org/10.5194/gmd-14-6863-2021>, 2021.
- 4359 Steele, L. P., Dlugokencky, E. J., Lang, P. M., Tans, P. P., Martin, R. C., and Masarie, K. A.: Slowing down of the
 4360 global accumulation of atmospheric methane during the 1980s, *Nature* 358, 313–316,
 4361 <https://doi.org/10.1038/358313a0>, 1992.
- 4362 Stephens, B. B., Gurney, K. R., Tans, P. P., Sweeney, C., Peters, W., Bruhwiler, L., Ciais, P., Ramonet, M.,
 4363 Bousquet, P., Nakazawa, T., Aoki, S., Machida, T., Inoue, G., Vinnichenko, N., Lloyd, J., Jordan, A., Heimann,
 4364 M., Shibistova, O., Langenfelds, R. L., Steele, L. P., Francey, R. J., and Denning, A. S.: Weak Northern and Strong
 4365 Tropical Land Carbon Uptake from Vertical Profiles of Atmospheric CO₂, *Science*, 316, 1732–1735,
 4366 <https://doi.org/10.1126/science.1137004>, 2007.
- 4367 Stephens, B. B., Keeling, R. F., Heimann, M., Six, K. D., Murnane, R., and Caldeira, K.: Testing global ocean
 4368 carbon cycle models using measurements of atmospheric O₂ and CO₂ concentration, *Glob. Biogeochem. Cycles*,
 4369 12, 213–230, <https://doi.org/10.1029/97GB03500>, 1998.
- 4370 Stock, C. A., Dunne, J. P., Luo, J. Y., Ross, A. C., Van Oostende, N., Zadeh, N., Cordero, T. J., Liu, X., and Teng,
 4371 Y.: Photoacclimation and Photoadaptation Sensitivity in a Global Ocean Ecosystem Model, *J Adv Model Earth*
 4372 *Syst*, 17, e2024MS004701, <https://doi.org/10.1029/2024MS004701>, 2025.
- 4373 Stocker, T., Qin, D., and Plattner, G.-K.: Climate Change 2013: The Physical Science Basis. Contribution of
 4374 Working Group I to the Fifth Assessment Report of the Intergovernmental Panel on Climate Change
 4375 [Intergovernmental Panel on Climate Change (eds.)], Cambridge University Press, Cambridge, ISBN:
 4376 9789291691388, 2013.
- 4377 Swart, N. C., Cole, J. N. S., Kharin, V. V., Lazare, M., Scinocca, J. F., Gillett, N. P., Anstey, J., Arora, V.,
 4378 Christian, J. R., Hanna, S., Jiao, Y., Lee, W. G., Majaess, F., Saenko, O. A., Seiler, C., Seinen, C., Shao, A.,
 4379 Sigmond, M., Solheim, L., von Salzen, K., Yang, D., and Winter, B.: The Canadian Earth System Model version 5
 4380 (CanESM5.0.3), *Geosci. Model Dev.*, 12, 4823–4873, <https://doi.org/10.5194/gmd-12-4823-2019>, 2019.
- 4381 SX Coal: Monthly coal consumption estimates, <http://www.sxcoal.com/>, last access: 23 October 2025, 2022.

Deleted: <https://doi.org/10.1029/2024MS004701>

- 4383 Takahashi, T., Sutherland, S. C., Wanninkhof, R., Sweeney, C., Feely, R. A., Chipman, D. W., Hales, B.,
4384 Friederich, G., Chavez, F., Sabine, C., Watson, A., Bakker, D. C. E., Schuster, U., Metzl, N., Yoshikawa-Inoue, H.,
4385 Ishii, M., Midorikawa, T., Nojiri, Y., Körtzinger, A., Steinhoff, T., Hoppema, M., Olafsson, J., Arnarson, T. S.,
4386 Tilbrook, B., Johannessen, T., Olsen, A., Bellerby, R., Wong, C. S., Delille, B., Bates, N. R., and de Baar, H. J. W.:
4387 Climatological mean and decadal change in surface ocean pCO₂, and net sea-air CO₂ flux over the global oceans,
4388 Deep Sea Research Part II: Topical Studies in Oceanography, 56, 554–577,
4389 <https://doi.org/10.1016/j.dsr2.2008.12.009>, 2009.
- 4390 Terhaar, J., Frölicher, T. L., and Joos, F.: Southern Ocean anthropogenic carbon sink constrained by sea surface
4391 salinity, *Sci. Adv.*, 7, eabd5964, <https://doi.org/10.1126/sciadv.abd5964>, 2021.
- 4392 Terhaar, J., Frölicher, T. L., and Joos, F.: Observation-constrained estimates of the global ocean carbon sink from
4393 Earth system models, *Biogeosciences*, 19, 4431–4457, <https://doi.org/10.5194/bg-19-4431-2022>, 2022.
- 4394 Terhaar, J., Goris, N., Müller, J. D., DeVries, T., Gruber, N., Hauck, J., Perez, F. F., and Séférian, R.: Assessment
4395 of Global Ocean Biogeochemistry Models for Ocean Carbon Sink Estimates in RECCAP2 and Recommendations
4396 for Future Studies. *Journal of Advances in Modeling Earth Systems*, 16(3), e2023MS003840,
4397 <https://doi.org/10.1029/2023MS003840>, 2024.
- 4398 Tian, H., Xu, X., Lu, C., Liu, M., Ren, W., Chen, G., Melillo, J., and Liu, J.: Net exchanges of CO₂, CH₄, and
4399 N₂O between China's terrestrial ecosystems and the atmosphere and their contributions to global climate warming,
4400 *J. Geophys. Res. Biogeosciences*, 116, G02011, <https://doi.org/10.1029/2010JG001393>, 2011.
- 4401 Tian, H., Chen, G., Lu, C., Xu, X., Hayes, D. J., Ren, W., Pan, S., Huntzinger, D. N., and Wofsy, S. C.: North
4402 American terrestrial CO₂ uptake largely offset by CH₄ and N₂O emissions: toward a full accounting of the
4403 greenhouse gas budget, *Climatic Change*, 129, 413–426, <https://doi.org/10.1007/s10584-014-1072-9>, 2015.
- 4404 Tjiputra, J. F., Schwinger, J., Bentsen, M., Morée, A. L., Gao, S., Bethke, I., Heinze, C., Goris, N., Gupta, A., He,
4405 Y.-C., Olivé, D., Seland, Ø., and Schulz, M.: Ocean biogeochemistry in the Norwegian Earth System Model
4406 version 2 (NorESM2), *Geosci. Model Dev.*, 13, 2393–2431, <https://doi.org/10.5194/gmd-13-2393-2020>, 2020.
- 4407 Tsujino, H., Nakano, H., Sakamoto, K., Urakawa, L. S., Toyama, K., Kosugi, N., Kitamura, Y., Ishii, M.,
4408 Nishikawa, S., Nishikawa, H., Sugiyama, T., and Ishikawa, Y.: Impact of increased horizontal resolution of an
4409 ocean model on carbon circulation in the North Pacific Ocean. *Journal of Advances in Modeling Earth Systems*,
4410 16, e2023MS003720, <https://doi.org/10.1029/2023MS003720>, 2024.
- 4411 Tubiello, F. N., Conchedda, G., Wanner, N., Federici, S., Rossi, S., and Grassi, G.: Carbon emissions and removals
4412 from forests: new estimates, 1990–2020, *Earth Syst. Sci. Data*, 13, 1681–1691, <https://doi.org/10.5194/essd-13-1681-2021>, 2021.
- 4414 Tubiello, F., Pekkarinen, A., Branthomme, A., Piccoli, M., Obli-Laryea, G., Ramadan, N., and Conchedda, G.:
4415 New FAOSTAT forest emissions and removals estimates: 1990–2025, *Earth Syst. Sci. Data Discussions*,
4416 <https://doi.org/10.5194/essd-2025-635>, 2025.
- 4417 Tuck, C.: 2022 Mineral Commodity Summary: Iron Ore, Tech. rep., U.S. Geological Survey,
4418 <https://pubs.usgs.gov/periodicals/mcs2022/mcs2022-iron-ore.pdf>, 2022.
- 4419 UNFCCC: Synthesis report for the technical assessment component of the first global stocktake, available at:
4420 <https://unfccc.int/documents/461466>, last access: 23 October 2025, 2022.
- 4421 Vale, M. M., Berenguer, E., Argollo de Menezes, M., Viveiros de Castro, E. B., Pugliese de Siqueira, L., and
4422 Portela, R. de C. Q.: The COVID-19 pandemic as an opportunity to weaken environmental protection in Brazil,
4423 *Biological Conservation*, 255, 108994, <https://doi.org/10.1016/j.biocon.2021.108994>, 2021.
- 4424 van der Laan-Luijckx, I. T., van der Velde, I. R., van der Veen, E., Tsuruta, A., Stanislawski, K., Babenhauerheide,
4425 A., Zhang, H. F., Liu, Y., He, W., Chen, H., Masarie, K. A., Krol, M. C., and Peters, W.: The CarbonTracker Data
4426 Assimilation Shell (CTDAS) v1.0: implementation and global carbon balance 2001–2015, *Geosci. Model Dev.*, 10,
4427 2785–2800, <https://doi.org/10.5194/gmd-10-2785-2017>, 2017.
- 4428 van der Velde, I. R., van der Werf, G. R., Houweling, S., Maasakkers, J. D., Borsdorff, T., Landgraf, J., Tol, P.,
4429 van Kempen, T. A., van Hees, R., Hoogeveen, R., Veeffkind, J. P., and Aben, I.: Vast CO₂ release from Australian

Deleted: <https://doi.org/10.5194/gmd-13-2393-2020>

- 4431 fires in 2019–2020 constrained by satellite, *Nature*, 597, 366–369, <https://doi.org/10.1038/s41586-021-03712-y>,
4432 2021.
- 4433 van der Werf, G. R., Randerson, J. T., Giglio, L., Collatz, G. J., Mu, M., Kasibhatla, P. S., Morton, D. C., DeFries,
4434 R. S., Jin, Y., and van Leeuwen, T. T.: Global fire emissions and the contribution of deforestation, savanna, forest,
4435 agricultural, and peat fires (1997–2009), *Atmospheric Chem. Phys.*, 10, 11707–11735, [https://doi.org/10.5194/acp-](https://doi.org/10.5194/acp-10-11707-2010)
4436 10-11707-2010, 2010.
- 4437 van der Werf, G. R., Randerson, J. T., Giglio, L., van Leeuwen, T. T., Chen, Y., Rogers, B. M., Mu, M., van Marle,
4438 M. J. E., Morton, D. C., Collatz, G. J., Yokelson, R. J., and Kasibhatla, P. S.: Global fire emissions estimates
4439 during 1997–2016, *Earth Syst. Sci. Data*, 9, 697–720, <https://doi.org/10.5194/essd-9-697-2017>, 2017.
- 4440 van Wees, D., van der Werf, G. R., Randerson, J. T., Andela, N., Chen, Y., and Morton, D. C.: The role of fire in
4441 global forest loss dynamics, *Glob. Change Biol.*, 27, 2377–2391, <https://doi.org/10.1111/gcb.15591>, 2021.
- 4442 von Bloh, W., Schaphoff, S., Müller, C., Rolinski, S., Waha, K., and Zaehle, S.: Implementing the nitrogen cycle
4443 into the dynamic global vegetation, hydrology, and crop growth model LPJmL (version 5.0), *Geosci. Model Dev.*,
4444 11, 2789–2812, <https://doi.org/10.5194/gmd-11-2789-2018>, 2018.
- 4445 Vaithinathan Ayar, P., Bopp, L., Christian, J. R., Ilyina, T., Krasting, J. P., Séférian, R., Tsujino, H., Watanabe, M.,
4446 Yool, A., and Tjiputra, J.: Contrasting projections of the ENSO-driven CO₂ flux variability in the equatorial
4447 Pacific under high-warming scenario, *Earth Syst. Dynam.*, 13, 1097–1118, [https://doi.org/10.5194/esd-13-1097-](https://doi.org/10.5194/esd-13-1097-2022)
4448 2022, 2022.
- 4449 Vuichard, N., Messina, P., Luysaert, S., Guenet, B., Zaehle, S., Ghattas, J., Bastrikov, V., and Peylin, P.:
4450 Accounting for carbon and nitrogen interactions in the global terrestrial ecosystem model ORCHIDEE (trunk
4451 version, rev 4999): multi-scale evaluation of gross primary production, *Geosci. Model Dev.*, 12, 4751–4779,
4452 <https://doi.org/10.5194/gmd-12-4751-2019>, 2019.
- 4453 Walker, A. P., Quaipe, T., Bodegom, P. M., De Kauwe, M. G., Keenan, T. F., Joiner, J., Lomas, M. R., MacBean,
4454 N., Xu, C., Yang, X., and Woodward, F. I.: The impact of alternative trait-scaling hypotheses for the maximum
4455 photosynthetic carboxylation rate (V_{cmax}) on global gross primary production, *New Phytol.*, 215, 1370–1386,
4456 <https://doi.org/10.1111/nph.14623>, 2017.
- 4457 Walker, A. P., De Kauwe, M. G., Bastos, A., Belmecheri, S., Georgiou, K., Keeling, R. F., McMahon, S. M.,
4458 Medlyn, B. E., Moore, D. J. P., Norby, R. J., Zaehle, S., Anderson-Teixeira, K. J., Battipaglia, G., Brienen, R. J.
4459 W., Cabugao, K. G., Cailleret, M., Campbell, E., Canadell, J. G., Ciais, P., Craig, M. E., Ellsworth, D. S., Farquhar,
4460 G. D., Faticchi, S., Fisher, J. B., Frank, D. C., Graven, H., Gu, L., Haverd, V., Heilman, K., Heimann, M., Hungate,
4461 B. A., Iversen, C. M., Joos, F., Jiang, M., Keenan, T. F., Knauer, J., Körner, C., Leshyk, V. O., Leuzinger, S., Liu,
4462 Y., MacBean, N., Malhi, Y., McVicar, T. R., Penuelas, J., Pongratz, J., Powell, A. S., Riutta, T., Sabot, M. E. B.,
4463 Schleucher, J., Sitch, S., Smith, W. K., Sulman, B., Taylor, B., Terrer, C., Torn, M. S., Treseder, K. K., Trugman,
4464 A. T., Trumbore, S. E., van Mantgem, P. J., Voelker, S. L., Whelan, M. E., and Zuidema, P. A.: Integrating the
4465 evidence for a terrestrial carbon sink caused by increasing atmospheric CO₂, *New Phytol.*, 229, 2413–2445,
4466 <https://doi.org/10.1111/nph.16866>, 2021.
- 4467 Watanabe, M., Tatebe, H., Koyama, H., Hajima, T., Watanabe, M., and Kawamiya, M.: Importance of El Niño
4468 reproducibility for reconstructing historical CO₂ flux variations in the equatorial Pacific, *Ocean Sci.*, 16, 1431–
4469 1442, <https://doi.org/10.5194/os-16-1431-2020>, 2020.
- 4470 Watson, A. J., Schuster, U., Shutler, J. D., Holding, T., Ashton, I. G. C., Landschützer, P., Woolf, D. K., and
4471 Goddijn-Murphy, L.: Revised estimates of ocean-atmosphere CO₂ flux are consistent with ocean carbon inventory,
4472 *Nat Commun*, 11, 4422, <https://doi.org/10.1038/s41467-020-18203-3>, 2020.
- 4473 Watson, R. T., Rohde, H., Oeschger, H., and Siegenthaler, U.: Greenhouse Gases and Aerosols, in: *Climate*
4474 *Change: The IPCC Scientific Assessment*. Intergovernmental Panel on Climate Change (IPCC), edited by:
4475 Houghton, J. T., Jenkins, G. J., and Ephraums, J. J., Cambridge University Press, Cambridge, ISBN: 978-
4476 0521403603, 1990.
- 4477 Wenzel, S., Cox, P. M., Eyring, V., and Friedlingstein, P.: Projected land photosynthesis constrained by changes in
4478 the seasonal cycle of atmospheric CO₂, *Nature*, 538, 499–501, <https://doi.org/10.1038/nature19772>, 2016.

- 4479 Wilkenskjeld, S., Kloster, S., Pongratz, J., Raddatz, T., and Reick, C. H.: Comparing the influence of net and gross
4480 anthropogenic land-use and land-cover changes on the carbon cycle in the MPI-ESM, *Biogeosciences*, 11, 4817–
4481 4828, <https://doi.org/10.5194/bg-11-4817-2014>, 2014.
- 4482 Wiltshire, A. J., Burke, E. J., Chadburn, S. E., Jones, C. D., Cox, P. M., Davies-Barnard, T., Friedlingstein, P.,
4483 Harper, A. B., Liddicoat, S., Sitch, S., and Zaehle, S.: JULES-CN: a coupled terrestrial carbon–nitrogen scheme
4484 (JULES vn5.1), 14, 2161–2186, <https://doi.org/10.5194/gmd-14-2161-2021>, 2021.
- 4485 Winkler, K., Yang, H., Ganzenmüller, R., Fuchs, R., Ceccherini, G., Duveiller, G., Grassi, G., Pongratz, J., Bastos,
4486 A., Shvidenko, A., Araza, A., Herold, M., Wigneron, J.-P., and Ciais, P.: Changes in land use and management led
4487 to a decline in Eastern Europe’s terrestrial carbon sink, *Commun. Earth Environ.*, 4, 1–14,
4488 <https://doi.org/10.1038/s43247-023-00893-4>, 2023.
- 4489 Woodward, F. I. and Lomas, M. R.: Vegetation dynamics – simulating responses to climatic change, *Biol. Rev.*, 79,
4490 643–670, <https://doi.org/10.1017/S1464793103006419>, 2004.
- 4491 Wright, R. M., Le Quéré, C., Buitenhuis, E., Pitois, S., and Gibbons, M. J.: Role of jellyfish in the plankton
4492 ecosystem revealed using a global ocean biogeochemical model, 18, 1291–1320, <https://doi.org/10.5194/bg-18-1291-2021>, 2021.
- 4494 Wunch, D., Wennberg, P. O., Osterman, G., Fisher, B., Naylor, B., Roehl, C. M., O’Dell, C., Mandrake, L., Viatte,
4495 C., Kiel, M., Griffith, D. W. T., Deutscher, N. M., Velasco, V. A., Notholt, J., Warneke, T., Petri, C., De Maziere,
4496 M., Sha, M. K., Sussmann, R., Rettinger, M., Pollard, D., Robinson, J., Morino, I., Uchino, O., Hase, F.,
4497 Blumenstock, T., Feist, D. G., Arnold, S. G., Strong, K., Mendonca, J., Kivi, R., Heikkinen, P., Iraci, L., Podolske,
4498 J., Hillyard, P. W., Kawakami, S., Dubey, M. K., Parker, H. A., Sepulveda, E., García, O. E., Te, Y., Jeseck, P.,
4499 Gunson, M. R., Crisp, D., and Eldering, A.: Comparisons of the Orbiting Carbon Observatory-2 (OCO-2) X CO2
4500 measurements with TCCON, *Atmos. Meas. Tech.*, 10, 2209–2238, <https://doi.org/10.5194/amt-10-2209-2017>,
4501 2017.
- 4502 Wunder, S., Kaimowitz, D., Jensen, S., and Feder, S.: Coronavirus, macroeconomy, and forests: What likely
4503 impacts?, *For. Policy Econ.*, 131, 102536, <https://doi.org/10.1016/j.forpol.2021.102536>, 2021.
- 4504 Xi, F., Davis, S. J., Ciais, P., Crawford-Brown, D., Guan, D., Pade, C., Shi, T., Syddall, M., Lv, J., Ji, L., Bing, L.,
4505 Wang, J., Wei, W., Yang, K.-H., Lagerblad, B., Galan, I., Andrade, C., Zhang, Y., and Liu, Z.: Substantial global
4506 carbon uptake by cement carbonation, *Nature Geosci.*, 9, 880–883, <https://doi.org/10.1038/ngeo2840>, 2016.
- 4507 Xia, J., Chen, Y., Liang, S., Liu, D., and Yuan, W.: Global simulations of carbon allocation coefficients for
4508 deciduous vegetation types, *Tellus B*, 67, 28016, <https://doi.org/10.3402/tellusb.v67.28016>, 2015.
- 4509 Xia, X., Ren, P., Wang, X., Liu, D., Chen, X., Dan, L., He, B., He, H., Ju, W., Liang, M., Lu, X., Peng, J., Qin, Z.,
4510 Xia, J., Zheng, B., Wei, J., Yue, X., Yu, G., Piao, S., and Yuan, W.: The carbon budget of China: 1980–2021,
4511 *Science Bulletin*, 69, 114–124, <https://doi.org/10.1016/j.scib.2023.11.016>, 2024.
- 4512 Yang, D., Liu, Y., Feng, L., Wang, J., Yao, L., Cai, Z., Zhu, S., Lu, N., and Lyu, D.: The First Global Carbon
4513 Dioxide Flux Map Derived from TanSat Measurements, *Adv. Atmospheric Sci.*, 38, 1433–1443,
4514 <https://doi.org/10.1007/s00376-021-1179-7>, 2021.
- 4515 Yang, X., Thornton, P., Ricciuto, D., Wang, Y., and Hoffman, F.: Global evaluation of terrestrial biogeochemistry
4516 in the Energy Exascale Earth System Model (E3SM) and the role of the phosphorus cycle in the historical
4517 terrestrial carbon balance, *Biogeosciences*, 20, 2813–2836, <https://doi.org/10.5194/bg-20-2813-2023>, 2023.
- 4518 Yao, Y., Joetzer, E., Ciais, P., Viovy, N., Cresto Aleina, F., Chave, J., Sack, L., Bartlett, M., Meir, P., Fisher, R.,
4519 and Luyssaert, S.: Forest fluxes and mortality response to drought: model description (ORCHIDEE-CAN-NHA
4520 r7236) and evaluation at the Caxiuana drought experiment, *Geosci. Model Dev.*, 15, 7809–7833,
4521 <https://doi.org/10.5194/gmd-15-7809-2022>, 2022.
- 4522 Yao, Y., Ciais, P., Viovy, N., Joetzer, E. and Chave, J.: How drought events during the last century have impacted
4523 biomass carbon in Amazonian rainforests. *Global Change Biology*, 29(3), pp.747-762,
4524 <https://doi.org/10.1111/gcb.16504>, 2023.
- 4525 You, Y., Tian, H., Pan, S., Shi, H., Bian, Z., Gurgel, A., Huang, Y., Kicklighter, D., Liang, X.-Z., Lu, C., Melillo,
4526 J., Miao, R., Pan, N., Reilly, J., Ren, W., Xu, R., Yang, J., Yu, Q., and Zhang, J.: Incorporating dynamic crop

Deleted: <https://doi.org/10.5194/amt-10-2209-2017>

Deleted: <https://doi.org/10.1016/j.scib.2023.11.016>

- 4529 growth processes and management practices into a terrestrial biosphere model for simulating crop production in the
4530 United States: Toward a unified modeling framework, *Agricultural and Forest Meteorology*, 325, 109144,
4531 <https://doi.org/10.1016/j.agrformet.2022.109144>, 2022.
- 4532 Yu, Z., Ciais, P., Piao, S., Houghton, R. A., Lu, C., Tian, H., Agathokleous, E., Kattel, G. R., Sitch, S., Goll, D.,
4533 Yue, X., Walker, A., Friedlingstein, P., Jain, A. K., Liu, S., and Zhou, G.: Forest expansion dominates China's land
4534 carbon sink since 1980, *Nat. Commun.*, 13, 5374, <https://doi.org/10.1038/s41467-022-32961-2>, 2022.
- 4535 Yue, X. and Unger, N.: The Yale Interactive terrestrial Biosphere model version 1.0: description, evaluation and
4536 implementation into NASA GISS ModelE2, *Geosci. Model Dev.*, 8, 2399–2417, <https://doi.org/10.5194/gmd-8-2399-2015>, 2015.
- 4538 Yue, X., Zhou, H., Tian, C., Ma, Y., Hu, Y., Gong, C., Zheng, H., and Liao, H.: Development and evaluation of the
4539 interactive Model for Air Pollution and Land Ecosystems (iMAPLE) version 1.0, *Geosci. Model Dev.*, 17, 4621–
4540 4642, <https://doi.org/10.5194/gmd-17-4621-2024>, 2024.
- 4541 Yuan, W., Liu, D., Dong, W., Liu, S., Zhou, G., Yu, G., Zhao, T., Feng, J., Ma, Z., Chen, J., Chen, Y., Chen, S.,
4542 Han, S., Huang, J., Li, L., Liu, H., Liu, S., Ma, M., Wang, Y., Xia, J., Xu, W., Zhang, Q., Zhao, X., and Zhao, L.:
4543 Multiyear precipitation reduction strongly decreases carbon uptake over northern China, *J. Geophys. Res.-Biogeo.*,
4544 119, 881–896, <https://doi.org/10.1002/2014JG002608>, 2014.
- 4545 Yue, C., Ciais, P., Zhu, D., Wang, T., Peng, S. S., and Piao, S. L.: How have past fire disturbances contributed to
4546 the current carbon balance of boreal ecosystems?, *Biogeosciences*, 13, 675–690, <https://doi.org/10.5194/bg-13-675-2016>, 2016.
- 4548 Zaehle, S. and Friend, A. D.: Carbon and nitrogen cycle dynamics in the O-CN land surface model: 1. Model
4549 description, site-scale evaluation, and sensitivity to parameter estimates: Site-scale evaluation of a C-N model,
4550 *Global Biogeochem. Cycles*, 24, GB1005, <https://doi.org/10.1029/2009GB003521>, 2010.
- 4551 Zaehle, S., Ciais, P., Friend, A. D., and Prieur, V.: Carbon benefits of anthropogenic reactive nitrogen offset by
4552 nitrous oxide emissions, *Nature Geosci*, 4, 601–605, <https://doi.org/10.1038/ngeo1207>, 2011.
- 4553 Zaehle, S., Medlyn, B. E., De Kauwe, M. G., Walker, A. P., Dietze, M. C., Hickler, T., Luo, Y., Wang, Y.-P., El-
4554 Masri, B., Thornton, P., Jain, A., Wang, S., Warland, D., Weng, E., Parton, W., Iversen, C. M., Gallet-Budynek, A.,
4555 McCarthy, H., Finzi, A., Hanson, P. J., Prentice, I. C., Oren, R., and Norby, R. J.: Evaluation of 11 terrestrial
4556 carbon–nitrogen cycle models against observations from two temperate Free-Air CO₂ Enrichment studies, *New
4557 Phytol.*, 202, 803–822, <https://doi.org/10.1111/nph.12697>, 2014.
- 4558 Zeng, J., Iida, Y., Matsunaga, T., and Shirai, T.: Surface ocean CO₂ concentration and air-sea flux estimate by
4559 machine learning with modelled variable trends, *Front. Mar. Sci.*, 9, <https://doi.org/10.3389/fmars.2022.989233>,
4560 2022.
- 4561 Zheng, B., Ciais, P., Chevallier, F., Chuvieco, E., Chen, Y., and Yang, H.: Increasing forest fire emissions despite
4562 the decline in global burned area, *Sci. Adv.*, 7, eabh2646, <https://doi.org/10.1126/sciadv.abh2646>, 2021.
- 4563 Zhu, Y., Xia, X., Canadell, J. G., Piao, S., Lu, X., Mishra, U., Wang, X., Yuan, W., and Qin, Z.: China's carbon
4564 sinks from land-use change underestimated, *Nat. Clim. Chang.*, 15, 428–435, <https://doi.org/10.1038/s41558-025-02296-z>, 2025.
- 4566 Zou, Y., Wang, Y., Ke, Z., Tian, H., Yang, J., and Liu, Y.: Development of a REgion-Specific Ecosystem
4567 Feedback Fire (RESFire) Model in the Community Earth System Model, *J. Adv. Model. Earth Syst.*, 11, 417–445,
4568 <https://doi.org/10.1029/2018MS001368>, 2019.
- 4569 Zscheischler, J., Mahecha, M. D., Avitabile, V., Calle, L., Carvalhais, N., Ciais, P., Gans, F., Gruber, N.,
4570 Hartmann, J., Herold, M., Ichii, K., Jung, M., Landschützer, P., Laruelle, G. G., Lauerwald, R., Papale, D., Peylin,
4571 P., Poulter, B., Ray, D., Regnier, P., Rödenbeck, C., Roman-Cuesta, R. M., Schwalm, C., Tramontana, G.,
4572 Tyukavina, A., Valentini, R., van der Werf, G., West, T. O., Wolf, J. E., and Reichstein, M.: Reviews and
4573 syntheses: An empirical spatiotemporal description of the global surface–atmosphere carbon fluxes: opportunities
4574 and data limitations, *Biogeosciences*, 14, 3685–3703, <https://doi.org/10.5194/bg-14-3685-2017>, 2017.

Deleted: <https://doi.org/10.1016/j.agrformet.2022.109144>

Deleted: <https://doi.org/10.5194/gmd-17-4621-2024>

Deleted: Chang., 15, 428–435,
<https://doi.org/10.1038/s41558-025-02296-z>

4579

Tables

4580

4581 **Table 1.** Factors used to convert carbon in various units (by convention, Unit 1 = Unit 2 × conversion).

Unit 1	Unit 2	Conversion	Source
GtC (gigatonnes of carbon)	ppm (parts per million) (a)	2.124 (b)	Ballantyne et al. (2012)
GtC (gigatonnes of carbon)	PgC (petagrams of carbon)	1	SI unit conversion
GtCO ₂ (gigatonnes of carbon dioxide)	GtC (gigatonnes of carbon)	3.664	44.01/12.011 in mass equivalent
(a) Measurements of atmospheric CO ₂ concentration have units of dry-air mole fraction. 'ppm' is an abbreviation for micromole/mol, dry air.			
(b) The use of a factor of 2.124 assumes that all the atmosphere is well mixed within one year. In reality, only the troposphere is well mixed and the growth rate of CO ₂ concentration in the less well-mixed stratosphere is not measured by sites from the NOAA network. Using a factor of 2.124 makes the approximation that the growth rate of CO ₂ concentration in the stratosphere equals that of the troposphere on a yearly basis.			

Formatted Table

4582

4583

Table 2. How to cite the individual components of the global carbon budget presented here.

Component	Primary reference
Global fossil CO ₂ emissions (EFOS), total and by fuel type	Andrew and Peters (2025)
National territorial fossil CO ₂ emissions (EFOS)	Erb and Marland (2025), UNFCCC (2022)
National consumption-based fossil CO ₂ emissions (EFOS) by country (consumption)	Peters et al. (2011a) updated as described in this paper
Net land-use change flux (ELUC)	This paper (see Table 4 for individual model references).
Growth rate in atmospheric CO ₂ concentration (GATM)	Lan et al. (2025)
Ocean and land CO ₂ sinks (SOCEAN and SLAND)	This paper (see Table 4 for individual model and data products references).

Formatted Table

Deleted: 2025a

4584

4586 **Table 3.** Main methodological changes in the global carbon budget this year (GCB2025). Empty cells mean
 4587 there were no methodological changes introduced that year. Table [S10](#) lists methodological changes from the
 4588 first global carbon budget publication up to 2024.

Deleted: S9

Fossil fuel emissions		LUC emissions	Reservoirs			Other changes
Global	Country (territorial)		Atmosphere	Ocean	Land	
	Projection available for Japan for the first time	Bookkeeping estimates derived from models that estimate ELUC based on transient carbon densities responding to environmental changes (BLUE, OSCAR, LUCE).	Include an assessment of satellite-derived growth rates	Adjustments applied for known underestimation of GOBMs and cool surface skin effect in fCO ₂ - product Suspension of 19 ocean data sets from SOCAT.	Include the RSS adjustment.	

Formatted Table

Deleted: products

4589

4594 **Table 4.** References for the process models, bookkeeping models, ocean data products, and atmospheric
 4595 inversions. All models and products are updated with new data to the end of year 2024.

4596

Model/data name	Reference	Change from Global Carbon Budget 2024 (Friedlingstein et al., 2025a)
Bookkeeping models for land-use change emissions		
BLUE	Hansis et al. (2015)	Transient C densities used to estimate ELUC
OSCAR	Gasser et al. (2020)	No change
LUCCE	Qin et al. (2024)	Transient C densities used to estimate ELUC
Dynamic global vegetation models		
CABLE-POP	Haverd et al. (2018)	corrected N deposition input data, minor parameter changes
CLASSIC	Melton et al. (2020), Gauthier et al. (2025), Kou-Giesbrecht and Arora (2022)	
CLM6.0	Lawrence et al. (2019)	New dust scheme, new BGC fire method, updates to MEGAN for BVOCs, parameter updates, new surface datasets, new N fixation method
CLM-FATES	Fisher et al. (2015), Koven et al. (2020)	New model
DLEM	Tian et al. (2015), You et al. (2022)	No change
EDv3	Moorcroft et al. (2001), Ma et al. (2022)	Updated meteorology inputs (i.e. hourly air temperature)
ELM	Yang et al.(2023), Burrows et al.(2020)	No change
ELM-FATES	Fisher et al. (2015), Koven et al. (2020), Needham et al. (2025)	New model
GDSTEM	Felzer et al. (2009), Felzer et al. (2011), Felzer (2012), Felzer and Jiang (2018)	New model
IBIS	Xia et al., (2024)	No change
iMAPLE	Yue et al. (2024)	No change.

Formatted Table

ISAM	Jain et al. (2013), Meiyappan et al. (2015), Shu et al. (2020)	Vertically resolved soil biogeochemistry (carbon and nitrogen) module, following Shu et al. (2020)
JSBACH	Mauritsen et al. (2019), Reick et al. (2021)	No change
JULES-ES	Wiltshire et al. (2021), Sellar et al. (2019), Burton et al. (2019)	Minor updates to wildfire parameters
LPI-GUESS	Smith et al. (2014)	Wood harvest without the LUH2 secondary mature, young, and non-forest harvest fraction info
LPI-mL	Schaphoff et al. (2018), von Bloh et al. (2018), Lutz et al., (2019), Heinke et al. (2023)	Switch from version 5.7.5 to 5.10.0 incorporating updates to soil temperature scheme, revised N demand and N uptake processes, revised tree phenology, as well as bugfixes and code improvements
LPI-EOSIM	Poulter et al. (2011) (d)	Incorporation of new respiration temperature responses and leaf respiration acclimation, updated the soil temperature and water scheme to have 8 layers
LPX-Bern	Lienert and Joos (2018)	No change
ORCHIDEEv3	Krinner et al. (2005), Zaehle and Friend (2010), Vuichard et al. (2019)	No change
SDGVM	Woodward and Lomas (2004), Walker et al. (2017)	Reverted to version used in Friedlingstein et al. (2022), but retaining the recent bug fix to monthly heterotrophic respiration output
VISIT	Ito and Inatomi (2012), Kato et al. (2013)	No change
VISIT-UT	Ito (2019)	New model
Intermediate complexity land carbon cycle model		
CARDAMOM	Bloom et al. (2016), Smallman et al. (2021)	Analysis resolution increased from 1 x1 to 0.5x0.5 degree. Estimates of fAPAR from MODIS collection 6.1. New prior constraint on the leaf carbon per unit area parameter (LCA). MODIS burned area forcing was replaced by GFEDv5 burned area estimate
Global ocean biogeochemistry models		
NEMO-PlankTOM12	Wright et al (2021)	No change
NEMO4.2-PISCES (IPSL)	Aumont et al. (2015)	No change to the model version, but switch to ERA5 forcing - A,B,C,D simulations have been re-run starting from GCB2024 simulation restart fields from 1940 onwards
MCOM-HAMOCC (NorESM1-OCv1.2)	Schwinger et al. (2016)	No change, model has been re-run to provide monthly CFC/SF ₆ outputs
MPIOM-	Lacroix et al. (2021)	No change

HAMOCC6		
NEMO3.6-PICESv2-gas (CNRM)	Berthet et al. (2019), Séférian et al. (2019)	Updated simulations using 1750 preindustrial conditions instead of 1850. No change in model configuration, except nudging of surface ocean fields applied to minimize the change of atm forcing. The methodology used is based on Sanchez-Gomez et al. (2024)
FESOM2.1-REcoM3	Gürses et al. (2023)	Switched to ERA5 forcing - A,B,C,D simulations have been re-run starting from GCB2024 simulation restart fields
MOM6-COBALTv3 (Princeton)	Stock et al., (2025)	New model configuration MOM6-COBALTv3 with ~1° horizontal resolution (360x210). 1) updated ocean biogeochemical module COBALTv3 with an additional fixed nitrogen removal process - anaerobic ammonium oxidation (anammox); 2) updated air-sea gas exchange scheme - wind-wave-bubble formulation; 3) updated riverine carbon and nutrient inputs following R2OMIP protocol (Lacroix et al., 2024, https://zenodo.org/records/13799103); 4) updated river water discharge files.
CESM-ETHZ	Doney et al. (2009)	Compared to the 2024 submission, we changed the forcing to ERA5. To this end, a new spinup was performed, extending over 500 years.
MRI-ESM2-4	Tsujino et al. (2024), Sakamoto et al. (2023)	Iron circulation is modified according to Moore and Braucher (2008) and iron limitation on primary production is adjusted according to this change. Updated atmospheric CO2 for simulations A and C. The JRA-3Q reanalysis (Kosaka et al. 2024) is used to physically force the model. The model is spun up for 1925 years with xCO2=278ppm.
ACCESS (CSIRO)	Law et al. (2017)	No change in model since GCB2024, but switched to ERA5 forcing and extended spinup.
fcO2-products		
VLIZ-SOMFFN	Landschützer et al. (2016)	Time period extended to 2024
Jena-MLS	Rödenbeck et al. (2014) updated to Rödenbeck et al (2022)	Time period extended to 2024
CMEMS-LSCE-FFNNv2	Chau et al. (2022)	Time period extended to 2024
UEXP-FNN-U	Watson et al. (2020) and Ford et al. (2024)	Updated to recalculated SOCATv2025 dataset (Ford et al. 2025). Updated salinity dataset to use a tiered approach (described in Gregor et al. 2024) including ESA CCI-SSS (v5.51) and CMEMS GLORYS12V1. Updated time period to 1980 to 2024
NIES-ML3	Zeng et al. (2022)	Time period extended to 2024.
JMA-MLR	Iida et al. (2021)	Time period extended to 2024. Updated to recalculated SOCATv2025 dataset (Ford et al. 2025)
OceanSODA-ETHZv2	Gregor et al. (2024)	Time period extended to 2024

LDEO-HPD	Gloege et al. (2022) and Bennington et al. (2022)	Time period extended to 2024
CSIR-ML6	Gregor et al. (2019)	Time period extended to 2024
Atmospheric inversions		
Jena CarboScope	Rödenbeck et al. (2018) & Stephens et al. (2007).	Slight change in station set. Numerical flux resolution 2x2. TM3 run on spatial resolution 6x4 (multiple of 2x2)
CarbonTracker Europe (CTE)	van der Laan-Luijkx et al. (2017)	Update of prior fluxes and assimilated observations.
NISMON-CO2	Niwa et al. (2022), Niwa et al. (2017).	Update of prior fluxes, specifically changed GFED to GBEI. Update of the meteorological input to JRA-3Q. Including more CO2 observations.
CT-NOAA	Jacobson et al. (2025), Byrne et al. (2023), Krol et al. (2005), Peiro et al. (2022)	New air-sea gas exchange and new terrestrial NBE (Jacobson et al., 2025). Unlike previous submissions, CT2025 uses only one set of priors.
CMS-Flux	Liu et al. (2021)	Update of prior fluxes and assimilated observations.
CAMS-Satellite	Chevallier et al. (2005) and Chevallier et al. (2025)	Update of the prior fluxes and assimilated observations.
GONGGA	Jin et al. (2024)	Update of the prior fluxes and assimilated observations.
COLA	Liu et al. (2022)	Update of the prior fluxes and assimilated observations.
GCASv2	Jiang et al. (2021) & Emmons et al. (2010)	Update of the prior fluxes and assimilated observations.
UoE	Feng et al. (2016) & Palmer et al. (2019)	Update of the prior fluxes and assimilated observations.
MROC-ACTM	Chandra et al. (2022) & Patra et al. (2018)	Update of assimilated observations and prior fluxes, specifically changed to MiCASA and GFED. Update of the meteorological input to JRA-3Q.
NTFVAR	Nayagam et al. (2025) & Maksyutov et al. (2021)	Update of prior fluxes and assimilated observations.
THU	Kong et al. (2022)	New this year, after missing out 1 year. Compared to the previous submission: update of prior fluxes and assimilated observations.
NISMON-CO2_GOSAT	Niwa et al. (2022), Niwa et al. (2017).	New this year.
Earth System Models		
CanESM5	Swart et al. (2019), Sospedra-Alfonso et al. (2021)	No change
EC-Earth3-CC	Döscher et al. (2021), Bilbao et al. (2021), Bernardello et al. (2024)	No change
IPSL-CM6A-CO2-LR	Boucher et al. (2020)	No change
MROC-ES2L	Watanabe et al. (2020)	No change

MPI-ESM1-2-LR	Mauritsen et al. (2019), Li et al. (2023)	No change
NorCPM-CC	Tjiputra et al. (2020), Bethke et al. (2021)	New this year.

4597

4598 **Table 5.** Comparison of results from the bookkeeping method and budget residuals with results from the
4599 DGVMs, as well as additional estimates from atmospheric oxygen, atmospheric inversions and Earth System
4600 Models (ESMs) for different periods, the last decade, and the last year available. All values are in GtC yr⁻¹. The
4601 best estimate for GCB2025 (E_{LUC}) is calculated with the bookkeeping models (1a) and used in the budget Table
4602 7, see Section 2 and Figure 7 for description of the bookkeeping component fluxes. The best estimate for
4603 GCB2025 (S_{LAND}) is calculated with the DGVMs including the RSS correction (2b), and used in the budget
4604 Table 7. The DGVM uncertainties represent ±1σ of the decadal or annual (for 2024) estimates from the
4605 individual DGVMs. For the inverse systems the mean and range of available results is given when the number
4606 of systems is less than 10, otherwise the ±1σ is provided. All values are rounded to the nearest 0.1 GtC and
4607 therefore columns do not necessarily add to zero.

		<i>Mean (GtC yr⁻¹)</i>							
		1960s	1970s	1980s	1990s	2000s	2010s	2015-2024	2024
Land-use change emissions (E _{LUC})	Bookkeeping (BK) Net flux (1a)	1.9±0.7	1.7±0.7	1.7±0.7	1.7±0.7	1.7±0.7	1.6±0.7	1.4±0.7	1.3±0.7
	BK - deforestation (total)	1.8 [1.6,2.1]	1.8 [1.6,2.1]	1.7 [1.5,1.9]	1.9 [1.6,2.1]	2 [1.7,2.2]	2 [1.6,2.4]	1.9 [1.5,2.3]	1.9 [1.4,2.4]
	BK - forest regrowth (total)	-0.9 [-1,0.7]	-0.9 [-1,0.8]	-0.9 [-1,0.8]	-1 [-1.1,0.8]	-1.1 [-1.2,0.9]	-1.3 [-1.4,1]	-1.3 [-1.5,1]	-1.3 [-1.6,1]
	BK - other transitions	0.3 [0.3,0.3]	0.2 [0.2,0.3]	0.2 [0.1,0.3]	0.1 [0.1,0.2]	0.1 [0,0.1]	0.2 [0.1,0.2]	0.1 [0.1,0.1]	0.1 [0.1,0.1]
	BK - peat drainage & peat fires	0.2 [0.1,0.2]	0.2 [0.1,0.2]	0.2 [0.2,0.2]	0.3 [0.2,0.3]	0.2 [0.2,0.3]	0.3 [0.3,0.3]	0.2 [0.2,0.3]	0.2 [0.2,0.2]
	BK - wood harvest & forest management	0.4 [0.1,0.6]	0.4 [0.1,0.6]	0.5 [0.1,0.7]	0.5 [0.1,0.7]	0.5 [0.1,0.7]	0.4 [0.1,0.7]	0.4 [0.1,0.7]	0.4 [0.1,0.7]
	DGVMs-net flux (1b)	1.3±0.5	1.2±0.5	1.2±0.5	1.2±0.5	1.2±0.6	1.1±0.6	1±0.6	0.9±0.5
Terrestrial sink (S _{LAND})	Residual sink from global budget (E _{FOS} +E _{LUC} (1a)-G _{ATM} -S _{OCEAN}) (2a)	1.9±0.8	2±0.8	1.7±0.9	2.6±0.9	2.9±0.9	3±0.9	2.4±0.9	0.3±1
	DGVMs (2b)	0.9±0.3	1.6±0.5	1.4±0.6	2±0.5	2.2±0.6	2.5±0.7	2.4±0.8	1.9±0.9
Net land fluxes (S _{LAND} -E _{LUC})	GCB2025 Budget (2b-1a)	-0.9±0.8	-0.1±0.9	-0.3±0.9	0.2±0.9	0.5±0.9	0.9±1	1±1	0.7±1.1
	Atmospheric O ₂	---	---	---	1.3±0.6	0.9±0.7	1±0.8	0.7±0.8	-

	1960s	1970s	1980s	1990s	2000s	2010s	2015-2024	2024
DGVMs-net (2b-1b)	-0.3±0.4	0.4±0.6	0.2±0.5	0.8±0.4	1±0.4	1.4±0.6	1.4±0.7	1.1±0.8
Inversions*	- [-,-]	- [-,-]	- [-,-]	0.7 [0.6,0.8] (2)	1.4 [1.3,1.6] (3)	1.5 [1.3,2.3] (8)	1.3±0.3 (14)	0.2±0.7 (14)
ESMs	0 [-0.7,0.5]	1.5 [1.2,2.2]	1.1 [0.5,1.4]	1.8 [1.2,2.4]	1.8 [0.4,2.7]	2 [0.7,3]	2.3 [-0.1,3.6]	0.8 [-2.9,3.3]

*Estimates are adjusted for the pre-industrial influence of river fluxes, for the cement carbonation sink, and adjusted to common EFOS (Sect. 2.7). The ranges given include varying numbers (in parentheses) of inversions in each decade (Table S4)

Formatted Table

Deleted: A4

Deleted: ¶

4609

4613 **Table 6:** Comparison of results for the un-adjusted ocean sinks from the $f\text{CO}_2$ -products, from global ocean
4614 biogeochemistry models (GOBMs), the best estimate for GCB2025 (adjusted So_{OCEAN}) calculated from $f\text{CO}_2$ -
4615 products and GOBMs) and used in the budget Table 7, as well as additional estimates from ocean interior
4616 observation-based changes in the dissolved inorganic carbon (DIC) inventory, atmospheric oxygen, atmospheric
4617 inversions and Earth System Models (ESMs) for different periods, the last decade, and the last year available.
4618 All values are in GtC yr^{-1} . Uncertainties represent $\pm 1\sigma$ of the estimates from the GOBMs and inversions ($n > 10$)
4619 and range of ensemble members is given for ensembles with $n < 10$ ($f\text{CO}_2$ -products, inversions, ocean interior,
4620 ESMs). The uncertainty of the GCB2025 budget estimate is based on expert judgement (Section 2 and
4621 Supplement S1 to S4) and for oxygen it is the standard deviation of a Monte Carlo ensemble (Section 2.8). Note
4622 that adjustments were applied to the $f\text{CO}_2$ -products and two of the ocean interior estimates to match the
4623 definition of So_{OCEAN} (see section 2.5.1 and S3.6).

4624

<i>Mean (GtC yr⁻¹)</i>								
Product	1960s	1970s	1980s	1990s	2000s	2010s	2015-2024	2024
GCB2025 Budget	1.3±0.4	1.6±0.4	2.1±0.4	2.3±0.4	2.6±0.4	3.1±0.4	3.2±0.4	3.4±0.4
$f\text{CO}_2$ -products	---	---	---	2.3 [2,3]	2.5 [2.4,2.9]	3.1 [2.9,3.5]	3.3 [2.9,3.9]	3.5 [2.8,4.2]
GOBMs	1.1±0.2	1.3±0.3	1.8±0.3	2.0±0.3	2.2±0.3	2.6±0.3	2.7±0.3	2.9±0.3
Atmospheric O ₂	---	---	---	2.0±0.4	2.8±0.4	3.4±0.5	3.5±0.5	-
Inversions	- [-,-]	- [-,-]	- [-,-]	2.4 [2.2,2.5] (2)	2.3 [2.2,2.4] (3)	2.9 [2.1,3.1] (8)	3±0.3 (14)	3±0.4 (14)
Ocean interior	1.1 [-,-]	1.3 [-,-]	1.8 [-,-]	2.1 [2,2.3]	2.2 [1.7,2.5]	3.3 [2.7,4]	---	-
ESMs	0.7 [0.1,1.1]	1 [0.4,1.4]	1.5 [0.7,2]	1.7 [1.1,2.1]	1.9 [1.5,2.2]	2.4 [2,2.7]	2.5 [2.2,2.8]	2.6 [2.2-3.1]

Formatted Table

Deleted: ¶
¶
¶
¶

4625

4632 **Table 7:** Decadal mean in the five components of the anthropogenic CO₂ budget for different periods, and last
 4633 year available. All values are in GtC yr⁻¹, and uncertainties are reported as ±1σ. Fossil CO₂ emissions include
 4634 cement carbonation. The table also shows the budget imbalance (B_{IM}), which provides a measure of the
 4635 discrepancies among the nearly independent estimates. A positive imbalance means the emissions are
 4636 overestimated and/or the sinks are too small. All values are rounded to the nearest 0.1 GtC and therefore
 4637 columns do not necessarily add to zero.

4638

		<i>Mean (GtC yr⁻¹)</i>								
		1960s	1970s	1980s	1990s	2000s	2010s	2015- 2024	2024	2025 (Proje ction)
Total emissi ons (E _{FOS} + E _{LUC})	Fossil CO ₂ emissi ons (E _{FOS})*	3±0.2	4.7±0 .2	5.4±0 .3	6.4±0 .3	7.8±0 .4	9.5±0 .5	9.8±0 .5	10.3± 0.5	10.4± 0.5
	Land- use chang e emissi ons (E _{LUC})	1.9±0 .7	1.7±0 .7	1.7±0 .7	1.7±0 .7	1.7±0 .7	1.6±0 .7	1.4±0 .7	1.3±0 .7	1.1±0 .7
	Total emissi ons	4.9±0 .7	6.4±0 .7	7.1±0 .8	8.1±0 .8	9.5±0 .8	11.1± 0.8	11.2± 0.9	11.6± 0.9	11.5± 0.9
Partiti oning	Growt h rate in atmos CO ₂ (G _{ATM})	1.7±0 .07	2.8±0 .07	3.4±0 .02	3.1±0 .02	4±0.0 2	5.1±0 .02	5.6±0 .02	7.9±0 .2	4.9±0 .2
	Ocean sink (S _{OCEA N})	1.3±0 .4	1.6±0 .4	2.1±0 .4	2.3±0 .4	2.6±0 .4	3.1±0 .4	3.2±0 .4	3.4±0 .4	3.2±0 .4
	Terres trial sink (S _{LAND})	0.9±0 .3	1.6±0 .5	1.4±0 .6	2±0.5	2.2±0 .6	2.5±0 .7	2.4±0 .8	1.9±0 .9	3.4±1
Budge t Imbal ance	BIM= E _{FOS} + E _{LUC} - (G _{ATM} +S _{OCEA})	0.9	0.5	0.3	0.7	0.7	0.4	0	-1.7	

	1960s	1970s	1980s	1990s	2000s	2010s	2015-2024	2024	2025 (Projection)
$N+S_{\text{land}}$									

*Fossil emissions excluding the cement carbonation sink amount to 3 ± 0.2 GtC yr⁻¹, 4.7 ± 0.2 GtC yr⁻¹, 5.5 ± 0.3 GtC yr⁻¹, 6.4 ± 0.3 GtC yr⁻¹, 7.9 ± 0.4 GtC yr⁻¹, and 9.7 ± 0.5 GtC yr⁻¹ for the decades 1960s to 2010s respectively and to 10 ± 0.5 GtC yr⁻¹ for 2024, and 10.5 ± 0.5 GtC yr⁻¹ for 2025.

Formatted Table

4640 **Table 8.** Cumulative CO₂ for different time periods in gigatonnes of carbon (GtC). Fossil CO₂ emissions
 4641 include cement carbonation. The budget imbalance (B_{IM}) provides a measure of the discrepancies among the
 4642 nearly independent estimates. All values are rounded to the nearest 5 GtC and therefore columns do not
 4643 necessarily add to zero. Uncertainties are reported as follows: E_{FOS} is 5% of cumulative emissions; E_{LUC} prior to
 4644 1959 is 1σ spread from the DGVMs, E_{LUC} post-1959 is 0.7*number of years (where 0.7 GtC yr⁻¹ is the
 4645 uncertainty on the annual E_{LUC} flux estimate); G_{ATM} uncertainty is held constant at 5 GtC for all time periods;
 4646 S_{OCEAN} uncertainty is 20% of the cumulative sink (20% relates to the annual uncertainty of 0.4 GtC yr⁻¹, which
 4647 is ~20% of the current ocean sink); and S_{LAND} is the 1σ spread from the DGVMs estimates.

4648 *Mean (GtC yr⁻¹)*

4649

		1750-2024	1850-2014	1850-2024	1960-2024	1850-2025
Emissions	Fossil CO ₂ emissions (E _{FOS})	500±25	400±20	495±25	415±20	510±25
	Land-use change emissions (E _{LUC})	280±65	235±55	250±60	110±45	250±60
	Total emissions	780±70	635±60	745±65	525±50	755±65
Partitioning	Growth rate in atmos CO ₂ (G _{ATM})	310±5	235±5	290±5	230±5	295±5
	Ocean sink (S _{OCEAN})	210±40	170±35	200±40	145±30	205±40
	Terrestrial sink (S _{LAND})	190±50	150±40	175±50	120±30	175±50
Budget imbalance	B _{IM} =E _{FOS} +E _{LUC} -(G _{ATM} +S _{OCEAN} +S _{LAND})	65	80	80	35	80

Formatted Table

4650
4651

Formatted: Font: Times New Roman, 10 pt

Formatted: Line spacing: single, Widow/Orphan control

Deleted: ¶
¶
¶
¶
¶

4659 **Table 9.** Average annual growth rate in fossil CO₂ emissions over the most recent decade (2015-2024) and the
4660 previous decade (2005-2014). The data for the World include the cement carbonation sink. IAS are emissions
4661 from international aviation and shipping. The rest of the world is defined as World minus China, USA, India,
4662 EU27, and IAS.
4663

	World	China	USA	India	EU27	OECD	Non-OECD	IAS	Rest of the World
2005-2014	2.1%	6.7%	-1.4%	6.4%	2.2%	-1.0%	4.6%	1.9%	1.8%
2015-2024	0.8%	2.5%	-1.2%	3.6%	-2.5%	-1.5%	2.1%	-1.4%	0.6%

Formatted Table

4664

Formatted: Font: Times New Roman, 10 pt, Bold

4665

Formatted: Space Before: 6 pt, After: 10 pt, Line spacing: 1.5 lines

Deleted: ¶

4681 **Table 10.** Major known sources of uncertainties in each component of the Global Carbon Budget, defined as
 4682 input data or processes that have a demonstrated effect of at least $\pm 0.3 \text{ GtC yr}^{-1}$.

Source of uncertainty	Time scale (years)	Location	Evidence
Fossil CO2 emissions (EFOS; Section 2.1)			
energy statistics	annual to decadal	global, but mainly China & major developing countries	(Korsbakken et al., 2016, Guan et al., 2012)
carbon content of coal	annual to decadal	global, but mainly China & major developing countries	(Liu et al., 2015)
system boundary	annual to decadal	all countries	(Andrew, 2020a)
Net land-use change flux (ELUC; section 2.2)			
land-cover and land-use change statistics	continuous	global; in particular tropics	(Houghton et al., 2012, Gasser et al., 2020, Ganzenmüller et al., 2022, Yu et al. 2022)
sub-grid-scale transitions	annual to decadal	global	(Wilkenskjeld et al., 2014, Bastos et al., 2021)
vegetation biomass	annual to decadal	global; in particular tropics	(Houghton et al., 2012, Bastos et al., 2021)
forest degradation (fire, selective logging)	annual to decadal	tropics; Amazon	(Aragão et al., 2018, Qin et al., 2021, Lapola et al., 2023)
wood and crop harvest	annual to decadal	global; SE Asia	(Arneth et al., 2017, Erb et al., 2018)
peat burning	multi-decadal trend	global	(van der Werf et al., 2010, 2017)
Atmospheric growth rate (GATM; section 2.4) no demonstrated uncertainties larger than $\pm 0.3 \text{ GtC yr}^{-1}$. The uncertainties in annual GATM have been estimated as $\pm 0.2 \text{ GtC yr}^{-1}$, although the conversion of the growth rate into a global annual flux assuming instantaneous mixing throughout the atmosphere introduces additional errors (see Section 2.4.2).			
Ocean sink (SOCEAN; section 2.5)			
sparsity in surface fCO2 observations	mean, decadal variability and trend	global, in particular southern hemisphere	(Gloege et al., 2021, Denvil-Sommer et al., 2021, Hauck et al., 2023a; Dong et al., 2024b)

Formatted Table

riverine carbon outgassing and its anthropogenic perturbation	annual to decadal	global, in particular partitioning between Tropics and South	(Aumont et al., 2001, Lacroix et al., 2020, Crisp et al., 2022)
Models underestimate interior ocean anthropogenic carbon storage	annual to decadal	global	(Friedlingstein et al., 2022a, this study, DeVries et al., 2023, Müller et al., 2023)
near-surface temperature and salinity gradients	mean on all time-scales	global	(Watson et al., 2020, Dong et al., 2022, Bellenger et al., 2023, Dong et al., 2024a)
Land sink (SLAND; section 2.6)			
strength of CO2 fertilisation	multi-decadal trend	global	(Wenzel et al., 2016; Walker et al., 2021)
response to variability in temperature and rainfall	annual to decadal	global; in particular tropics	(Cox et al., 2013; Jung et al., 2017; Humphrey et al., 2018; 2021)
nutrient limitation and supply	annual to multi-decadal	global	(Zaehle et al., 2014)
carbon allocation and tissue turnover rates	annual to decadal	global	(De Kauwe et al., 2014; O'Sullivan et al., 2022)
tree mortality	annual	global in particular tropics	(Hubau et al., 2021; Brienen et al., 2020)
response to diffuse radiation	annual	global	(Mercado et al., 2009; O'Sullivan et al., 2021)

Formatted: English (UK)

Formatted: English (UK)

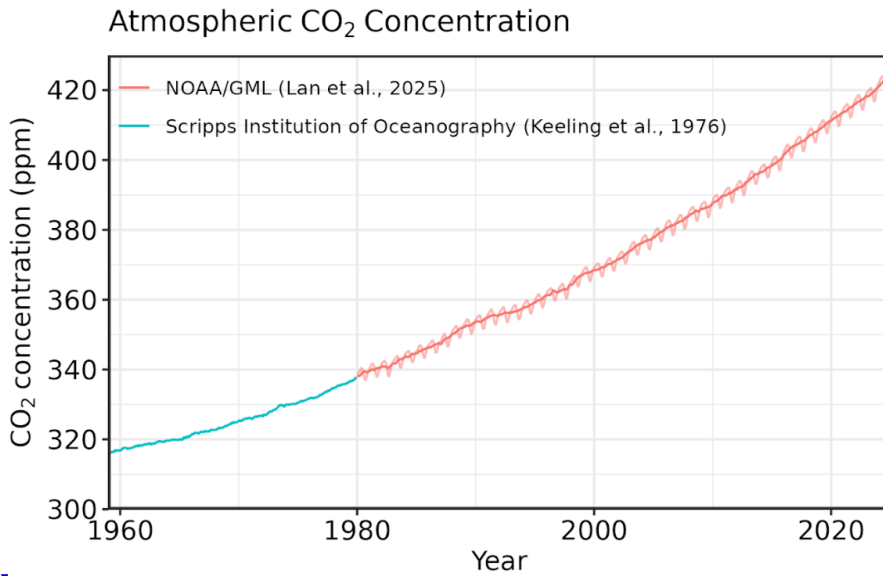
Formatted: Normal

4683

4684

4685

Figures

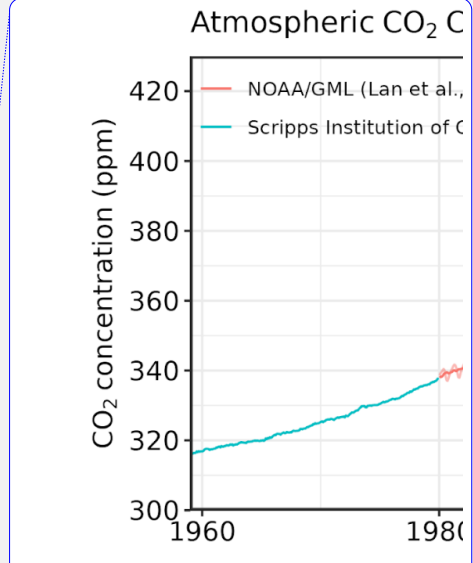


4686

4687 **Figure 1.** Surface average atmospheric CO₂ concentration (ppm). Since 1980, monthly data are from
 4688 NOAA/GML (Lan et al., 2025) and are based on an average of direct atmospheric CO₂ measurements from
 4689 multiple stations in the marine boundary layer (Masarie and Tans, 1995). The 1958-1979 monthly data are from
 4690 the Scripps Institution of Oceanography, based on an average of direct atmospheric CO₂ measurements from the
 4691 Mauna Loa and South Pole stations (Keeling et al., 1976). To account for the difference of mean CO₂ and
 4692 seasonality between the NOAA/GML and the Scripps station networks used here, the Scripps surface average
 4693 (from two stations) was de-seasonalised and adjusted to match the NOAA/GML surface average (from multiple
 4694 stations) by adding the mean difference of 0.667 ppm, calculated here from overlapping data during 1980-2012.

4695

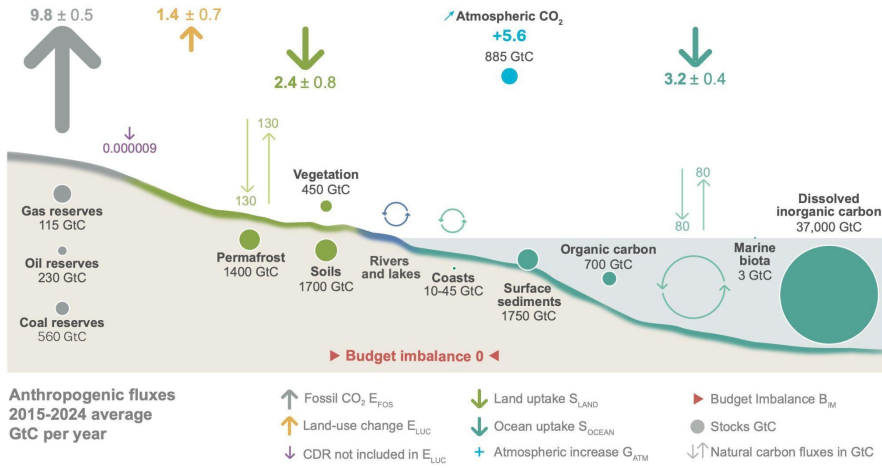
Deleted: [Image icon]



Deleted: Deleted: 2025a

Deleted: [Image icon] Page Break [Image icon] ... [9]

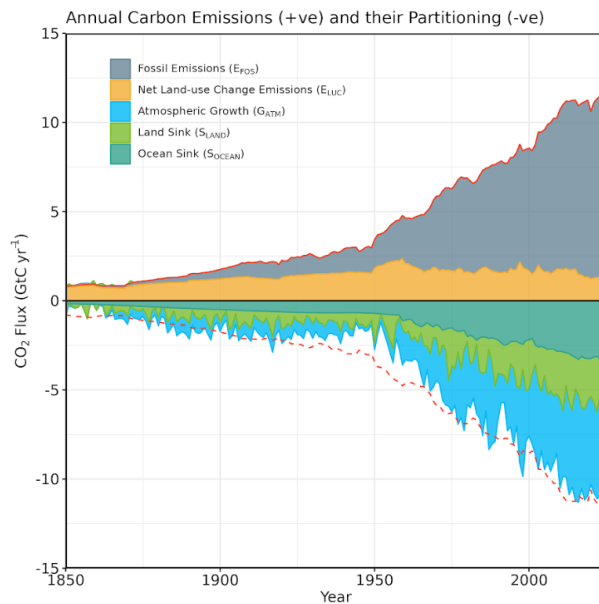
The global carbon cycle



4712

4713 **Figure 2.** Schematic representation of the overall perturbation of the global carbon cycle caused by
 4714 anthropogenic activities, averaged globally for the decade 2015-2024. See legends for the corresponding
 4715 Fluxes estimates and their 1 standard deviation uncertainty are as reported in Table 7. The CDR estimate is for the
 4716 year 2024. The uncertainty in the atmospheric CO₂ growth rate is very small ($\pm 0.02 \text{ GtC yr}^{-1}$) and is neglected for
 4717 the figure. The anthropogenic perturbation occurs on top of an active carbon cycle, with fluxes and stocks
 4718 represented in the background and taken from Canadell et al. (2021) for all numbers, except for the carbon
 4719 stocks in coasts which is from a literature review of coastal marine sediments (Price and Warren, 2016). Fluxes
 4720 are in GtC yr⁻¹ and reservoirs in GtC. This figure was produced by Nigel Hawtin.

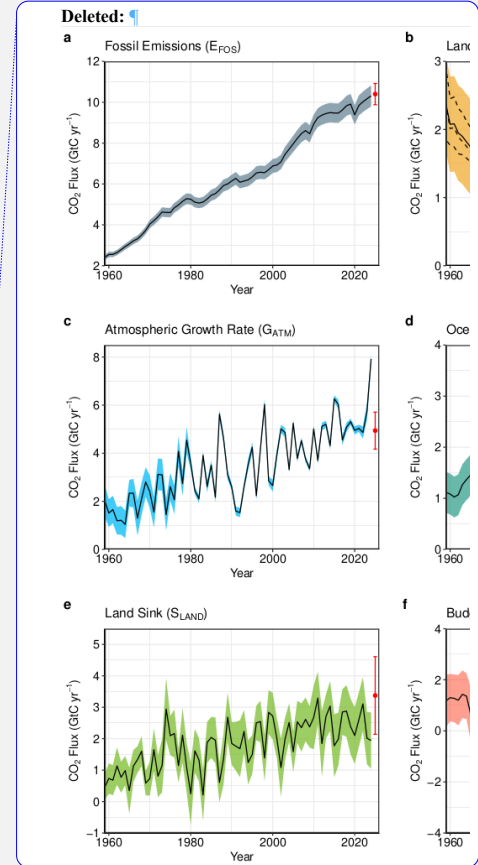
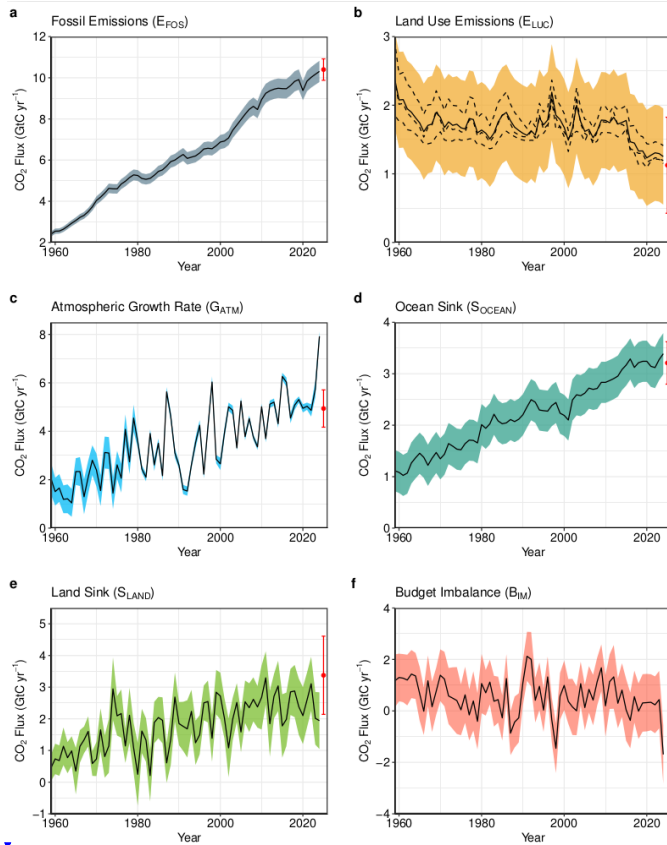
4721



4722
 4723 **Figure 3.** Combined components of the global carbon budget as a function of time, for fossil CO₂ emissions
 4724 (E_{FOS}, including a small sink from cement carbonation; grey) and emissions from land-use change (E_{LUC};
 4725 brown), as well as their partitioning among the atmosphere (G_{ATM}; cyan), ocean (S_{OCEAN}; blue), and land (S_{LAND};
 4726 green). The figure shows annual estimates of each flux (in GtC yr⁻¹) since the year 1850. The partitioning is
 4727 based on nearly independent estimates from observations (for G_{ATM}) and from process model ensembles
 4728 constrained by data (for S_{OCEAN} and S_{LAND}) and does not exactly add up to the sum of the emissions, resulting in
 4729 a budget imbalance (BIM) which is represented by the difference between the bottom red line (mirroring total
 4730 emissions) and the sum of carbon fluxes in the ocean, land, and atmosphere reservoirs. The E_{FOS} estimate is
 4731 based on a mosaic of different datasets and has an uncertainty of ±5% (±1σ). The E_{LUC} estimate is from three
 4732 bookkeeping models (Table 4) with uncertainty of ±0.7 GtC yr⁻¹. The G_{ATM} estimates prior to 1959 are from
 4733 Joos and Spahni (2008) with uncertainties equivalent to about ±0.1-0.15 GtC yr⁻¹ and from Lan et al. (2025)
 4734 since 1959 with uncertainties of about ±0.07 GtC yr⁻¹ during 1959-1979 and ±0.02 GtC yr⁻¹ since 1980. The
 4735 S_{OCEAN} estimate prior to 1959 is the average from Khatiwala et al. (2013) and DeVries (2014) with uncertainty
 4736 of about ±30%. After 1959, it is the average of an ensemble of models (GOBMs) and an ensemble of fCO₂-
 4737 products (with adjustments, Table 4) with uncertainties of about ±0.4 GtC yr⁻¹. The S_{LAND} estimate is the
 4738 average of an ensemble of models (DGVMs) (Table 4) with uncertainties of about ±1 GtC yr⁻¹. See the text for
 4739 more details of each component and their uncertainties.

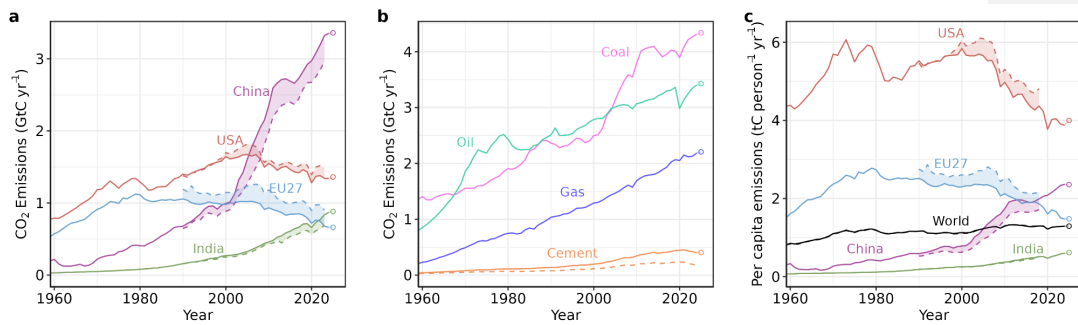
Deleted: <object>

Deleted: 2025a



4742
 4743 **Figure 4.** Components of the global carbon budget and their uncertainties as a function of time, presented
 4744 individually for (a) fossil CO₂, including cement carbonation emissions (E_{FOS}), (b) emissions from land-use
 4745 change (E_{LUC}), (c) growth rate in atmospheric CO₂ concentration (G_{ATM}), (d) the ocean CO₂ sink (S_{OCEAN}), (e)
 4746 the land CO₂ sink (S_{LAND}), (f) the budget imbalance (B_{IM}) that is not accounted for by the other terms. Individual
 4747 estimates from the three bookkeeping models are shown as dashed lines for E_{LUC} in panel (b). Positive values of
 4748 S_{LAND} and S_{OCEAN} represent a flux from the atmosphere to land or the ocean. All data are in GtC yr⁻¹ with the
 4749 uncertainty bounds representing ± 1 standard deviation in shaded colour. Data sources are as in Figure 3. The red
 4750 dots indicate our projections for the year 2025 and the red error bars the uncertainty in the 2025 projections (see
 4751 methods).

Formatted: Font: Bold

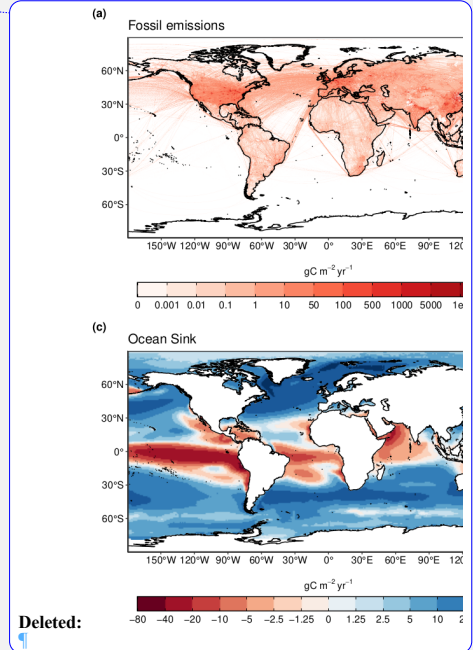


4754
 4755 **Figure 5.** Fossil CO₂ emissions for (a) territorial (solid lines) and consumption (dashed lines) emissions for the
 4756 top three country emitters (USA, China, India) and for the European Union (EU27), (b) global emissions by fuel
 4757 type, including coal, oil, gas, and cement, and cement minus cement carbonation (dashed), and (c) per-capita
 4758 emissions the world and for the large emitters as in panel (a). Territorial emissions are from Andrew & Peters
 4759 (2025), while consumption-based emissions are updated from Peters et al. (2011a). See Section 2.1 and
 4760 Supplement S.1 for details of the calculations and data sources.

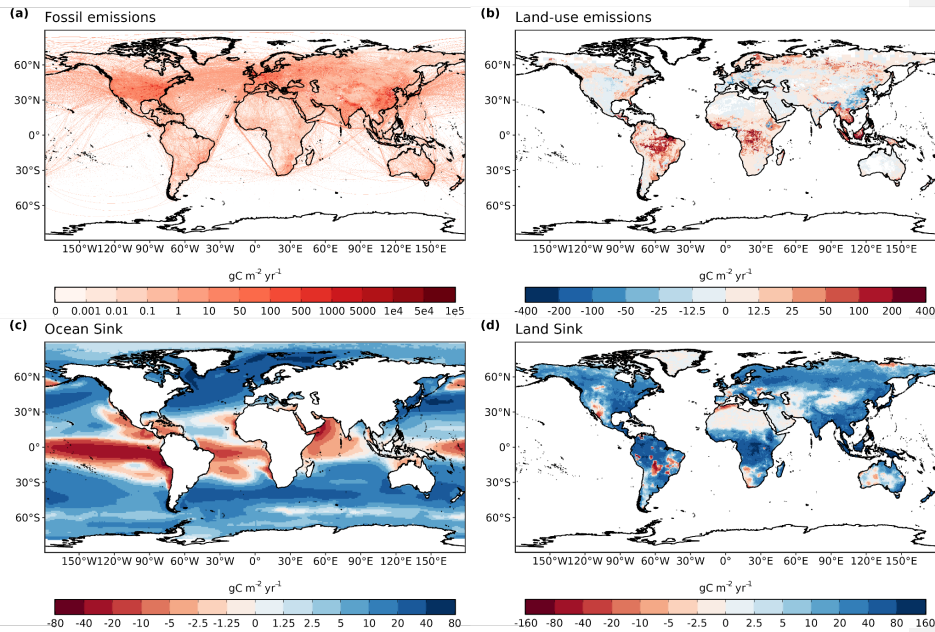
Deleted: ~~<object>~~

Deleted:Page Break.....

Formatted: Font: Not Bold



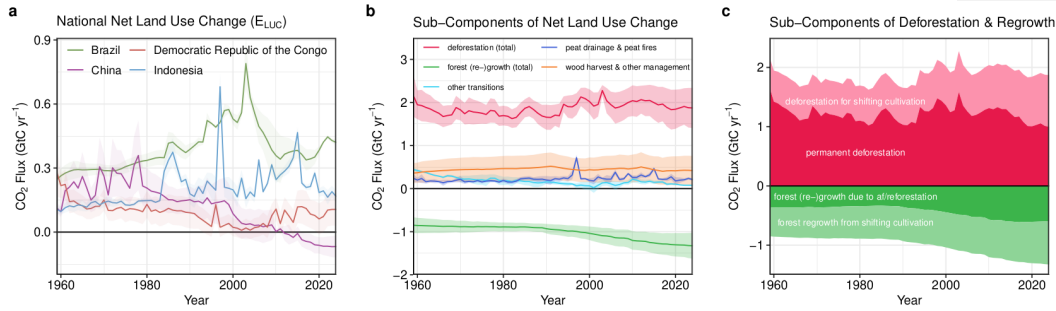
Deleted:



4767
 4768 **Figure 6.** The 2015-2024 decadal mean components of the global carbon budget, presented for (a) fossil CO₂
 4769 emissions (E_{FOS}), (b) land-use change emissions (E_{LUC}), (c) the ocean CO₂ sink (S_{OCEAN}), and (d) the land CO₂
 4770 sink (S_{LAND}). Positive values for E_{FOS} and E_{LUC} represent a flux to the atmosphere, whereas positive values of
 4771 S_{OCEAN} and S_{LAND} represent a flux from the atmosphere to the ocean or the land (carbon sink). In all panels, red
 4772 colours represent a source (flux from the land/ocean to the atmosphere), blue colours represent a sink (flux from
 4773 the atmosphere into the land/ocean). All units are in gC m⁻² yr⁻¹. Note the different scales in each panel. E_{FOS}
 4774 data shown is from GCP-GridFEDv2025.0 and does not include cement carbonation. The E_{LUC} map shows the
 4775 average E_{LUC} from the three bookkeeping models plus emissions from peat drainage and peat fires. BLUE and
 4776 LUCE provide spatially explicit estimates at 0.25° resolution. Gridded E_{LUC} estimates for OSCAR are derived
 4777 by spatially distributing their national data based on the spatial patterns of BLUE gross fluxes in each country
 4778 (see Schwingshackl et al., 2022, for more details about the methodology). S_{OCEAN} data shown is the average of
 4779 un-adjusted GOBMs and fCO₂-products means, using GOBMs simulation A, no adjustment for bias and drift
 4780 applied to the gridded fields (see Section 2.5). S_{LAND} data shown is the average of the DGVMs for simulation
 4781 S2, no adjustment for bias and drift applied to the gridded fields (see Section 2.6).

Deleted: with the RSS
 Deleted: included

4784



4785

4786

4787

4788

4789

4790

4791

4792

4793

4794

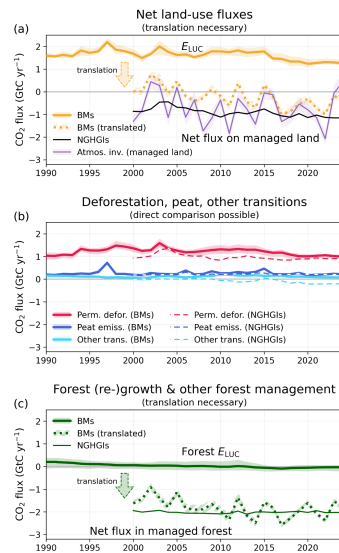
4795

4796

4797

Figure 7. Net CO₂ exchanges between the atmosphere and the terrestrial biosphere related to land use change. (a) Net CO₂ emissions from land-use change from the four countries with largest cumulative emissions since 1959. Values shown are the average of the three bookkeeping models, with shaded regions as ±1σ uncertainty. (b) Sub-components of E_{LUC}: (i) emissions from deforestation (including permanent deforestation and deforestation in shifting cultivation cycles), (ii) emissions from peat drainage & peat fires, (iii) removals from forest (re-)growth (including forest (re-)growth due to afforestation and reforestation and forest regrowth in shifting cultivation cycles), (iv) fluxes from wood harvest and other forest management (comprising slash and product decay following wood harvest, regrowth after wood harvest, and fire suppression), and (v) emissions and removals related to other land-use transitions. The sum of the five components is E_{LUC} shown in Figure 4b. (c) Sub-components of ‘deforestation (total)’ and of ‘forest (re-)growth (total)’: (i) deforestation in shifting cultivation cycles, (ii) permanent deforestation, (iii) forest (re-)growth due to afforestation and/or reforestation, and (iv) forest regrowth in shifting cultivation cycles.

Deleted: <object>



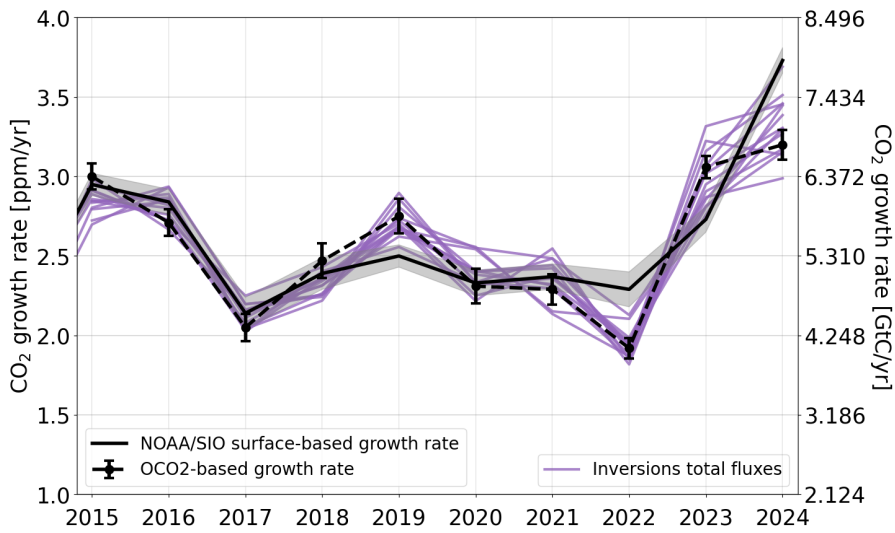
4799

4800 **Figure 8.** Comparison of land-use flux estimates from bookkeeping models (BMs; following the GCB
 4801 definition of E_{LUC}), national GHG inventories (NGHGIs; following IPCC guidelines and thus including all
 4802 carbon fluxes on managed land), and atmospheric inversion systems (considering fluxes on managed land only).
 4803 To compare BM results with NGHGIS, a translation is necessary for some subcomponents. (a) Net land-use
 4804 fluxes, for which a translation of BMs is necessary, (b) subcomponents permanent deforestation, peat drainage
 4805 & peat fires, and other transitions, which can be directly compared and (c) subcomponent forest (re-)growth &
 4806 other forest management, for which a translation is necessary. The lines represent the mean of 3 BMs and 14
 4807 atmospheric inversion estimates, respectively; Shaded areas denote the full range across BM estimates and the
 4808 standard deviation for atmospheric inversions, respectively. The subcomponent forest (re-)growth & other forest
 4809 management includes removals from forest (re-)growth (permanent), emissions and removals from wood
 4810 harvest & other forest management, and emissions and removals in shifting cultivation cycles. The translation of
 4811 BM estimates to NGHGI estimates in (a) and (c) is done by adding the natural land sink in managed forests to
 4812 the BM estimates (see also Table S11). The GCB definition of E_{LUC} and the NGHGI definition of land-use
 4813 fluxes are equally valid, each in its own context. For illustrative purposes we only show the translation of BM
 4814 estimates to the NGHGI definition. NGHGI data are from the LULUCF data hub V3.1 (Melo et al. 2025).

Deleted: <object>

Deleted: S10

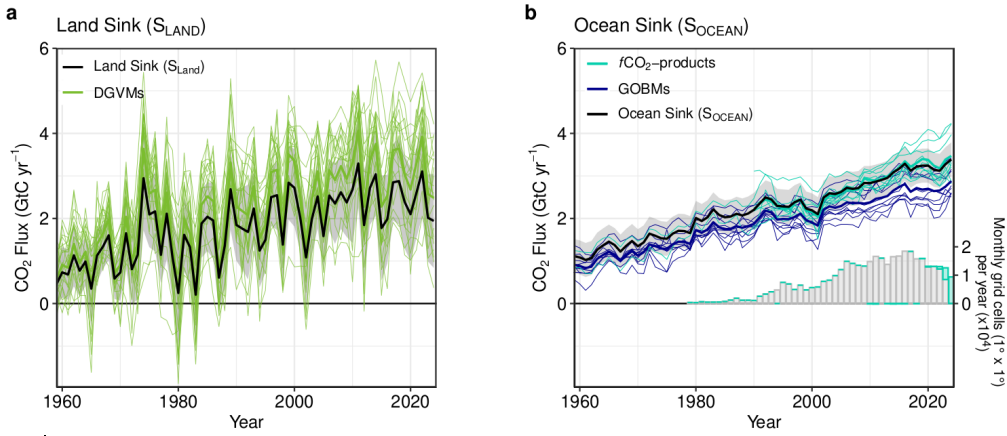
Formatted: Font: Bold



4817

4818 **Figure 9:** Annual atmospheric CO₂ growth rates based on observations from the surface network (by NOAA
 4819 (National Oceanic and Atmospheric Administration) and SIO (Scripps Institution of Oceanography), as well as
 4820 using the Growth Rate from Satellite Observations (GRESO) approach using OCO-2 based XCO₂ observations
 4821 in ppm yr⁻¹ with uncertainties. To obtain G_{ATM}, the surface observation-based growth rate in units of ppm yr⁻¹ is
 4822 converted to units of GtC yr⁻¹ by multiplying by a conversion factor (CF) of 2.124 GtC per ppm, assuming
 4823 instantaneous mixing of CO₂ throughout the atmosphere. The purple lines are the atmospheric growth rates (in
 4824 GtC yr⁻¹) calculated as the sum of the fluxes derived by the atmospheric inversions. Note that the right hand axis
 4825 shows the growth rate in GtC yr⁻¹, with intervals of the conversion factor.

Deleted:Page Break.....
 <object>



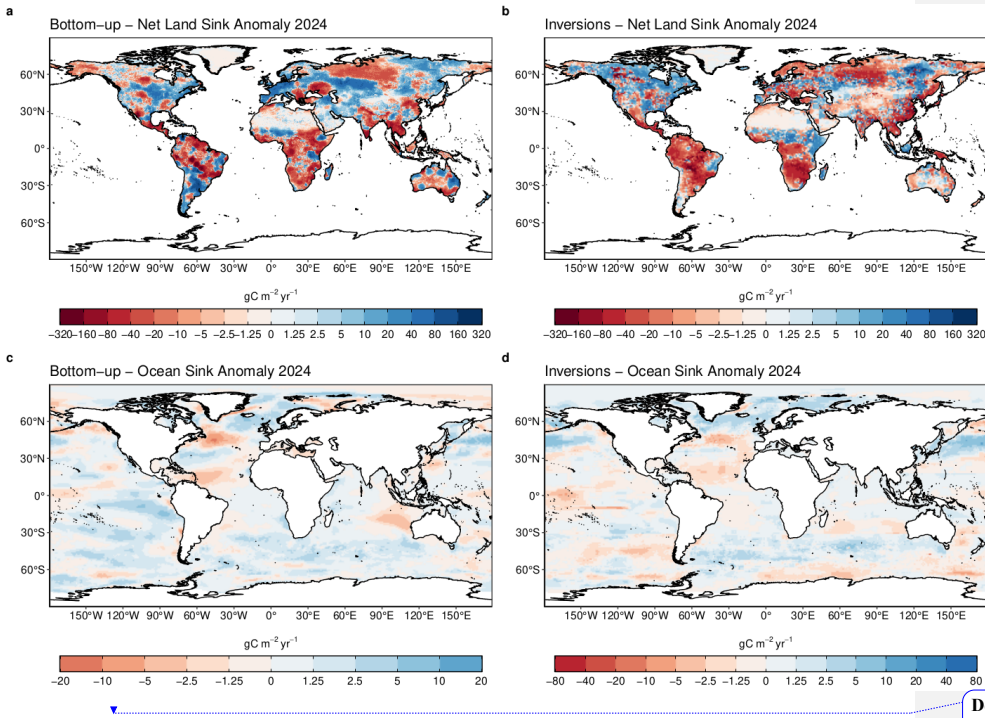
4829 **Figure 10.** (a) The land CO₂ sink (S_{LAND}) estimated by individual DGVMs (thin green lines). The DGVM multi-
 4830 model mean is shown as the thick green line. The S_{LAND} budget estimate (black with $\pm 1\sigma$ uncertainty), is the
 4831 DGVM multi-model mean adjusted for the RSS bias (i.e. reduced by 19%). (b) Comparison of the
 4832 anthropogenic atmosphere-ocean CO₂ flux showing the budget values of S_{OCEAN} (black; with the uncertainty in
 4833 grey shading), individual ocean models (royal blue), and the ocean fCO_2 -products (cyan). Adjustments were
 4834 applied to S_{OCEAN} (black) for the known underestimation in GOBMs and the warm layer/cool skin effect for
 4835 fCO_2 -products. Individual model lines as well as GOBMs and fCO_2 -product ensemble means (thick cyan and
 4836 royal blue lines) do not include these adjustments, with the exception of 2 fCO_2 -products (UExp-FNN-U and
 4837 JMA-MLR) that include temperature corrections as part of their air-sea CO₂ flux calculation (see section 2.5).
 4838 Two fCO_2 -products (Jena-MLS, LDEO-HPD) extend back to 1959. All fCO_2 -products were adjusted for the pre-
 4839 industrial ocean source of CO₂ from river input to the ocean, by subtracting a source of 0.65 GtC yr⁻¹ to make
 4840 them comparable to S_{OCEAN} (see Section 2.5). The bar-plot in the lower right illustrates the number of monthly
 4841 gridded values in the SOCAT v2025 dataset (Bakker et al., 2025a). Grey bars indicate the number of grid cells
 4842 in SOCAT v2024, and coloured bars indicate the newly added grid cells in v2025.

Deleted: ¶

Page Break

Deleted: <object>

Formatted: Font: Bold



4850

4851

4852

4853

4854

4855

4856

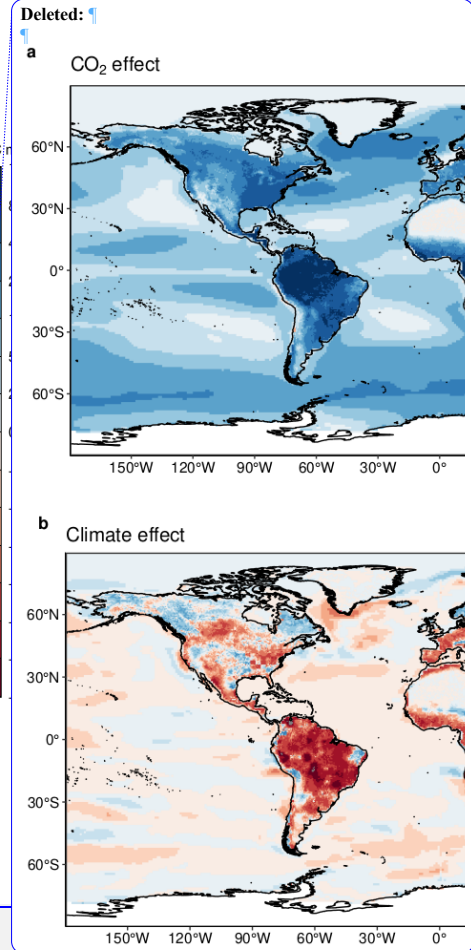
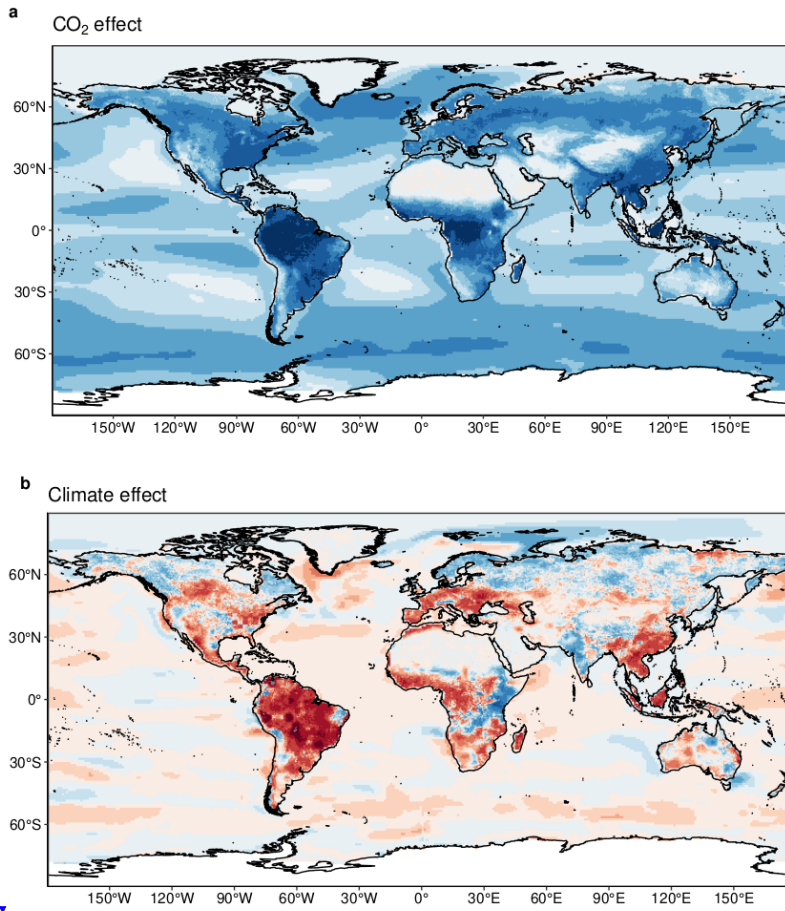
4857

Figure 11. Anomalies in land and ocean sinks for 2024. Maps show the 2024 fluxes relative to the 2015-2024 decadal mean. Units are $\text{gC m}^{-2} \text{yr}^{-1}$. (a) The bottom-up anomaly in the net land flux combines both the anomaly in S_{LAND} from DGVMs and in $ELUC$ from bookkeeping models, although the $ELUC$ contribution to the anomaly is minimal. Panel (b) shows the mean anomaly in the net land flux across 14 inversions. Panel (c) shows the mean anomaly from GOBMs and $f\text{CO}_2$ product ensemble means. The mean anomaly for GOBMs and $f\text{CO}_2$ products is first calculated, and then the mean of the two products is shown. Panel (d) shows the mean anomaly in ocean fluxes across 14 inversions.

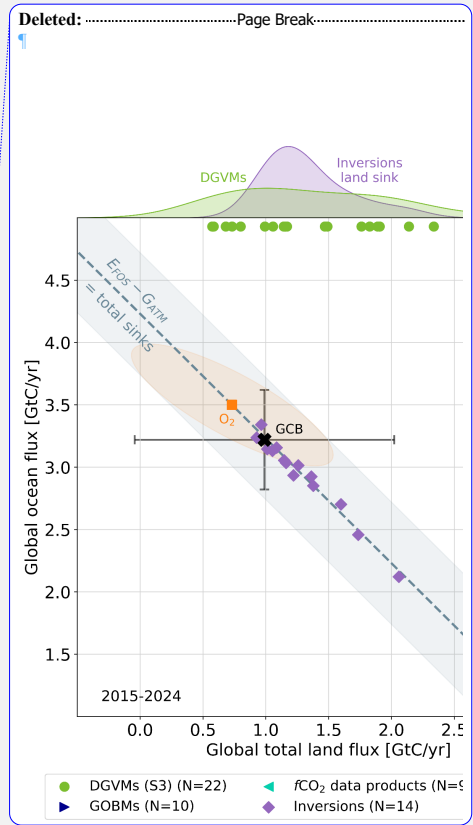
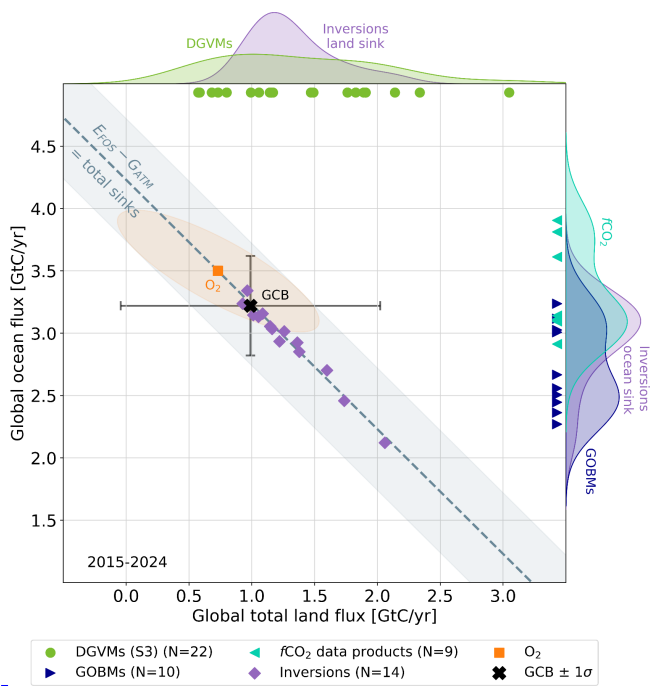
Deleted:Page Break.....

<object>

Formatted: Font: Bold

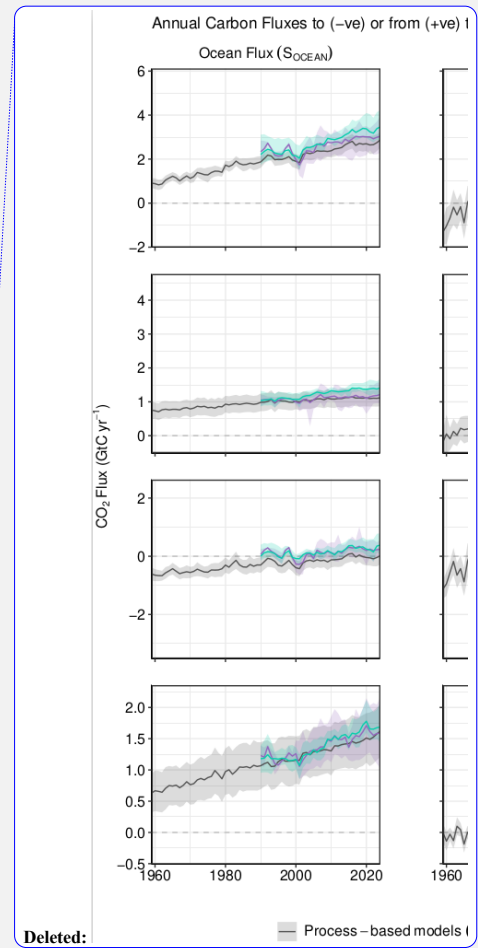
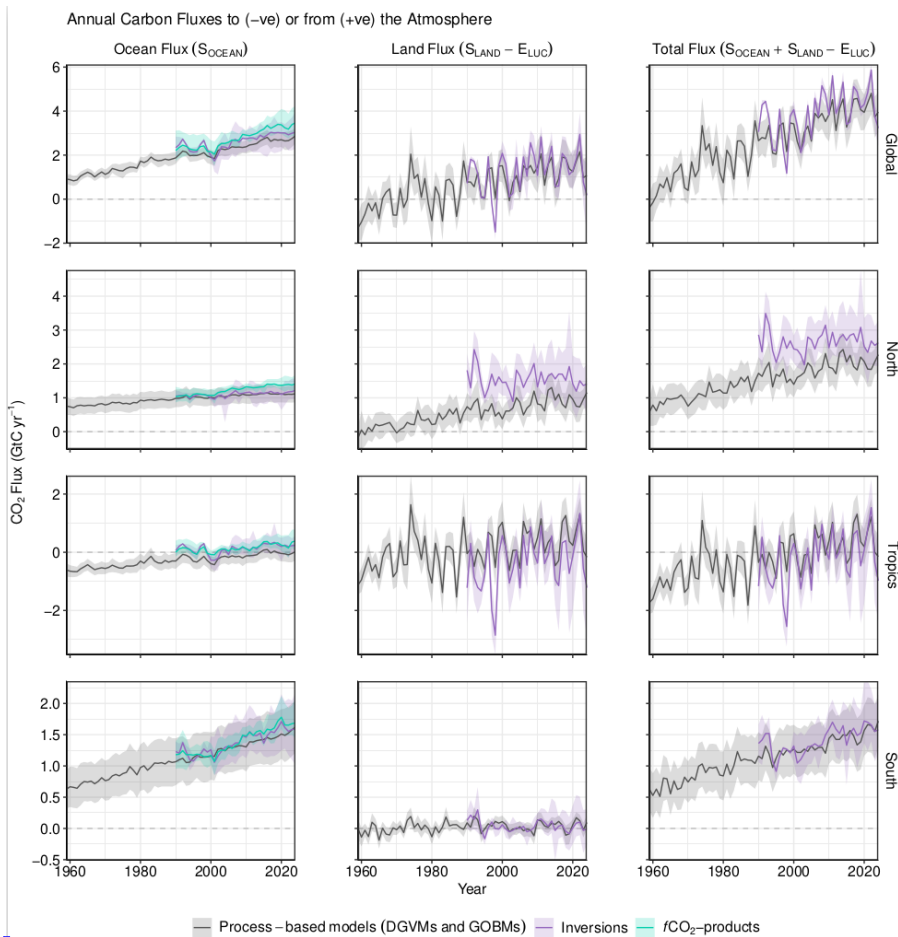


4861
 4862 **Figure 12.** Attribution of the atmosphere-ocean (S_{OCEAN}) and atmosphere-land (S_{LAND}) CO₂ fluxes to (a)
 4863 increasing atmospheric CO₂ concentrations and (b) changes in climate, averaged over the previous decade 2015-
 4864 2024. All data shown is from the processed-based GOBMs and DGVMs. Note that the sum of ocean CO₂ and
 4865 climate effects shown here will not equal the ocean sink shown in Figure 6, which includes the fCO_2 -products.
 4866 No adjustments were applied to the DGVMs or GOBMs. See Supplement S.3.2 and S.4.1 for attribution
 4867 methodology. Units are in gC m⁻² yr⁻¹ (note the non-linear colour scale). Positive values (blue) are CO₂ sinks,
 4868 negative values (red) are CO₂ sources.



4872

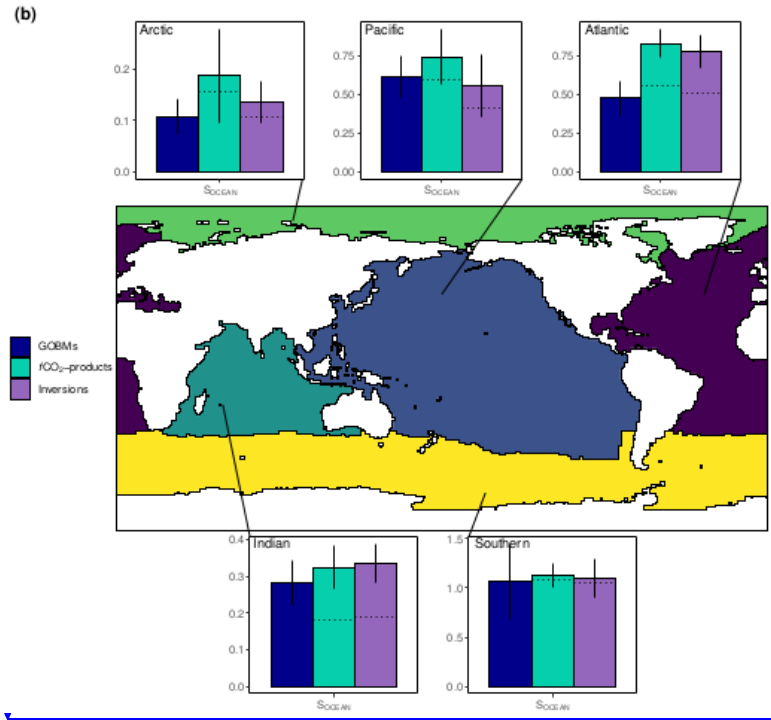
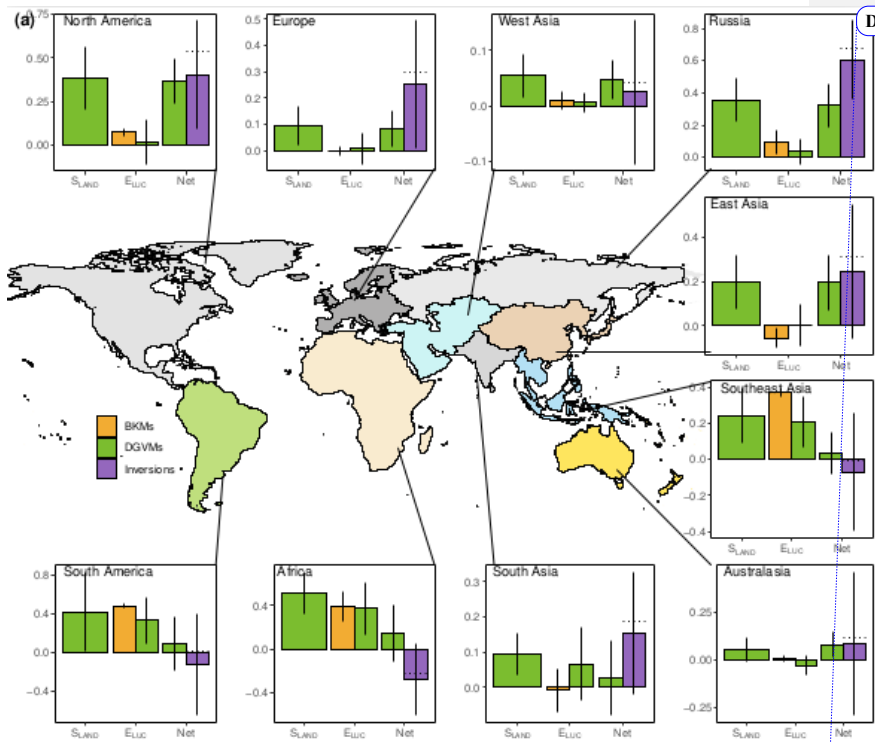
4873 **Figure 13.** The 2015-2024 decadal mean global net atmosphere-ocean and net atmosphere-land fluxes derived
 4874 from the ocean models and $f\text{CO}_2$ products (y-axis, right and left pointing blue triangles respectively), and from
 4875 the DGVMs (x-axis, green symbols), and the same fluxes estimated from the atmospheric inversions (purple
 4876 symbols). The shaded distributions show the densities of the ensembles of individual estimates. The black
 4877 central cross ('GCB') is the mean ($\pm 1\sigma$) of S_{OCEAN} and ($S_{\text{LAND}} - E_{\text{LUC}}$) as assessed in this budget. The grey
 4878 diagonal line represents the constraint on the global land + ocean net flux, i.e. global fossil fuel emissions minus
 4879 the atmospheric growth rate from this budget ($E_{\text{FOS}} - G_{\text{ATM}}$). The orange square represents the same global net
 4880 atmosphere-ocean and atmosphere-land fluxes as estimated from the atmospheric O_2 constraint (the ellipse
 4881 drawn around the central atmospheric O_2 estimate is a contour representing the 1σ uncertainty of the land and
 4882 ocean fluxes as a joint probability distribution). Positive values are CO_2 sinks. Note that the inverse estimates
 4883 have been scaled for a minor difference between E_{FOS} and GridFEDv2025.1 (Jones et al., 2025). The 'GCB'
 4884 central mean estimate includes the S_{LAND} and S_{OCEAN} global adjustments. The inversions and $f\text{CO}_2$ products
 4885 include the river adjustment (see Section 2). No further adjustments were applied to the individual bottom-up
 4886 estimates.



4890
 4891 **Figure 14.** CO₂ fluxes between the atmosphere and the Earth's surface separated between land and oceans,
 4892 globally and in three latitude bands. The ocean flux is S_{OCEAN} and the land flux is the net atmosphere-land fluxes
 4893 from the DGVMs. The latitude bands are (top row) global, (2nd row) north (>30°N), (3rd row) tropics (30°S-
 4894 30°N), and (bottom row) south (<30°S), and over ocean (left column), land (middle column), and total (right
 4895 column). Estimates are shown for: process-based models (DGVMs for land, GOBMs for oceans); inversion
 4896 systems (land and ocean); and $f\text{CO}_2$ -products (ocean only). Positive values are CO₂ sinks. Mean estimates from
 4897 the combination of the process models for the land and oceans are shown (black line) with $\pm 1 \sigma$ of the model
 4898 ensemble (grey shading). For the total uncertainty in the process-based estimate of the total sink, uncertainties
 4899 are summed in quadrature. Mean estimates from the atmospheric inversions are shown (purple lines) with their
 4900 full spread (purple shading). Mean estimates from the $f\text{CO}_2$ -products are shown for the ocean domain (light blue

4902 lines) with full model spread (light blue shading). The global SO_{CEAN} (upper left) and the sum of SO_{CEAN} in all
4903 three regions represents the anthropogenic atmosphere-to-ocean flux based on the assumption that the pre-
4904 industrial ocean sink was 0 GtC yr^{-1} when riverine fluxes are not considered. This assumption does not hold at
4905 the regional level, where pre-industrial fluxes can be significantly different from zero. Hence, the regional
4906 panels for SO_{CEAN} represent a combination of natural and anthropogenic fluxes.

Formatted: Font: 9 pt, Bold



4912 **Figure 15.** Decadal mean (a) land and (b) ocean fluxes for RECCAP-2 regions over 2015-
4913 2024. For land fluxes, S_{LAND} is estimated by the DGVMs (green bars), with the error bar as
4914 $\pm 1\sigma$ spread among models. A positive S_{LAND} is a net transfer of carbon from the atmosphere to
4915 the land. E_{LUC} fluxes are shown for both DGVMs (green) and bookkeeping models (orange),
4916 again with the uncertainty calculated as the $\pm 1\sigma$ spread. Note, a positive E_{LUC} flux indicates a
4917 loss of carbon from the land. For the DGVMs, S_{LAND} and E_{LUC} are adjusted for RSS bias. The
4918 net land flux is shown for both DGVMs (green) and atmospheric inversions (purple),
4919 including the full model spread for inversions. The ocean sink (S_{OCEAN}) is estimated by
4920 GOBMs (royal blue), fCO_2 -products (cyan), and atmospheric inversions (purple). No
4921 adjustments were applied to GOBMs and fCO_2 -products at regional scale. Uncertainty is
4922 estimated as the $\pm 1\sigma$ spread for GOBMs, and the full model spread for the other two datasets.
4923 The dotted lines show the fCO_2 -products and inversion results without river flux adjustment.
4924 Positive values are CO_2 sinks.

Page 31: [1] Deleted Friedlingstein, Pierre 27/03/2026 15:40:00

▼

Page 31: [1] Deleted Friedlingstein, Pierre 27/03/2026 15:40:00

▼

Page 31: [1] Deleted Friedlingstein, Pierre 27/03/2026 15:40:00

▼

Page 31: [1] Deleted Friedlingstein, Pierre 27/03/2026 15:40:00

▼

Page 31: [1] Deleted Friedlingstein, Pierre 27/03/2026 15:40:00

▼

Page 31: [1] Deleted Friedlingstein, Pierre 27/03/2026 15:40:00

▼

Page 31: [1] Deleted Friedlingstein, Pierre 27/03/2026 15:40:00

▼

Page 31: [1] Deleted Friedlingstein, Pierre 27/03/2026 15:40:00

▼

Page 31: [1] Deleted Friedlingstein, Pierre 27/03/2026 15:40:00

▼

Page 31: [1] Deleted Friedlingstein, Pierre 27/03/2026 15:40:00

▼

Page 31: [1] Deleted **Friedlingstein, Pierre** **27/03/2026 15:40:00**

▼

Page 31: [1] Deleted **Friedlingstein, Pierre** **27/03/2026 15:40:00**

▼

Page 31: [2] Deleted **Friedlingstein, Pierre** **27/03/2026 15:40:00**

▼

Page 31: [2] Deleted **Friedlingstein, Pierre** **27/03/2026 15:40:00**

▼

Page 31: [2] Deleted **Friedlingstein, Pierre** **27/03/2026 15:40:00**

▼

Page 31: [2] Deleted **Friedlingstein, Pierre** **27/03/2026 15:40:00**

▼

Page 31: [2] Deleted **Friedlingstein, Pierre** **27/03/2026 15:40:00**

▼

Page 31: [2] Deleted **Friedlingstein, Pierre** **27/03/2026 15:40:00**

▼

Page 31: [3] Deleted **Friedlingstein, Pierre** **27/03/2026 15:40:00**

▼

Page 31: [3] Deleted **Friedlingstein, Pierre** **27/03/2026 15:40:00**

▼

Page 31: [3] Deleted Friedlingstein, Pierre 27/03/2026 15:40:00

▼

Page 31: [3] Deleted Friedlingstein, Pierre 27/03/2026 15:40:00

▼

Page 31: [3] Deleted Friedlingstein, Pierre 27/03/2026 15:40:00

▼

Page 31: [3] Deleted Friedlingstein, Pierre 27/03/2026 15:40:00

▼

Page 31: [3] Deleted Friedlingstein, Pierre 27/03/2026 15:40:00

▼

Page 31: [3] Deleted Friedlingstein, Pierre 27/03/2026 15:40:00

▼

Page 31: [3] Deleted Friedlingstein, Pierre 27/03/2026 15:40:00

▼

Page 31: [3] Deleted Friedlingstein, Pierre 27/03/2026 15:40:00

▼

Page 31: [4] Deleted Friedlingstein, Pierre 27/03/2026 15:40:00

▼

Page 31: [4] Deleted Friedlingstein, Pierre 27/03/2026 15:40:00

▼

Page 31: [4] Deleted Friedlingstein, Pierre 27/03/2026 15:40:00

▼

Page 31: [4] Deleted Friedlingstein, Pierre 27/03/2026 15:40:00

▼

Page 31: [4] Deleted Friedlingstein, Pierre 27/03/2026 15:40:00

▼

Page 31: [4] Deleted Friedlingstein, Pierre 27/03/2026 15:40:00

▼

Page 31: [4] Deleted Friedlingstein, Pierre 27/03/2026 15:40:00

▼

Page 31: [4] Deleted Friedlingstein, Pierre 27/03/2026 15:40:00

▼

Page 31: [5] Deleted Friedlingstein, Pierre 27/03/2026 15:40:00

▼

Page 31: [5] Deleted Friedlingstein, Pierre 27/03/2026 15:40:00

▼

Page 31: [5] Deleted Friedlingstein, Pierre 27/03/2026 15:40:00

▼

Page 31: [5] Deleted Friedlingstein, Pierre 27/03/2026 15:40:00

▼

Page 31: [5] Deleted Friedlingstein, Pierre 27/03/2026 15:40:00

▼

Page 31: [5] Deleted Friedlingstein, Pierre 27/03/2026 15:40:00

▼

Page 31: [5] Deleted Friedlingstein, Pierre 27/03/2026 15:40:00

▼

Page 31: [6] Deleted Friedlingstein, Pierre 27/03/2026 15:40:00

▼

Page 31: [6] Deleted Friedlingstein, Pierre 27/03/2026 15:40:00

▼

Page 31: [6] Deleted Friedlingstein, Pierre 27/03/2026 15:40:00

▼

Page 31: [6] Deleted Friedlingstein, Pierre 27/03/2026 15:40:00

▼

Page 31: [7] Deleted Friedlingstein, Pierre 27/03/2026 15:40:00

▼

Page 31: [7] Deleted Friedlingstein, Pierre 27/03/2026 15:40:00

▼

Page 31: [7] Deleted Friedlingstein, Pierre 27/03/2026 15:40:00

▼

Page 31: [7] Deleted **Friedlingstein, Pierre** **27/03/2026 15:40:00**

▼

Page 31: [7] Deleted **Friedlingstein, Pierre** **27/03/2026 15:40:00**

▼

Page 31: [7] Deleted **Friedlingstein, Pierre** **27/03/2026 15:40:00**

▼

Page 31: [7] Deleted **Friedlingstein, Pierre** **27/03/2026 15:40:00**

▼

Page 31: [7] Deleted **Friedlingstein, Pierre** **27/03/2026 15:40:00**

▼

Page 31: [7] Deleted **Friedlingstein, Pierre** **27/03/2026 15:40:00**

▼

Page 31: [7] Deleted **Friedlingstein, Pierre** **27/03/2026 15:40:00**

▼

Page 31: [7] Deleted **Friedlingstein, Pierre** **27/03/2026 15:40:00**

▼

Page 31: [7] Deleted **Friedlingstein, Pierre** **27/03/2026 15:40:00**

▼

Page 31: [7] Deleted **Friedlingstein, Pierre** **27/03/2026 15:40:00**

▼

Page 31: [7] Deleted **Friedlingstein, Pierre** **27/03/2026 15:40:00**

▼

Page 31: [7] Deleted **Friedlingstein, Pierre** **27/03/2026 15:40:00**

▼

Page 31: [8] Deleted **Friedlingstein, Pierre** **27/03/2026 15:40:00**

▼

Page 31: [8] Deleted **Friedlingstein, Pierre** **27/03/2026 15:40:00**

▼

Page 31: [8] Deleted **Friedlingstein, Pierre** **27/03/2026 15:40:00**

▼

Page 31: [8] Deleted **Friedlingstein, Pierre** **27/03/2026 15:40:00**

▼

Page 124: [9] Deleted **Friedlingstein, Pierre** **27/03/2026 15:40:00**

▼

Page 139: [10] Deleted **Friedlingstein, Pierre** **27/03/2026 15:40:00**

▼